EPISTEMIC UNCERTAINTY IN THE ANALYTICALLY DERIVED FRAGILITY FUNCTIONS: MULTIPLE STRIPE ANALYSIS VERSUS CLOUD ANALYSIS

by

Zeynep Eda Önder

B.S., Civil Engineering, Istanbul Technical University, 2019

Submitted to Kandilli Observatory and Earthquake Research Institute
in partial fulfillment of the requirements for the degree of
Master of Science

Graduate Program in Earthquake Engineering
Boğaziçi University
2022

EPISTEMIC UNCERTAINTY IN THE ANALYTICALLY DERIVED FRAGILITY FUNCTIONS: MULTIPLE STRIPE ANALYSIS VERSUS CLOUD ANALYSIS

DATE OF APPROVAL: 29.07.2022

ACKNOWLEDGEMENTS

First and foremost, I would like to thank my thesis supervisor, Ufuk Hancılar, for all the possibilities he gave me during my master's degree as well as for his support, direction, and kind approach during the preparation of my thesis.

Besides my advisor, I would like to express my deep and sincere gratitude to my dear friends Erkan Şenol and Mahir Çetin for providing me full support during my master's education.

Most of all I am extremely grateful to my dear family for their unconditional love and spiritual support throughout my life.

ABSTRACT

EPISTEMIC UNCERTAINTY IN THE ANALYTICALLY DERIVED FRAGILITY FUNCTIONS: MULTIPLE STRIPE ANALYSIS VERSUS CLOUD ANALYSIS

This study aims to examine the effects of epistemic uncertainty arising from different analysis approaches on the derived fragility functions. To this end, fragility functions are developed by using two different methods namely multiple stripe analysis (MSA) and cloud analysis, and compared for low-rise and mid-rise (3 and 6-story), reinforced concrete (RC), moment-resisting frame (MRF) buildings designed as per the Turkish Seismic Codes (TSC) published in 1975 and 2018. Each building's preliminary design complies with the minimum requirements specified in the relevant seismic codes. A total of four buildings are studied considering different heights and different seismic codes. The OpenSees Program (the Open System for Earthquake Engineering Simulation) is used to perform nonlinear dynamic analyses of the structures. While spectral displacement (Sd), spectral acceleration (Sa) and peak ground acceleration (PGA) are chosen as intensity measures, maximum inter-story drift ratio (MIDR) and top displacement (Dtop) are selected as engineering demand parameters. For the damage state definitions through threshold values on the EDPs, nonlinear static (pushover) analyses are conducted to pick the limit values of top displacements from the idealized pushover curves whereas limit values for MIDR are drawn from the Hazus MR4 Technical Document. For MSA, 11 stripes and 22 pairs of earthquake records for each stripe are used, while 44 sets of record pairs are used for cloud analysis. Fragility functions for the aforementioned buildings are developed by using two methods and compared to account for the epistemic uncertainty in the derivation of fragility functions.

ÖZET

KIRILGANLIK FONKSİYONLARININ TÜRETİMİNDE EPİSTEMİK BELİRSİZLİĞİN DEĞERLENDİRİLMESİ: ÇOKLU ÇİZGİ ANALİZİ VE BULUT ANALİZİ

Bu çalışma, farklı analiz yaklaşımları ile türetilmiş kırılganlık eğrilerinin, farklılıklarından kaynaklanan epistemik belirsizliğin etkilerini incelemeyi amaçlamaktadır. Bu amaçla kırılganlık fonksiyonları; iki farklı yöntem olan çoklu çizgi analizi ve bulut analizi kullanılarak, 1975 ve 2018 Türkiye Deprem Yönetmeliklerine göre İstanbul'da inşa edilen alçak ve orta katlı (3 ve 6 katlı), moment aktaran betonarme çerçeve yapıları için geliştirilmiş ve karşılaştırılmıştır. Her binanın ön tasarımı için ilgili deprem yönetmeliğinde belirtilen minimum standartlara uyulmuştur. Farklı kat seviyeleri ve farklı deprem yönetmelikleri dikkate alınarak toplamda dört bina incelenmiştir. Yapıların doğrusal olmayan dinamik analizlerini gerçekleştirmek için OpenSees Programı kullanılmıştır. Spektral ivme (Sa), spektral yer değiştirme (Sd) ve maksimum yer ivmesi (PGA) şiddet ölçü birimi olarak (IM) kullanılırken, maksimum göreli kat ötelenmesi (MIDR) ve çatı yer değiştirmesi (Dtop) mühendislik talep parametreleri (EDP) olarak bu analizlerde kullanılmıştır. Mühendislik talep parametreleri (EDP) için hasar sınır durumları ile ilgili olarak, MIDR sınır değerleri Hazus MR4 teknik el kitabından alınırken, Dtop için limit değerleri belirlerken doğrusal olmayan statik itme analizi kullanılmıştır. Çoklu çizgi analizleri için 11 çizgi ve her çizgi için 22 çift deprem kaydı kullanılırken, bulut analizleri için 44 çift deprem kaydı kullanılmıştır. Bu çalışmada, kırılganlık eğrileri iki farklı yöntem kullanılarak türetilmiş ve türetilmesindeki epistemik belirsizliğini görmek amacıyla karşılaştırma yapılmıştır.

TABLE OF CONTENTS

LIST OF FIGURES

LIST OF TABLES

LIST OF SYMBOLS

g	gravitational acceleration, 9.80665 m/s^2
Ss	Coefficient of map spectral acceleration corresponding to the T=0.2-second-short period
S_1	Coefficient of map spectral acceleration corresponding to the T=1.0-second-long period
T_1	First-mode period
$(V_s)_{30}$	Shear wave velocities at 30 m below the top of the soil layer
$\phi(\ )$	Standard normal cumulative distribution function (CDF)
β	Standard deviation of lnIM
Θ	median of the fragility function (the IM level with 50 percent probability of collapse)
Π	Mathematical constant, approximately equal to 3.14159

LIST OF ACRONYMS/ABBREVIATIONS

2D	Two Dimensional
3D	Three Dimensional
AI	Arias intensity
ASCE	American society of civil engineers
ATC	Applied Technology Council
C1L	Low-rise concrete moment frame
CAV	Cumulative absolute velocity
CDF	Cumulative distribution function
CP	Collapse prevention
DS	Damage state
Dtop	Maximum top displacement
EDP	Engineering demand parameter
ELF	Equivalent Lateral Force
EMS98	European Macroseismic Scale
FE	Finite element
FEMA	Federal Emergency Management Agency
FL	Failure limit
G	Dead load
HAZUS	Hazards United States
IDA	Incremental dynamic analysis
IM	Intensity measure
IO	Immediate occupancy
kN	Kilonewton
LS	Life safety
m	Meter
MFA	Maximum floor acceleration
MIDR	Maximum interstory drift ratio
ML	Minimum damage limit

MLE	Maximum likelihood estimation
MMI	Modified Mercalli Intensity
MPa	Megapascal
MPR	Maximum plastic end rotation
MRF	Moment resisting frame
MSA	Multiple stripe analysis
M_W	Moment magnitude
NAFZ	North Anatolian Fault Zone
NRHA	Nonlinear response history analysis
PEER	Pacific Earthquake Engineering Research
PGA	Peak ground acceleration
PGV	Peak ground velocity
pSa	Pseudo spectral acceleration
Q	Live load
RC	Reinforced concrete
R_{JB}	Joyner-Boore distance
s	Second
S_a	Spectral acceleration
SCWB	Strong column weak beam
S_d	Spectral displacement
S_{D1}	Design spectral acceleration coefficient for long period
S_{DS}	Design spectral acceleration coefficient for short period
SL	Safety limit
S_v	Spectral velocity
TSC	Turkish Seismic Code

1. INTRODUCTION

An abrupt shaking of the earth's crust is referred to as an earthquake. Earthquakes may range in magnitude from hardly felt to severe enough to fling humans outside or wiped out entire towns. Unbearable and catastrophic results may occur from an earthquake. It causes extensive house, hospital, and other structure destruction. Many humans suffer fatal, serious injuries and financial, material losses. It has an impact on everyone's physically and mentally well-being. In addition, in structures that don't get the proper engineering servicing, we see that these impacts grow exponentially.

While being an earthquake-prone nation, Turkey faces serious and unavoidable earthquake-related problems. Turkey is located on active fault lines, and many of the nation's major cities are located quite close to these faults. The North Anatolian Fault Zone (NAFZ), which passes under the Sea of Marmara, it is thought that its impact on a metropolitan city like Istanbul will be more serious. Especially in Turkey, it is observed that the structures built before 2000s are weak in terms of engineering service during the design and construction stages. Therefore, it is thought that the capacities of these structures will not be able to meet the possible large seismic demands. For this reason, it is necessary to take serious measures and evaluate the structures according to the new regulations and take the necessary actions immediately. Recently, governments have started to give importance to earthquake risk assessment. Thanks to the risk assessment, loss estimates are made according to the regions. With risk assessment, the type and degree of damage to buildings can be determined and can be concentrated on those areas in order to take precautions. Earthquake hazard, fragility, and inventory of assets that are subjected to hazards are major determinants of seismic risk assessment [1].

The focus of this study is the development and assessment of fragility functions by using two different methods namely, multiple stripe analysis and cloud analysis, to account for epistemic uncertainty in the development of fragility functions for low to mid-rise reinforced concrete (RC) structures that are designed in accordance with the 1975 and 2018 Turkish Seismic Code requirements.

Uncertainty can be divided in two types which are epistemic and aleatory uncertainty. Epistemic uncertainty derives from the lack of knowledge of a parameter or process, while aleatory uncertainty refers to uncertainty caused by probabilistic variations in a random event. In addition, epistemic uncertainty can be reduced by changing model or data. In this study, to account for the epistemic uncertainty in developing fragility functions, two different models are used.

The approaches to create fragility functions are briefly covered in the next section, along with its primary components. Following that, a study of the literature is summarized, finally, the aims and scope of this study are explained.

1.1. Four Methods for Obtaining Fragility Functions

Fragility function is a cumulative distribution function (CDF) that shows the probability of a building exceeding a damage limit such as safety and failure limits against a ground motion intensity measure (IM) like Sd and Sa or peak ground motion intensity parameters (PGA, PGV, etc.). There are four methods to obtain a fragility function, which are, in decreasing reliability, empirical, analytical, expert opinion or judgmental, and hybrid methods [2].

Empirical (observational) fragility functions are generated by using post- earthquake results and observations. Although the most realistic results are obtained from this method, it has some disadvantages such as the lack of real earthquakes with high magnitudes that the analysts can exploit.

Analytical (predicted) fragility functions are obtained by analyzing the mathematical- analytical models of buildings. Analysts can scale the ground motions to represent large earthquakes or can simulate ground motions when there are not enough recorded accelerograms. Analysts can make some assumptions when using this method, but they must be careful not to include unrealistic parameters in the analyses.

The judgmental fragility functions are generated by making use of expert opinions. Experts know failure. Their thoughts about failures are collected in a pool and used. The main drawback of this method is its lack of credibility.

In the hybrid methods, fragility functions are generated by using the combination of the methods explained above. For instance, the analytical method can be used to generate fragility functions for collapse limit state while the empirical method is used to generate fragility function for light limit damage state.

1.2. Elements of Fragility Functions

Structural model, damage state, and intensity measure are the three main elements of fragility functions [3]. Typology of structures is also an important parameter since the structures' features play a crucial role in obtaining the correct fragility function. The geometry of the building, the height of the story, material properties, seismic code, and structural system also affect the fragility function's character. For example, for the same building, different design parameters due to earthquake codes differentiate the fragility functions. Moreover, region-to-region fragility functions show big changes due to soil and design parameters. Story number is also an important factor and is considered by the analysts to obtain its effect on the structures. Buildings with high story numbers have high damage levels [4].

Damage state (DS) is an important element of fragility function. For instance, minimum damage limit (ML), safety limit (SL), and failure limit (FL) are damage limits defined by the Turkish seismic codes (TSC) 2007. Damage states are classified as minor, moderate, substantial, or complete, according to FEMA 356 [5]. Limit values of damage states are related to the level of engineering demand parameters (EDP) that are used to measure the response. EDPs are classified as global and local demand parameters. While base shear, top displacement, roof drift ratio, maximum inter-story drift ratio (maximum inter-story drift normalized by story height) are examples of global engineering demand parameters, strain and chord rotation are examples of local demand parameters. EDPs should be appropriate with the structure's behavior. The analyst should be careful not to select ill-defined EDPs. For example, while base shear force is not an appropriate EDP for structures with high periods, the inter-story drift ratio is a meaningful measure for ductile structures.

Intensity measure (IM) is another important element of fragility function. Peak ground motion intensity values (PGA, PGV, etc.), spectral values (Sa, Sd) for the first natural vibration period, arias intensity (AI), cumulative absolute velocity (CAV) are the examples of intensity measures [6]. AI and CAV are energy-based parameters. IM should be efficient and sufficient. Intensity measures should be selected attentively, and the response of structures (EDP) should be well correlated with the intensity measures. For instance, low-rise and brittle structures' EDPs are convenient with peak ground acceleration (PGA) whereas spectral displacement (Sd) and spectral acceleration (Sa) are good IMs for ductile structures. Sa(T1) is a very prevalent intensity measure in developing fragility curves.

Spectral acceleration with the five percent damping ratio for the first mode is not fully sufficient when an analyst uses the high scale factor for ground motion records to obtain collapse state especially for the structures that are designed according to high codes [7].

In a fragility plot, the vertical axis indicates the cumulative probability of structural damage reaching or exceeding the threshold of a given damage state and the horizontal axis shows the ground motion intensity measure [6]. An example of a fragility curve is shown in Figure 1.1 [8].

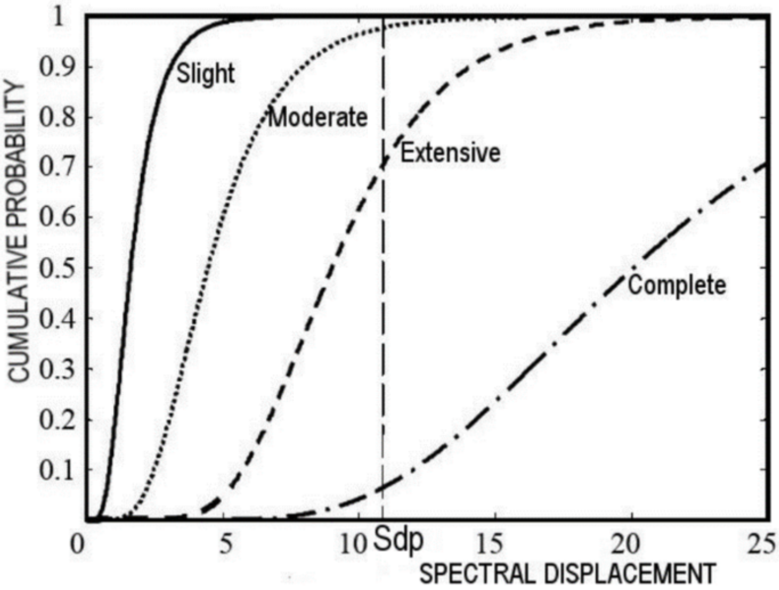

Figure 1.1. Example of fragility curves (Source: Hancilar et. al., 2010).

1.3. Literature Survey

There are plenty of studies about the derivation of fragility functions to evaluate the probabilistic structural assessment of structures. The literature survey at this study is focused on the studies that are related to the structures in Turkey.

Duran (2020) developed fragility functions (curves) for mid-rise, no-code RC frame structures. He used sixteen different types of buildings to represent the typologies of 800 buildings that are located in the district of Zeytinburnu in Istanbul. He classified the buildings into two groups according to the confinement conditions of their structural members, namely, confined and unconfined. He used the maximum interstory drift ratio (MIDR) as engineering demand parameter (EDP), and peak ground acceleration (PGV) as intensity measure (IM). He utilized incremental dynamic analysis (IDA) and nonlinear static analysis (pushover) to evaluate the responses of the buildings, he compared the responses that are obtained from these two types of analyses. He used the maximum likelihood method to obtain the fragility curves [3].

Akkar et al. (2005) generated fragility functions for low and mid-rise reinforced concrete buildings. Thirty-two reinforced concrete buildings with 2 and 3-stories were analyzed. These buildings represent the typology of buildings that were affected by the 1999 Düzce earthquake in Turkey. Fragility functions were obtained by using the hybrid method. When generating fragility functions, the lateral deformation capacity, strength, and stiffness of the buildings are obtained from the field observation database. He performed nonlinear response history analysis (NRHA). He used the global(roof) drift ratio as EDP and PGV as intensity measures because of its good correlation with the response of these types of buildings. The author indicated that the story number of buildings is an important parameter when developing fragility function [4].

Hancılar et al. (2014) generated fragility functions for mid-rise RC frames and RC shear buildings that were constructed in the 1990s. Fifty-five public school buildings in Istanbul were examined in this study and a standardized school building was modeled. Material and geometrical properties and dimensions of the structural elements were considered aleatory uncertainty, while the direction of ground motion excitation was considered epistemic uncertainty. The Monte Carlo approach was used in the study to see the effects of these uncertainties. The analytical method was used for generating the fragility functions. 107 earthquake records were utilized for the nonlinear dynamic analyses of the buildings. Five damage states (no damage, slight, moderate, extensive, complete) and three intensity measures (PGA, PGV, Sd (T1)) were used to develop fragility curves. The maximum inter-story drift ratio was also selected as the engineering demand parameter. This study showed that the uncertainties and control mechanisms to implement the standards have big effects on the fragility functions of buildings [9].

Kırçıl and Polat (2006) developed fragility functions for mid-rise RC frame buildings which were designed according to the 1975 Turkish seismic code (TSC 1975). Buildings were classified by their story numbers. (3-, 5-, 7- story). Yielding and collapse limits were chosen for damage levels. Maximum inter-story drift ratio (MIDR) was used as the engineering demand parameter to measure structures' response and first mode spectral acceleration, spectral displacement, and peak ground acceleration were used as the intensity measures. Incremental dynamic analyses were performed. The limit of yield capacity was defined as a point when the linear IDA curve became nonlinear, while the limit of collapse capacity was defined as a point when little increment of spectral acceleration leads to infinite MIDR. Fragility curves were developed based on Sa, Sd, and PGA as IM [10].

Tüzün (2008) developed analytical fragility curves for RC-MRF structures with story numbers ranging between two to seven. Building data were gathered from the existing RC frame buildings in Bolu, Turkey. He classified these structures into six groups according to their story numbers. Fragility curves were developed by using the analytical method. Spectrum-based ground motions were used for nonlinear dynamic analysis. He scaled the records with 0.05 g increments up to 1.00 g fır IDA. The Park-Ang damage index was used to define the damage levels. Sa(T1) and Sd(T1) were used as intensity measures. He showed that the near-field effect of ground motion, material uncertainty, and structural geometry has important effects on the fragility curves [11].

Dolağan (2019) generated fragility functions for mid-rise RC frame buildings which do not conform to any seismic code released after 1975. She used sixteen different types of buildings to represent the typologies of 800 buildings which are located in the district of Zeytinburnu in Istanbul. Nonlinear time-history analyses of the buildings were conducted with the use of OpenSees. She utilized incremental dynamic analysis (IDA) to evaluate the responses of the buildings. PGA was chosen as the intensity measure due to its convenience with pre-code structures' responses, and the maximum inter-story drift ratio was used as the engineering demand parameter. Damage levels were defined as strain values of structural members by considering TSC 2018. She indicated that structure's low geometrical and material quality cause early dynamic instability [12].

Hancılar and Çaktı (2015) studied the correlation between the engineering demand parameters (EDPs) and ıntensity measures (IMs). Buildings were classified by their story numbers as 5-, 10-, 15-, and 20- stories in this study. Unscaled ground motion records were used for nonlinear time history analysis (NRHA) to develop fragility curves. In this study, peak ground acceleration, velocity, and displacement (PGA, PGV, PGD), spectral acceleration, velocity, and displacement for first mode vibration period (Sa(T1), Sv(T1), Sd(T1)), arias intensity (AI), cumulative absolute velocity (CAV) were used as intensity measures. Maximum plastic end rotation (MPR), strain, maximum inter-story drift ratio (MIDR), maximum floor acceleration (MFA) were used as engineering demand parameters by the authors. According to this study, maximum inter-story drift ratio and plastic end rotation are well correlated with the first mode spectral acceleration for 5,10-story buildings, while for 15, 20-story buildings, maximum inter-story drift ratio, and plastic end rotation demand parameters show a good correlation with PGV. For low-rise buildings, peak ground acceleration is also well correlated with MFAs [6].

From the literature surveys, we conclude that there are various ways to develop fragility functions (curves). Intensity measure, engineering demand parameter, structure typology, material properties, geometrical configuration, ground motion selection, design code rules, etc. are the factors that affect fragility functions. Difference, deficiency, and uncertainty of any of these components can lead to different results when creating the fragility function. While defining damage states, analysts can prefer global or local engineering demand levels according to their time and effort. Some researchers may define the limit of engineering demand parameters by using capacity curves by converting the capacity curves to bilinear elastic-perfectly curves with the equal energy principle. Damage thresholds can be obtained by using yield and ultimate spectral displacement values.

Methods that are used to generate fragility functions are another factor that leads to different results. Most accurate results are obtained from the empirical method which does not give reliable results for high magnitude earthquakes. The analytical method is the second most chosen method to develop an accurate fragility curve.

Different building's finite element (FE) models also lead to different fragility functions. Since 2D models are easy to develop, analysts often prefer to use them but, they cause more uncertainties than 3D models.

1.4. Scope and Objective of Thesis

The aim of this thesis is to account for the epistemic uncertainty in the development of fragility functions by using two different methods namely, multiple stripe analysis and cloud analysis. The fragility functions are developed and compared for low-rise and mid-rise (3 and 6-story) reinforced concrete-moment resisting frame buildings designed in accordance with the TSC 1975 and TSC 2018 minimum standards. Four buildings are designed taking into account, two different story numbers (3 and 6-story), and two seismic regulations (TSC 1975 and TSC 2018). Four categories are made up of these buildings: two 6-story buildings designed per TSC 1975 and TSC 2018, two 3-story buildings designed per TSC 1975 and TSC 2018.

The OpenSees Software is used to perform the nonlinear dynamic analyses of the structures. Multiple stripe analysis (MSA) and cloud analysis approaches are used to obtain the fragility functions for the specified buildings. While spectral displacement (Sd), spectral acceleration (Sa) and peak ground acceleration (PGA) are chosen as intensity measures (IM), maximum inter-story drift ratio (MIDR) and top displacement (Dtop) are used as engineering parameters (EDP).

Regarding the threshold values of maximum inter-story drift ratio (MIDR), those are drawn from the Hazus MR4 Document while pushover curves are utilized to determine the limit values for Dtop. There are eleven stripes for multiple stripe analysis (MSA), and 22 couples of earthquake record sets are chosen for each stripe. For cloud analysis 44 pairs of records are utilized. All the records are taken from the PEER data base.

For low-rise and mid-rise RC buildings (3 and 6-story) designed per TSC 1975 and TSC 2018, fragility functions based on several types of intensity measures (IM) such as spectral acceleration (Sa), spectral displacement (Sd) and peak ground acceleration (PGA) and several types of engineering demand parameters (EDP) such as maximum inter-story drift ratio (MIDR) and top displacement (Dtop) are generated and compared.

2. STRUCTURAL SYSTEMS AND GROUND MOTION SELECTION

2.1. Definition of Structural Models

For 3 and 6-story buildings, fragility functions are developed by using two different methods in this study. The buildings are designed considering the minimum standards specified in the relevant seismic codes (TSC 1975 and TSC 2018). In addition, consideration is given to the capacity design principles described in the seismic codes.

Figure 2.1. Site location in Istanbul (Source: Google Earth).

A location in Istanbul is chosen, and 3 and 6-story buildings are designed there in accordance with the earthquake hazard characteristics on the specified site. This site is depicted in Figure 2.1. Table 2.1 lists the longitude and latitude and the related shear wave velocity to 30 meters, $(Vs)_{30}$. Four buildings in total, two with various story numbers and two with distinct design codes, analyzed and developed. Figure 2.2

and Figure 2.3 show the layouts for the 3 and 6-story structures. Figure 2.4 shows the structures' 3D finite element (FE) models.

Table 2.1. Location parameters.

Location ID	Coordinates	$(\text{Vs})_{30}[m/s]$
1	28.705, 41.045	178

The minimum requirements of TSC 1975 and TSC 2018 are being used to analyze and design the buildings. Table 2.2 lists the design criteria for both seismic codes. The preliminary design and analysis of the buildings are done using ETABS programme [13]. Buildings' linear analyses are conducted using the equivalent lateral force (ELF) approach. Figures 2.5 and 2.6 show the first three mode shapes for 3 and 6-story buildings.

Table 2.3 contains information on the free vibration periods of the 3 and 6-story buildings. The need for the cracked sectional stiffness of components is not obligatory in the TSC 1975. Therefore, even though their elasticity modulus values are lower than those of the structures that are designed in accordance with the TSC 2018, the structures that are designed in accordance with the TSC 1975 have lower periods.

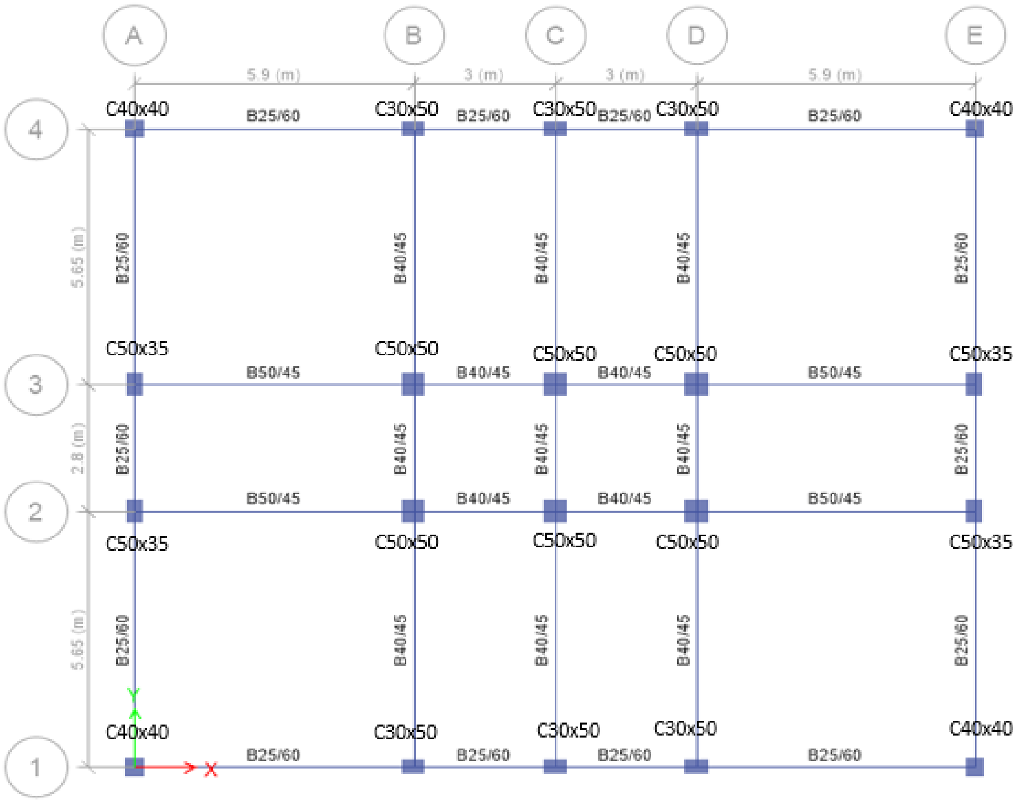

(a) 3-story

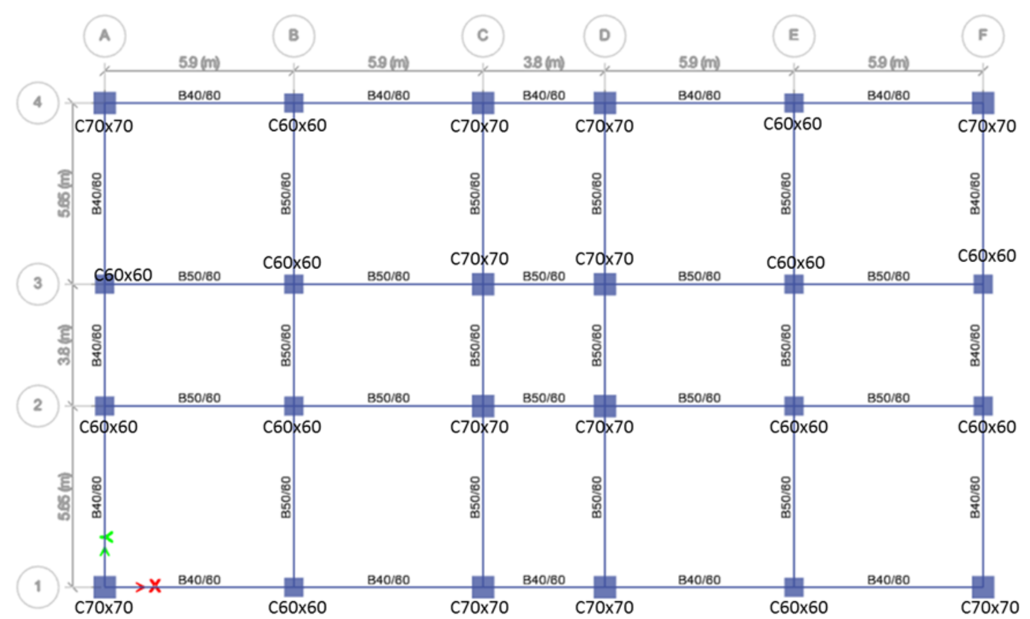

(b) 6-story

Figure 2.2. Floor plans and dimensions for the buildings designed as per the TSC 2018.

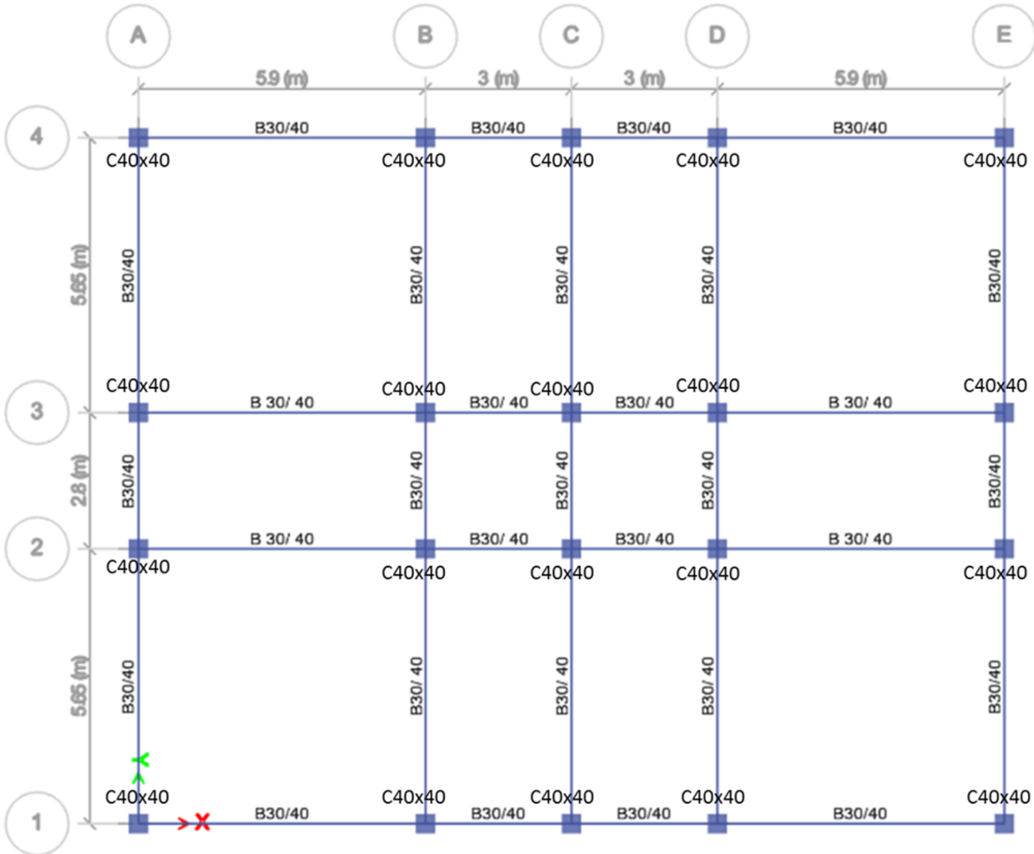

(a) 3-story

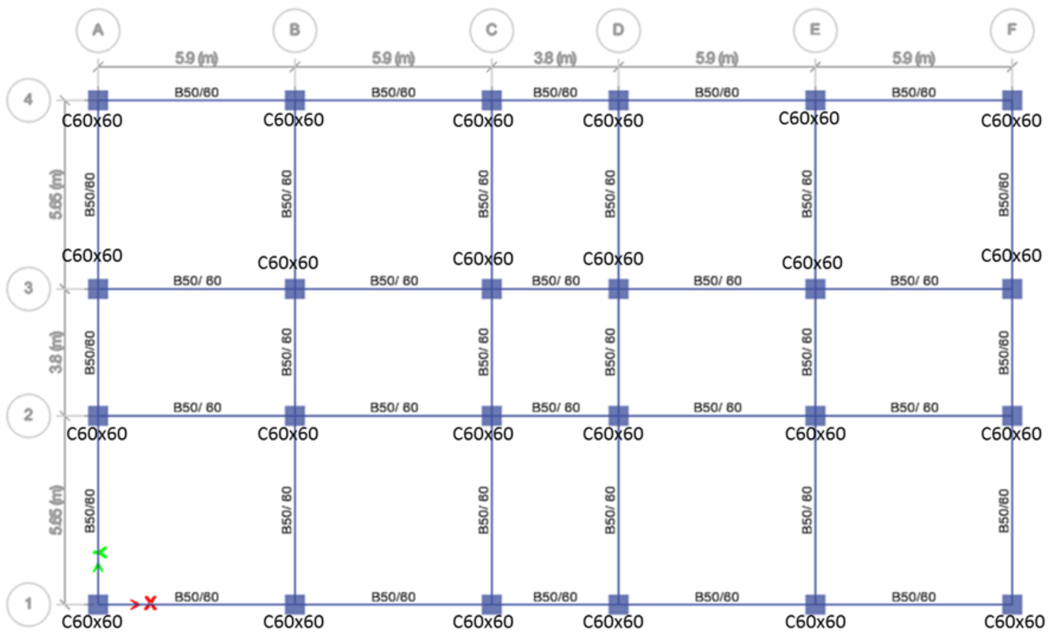

(b) 6-story

Figure 2.3. Floor plans and dimensions for the buildings designed as per the TSC 1975.

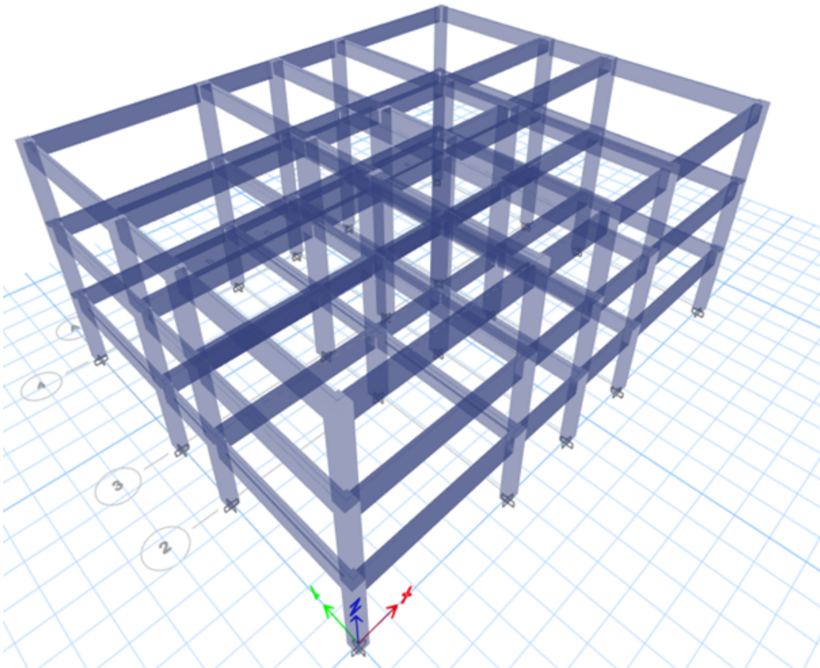

(a) 3-story buildings

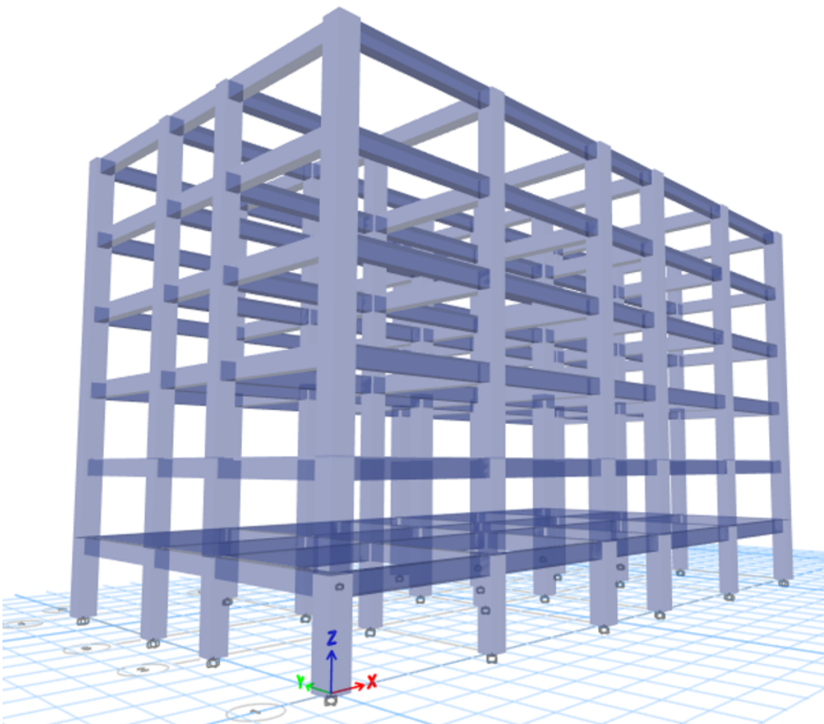

(b) 6-story buildings

Figure 2.4. Representative 3D views of the FEM models.

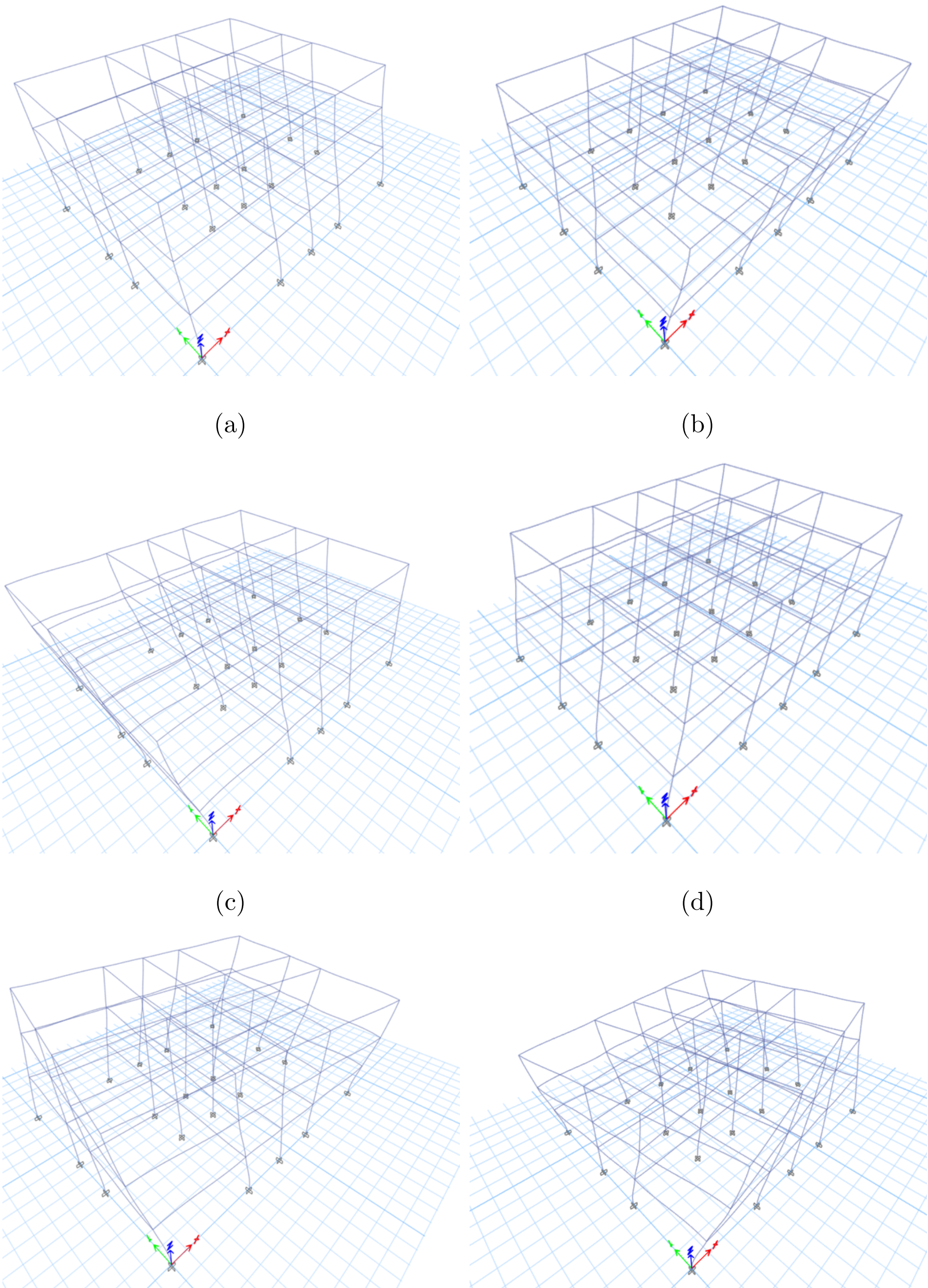

(a) (b)

(c) (d)

(e) (f)

Figure 2.5. The first three mode shapes of 3-story buildings designed per 1975 TSC (left) and 2018 TSC (right). The top row shows the first modes, the last row shows the third modes.

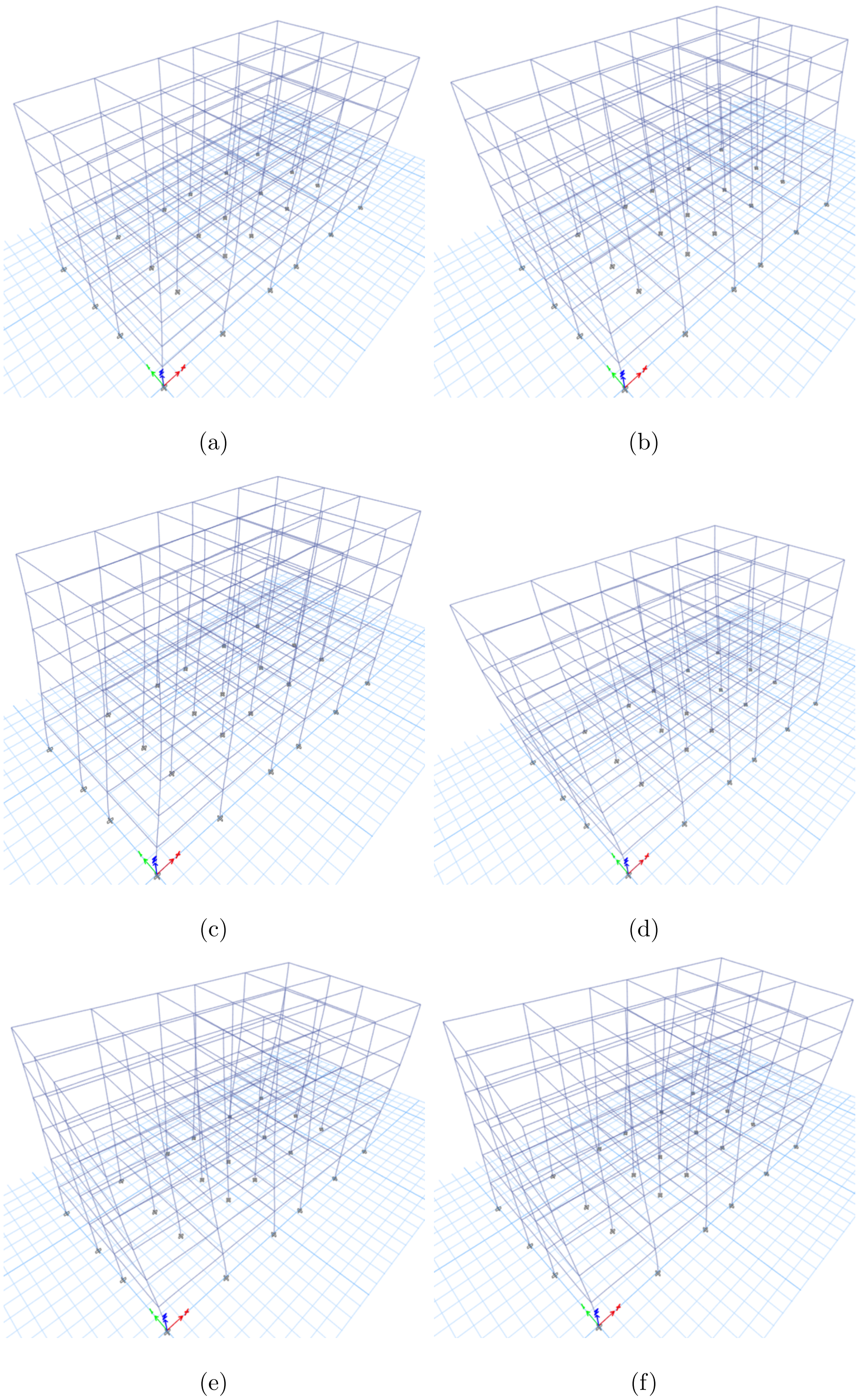

Figure 2.6. The first three mode shapes of 6-story buildings designed per 1975 TSC (left) and 2018 TSC (right). The top row shows the first modes, the last row shows the third modes.

Table 2.2. Design parameters.

Design Parameters	TSC,1975	TSC,2018
Concrete Class	C16	C25
Reinforcing Steel Grade	S220	S420
Building usage purpose	Residential	Residential
h basement, m	2.9	2.9
h normal, m	2.9	2.9
Footprint Area, m^2	101.4(for 3-story)	101.4(for 3-story)
Footprint Area, m^2	413.74(for 6-story)	413.74(for 6-story)
Slab thickness, mm	120.0(for 3-story)	120.0(for 3-story)
Slab thickness, mm	160.0(for 6-story)	160.0(for 6-story)
Type of The Lateral Load Resisting System	MRF	MRF
Super-imposed Dead Load, kN/m^2	2	2
Peripheral wall load, kN/m^2	4.325	4.325
Interior wall load, kN/m^2	2.5	2.5
Live Load, kN/m^2	2	2
Super-imposed Dead Load (roof), kN/m^2	4	4
Live Load (roof), kN/m^2	1.5	1.5
Analysis Type	ELF method	ELF method

Table 2.3. The free vibration periods of the buildings in seconds.

	First Mode	Second Mode	Third Mode
3-story,1975	0.530	0.513	0.483
3-story,2018	0.309	0.277	0.245
6-story,1975	0.541	0.531	0.500
6-story,2018	0.727	0.724	0.679

During the design stages, the capacity design concepts are considered. By taking into account the capacity design principles, the nonlinear ductile behavior at the load-carrying mechanism is assured, allowing the energy of an earthquake to be dampened with the deformation of structural parts that are built as ductile. Shear deformation failures occur suddenly, whereas flexural failures happen gradually in a ductile manner. By increasing the shear capacity of the structural members, brittle failures are avoided. The internal forces of the structure rise during the earthquake, but because of the capacity design concepts, the structural elements may securely adapt by utilising their inelastic deformation capabilities in a ductile way. The structural member shear force capacities have to be high enough to guarantee the bending type yielding. The strong column-weak beam concept is maintained. Additionally, frame joints are designed to also be strong enough to distribute moments among frame parts.

2.2. Differences Between TSC 1975 and TSC 2018 for Low-Rise and Mid-Rise RC MRF Buildings

There are a few distinctions between these two seismic codes, so in this chapter, those distinctions which come up during the structure's design phases are highlighted.

Firstly, Turkey is classified into four earthquake zones in the TSC 1975 seismic code. The computation of the earthquake effects is further clarified in the TSC 1975 seismic code compared to the previous ones and spectral acceleration is first included in this seismic code. The earthquake coefficient (C) is calculated by using earthquake zone coefficients (C_0) that are established in accordance with the earthquake zones named as 1, 2, 3 and 4.

In the TSC 2018 seismic code, on the other hand, building performance objective is established based on the seismic design category and building height class, after which design method is chosen for new structures. The vertical design spectrum and the seismic hazard according to the location are both specified. The significant distinction between this code and others including TSC 1975 is that it allows the design of structures in accordance with multiple building performance objective. In addition to this, the TSC 2018 seismic code bases its assessment of earthquake hazard on a point's location rather than the seismic hazard maps that are used in the previous codes, which divided Turkey into seismic zones. In this regard, the site effect and seismic hazard parameters, which together make up the conventional acceleration spectrum, have drastically changed. Lastly, earthquake hazard is defined not at a single ground motion level, but at four different levels namely, DD1, DD2, DD2 and DD4 levels.

There are also more variations between the two seismic codes throughout the design phase of RC structural elements. The lowest level of concrete class is one of them. While C14 is the minimal concrete class in TSC 1975, C25 is the minimum allowable concrete class in TSC 2018. The other is the dimensions of the column sections; in TSC 2018, the minimum section of the column sections is 300 mm, whereas in TSC 1975, the minimum column section dimension is 250 mm.

2.3. Nonlinear Modelling

Using OpenSees software is used to perform the nonlinear dynamic analyses. The software's "nonlinearBeamColumn" component is used to simulate columns, while its "beamWithHinges" component is used to simulate beams. Figure 2.7 shows the stress-strain hysteresis produced by using concrete04 and steel02 models.

The structural components' cross-sections are divided into several fibers. The "Concrete04" material of OpenSees Programme is utilized for the core and cover concrete in the concrete model. The identical concrete model put out by Mander et al. (1988) is generated with the command "Concrete04". The concrete model's tensile strength is disregarded. The OpenSees "Steel02" material is utilized for the reinforcing model. Using the "Section Aggregator" OpenSees Programme command, torsional and shear behavior of sections are treated as elastic and are executed in the analyses.

Although the slab and foundation are not represented in the models, gravity analysis takes slab weight into account. At the base level, the columns' degrees of freedom are fixed. To take into account the in-plane behavior of slabs and to convey

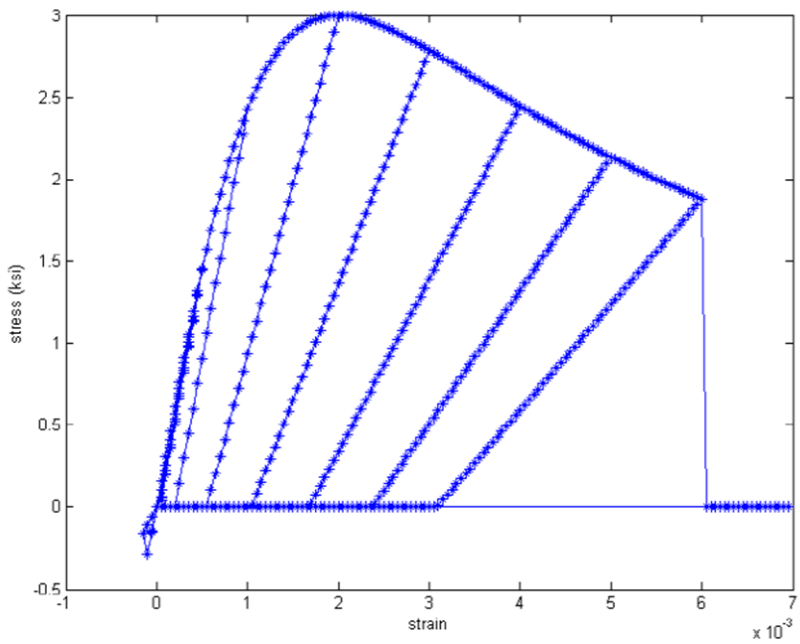

(a)

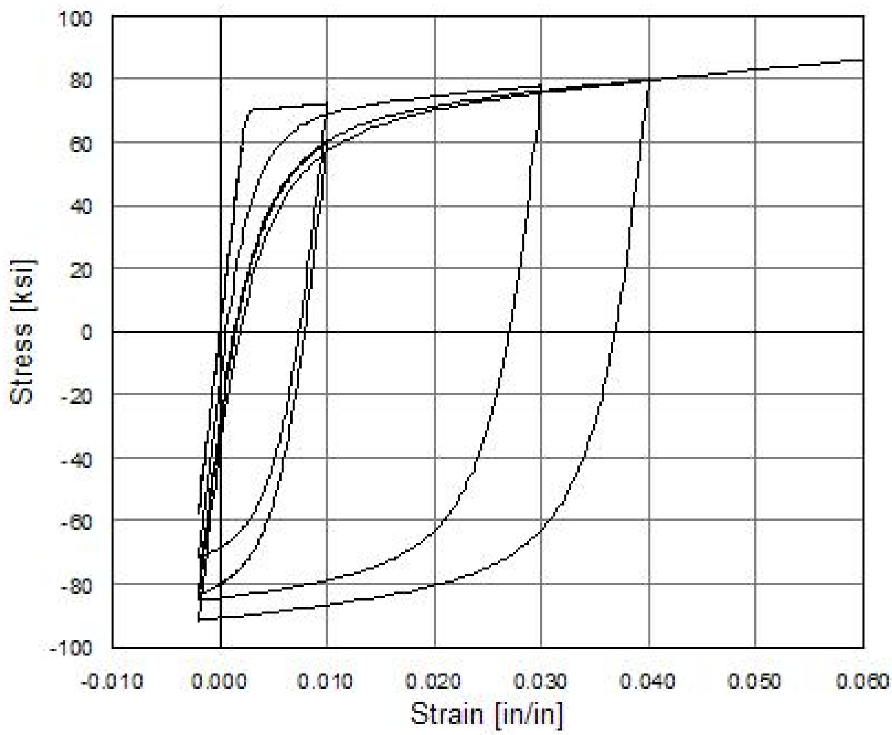

(b)

Figure 2.7. (a) Stress-strain model for concrete04 (Opensees 3.0.3 user command -language manuel), (b) Hysteretic behavior of steel02 model w/o isotropic hardening (Opensees 3.0.3 user command -language manual).

the seismic loads to the columns, slabs are modeled as rigid diaphragms. In addition, in order to examine the second-order effects, the P-Delta effect is taken into consideration in the thesis. Also, the implementation of masses at nodes at each story level is based on the notion that they represent a dead load and a third of the live load (G+0.3Q). Rayleigh damping is used with 5% damping ratio for the first and third modes.

2.4. Ground Motion Selection and Scaling

In this study, fragility functions are created by using multiple stripe analysis (MSA) and cloud analysis to account for epistemic uncertainty. It takes a significant number of ground motion data to obtain a reliable structural response. According to ATC-58 [7] [14] the usage of 11 couples of ground motions is advised for non-linear dynamic analysis. For multiple stripe analysis (MSA), 11 stripe which are made up of 22 pairs of ground motion recordings, are specified in this thesis to illustrate intensity measure levels, Sa(T1), and are used to develop one of the fragility curves for each structure . A code-based target response spectrum is initially established for each IM level in order to choose the ground motion records for each stripe. Next, 22 couples of ground motion recordings are chosen from the PEER Ground Motion Database using each given target response spectrum.

The Disaster and Emergency Management Authority (AFAD) provided four design spectra based on seismic ground motion levels with 43, 72, 475, and 2475 years return periods that took into account the structures' site and soil class. The basic period spectral acceleration values for the four design spectra are then calculated. Figure 2.8 shows four lateral elastic design spectra.

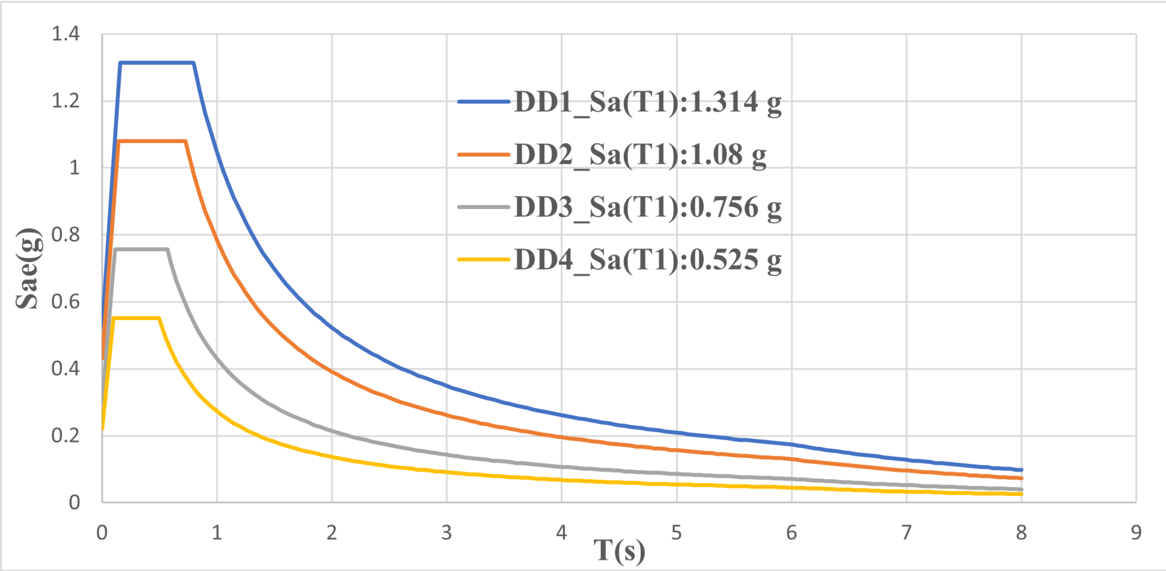

Figure 2.8. 5% damped horizontal elastic design spectra.

11 stripes (IM levels) are created between 0.1 g and 2.90 g with the increments of 0.30 g (0.1 g, 0.25 g, 0.50 g, 0.8 g, 1.10 g, 1.40 g, 1.70 g, 2.00 g, 2.30 g, 2.60 g, and 2.90 g). To select ground motions, a design spectrum for each IM level is created. While creating the 11 design spectra for each IM level, DD1, DD2, DD3, and DD4 earthquake ground motion levels are scaled to obtain eleven IM levels (0.1 g, 0.25 g, 0.50 g, 0.8 g, 1.10 g, 1.40 g, 1.70 g, 2.00 g, 2.30 g, 2.60 g, and 2.90 g). Eleven scaled lateral elastic design spectra are given in Figure 2.9.

With increments of 0.30 g, 11 stripes (IM levels) are produced between 0.1 g and 2.90 g. A design spectrum is made for each IM level in order to choose the ground motions. Earthquake ground motion levels DD1, DD2, DD3, and DD4 are scaled to produce eleven IM levels while developing the 11 design spectra for each IM level. Figure 2.9 presents eleven scaled lateral elastic design spectra.

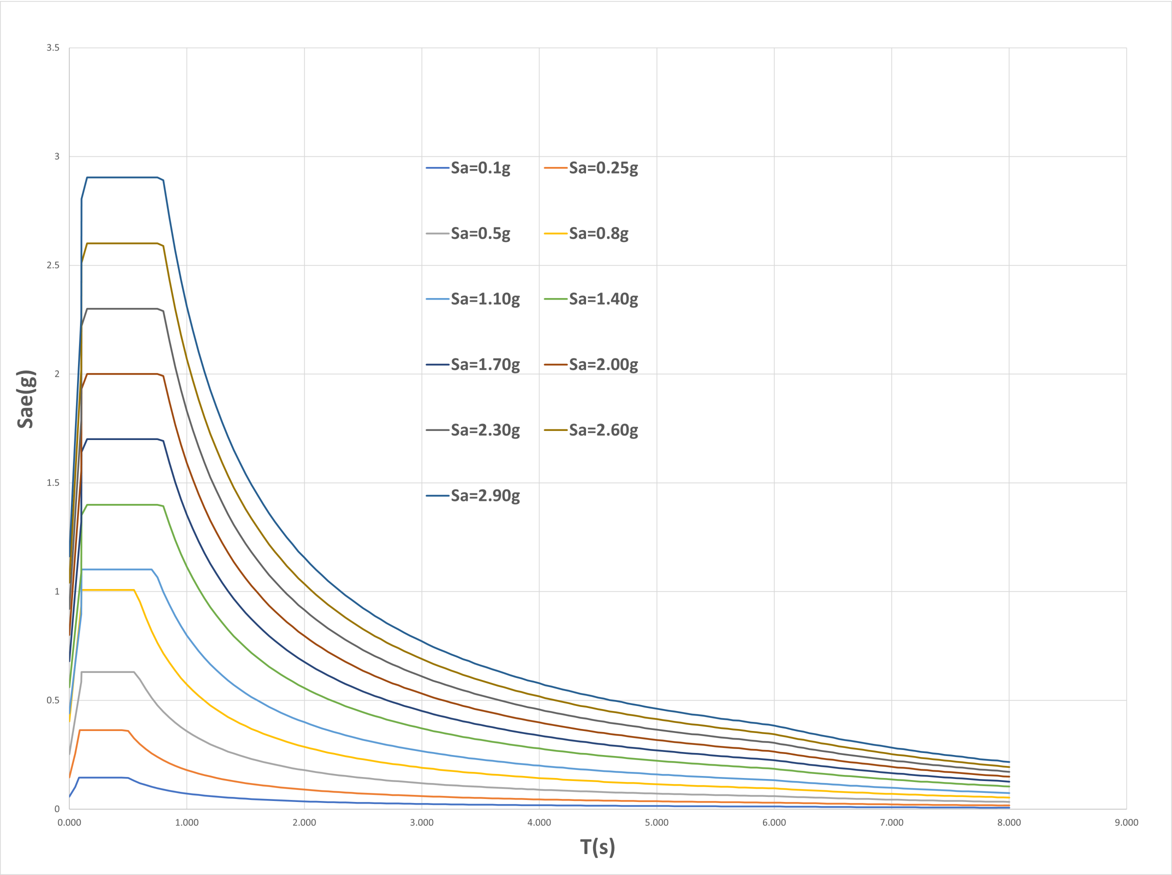

Figure 2.9. Scaled lateral elastic design spectra.

When developing the design spectra for the 11 IM levels, the DD4 spectrum, whose Sa(T1) value is 0.525 g, is scaled to provide the design spectrum for the intensity measure of Sa(T1)=0.1 g, the DD4 spectrum, whose Sa(T1) value is 0.525 g, is scaled to provide the design spectrum for the intensity measure of Sa(T1)=0.25 g, the DD4 spectrum, whose Sa(T1) value is 0.525 g, is scaled to provide the design spectrum for the intensity measure of Sa(T1)=0.50 g, the DD3 spectrum, whose Sa(T1) value is 0.756 g, is scaled to provide the design spectrum for the intensity measure of Sa(T1)=0.80 g, the DD2 spectrum, whose Sa(T1) value is 1.08 g, is scaled to provide the design spectrum for the intensity measure of Sa(T1)=1.10 g, the DD1 spectrum, whose Sa(T1) value is 1.314 g, is scaled to provide the design spectrum for the intensity measure of Sa(T1)=1.40 g,the DD1 spectrum, whose Sa(T1) value is 1.314 g, is scaled to provide the design spectrum for the intensity measure of Sa(T1)=1.70 g, the DD1 spectrum, whose Sa(T1) value is 1.314 g, is scaled to provide the design spectrum for the intensity measure of Sa(T1)=2.00 g, the DD1 spectrum, whose Sa(T1) value is 1.314 g, is scaled to provide the design spectrum for the intensity measure of Sa(T1)=2.30 g, the DD1 spectrum, whose Sa(T1) value is 1.314 g, is scaled to provide the design spectrum for the intensity measure of Sa(T1)=2.60 g, the DD1 spectrum, whose Sa(T1) value is 1.314 g, is scaled to provide the design spectrum for the intensity measure of Sa(T1)=2.90 g.

To account for the directional uncertainty in the perpendicular components of the records, the chosen ground motions are scaled by a ratio of 1.3. Table 2.4 lists an illustration of the search criteria used to choose the ground motions from PEER for assessments of structures. Figure 2.10 provides an illustration of the scaled ground motion spectrum for the third stripe used for the analyses of 3-story building according to the built in TSC 1975.

Regarding the cloud analysis, 44 pairs of records are chosen from the PEER Database with uniform distribution of PGA ranging from 0.1 g to 1.5 g. Figure 2.11 shows the 5% response spectra of the selected 44 pairs of records.

Table 2.4. Ground motion search parameters for 3-story building (TSC 1975).

Fault type	Strike-Slip
Magnitude	6.0 - 8.0
R_{JB} (km)	15 - 300
Vs (m/s)	150 - 260
Spectral Ordinate	Geomean
ScaleFactor	0.8 - 9.0
Scaling Period	0.53

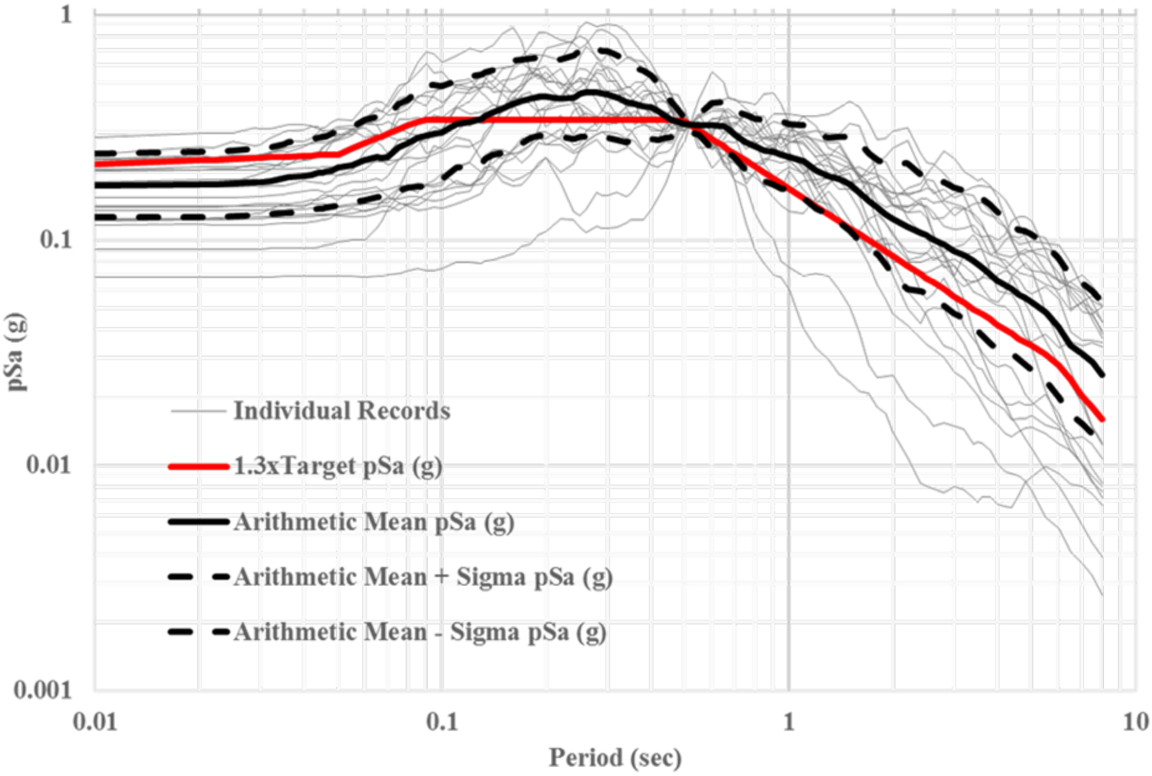

Figure 2.10. Response spectra of the scaled ground motions for the second stripe (Sa=0.25 g) used for the analyses of 3-story building.

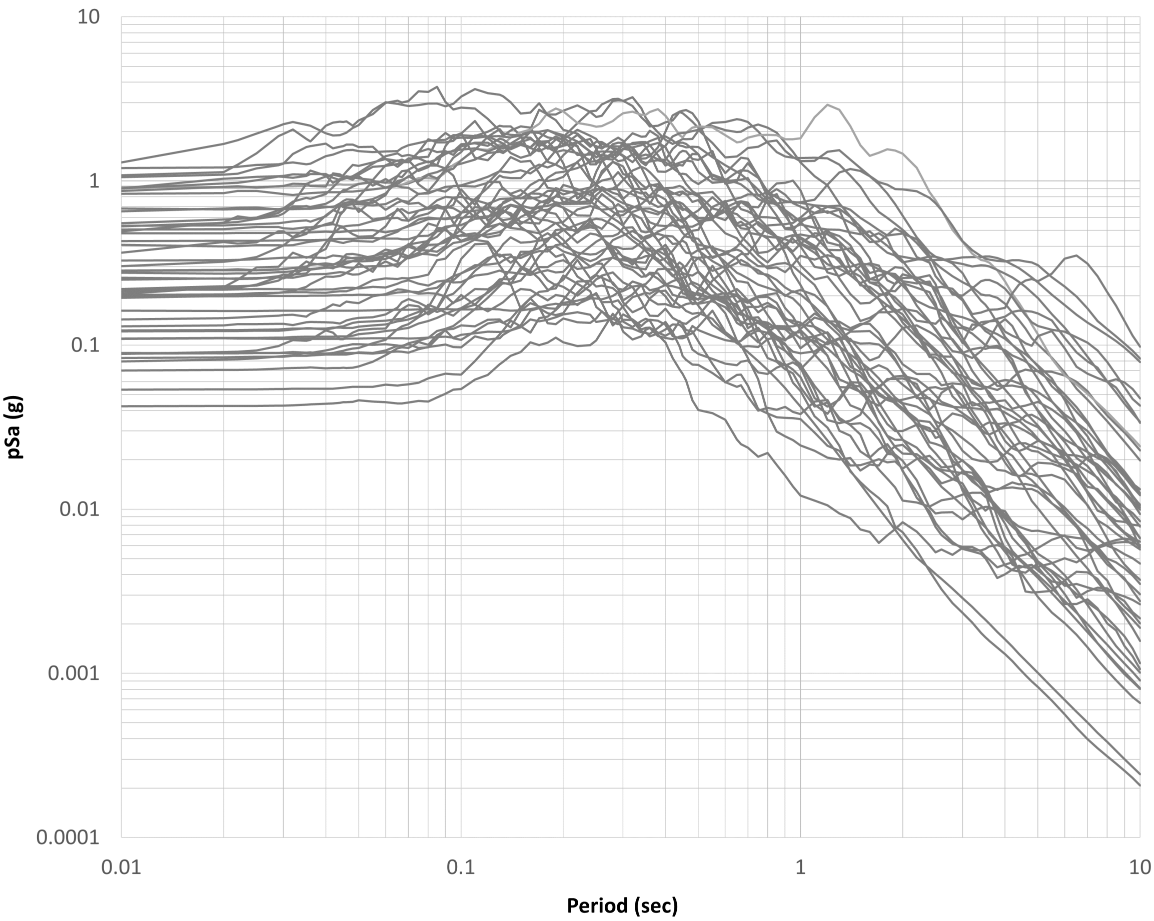

Figure 2.11. Response spectra of the ground motions used for the cloud analyses of 3 and 6-story buildings.

3. DETERMINATION OF DAMAGE STATE LIMITS AND INTENSITY MEASURES

3.1. Determination of the Damage State Limits

We must describe the damage states and their EDP limitations for which the fragility functions are designed in order to establish the fragility functions for the structures. The choice of the intensity measurements and the determination of the damage state limitations are covered in the this section.

For the various performance levels of the structures, the threshold values of damage states must be specified. Engineering demand parameters are used to assess the structural responses to a specific degree of intensity measure (IM). Although there are many different kinds of EDPs, they are categorized into two: global and local EDPs. For local EDPs, end rotation and strain of structural components are employed, whereas maximum inter-story drift ratio (MIDR), permanent deformation, and roof displacement are used for global EDPs. Local EDPs are not time efficient as the number of structures rises. There are four buildings in this study, and several nonlinear dynamic analyses have been done on each one of them. As a result, MIDR and top displacement are chosen as the EDP parameters in this thesis.

By doing a pushover analysis and obtaining a pushover curve for each building, we were able to identify the upper and lower bounds of top displacement. By analyzing the pushover curves and idealizing them, we chose the limit values. The mean of the limit values from all pushover curves is chosen as the limit value for that building type and for that damage state for determining the top displacement limit value for one building type (i.e., 3-story or 6-story) and one damage state. Regarding the MIDR limit values, they are drawn from the Hazus MR4 Technical Manual, which is intended for MRF constructions.

By utilizing the global capacity curve in Equation (3.1), Lagomarsino and Giovinazzi (2006) were able to distinguish between the following four damage states: slight, moderate, extensive, and complete [7]. In Figure 3.1, a pushover curve is shown together with an idealized one.

$$
\begin{aligned}
S_{slight} &= S_{dy} \\
S_{moderate} &= 1.5 \times S_{dy} \\
S_{extensive} &= 1.5 \times (S_{dy} + S_{Sdu}) \\
S_{complete} &= S_{du}
\end{aligned}
\tag{3.1}
$$

The global damage threshold values for MIDR are specified in the Hazus MR4 Technical Manual. According to this document, the load bearing capacity, code class, and building height class are taken into account when determining the MIDR threshold values [15]. In this technical handbook, C1 is used for the structural type such as concrete moment frame while L and M are used for height type such as low-rise and mid-rise.

Table 3.1 lists the global damage threshold values (MIDR) that were derived from the Hazus MR4 Technical Manual for buildings 3-story TSC 2018, 6-story TSC 2018, 3-story TSC 1975, and 6-story TSC 1975, respectively. While, Figures 3.2 and 3.3 provide pushover curves for 3 and 6-story buildings, Figures 3.4 and 3.5 provide capacity curves for 3 and 6-story buildings. The number of stories, the axis of the study, and the seismic design code year are shown in the explanations written over the figures.

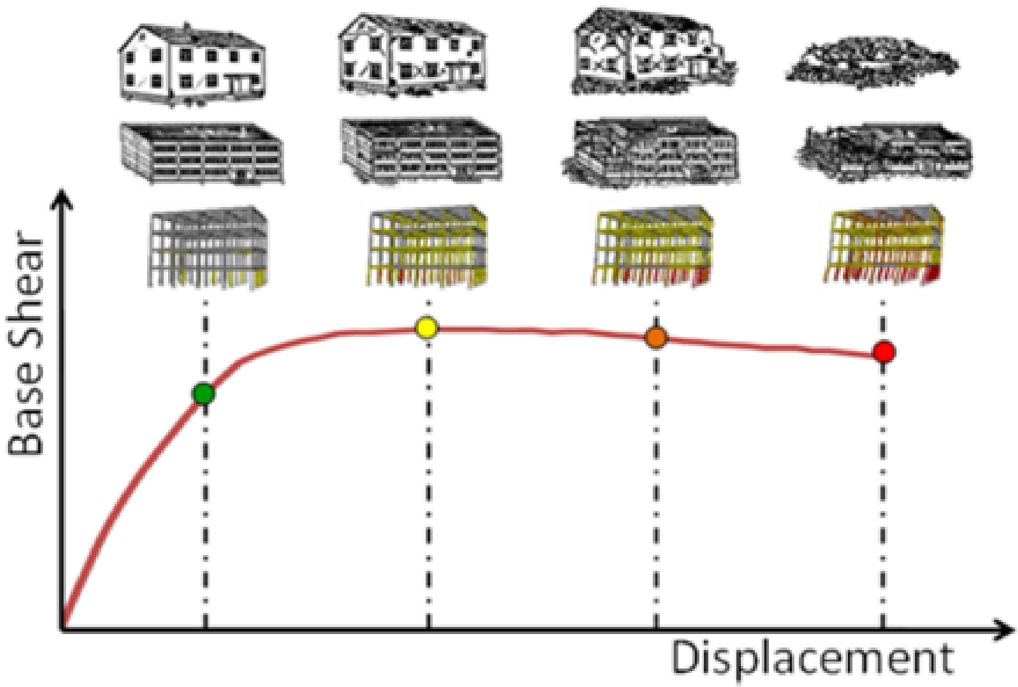

(a)

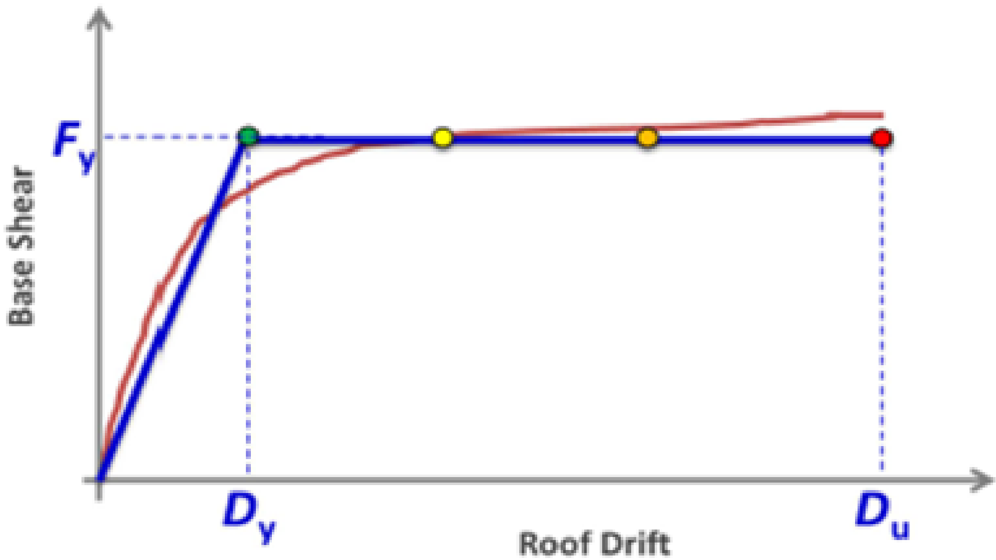

(b)

Figure 3.1. (a) Example of pushover curve and damage thresholds (Source: GEM Technical Report 2014-12 V1.0.0)), (b) Idealized pushover curve. (Source: GEM Technical Report 2014-12 V1.0.0).

Table 3.1. Limit values for the maximum inter-story drift ratio (MIDR)

Building Properties	Interstory Drift at Tresholds of Damage State			
	Slight	Moderate	Extensive	Complete
C1L	0.005	0.01	0.03	0.08
C1M	0.0033	0.0067	0.02	0.0533
C1L	0.005	0.008	0.02	0.05
C1M	0.0033	0.0053	0.0133	0.0333

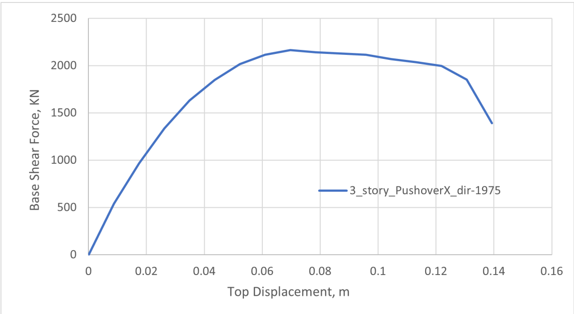

(a) 3-story 1975 in x-direction

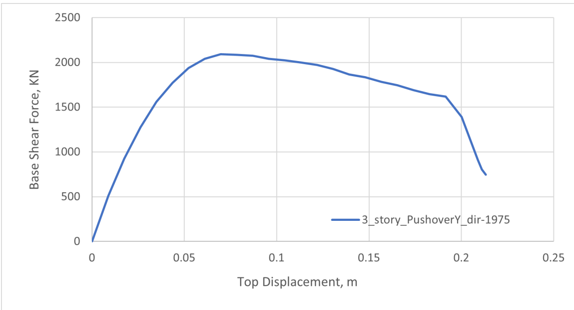

(b) 3-story 1975 in y-direction

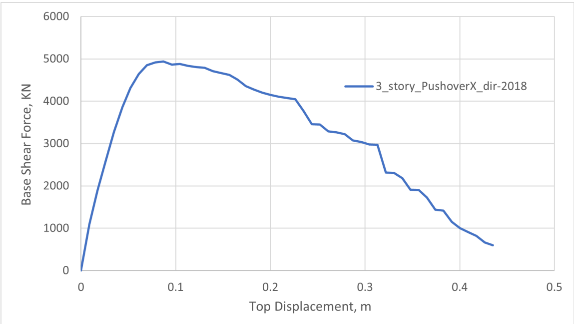

(c) 3-story 2018 in x-direction

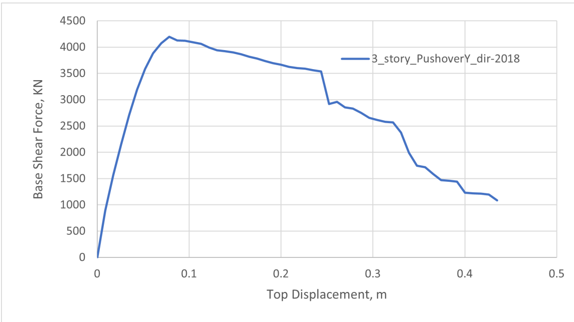

(d) 3-story 2018 in y-direction

Figure 3.2. Pushover curves for 3-story buildings.

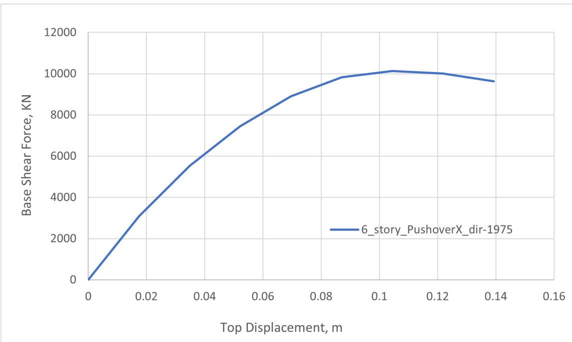

(a) 6-story 1975 in x-direction

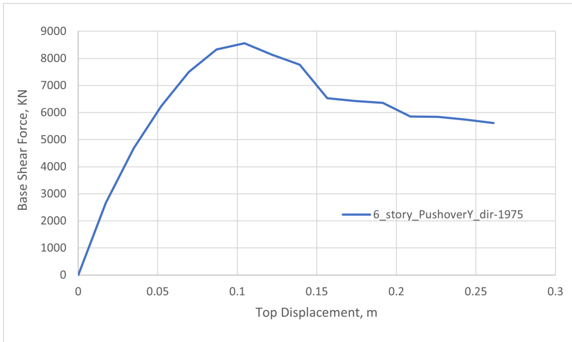

(b) 6-story 1975 in y-direction

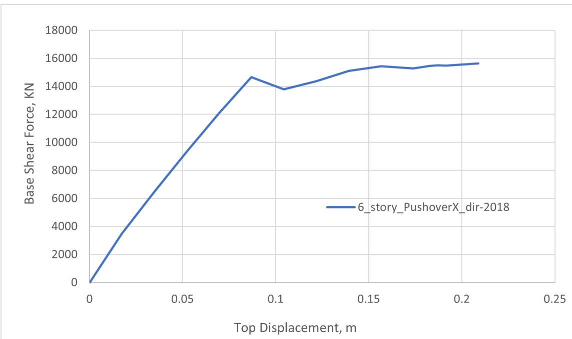

(c) 6-story 2018 in x-direction

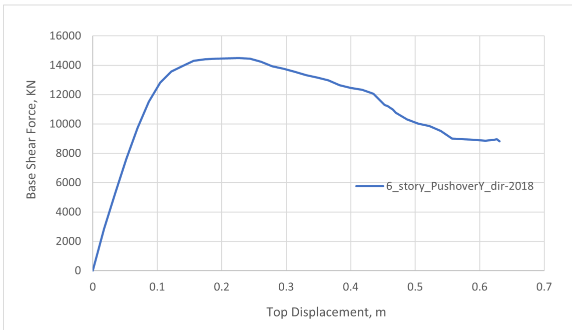

(d) 6-story 2018 in y-direction

Figure 3.3. Pushover curves for 6-story buildings.

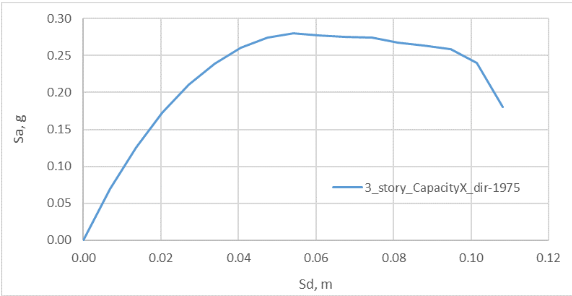

(a) 3-story 1975 in x-direction

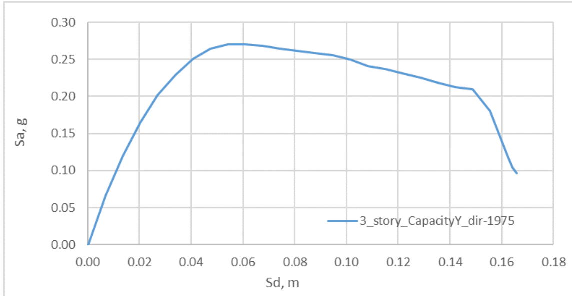

(b) 3-story 1975 in y-direction

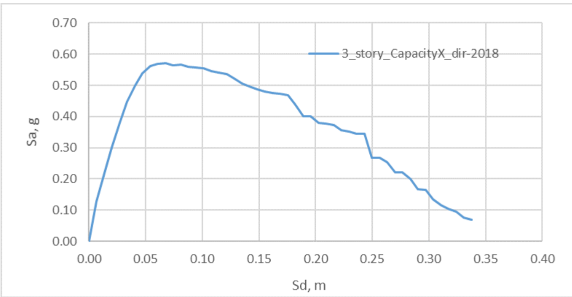

(c) 3-story 2018 in x-direction

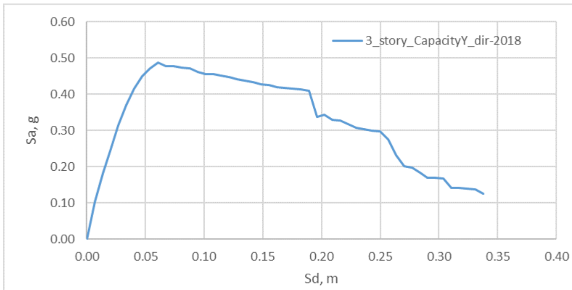

(d) 3-story 2018 in y-direction

Figure 3.4. Capacity curves for 3-story buildings.

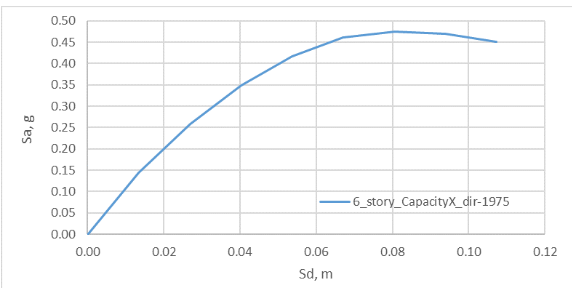

(a) 6-story 1975 in x-direction

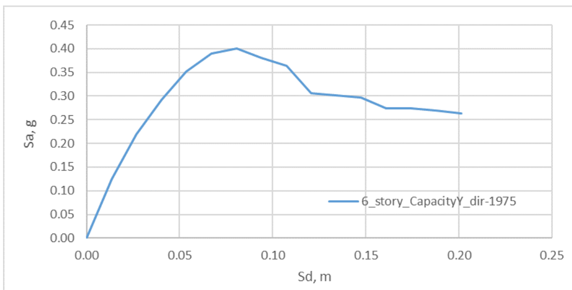

(b) 6-story 1975 in y-direction

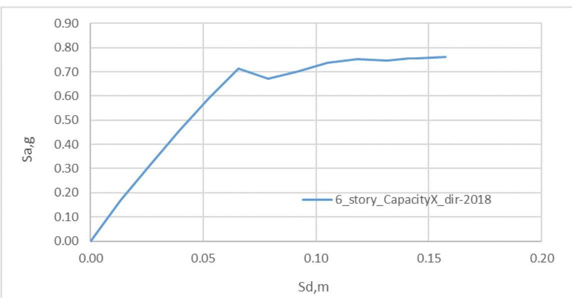

(c) 6-story 2018 in x-direction

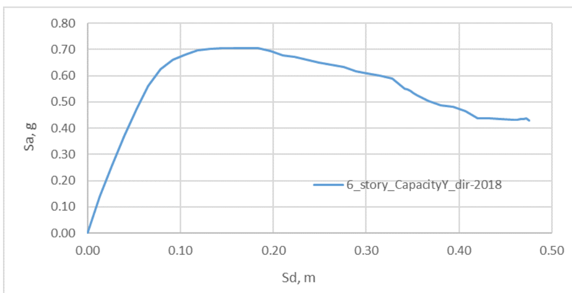

(d) 6-story 2018 in y-direction

Figure 3.5. Capacity curves for 6-story buildings.

3.2. Selection of the Intensity Measures

Experimental and instrumental intensity measures are two separate categories of intensity measurements. Two examples of experimental intensity measurements are the EMS98 scale and the Modified Mercalli Intensity Scale (MMI). The spectral acceleration (Sa), spectral velocity (Sv), spectral displacement (Sd), peak ground acceleration (PGA), peak ground velocity (PGV), peak ground displacement (PGD), and arias intensity (AI) are some examples of the instrumental intensity measurements [6]. Because they provide more precise findings, correctly depict the structure's response, and take ground motion uncertainty into account, instrumental intensity measurements are the most practical and effective intensity measures. When choosing an intensity measure, the type of building and the number of stories are crucial factors.

Since intensity measure (IM) is a crucial fragility criterion, it must be effective and adequate. The chosen intensity measure type should be consistent with the engineering demand parameter type. The response of structures (EDP) should be well associated with intensity measures, and intensity measures should be carefully chosen. For instance, peak ground acceleration (PGA) and EDPs for low-rise and brittle structures are closely associated, but spectral displacement (Sd) and spectral acceleration (Sa) are closely related to the response of ductile structures. Period independent intensity measurements (i.e., PGA) are more effective to utilize when the number of buildings to be evaluated rises [6]. Buildings in this research are ductile, low and mid-rise, and the major vibration periods are those of the first mode. As a result, the intensity measurements are based on spectral displacements and spectral accelerations at the initial natural vibration periods. Additionally, pga is used as IM parameter to see its effects on the fragility functions.

4. DEVELOPMENT OF FRAGILITY CURVES

The likelihood of going beyond a specific damage state versus various intensity measure (IM) levels is provided by fragility functions. The statistical technique of maximum likelihood estimation and simple logarithmic regression are employed in this study to create fragility curves from the findings of nonlinear dynamic analyses. Numerous nonlinear dynamic analyses are conducted in this study, and the results are compiled to produce the fragility curves. Different methods can be used for nonlinear dynamic analysis. The two most often used analysis methods for creating fragility functions are multiple stripe analysis (MSA) and incremental dynamic analysis (IDA).

In order to determine the response for the incremental dynamic analysis (IDA) presented by Vamvatsikos and Cornel (2002), a set of ground motion records are increased incrementally up until the structure approaches the dynamic instability. From there, the intensity measure level that correlates to the damage level is generated [16]. The content of the ground motions is corrupted by the technique's use of unrealistically high scaling factors, which is one of its main drawbacks. However, the structural response is determined for several sets of ground motions that are chosen to reflect a certain degree of intensity measure for the MSA. Instead of scaling identical set of ground motion data repeatedly, separate sets of ground motion records are utilized for various intensity metrics. Analysts have the opportunity to restrict the scale factors of ground motion records so as to prevent the content of such records from being tainted since different sets of ground motion can be utilized for various IM levels. Additionally, the uncertainty brought on by record-to-record variability is compensated for to some extent since alternative sets of ground motions can be employed.

4.1. Multiple Stripe Analysis of the Buildings

Based on the IM parameters of Sa(T1), Sa(T1) and PGA eleven IM levels (stripes) are created, and 22 couples of records are employed for the nonlinear dynamic analyses for every stripe.

The relevant ground motion pairings are applied to the structure for each type of structure and each IM level (stripe), and the associated EDP (MIDR and Dtop) values are stored. The results of MSA for different IM parameters (Sa, Sd and PGA) and the EDPs (MIDR and Dtop) are given in Figures 4.1 to 4.18 which are developed in MATLAB [17]. Also, the damage state limits in terms of the selected EDP are shown in these figures with vertical red dotted lines. The number of EDP values exceeding the limit values can easily be seen in the figures.

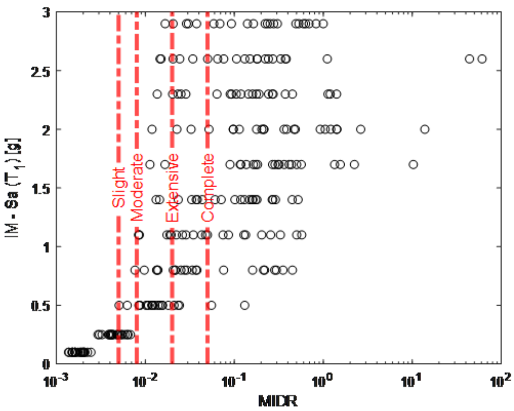

(a) 3-story 1975 in x-direction

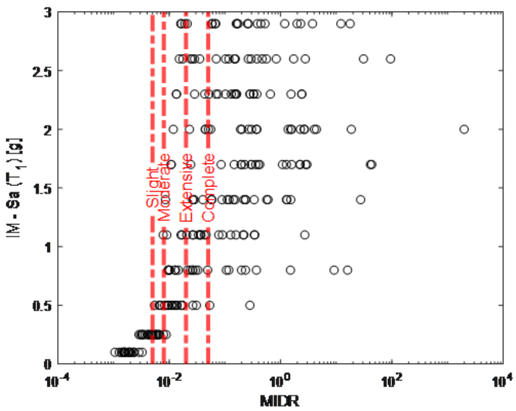

(b) 3-story 1975 in y-direction

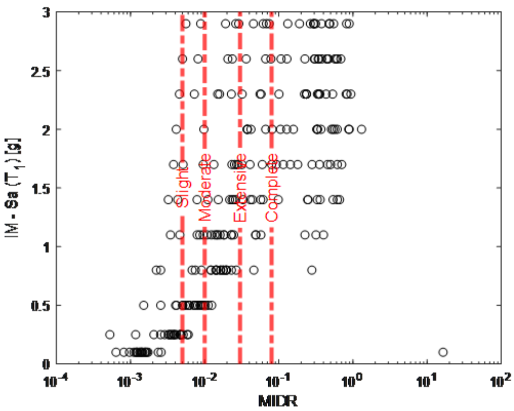

(c) 3-story 2018 in x-direction

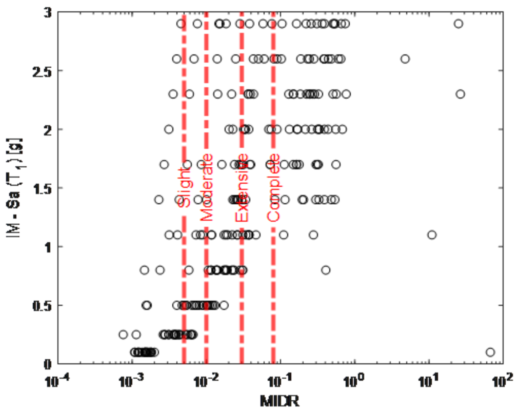

(d) 3-story 2018 in y-direction

Figure 4.1. Results of MSA for 3-story buildings, IM(Sa)-EDP(MIDR). The black circles show the MIDR values obtained from nonlinear dynamic analyses, and the vertical red dashed lines denote slight, moderate, extensive and complete damage state thresholds from left to the right, respectively.

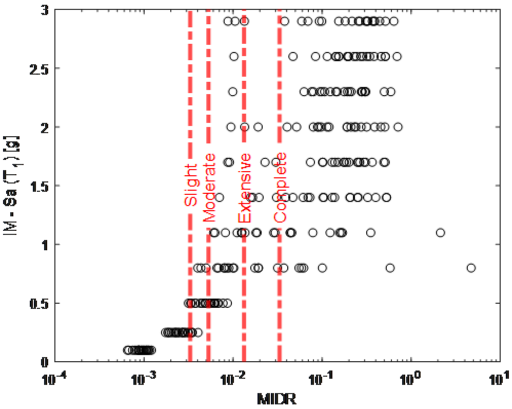

(a) 6-story 1975 in x-direction

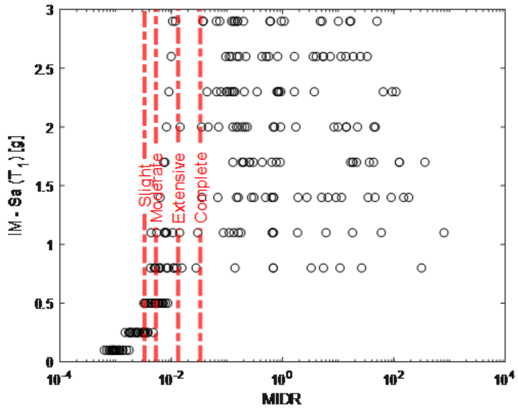

(b) 6-story 1975 in y-direction

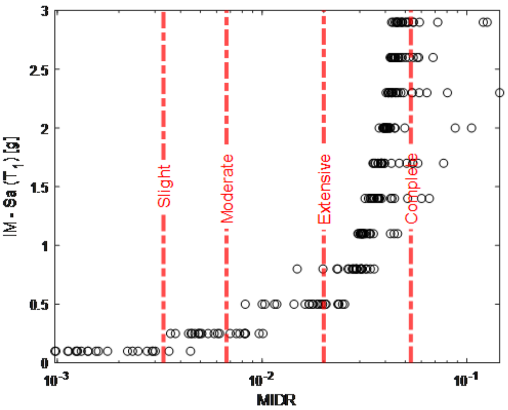

(c) 6-story 2018 in x-direction

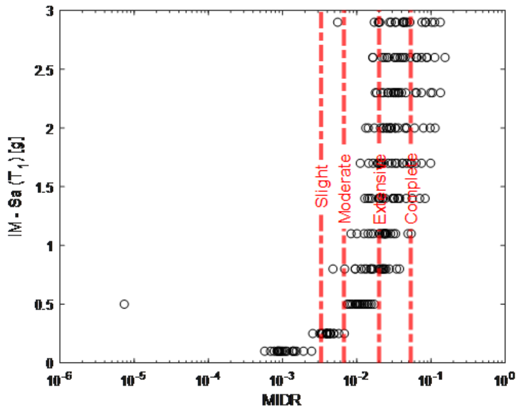

(d) 6-story 2018 in y-direction

Figure 4.2. Results of MSA for 6-story buildings, IM(Sa)-EDP(MIDR). The black circles show the MIDR values obtained from nonlinear dynamic analyses, and the vertical red dashed lines denote slight, moderate, extensive and complete damage state thresholds from left to the right, respectively.

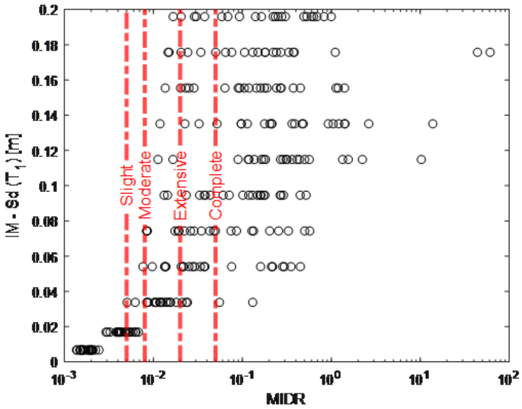

(a) 3-story 1975 in x-direction

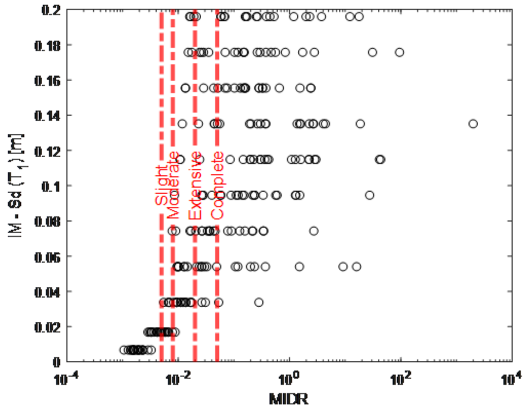

(b) 3-story 1975 in y-direction

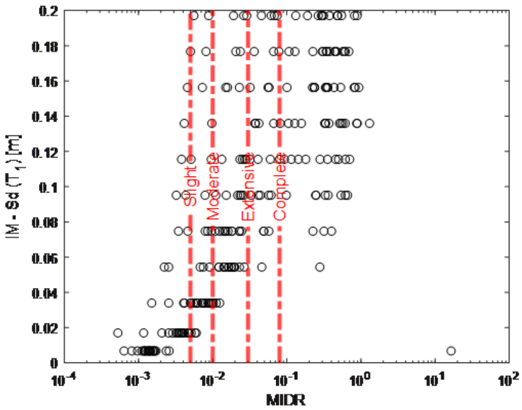

(c) 3-story 2018 in x-direction

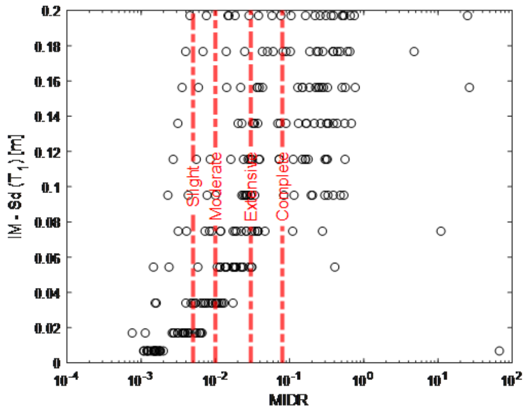

(d) 3-story 2018 in y-direction

Figure 4.3. Results of MSA for 3-story buildings, IM(Sd)-EDP(MIDR). The black circles show the MIDR values obtained from nonlinear dynamic analyses, and the vertical red dashed lines denote slight, moderate, extensive and complete damage state thresholds from left to the right, respectively.

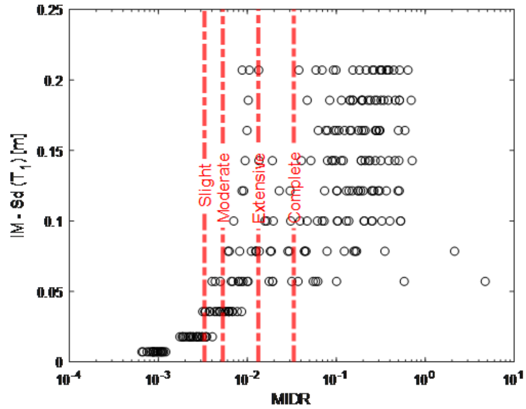

(a) 6-story 1975 in x-direction

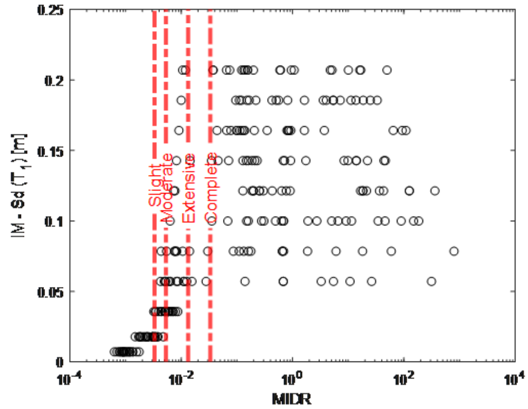

(b) 6-story 1975 in y-direction

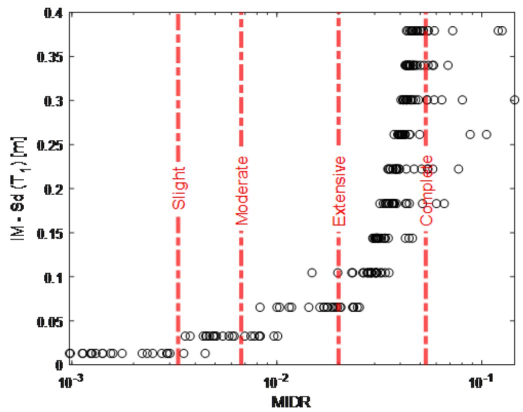

(c) 6-story 2018 in x-direction

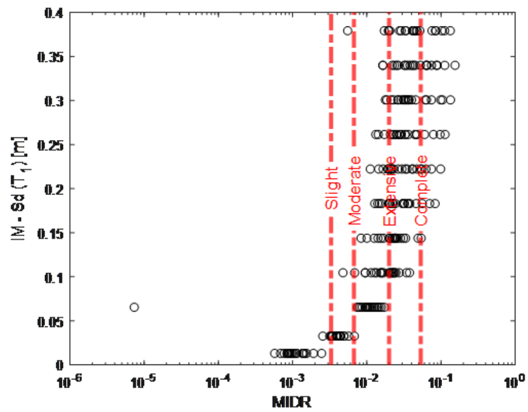

(d) 6-story 2018 in y-direction

Figure 4.4. Results of MSA for 6-story buildings, IM(Sd)-EDP(MIDR). The black circles show the MIDR values obtained from nonlinear dynamic analyses, and the vertical red dashed lines denote slight, moderate, extensive and complete damage state thresholds from left to the right, respectively.

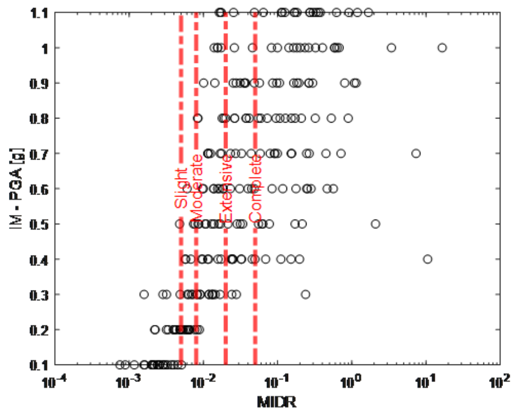

(a) 3-story 1975 in x-direction

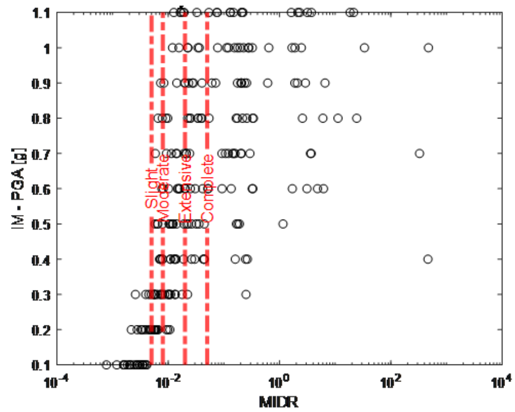

(b) 3-story 1975 in y-direction

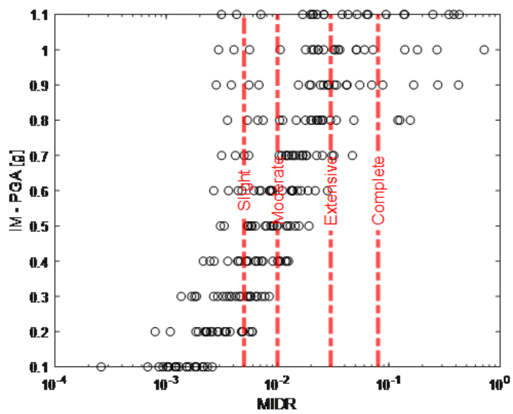

(c) 3-story 2018 in x-direction

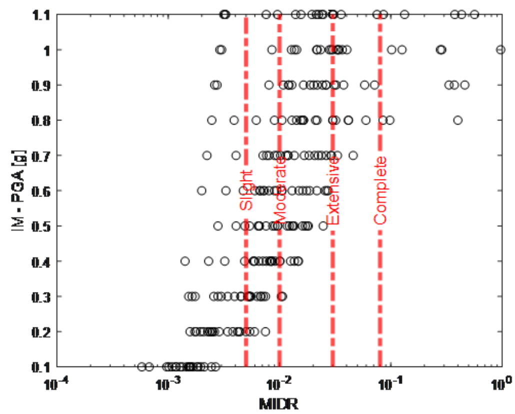

(d) 3-story 2018 in y-direction

Figure 4.5. Results of MSA for 3-story buildings, IM(PGA)-EDP(MIDR). The black circles show the MIDR values obtained from nonlinear dynamic analyses, and the vertical red dashed lines denote slight, moderate, extensive and complete damage state thresholds from left to the right, respectively.

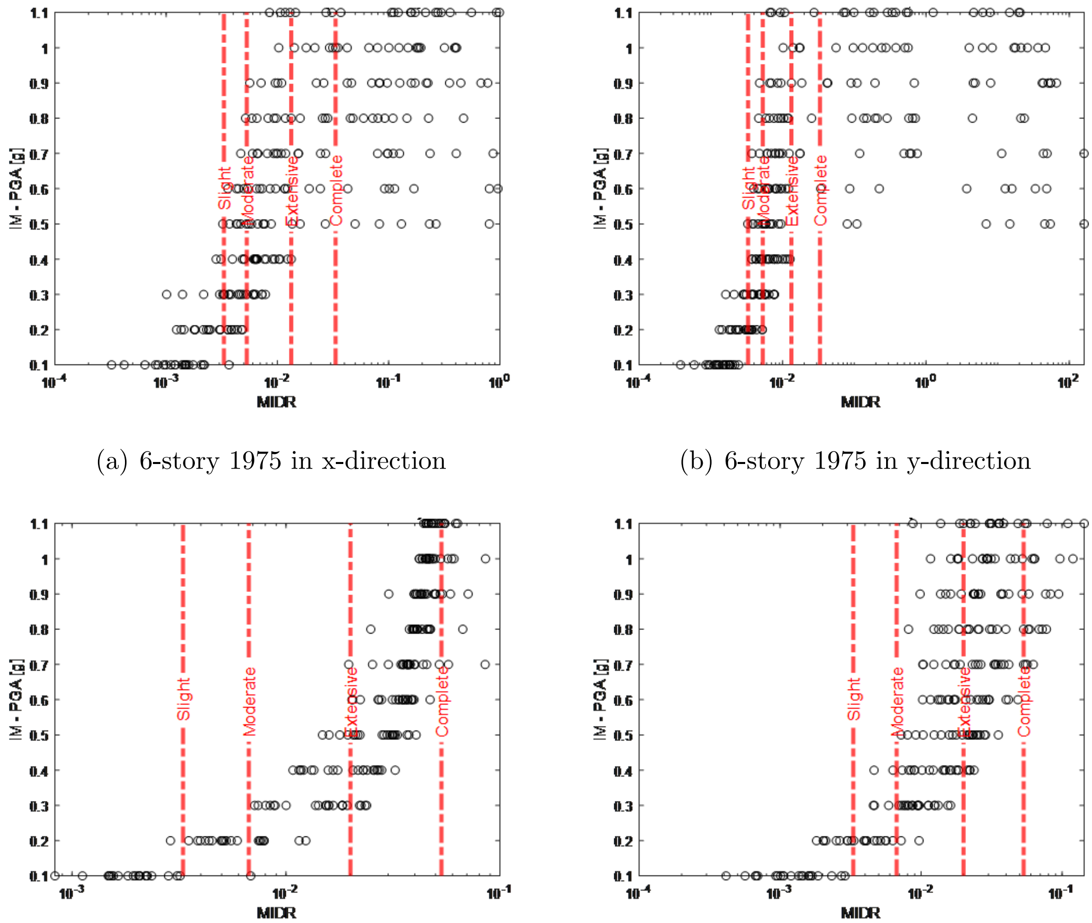

(a) 6-story 1975 in x-direction

(b) 6-story 1975 in y-direction

(c) 6-story 2018 in x-direction

(d) 6-story 2018 in y-direction

Figure 4.6. Results of MSA for 6-story buildings, IM(PGA)-EDP(MIDR). The black circles show the MIDR values obtained from nonlinear dynamic analyses, and the vertical red dashed lines denote slight, moderate, extensive and complete damage state thresholds from left to the right, respectively.

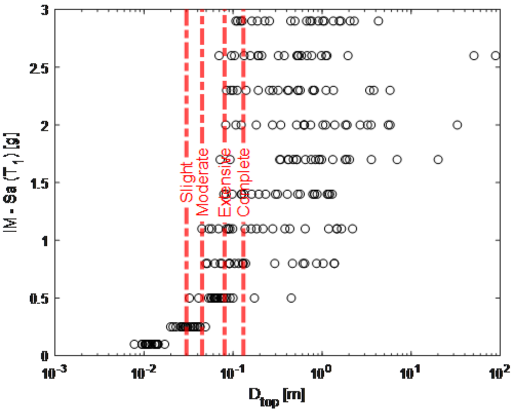

(a) 3-story 1975 in x-direction

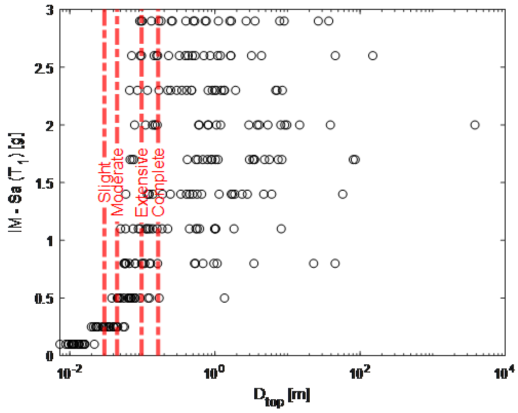

(b) 3-story 1975 in y-direction

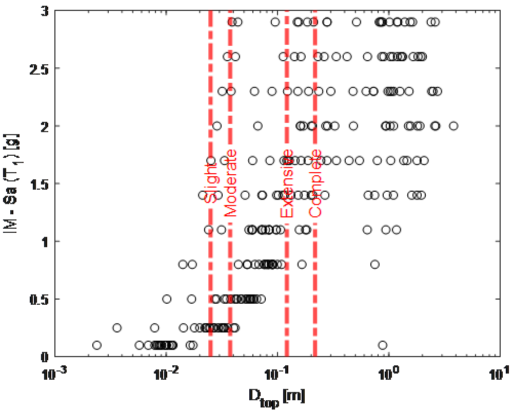

(c) 3-story 2018 in x-direction

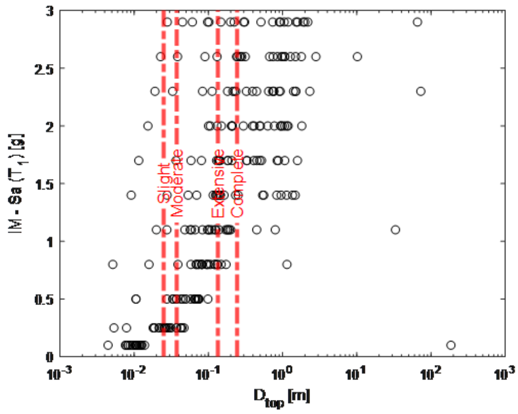

(d) 3-story 2018 in y-direction

Figure 4.7. Results of MSA for 3-story buildings, IM(Sa)-EDP(Dtop). The black circles show the Dtop values obtained from nonlinear dynamic analyses, and the vertical red dashed lines denote slight, moderate, extensive and complete damage state thresholds from left to the right, respectively.

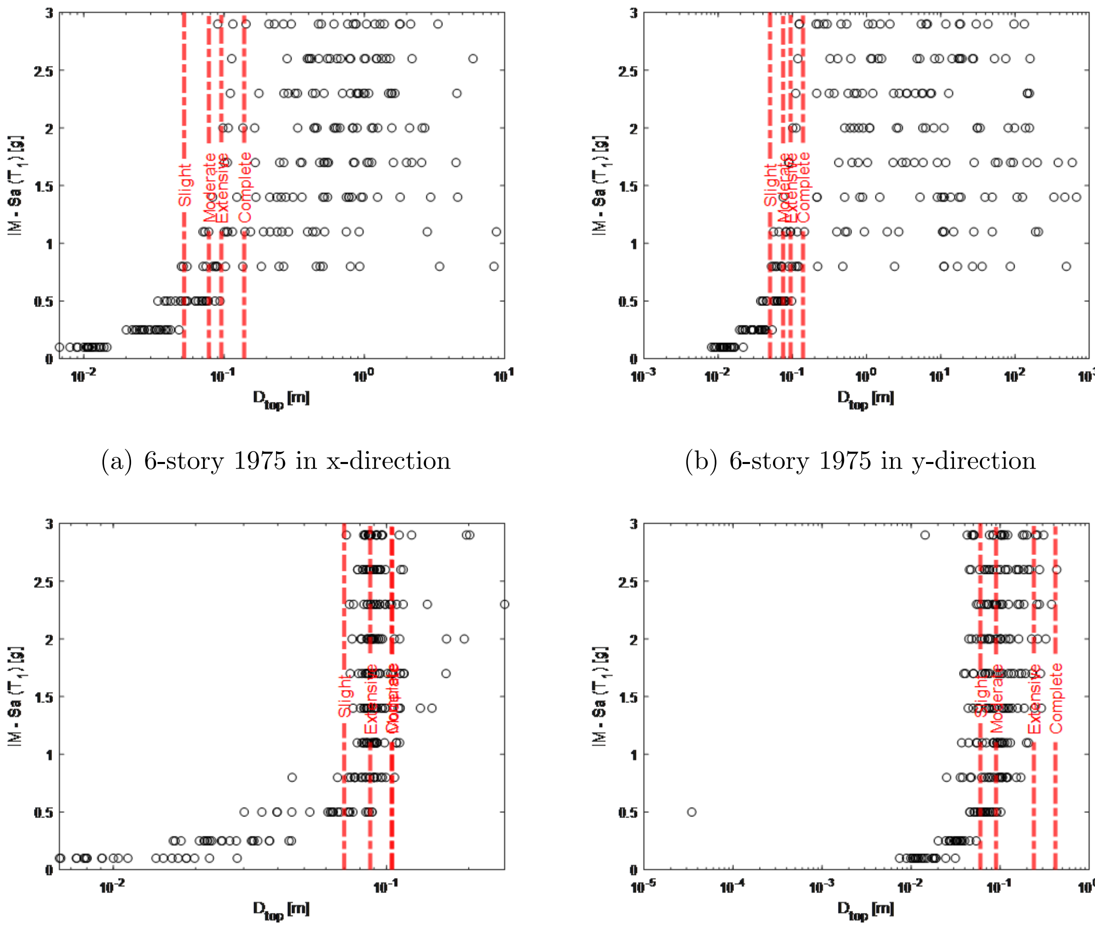

(a) 6-story 1975 in x-direction

(b) 6-story 1975 in y-direction

(c) 6-story 2018 in x-direction

(d) 6-story 2018 in y-direction

Figure 4.8. Results of MSA for 6-story buildings, IM(Sa)-EDP(Dtop). The black circles show the Dtop values obtained from nonlinear dynamic analyses, and the vertical red dashed lines denote slight, moderate, extensive and complete damage state thresholds from left to the right, respectively.

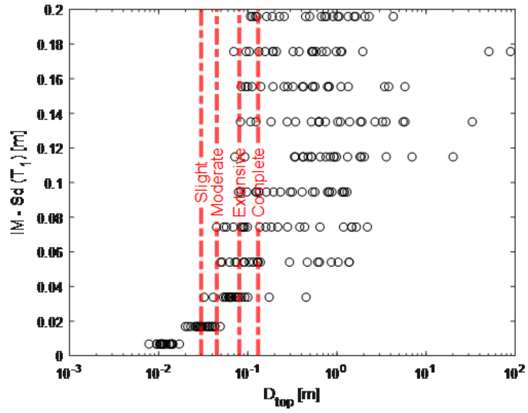

(a) 3-story 1975 in x-direction

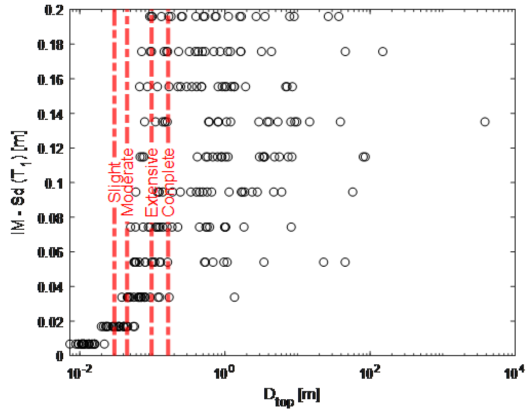

(b) 3-story 1975 in y-direction

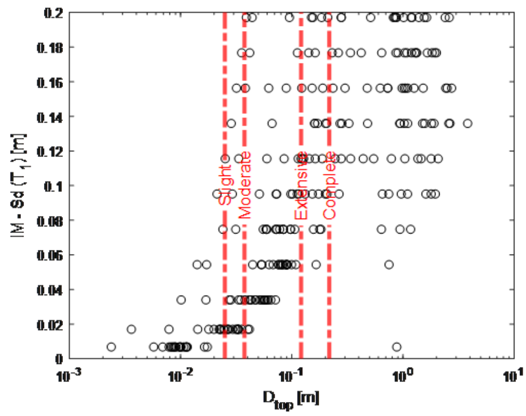

(c) 3-story 2018 in x-direction

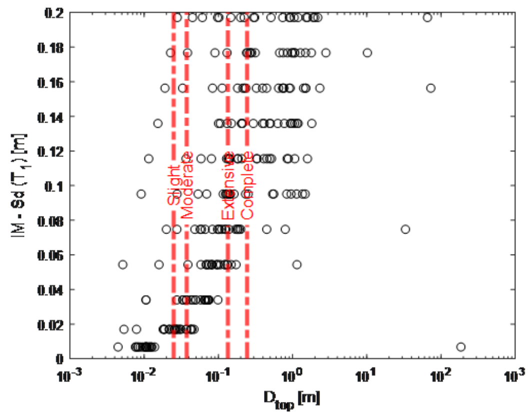

(d) 3-story 2018 in y-direction

Figure 4.9. Results of MSA for 3-story buildings, IM(Sd)-EDP(Dtop). The black circles show the Dtop values obtained from nonlinear dynamic analyses, and the vertical red dashed lines denote slight, moderate, extensive and complete damage state thresholds from left to the right, respectively.

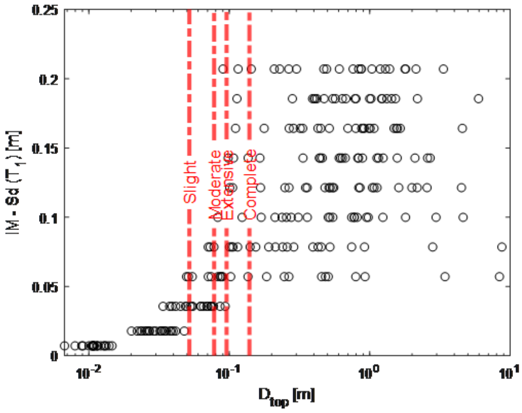

(a) 6-story 1975 in x-direction

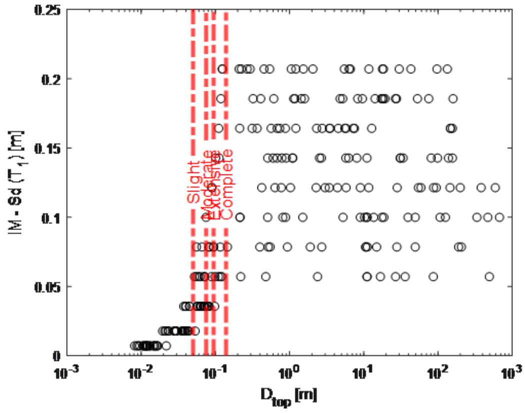

(b) 6-story 1975 in y-direction

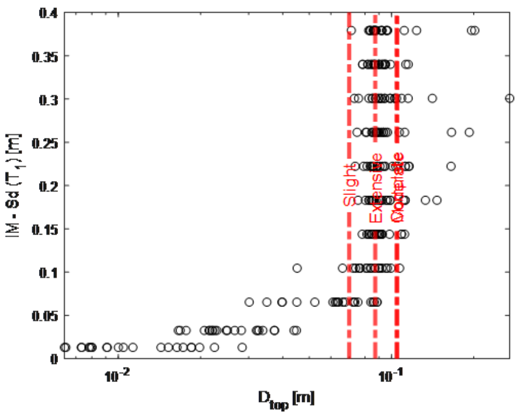

(c) 6-story 2018 in x-direction

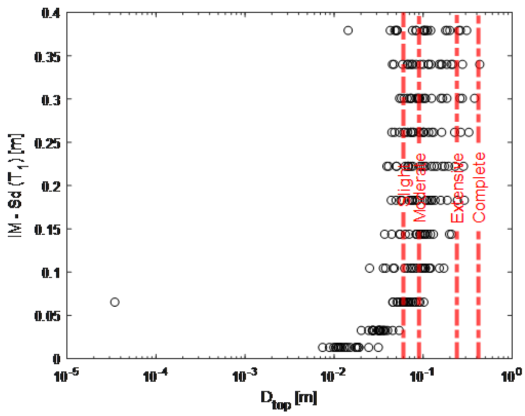

(d) 6-story 2018 in y-direction

Figure 4.10. Results of MSA for 6-story buildings, IM(Sd)-EDP(Dtop). The black circles show the Dtop values obtained from nonlinear dynamic analyses, and the vertical red dashed lines denote slight, moderate, extensive and complete damage state thresholds from left to the right, respectively.

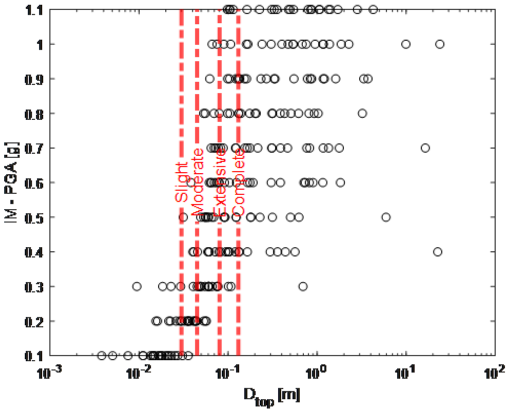

(a) 3-story 1975 in x-direction

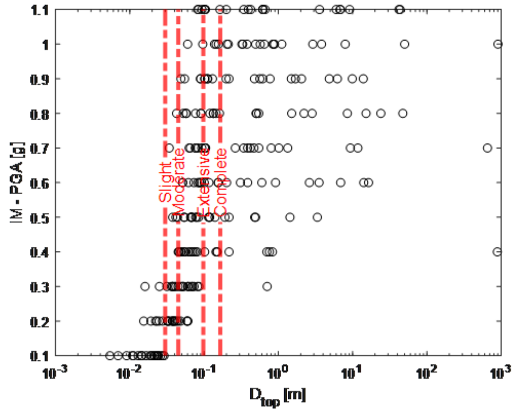

(b) 3-story 1975 in y-direction

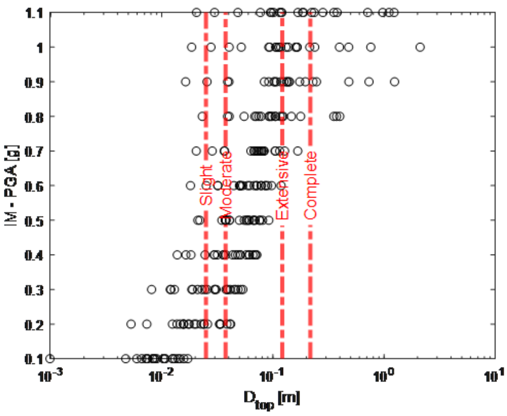

(c) 3-story 2018 in x-direction

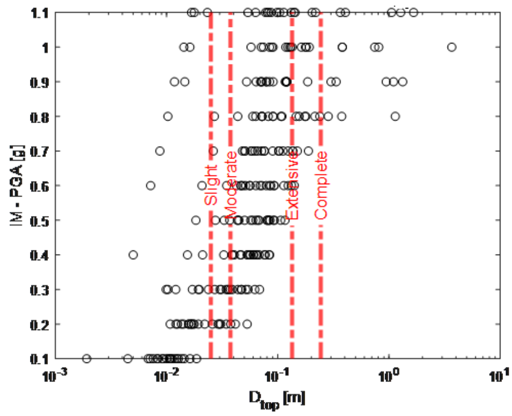

(d) 3-story 2018 in y-direction

Figure 4.11. Results of MSA for 3-story buildings designed per TSC 2018, IM(PGA)-EDP(Dtop). The black circles show the Dtop values obtained from nonlinear dynamic analyses, and the vertical red dashed lines denote slight, moderate, extensive and complete damage state thresholds from left to the right, respectively.

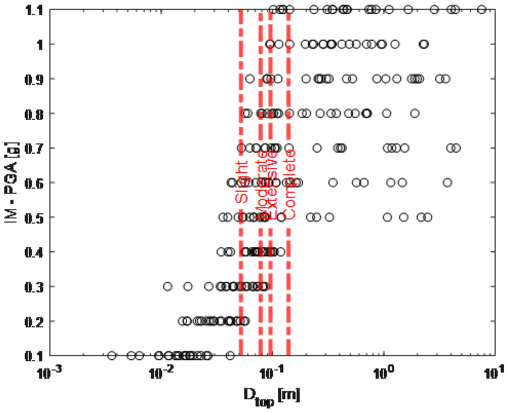

(a) 6-story 1975 in x-direction

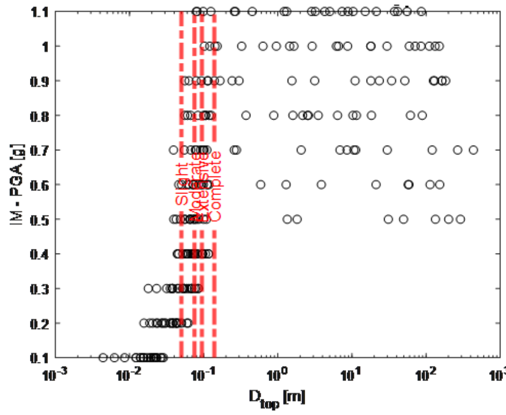

(b) 6-story 1975 in y-direction

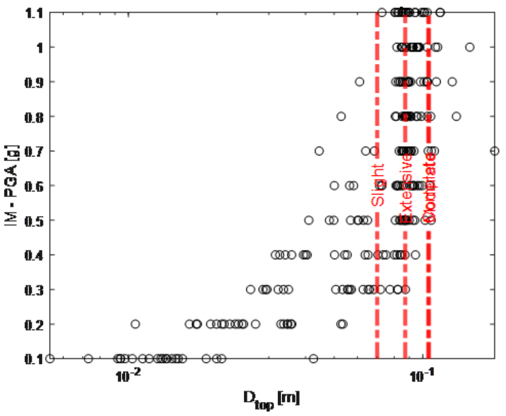

(c) 6-story 2018 in x-direction

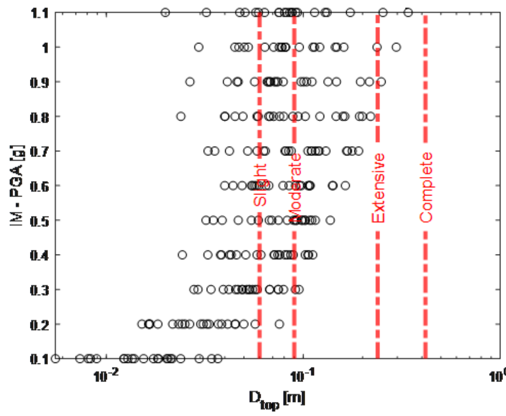

(d) 6-story 2018 in y-direction

Figure 4.12. Results of MSA for 6-story buildings, IM(PGA)-EDP(Dtop). The black circles show the Dtop values obtained from nonlinear dynamic analyses, and the vertical red dashed lines denote slight, moderate, extensive and complete damage state thresholds from left to the right, respectively.

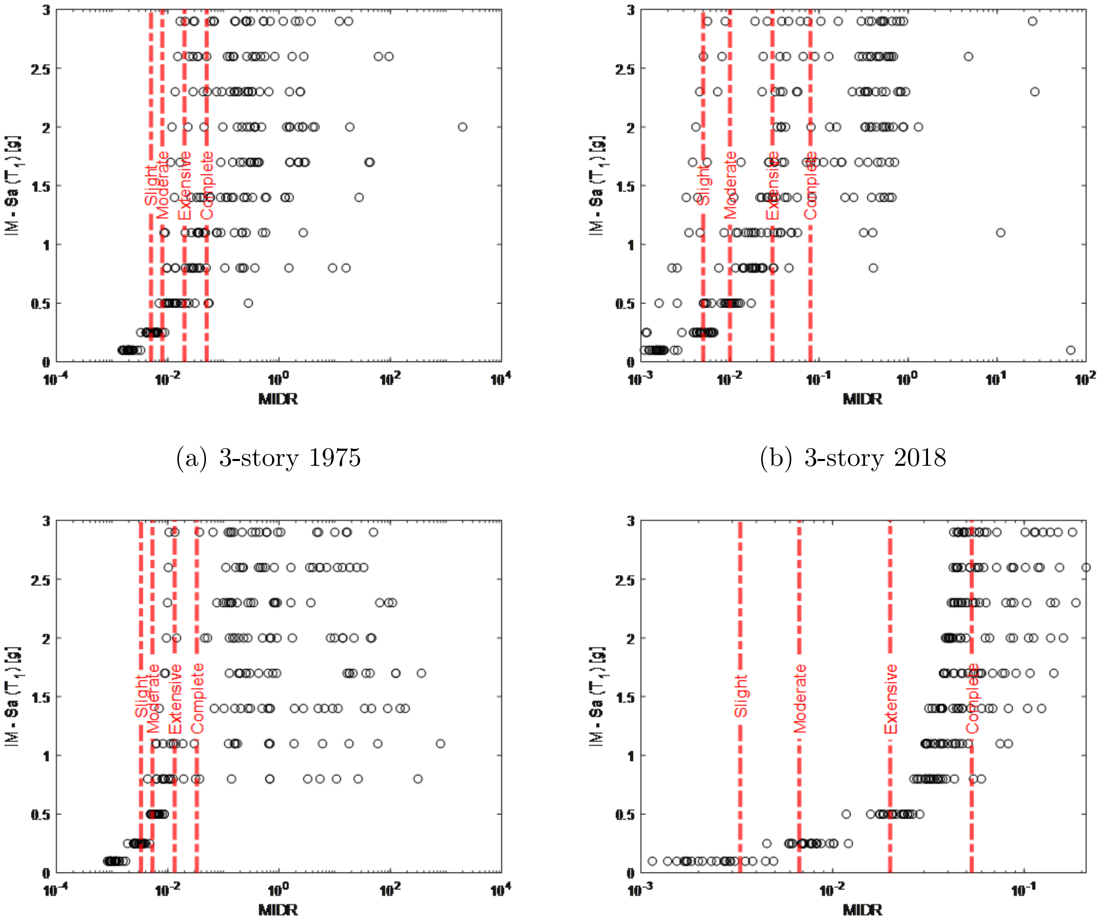

(a) 3-story 1975

(b) 3-story 2018

(c) 6-story 1975

(d) 6-story 2018

Figure 4.13. Direction-free results of MSA for all buildings, IM(Sa)-EDP(MIDR). The black circles show the MIDR values obtained from nonlinear dynamic analyses, and the vertical red dashed lines denote slight, moderate, extensive and complete damage state thresholds from left to the right, respectively.

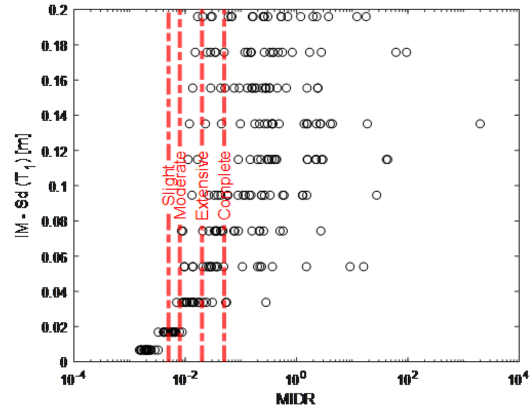

(a) 3-story 1975

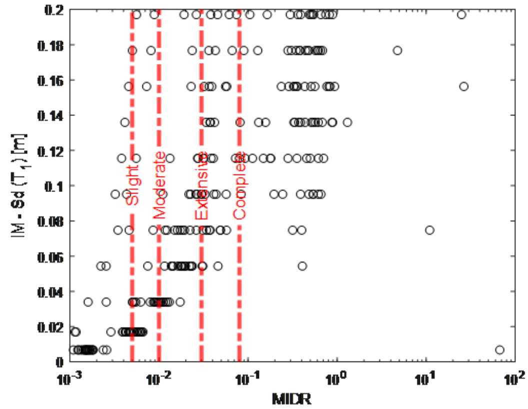

(b) 3-story 2018

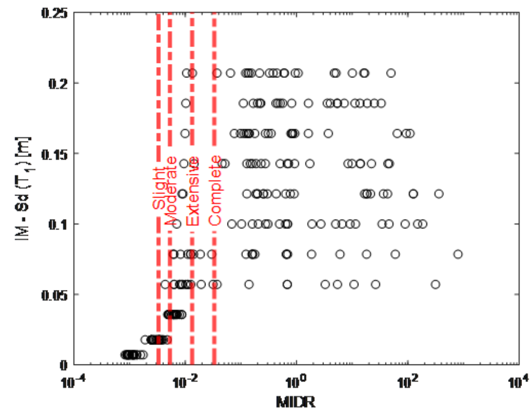

(c) 6-story 1975

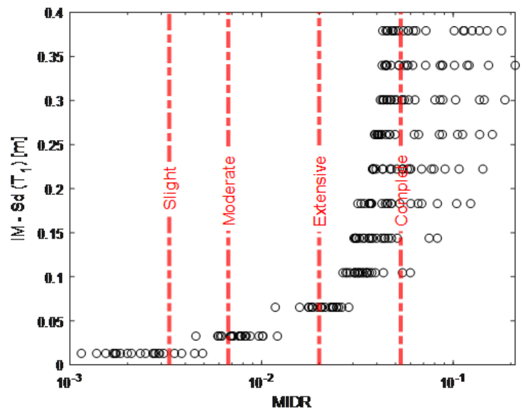

(d) 6-story 2018

Figure 4.14. Direction-free results of MSA for all buildings, IM(Sd)-EDP(MIDR). The black circles show the MIDR values obtained from nonlinear dynamic analyses, and the vertical red dashed lines denote slight, moderate, extensive and complete damage state thresholds from left to the right, respectively.

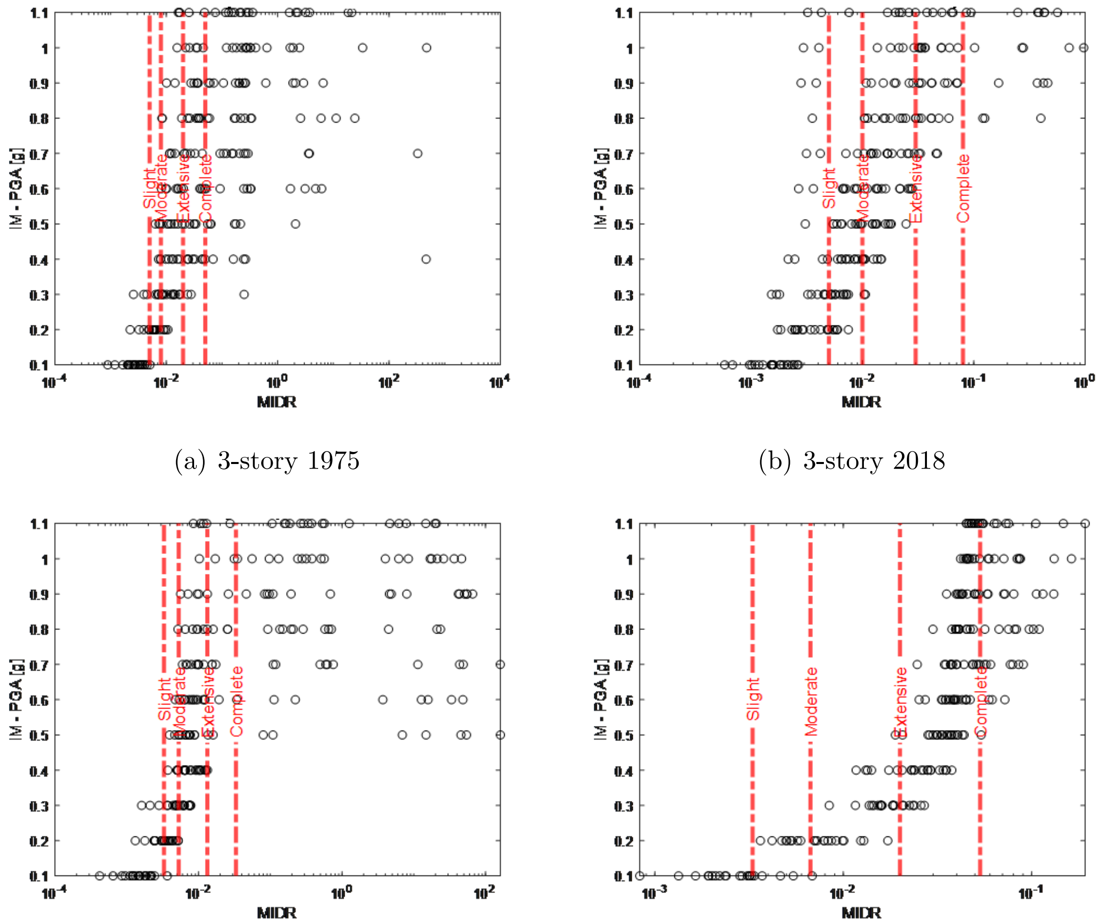

(a) 3-story 1975

(b) 3-story 2018

(c) 6-story 1975

(d) 6-story 2018

Figure 4.15. Direction-free results of MSA for all buildings, IM(PGA)-EDP(MIDR). The black circles show the MIDR values obtained from nonlinear dynamic analyses, and the vertical red dashed lines denote slight, moderate, extensive and complete damage state thresholds from left to the right, respectively.

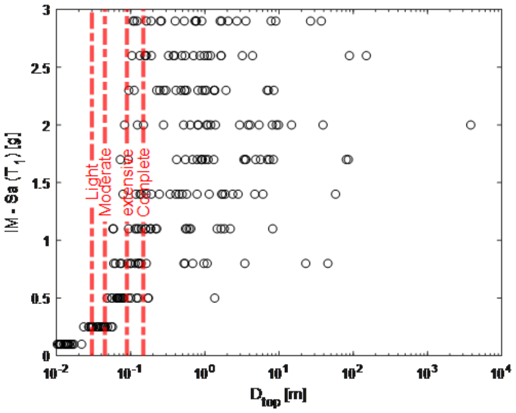

(a) 3-story 1975

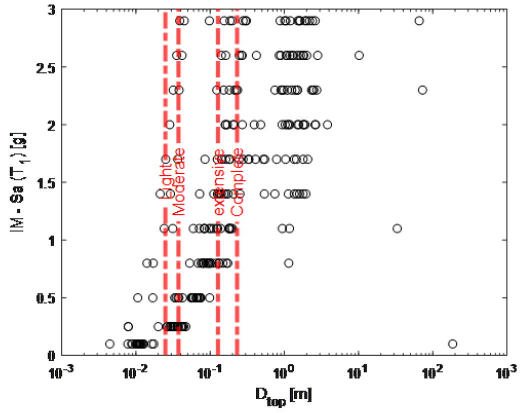

(b) 3-story 2018

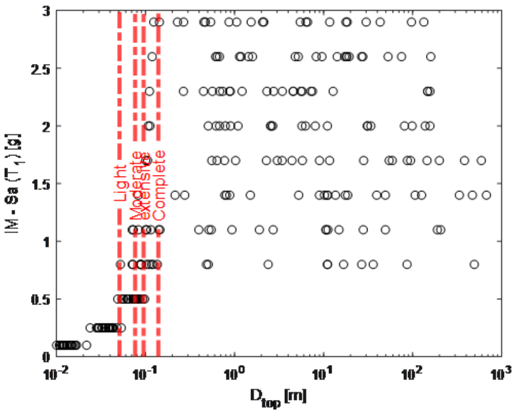

(c) 6-story 1975

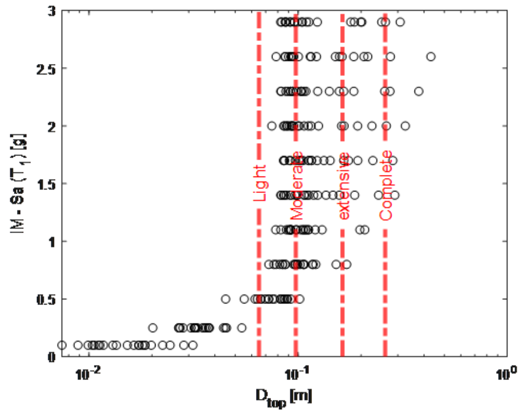

(d) 6-story 2018

Figure 4.16. Direction-free results of MSA for all buildings, IM(Sa)-EDP(Dtop). The black circles show the Dtop values obtained from nonlinear dynamic analyses, and the vertical red dashed lines denote slight, moderate, extensive and complete damage state thresholds from left to the right, respectively.

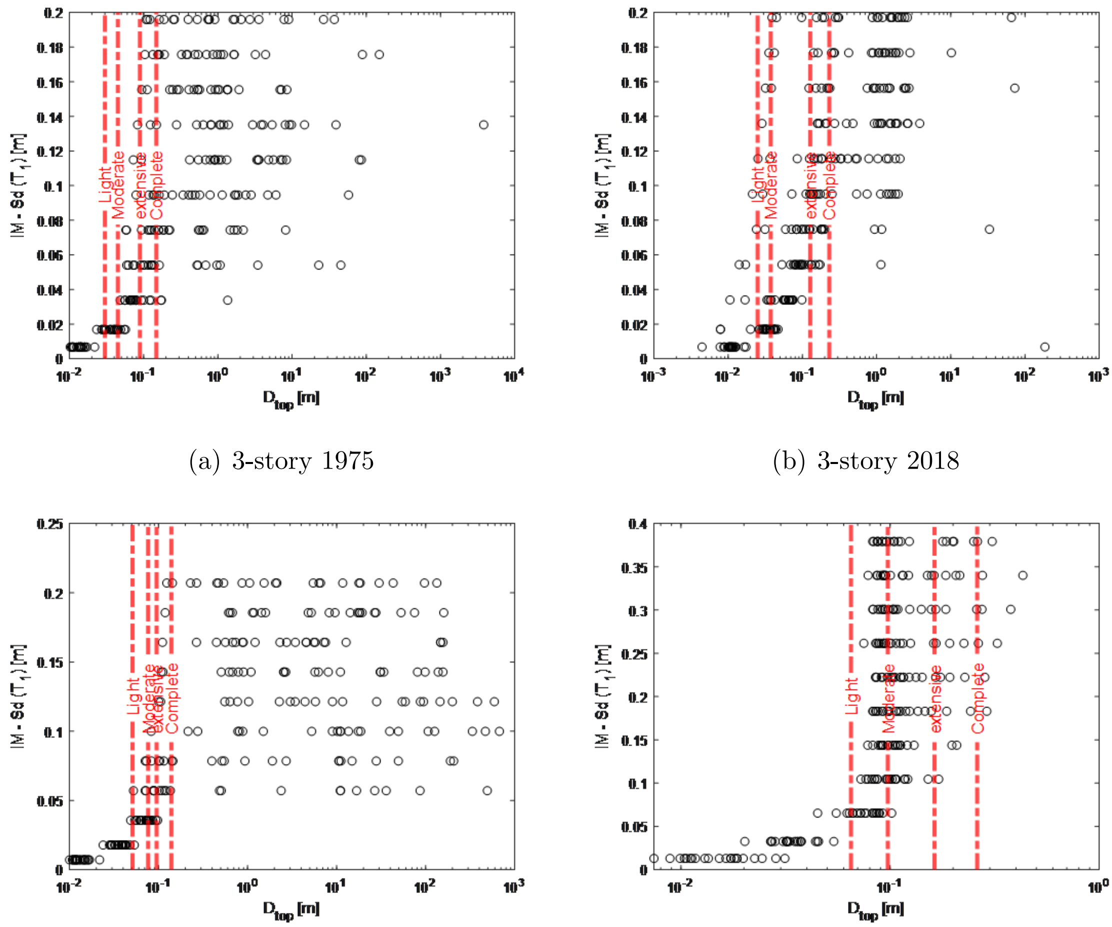

(a) 3-story 1975

(b) 3-story 2018

(c) 6-story 1975

(d) 6-story 2018

Figure 4.17. Direction-free results of MSA for all buildings, IM(Sd)-EDP(Dtop). The black circles show the Dtop values obtained from nonlinear dynamic analyses, and the vertical red dashed lines denote slight, moderate, extensive and complete damage state thresholds from left to the right, respectively.

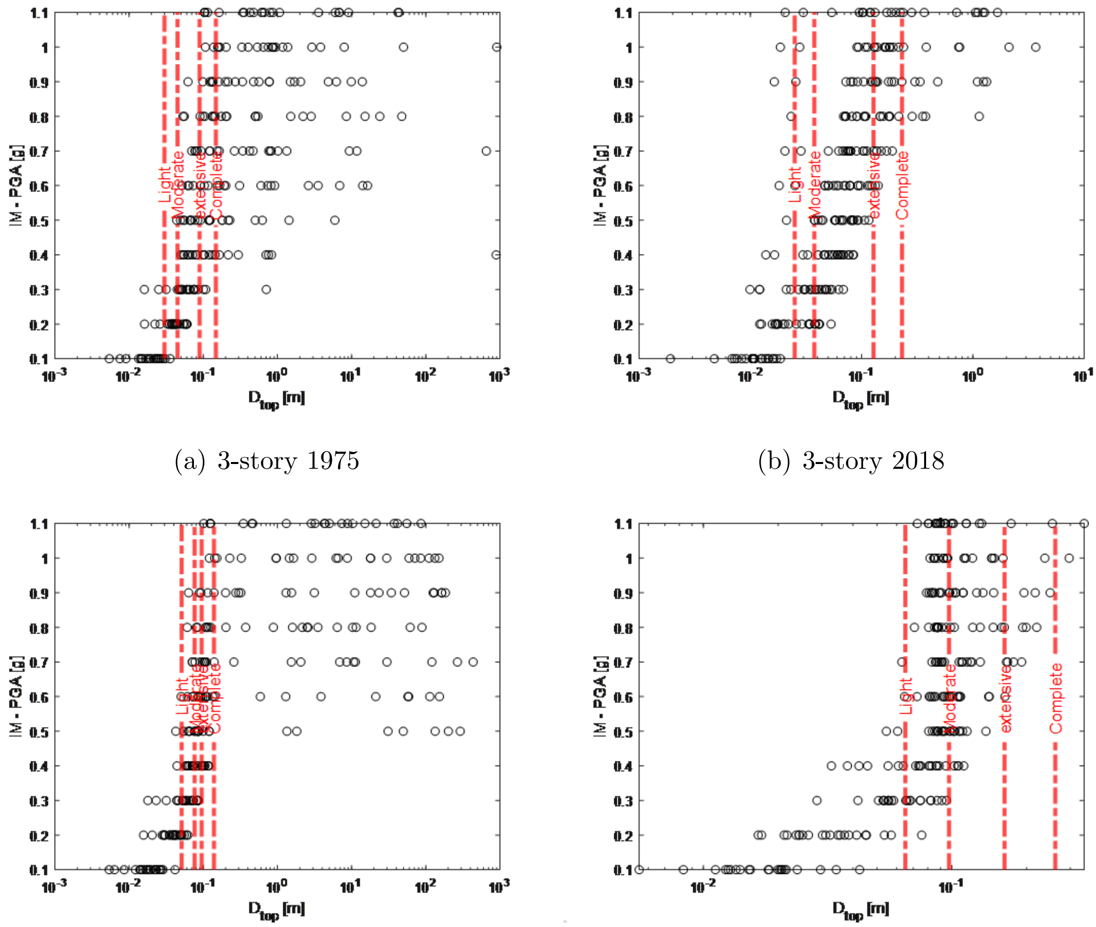

(a) 3-story 1975

(b) 3-story 2018

(c) 6-story 1975

(d) 6-story 2018

Figure 4.18. Direction-free results of MSA for all buildings, IM(PGA)-EDP(Dtop). The black circles show the Dtop values obtained from nonlinear dynamic analyses, and the vertical red dashed lines denote slight, moderate, extensive and complete damage state thresholds from left to the right, respectively.

4.2. Cloud Analysis of the Buildings

Compared with IDA and MSA, Cloud Analysis is much more efficient, which requires a relatively smaller number of nonlinear dynamic analyses to develop a simple regression (e.g., linear) in the logarithmic space of structural responses versus IM based on a set of ground motions with a wide range of intensities. The quality of the simple linear regression is not only sensitive to the selected set of ground motions, but also influenced by the collapse data [18], thus may noticeably reducing the accuracy of fragility estimates [19].

Cloud analysis uses the linear regression in the logarithmic scale by least squares to establish the relationship between engineering demand parameter (EDP) and intensity measure (IM) [20] as follows:

$$E\left[ln\left(EDP\right) = DS \mid IM\right] = ln\left(\mu_d\right) = ln\left(a\right) + bln\left(IM\right) \tag{4.1}$$

$$\sigma_d = \sqrt{\sum_{j=1}^{N} \frac{\left[ln(EDP_j) - ln(\mu_d)\right]^2}{(N-2)}}, \tag{4.2}$$

where $E\left[ln\left(EDP\right) \mid IM\right]$ is expected value for the logarithm of EDP given IM, μ_d is median of EDP given IM, σ_d is dispersion of EDP given IM, EDP_j is EDP obtained from the j-th ground motion, a and b are regression coefficients; and N is number of ground motions. The fragility function is expressed as the damage probability that EDP exceeds the pre-defined value threshold for each damage state (DS) conditional on IM, which can be derived based on the above linear relationship between EDP and IM under the lognormal probability distribution as follows:

$$P_f[EDP \geq DS \mid IM, \theta, \beta] = \Phi\left[\frac{ln(\mu_d) - ln(DS)}{\sigma_d}\right] = \Phi\left[\frac{ln(IM) - ln(\theta)}{\beta}\right], \tag{4.3}$$

where $\Phi(.)$ is standard normal cumulative distribution function (CDF); θ is median of the fragility function, i.e., $ln\left(\theta\right) = [ln(DS) - ln(a)]/b$, and β is dispersion of the fragility function, i.e., $\beta = \sigma_d/b$ given IM.

The results of Cloud Analysis for different IM parameters (Sa, Sd and PGA) and EDPs (MIDR and Dtop) are given in Figures 4.19 to 4.36 which are developed in MATLAB [17]. Also, the damage state limits in terms of the selected EDP are shown in these figures with vertical red dotted lines. The number of EDP values exceeding the limit values can easily be seen in the figures.

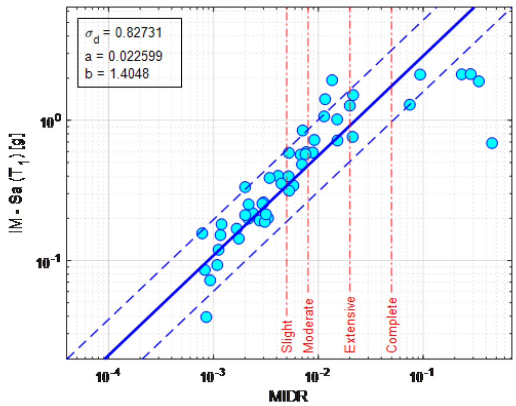

(a) 3-story 1975 in x-direction

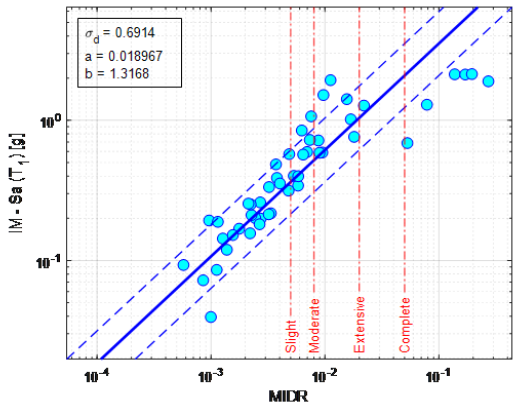

(b) 3-story 1975 in y-direction

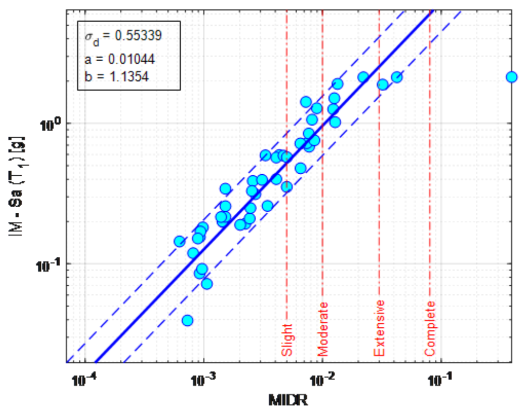

(c) 3-story 2018 in x-direction

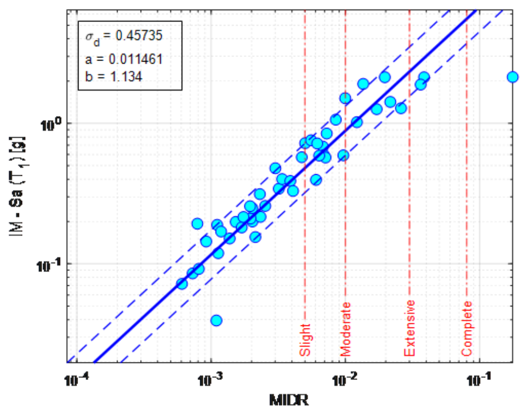

(d) 3-story 2018 in y-direction

Figure 4.19. Results of Cloud Analysis for 3-story buildings, IM(Sa)-EDP(MIDR). The blue circles show the MIDR values obtained from nonlinear dynamic analyses, and the vertical red dashed lines denote slight, moderate, extensive and complete damage state thresholds from left to the right, respectively.

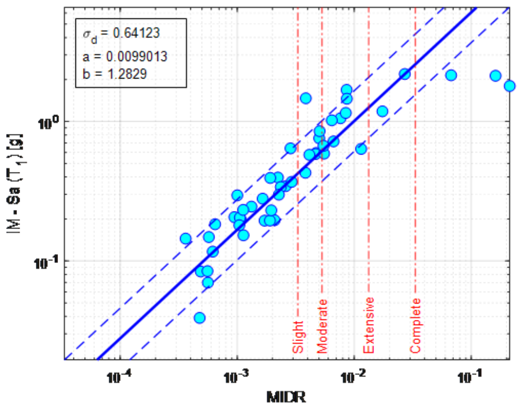

(a) 6-story 1975 in x-direction

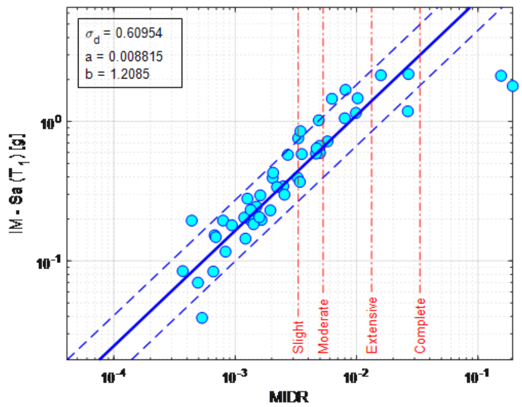

(b) 6-story 1975 in y-direction

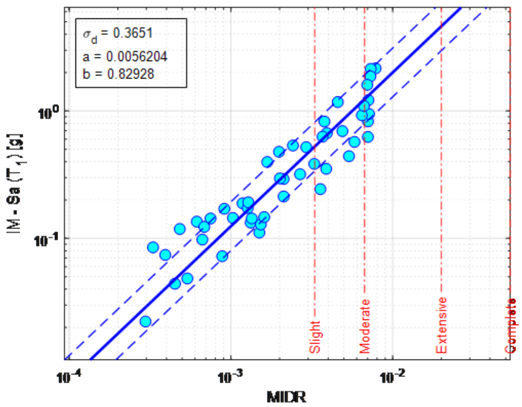

(c) 6-story 2018 in x-direction

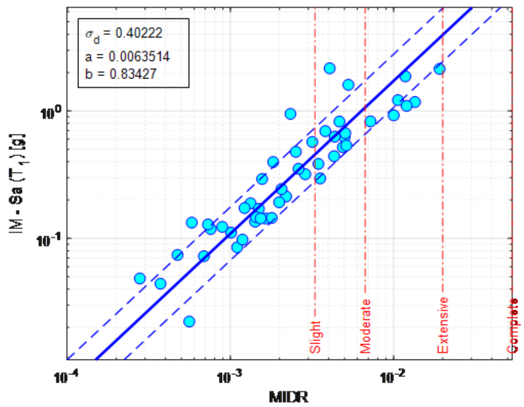

(d) 6-story 2018 in y-direction

Figure 4.20. Results of Cloud Analysis for 6-story buildings, IM(Sa)-EDP(MIDR). The blue circles show the MIDR values obtained from nonlinear dynamic analyses, and the vertical red dashed lines denote slight, moderate, extensive and complete damage state thresholds from left to the right, respectively.

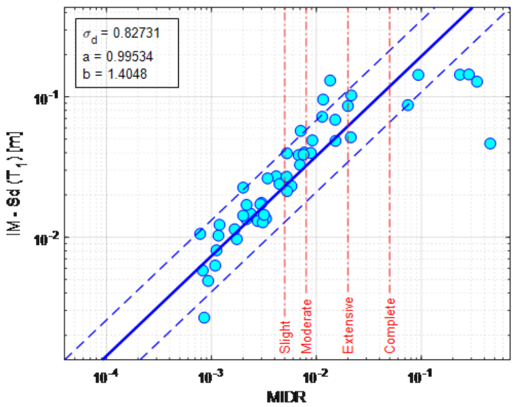

(a) 3-story 1975 in x-direction

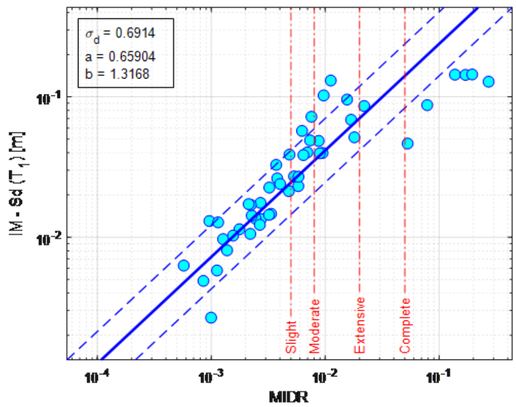

(b) 3-story 1975 in y-direction

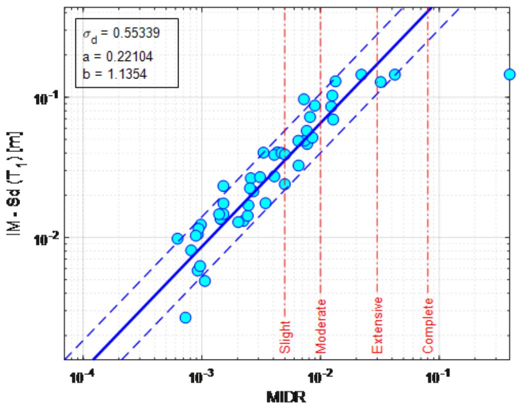

(c) 3-story 2018 in x-direction

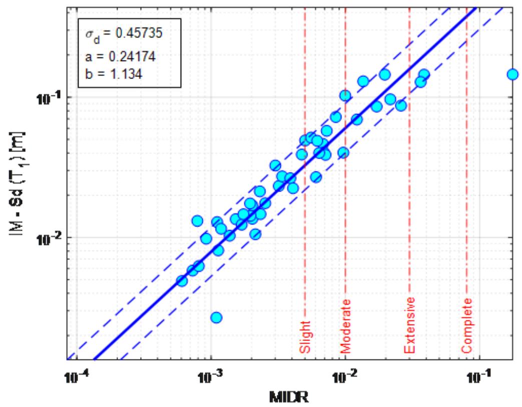

(d) 3-story 2018 in y-direction

Figure 4.21. Results of Cloud Analysis for 3-story buildings, IM(Sd)-EDP(MIDR). The blue circles show the MIDR values obtained from nonlinear dynamic analyses, and the vertical red dashed lines denote slight, moderate, extensive and complete damage state thresholds from left to the right, respectively.

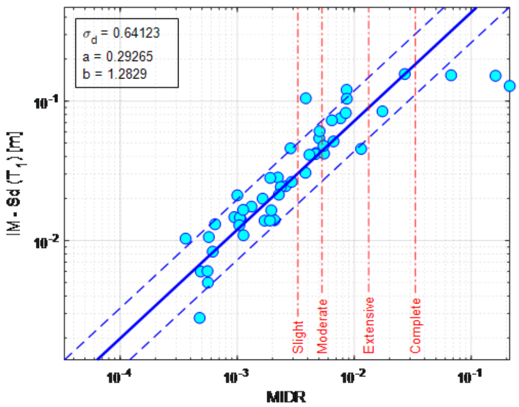

(a) 6-story 1975 in x-direction

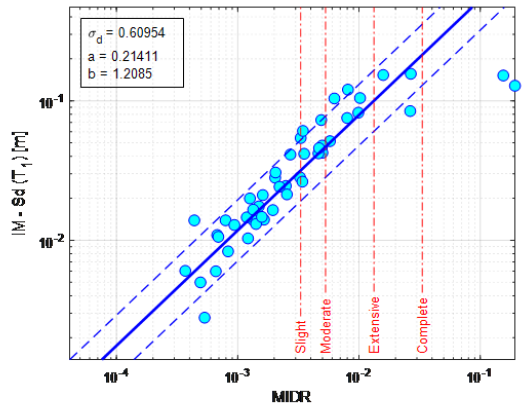

(b) 6-story 1975 in y-direction

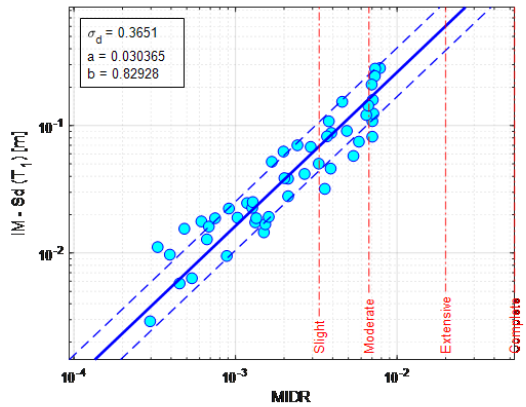

(c) 6-story 2018 in x-direction

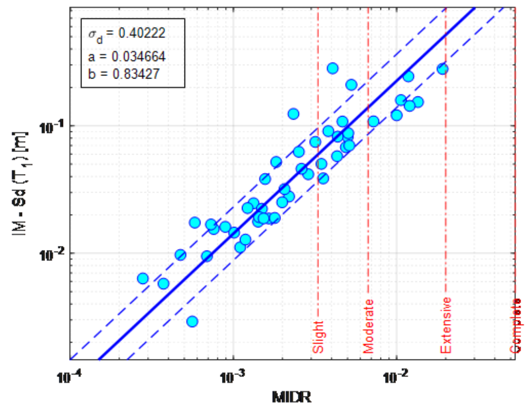

(d) 6-story 2018 in y-direction

Figure 4.22. Results of Cloud Analysis for 6-story buildings, IM(Sd)-EDP(MIDR). The blue circles show the MIDR values obtained from nonlinear dynamic analyses, and the vertical red dashed lines denote slight, moderate, extensive and complete damage state thresholds from left to the right, respectively.

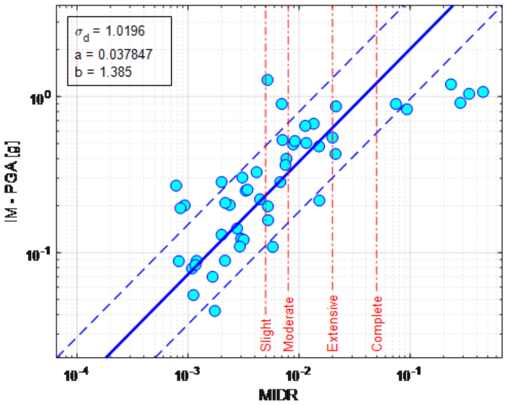

(a) 3-story 1975 in x-direction

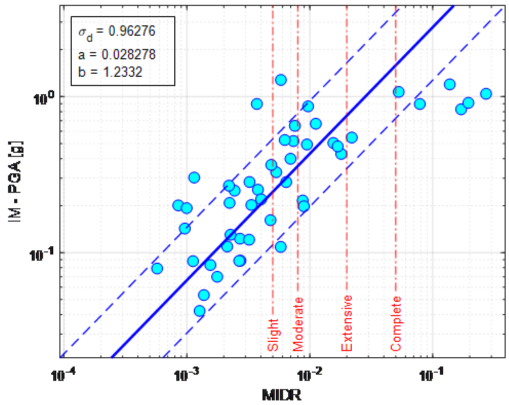

(b) 3-story 1975 in y-direction

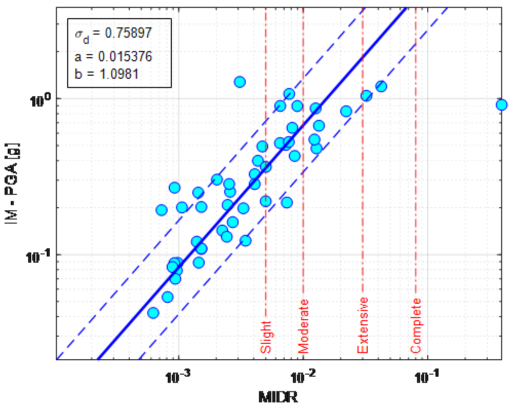

(c) 3-story 2018 in x-direction

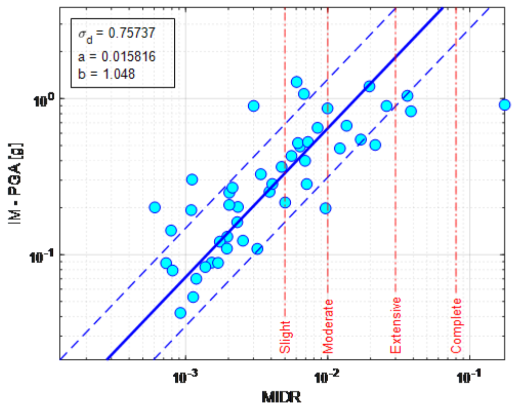

(d) 3-story 2018 in y-direction

Figure 4.23. Results of Cloud Analysis for 3-story buildings, IM(PGA)-EDP(MIDR). The blue circles show the MIDR values obtained from nonlinear dynamic analyses, and the vertical red dashed lines denote slight, moderate, extensive and complete damage state thresholds from left to the right, respectively.

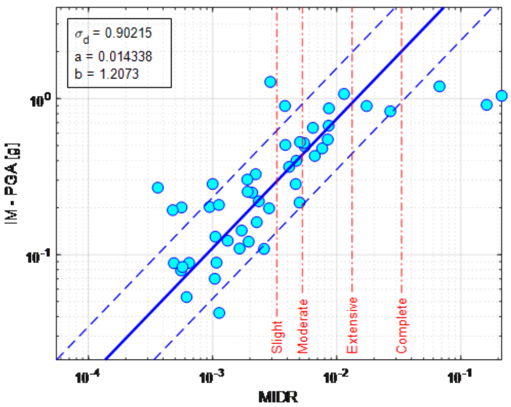

(a) 6-story 1975 in x-direction

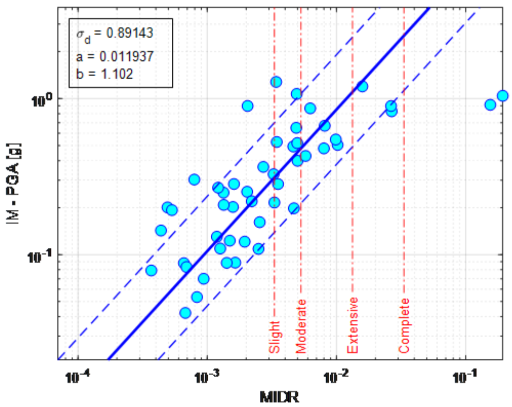

(b) 6-story 1975 in y-direction

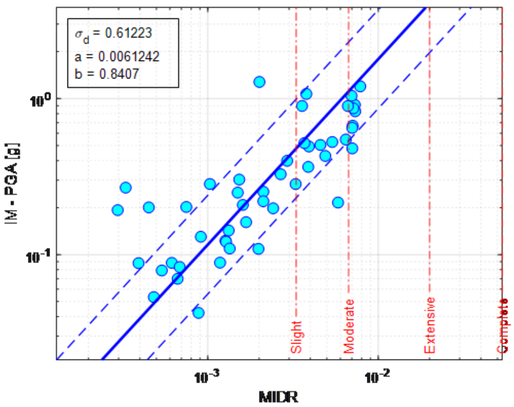

(c) 6-story 2018 in x-direction

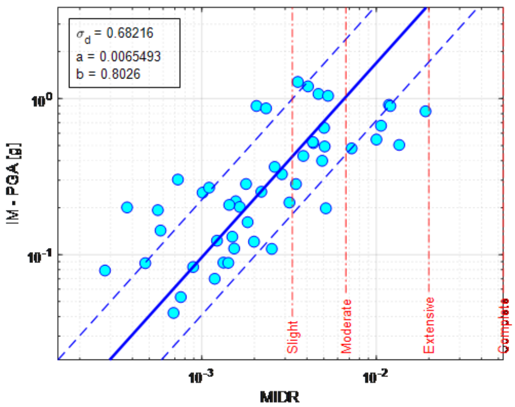

(d) 6-story 2018 in y-direction

Figure 4.24. Results of Cloud Analysis for 6-story buildings, IM(PGA)-EDP(MIDR). The blue circles show the MIDR values obtained from nonlinear dynamic analyses, and the vertical red dashed lines denote slight, moderate, extensive and complete damage state thresholds from left to the right, respectively.

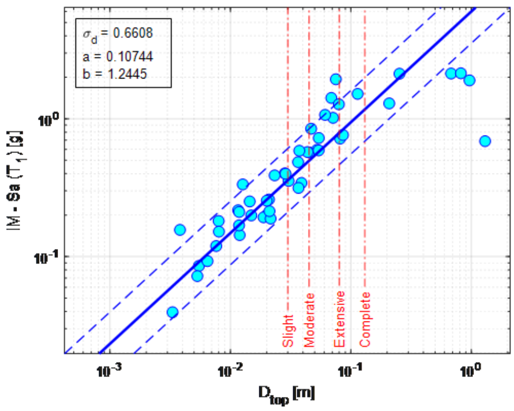

(a) 3-story 1975 in x-direction

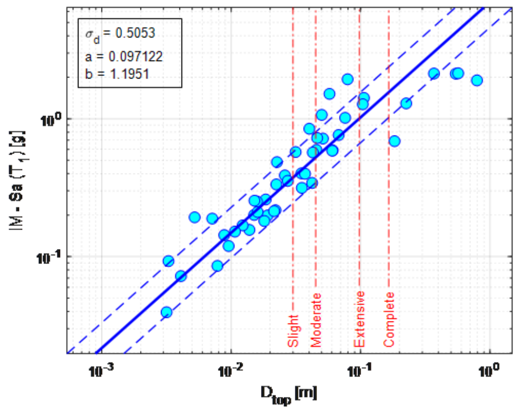

(b) 3-story 1975 in y-direction

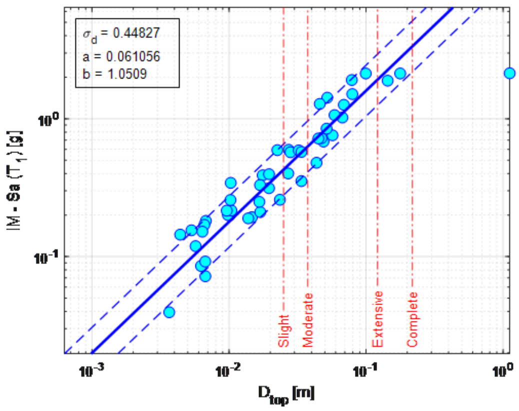

(c) 3-story 2018 in x-direction

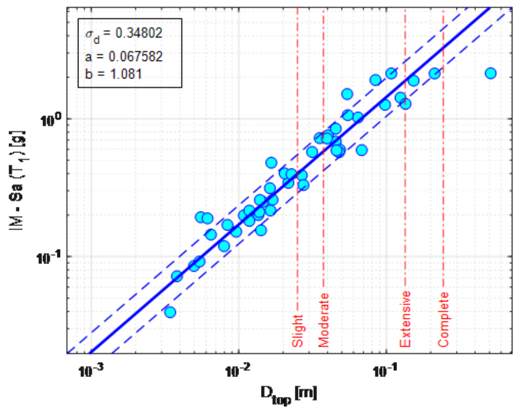

(d) 3-story 2018 in y-direction

Figure 4.25. Results of Cloud Analysis for 3-story buildings, IM(Sa)-EDP(Dtop). The blue circles show the Dtop values obtained from nonlinear dynamic analyses, and the vertical red dashed lines denote slight, moderate, extensive and complete damage state thresholds from left to the right, respectively.

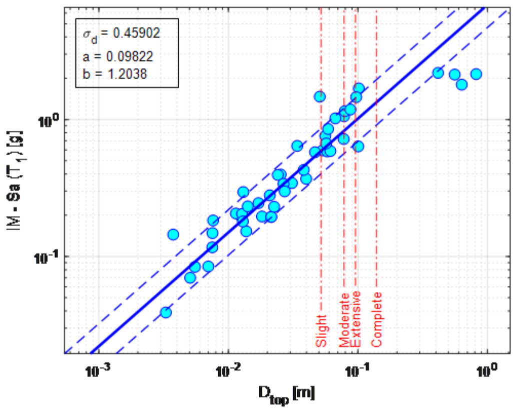

(a) 6-story 1975 in x-direction

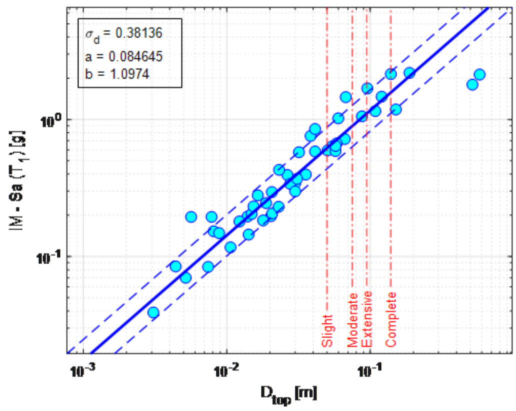

(b) 6-story 1975 in y-direction

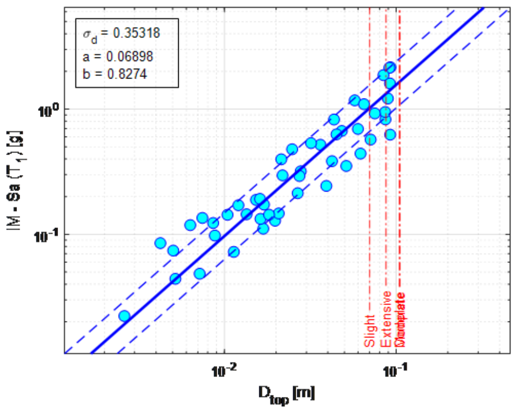

(c) 6-story 2018 in x-direction

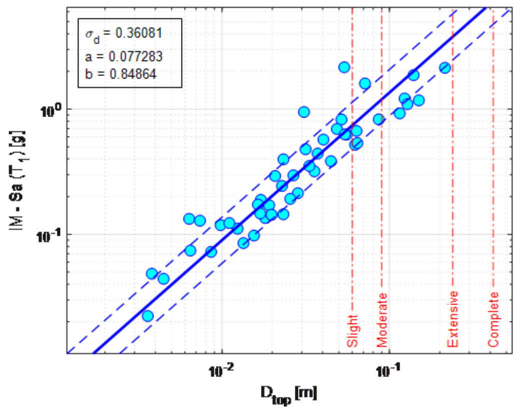

(d) 6-story 2018 in y-direction

Figure 4.26. Results of Cloud Analysis for 6-story buildings, IM(Sa)-EDP(Dtop). The blue circles show the Dtop values obtained from nonlinear dynamic analyses, and the vertical red dashed lines denote slight, moderate, extensive and complete damage state thresholds from left to the right, respectively.

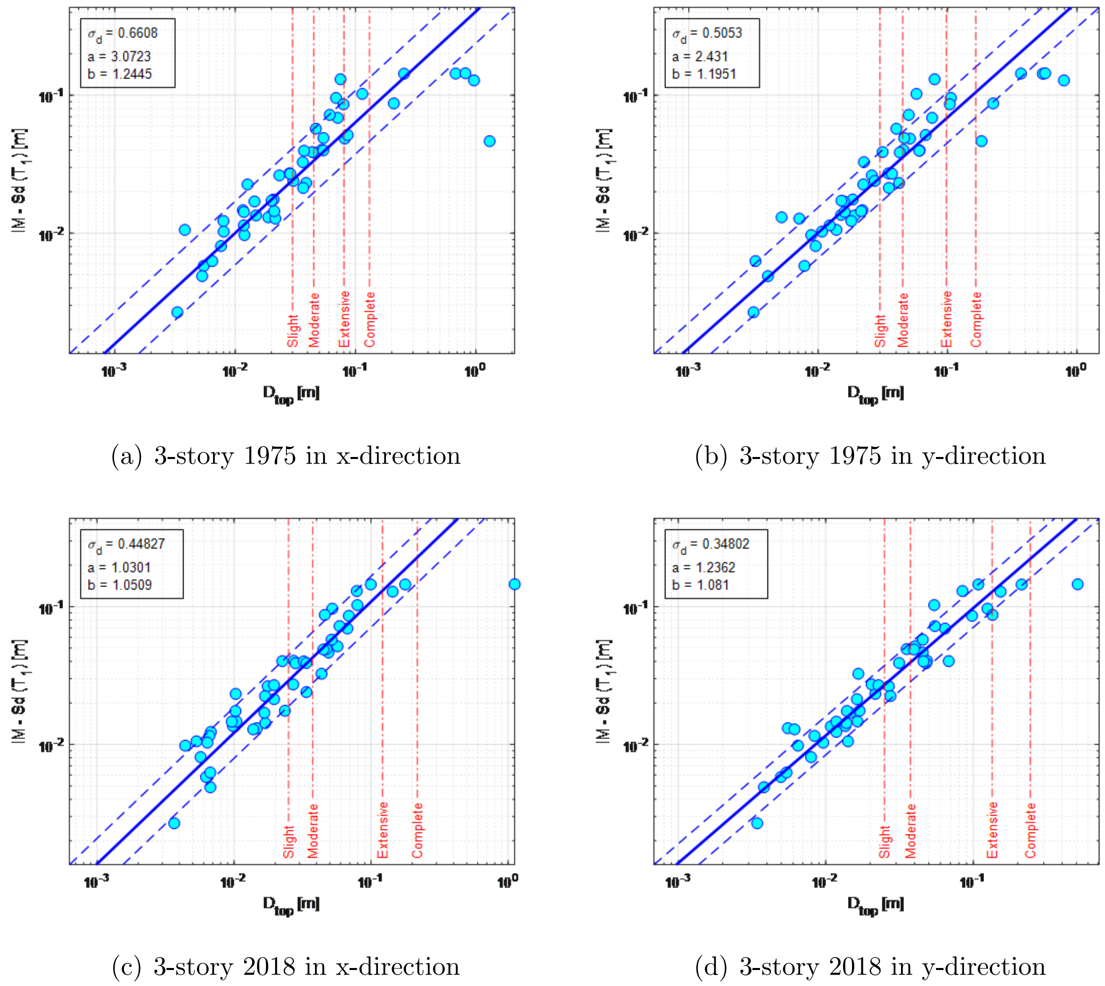

Figure 4.27. Results of Cloud Analysis for 3-story buildings, IM(Sd)-EDP(Dtop). The blue circles show the Dtop values obtained from nonlinear dynamic analyses, and the vertical red dashed lines denote slight, moderate, extensive and complete damage state thresholds from left to the right, respectively.

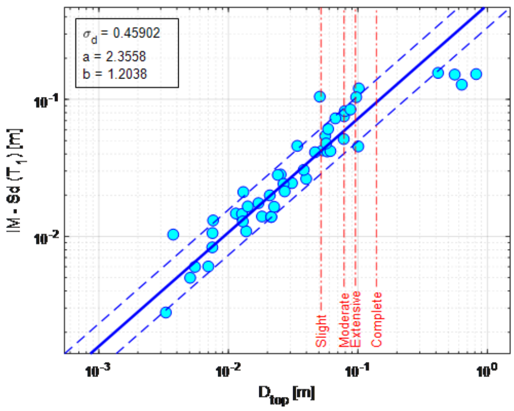

(a) 6-story 1975 in x-direction

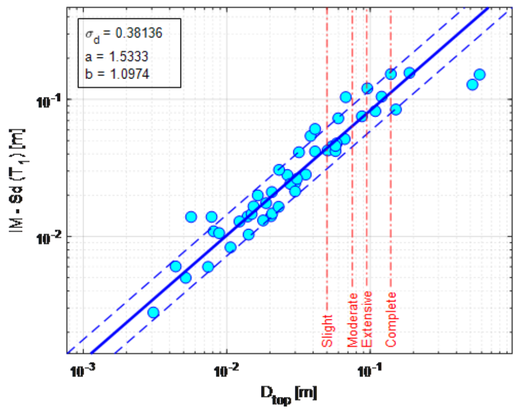

(b) 6-story 1975 in y-direction

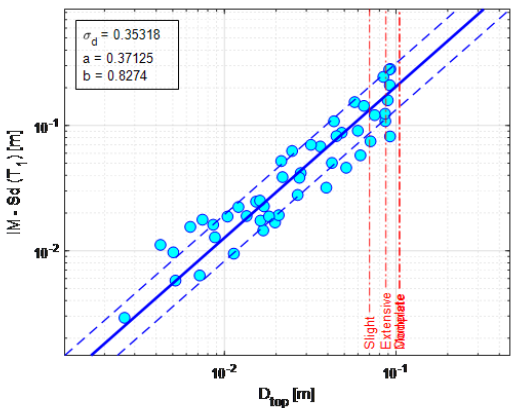

(c) 6-story 2018 in x-direction

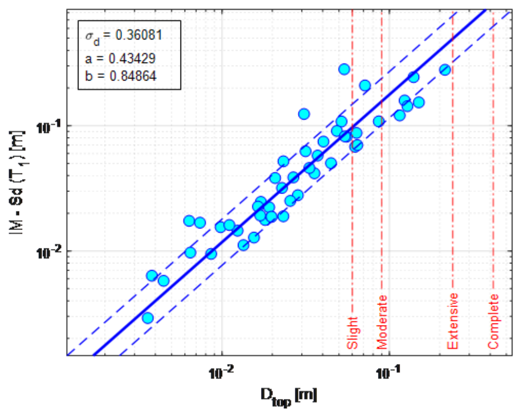

(d) 6-story 2018 in y-direction

Figure 4.28. Results of Cloud Analysis for 6-story buildings, IM(Sd)-EDP(Dtop). The blue circles show the Dtop values obtained from nonlinear dynamic analyses, and the vertical red dashed lines denote slight, moderate, extensive and complete damage state thresholds from left to the right, respectively.

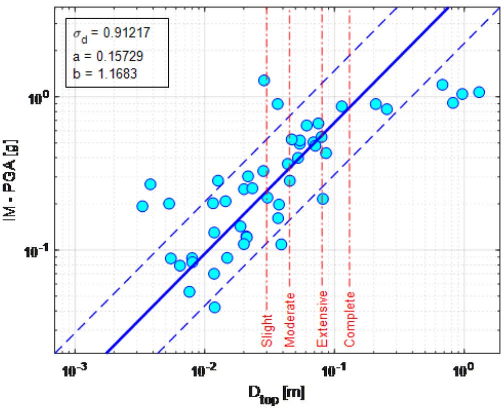

(a) 3-story 1975 in x-direction

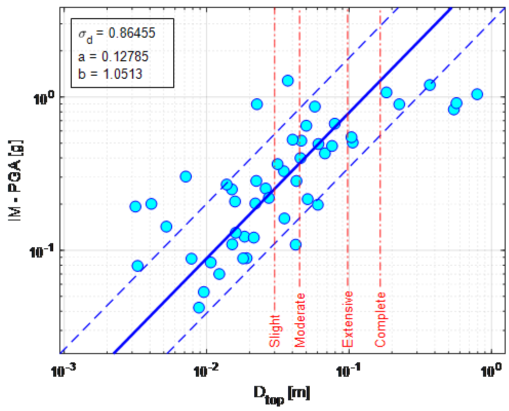

(b) 3-story 1975 in y-direction

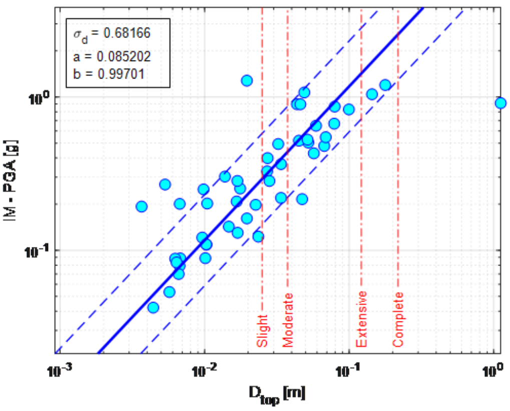

(c) 3-story 2018 in x-direction

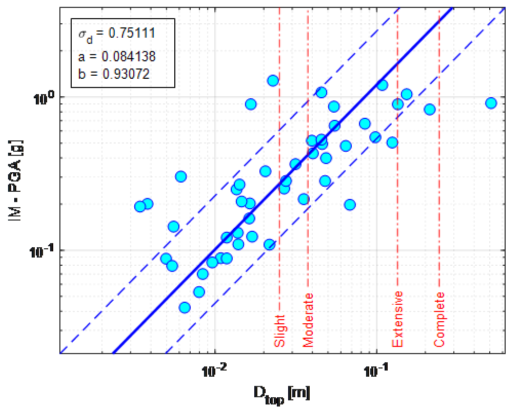

(d) 3-story 2018 in y-direction

Figure 4.29. Results of Cloud Analysis for 3-story buildings, IM(PGA)-EDP(Dtop). The blue circles show the Dtop values obtained from nonlinear dynamic analyses, and the vertical red dashed lines denote slight, moderate, extensive and complete damage state thresholds from left to the right, respectively.

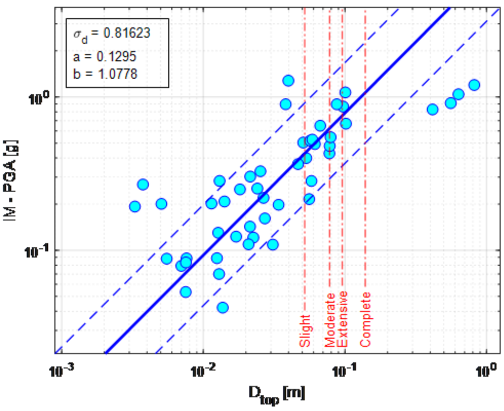

(a) 6-story 1975 in x-direction

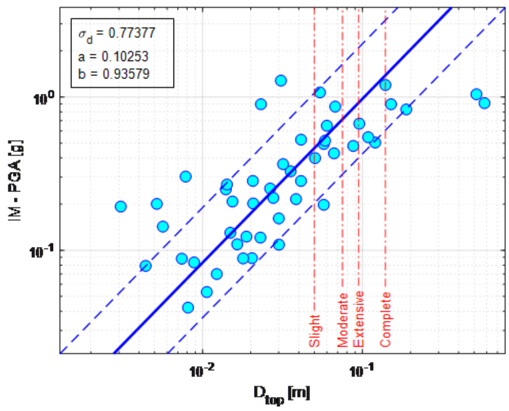

(b) 6-story 1975 in y-direction

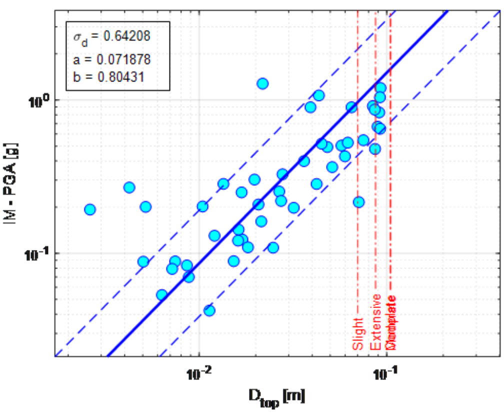

(c) 6-story 2018 in x-direction

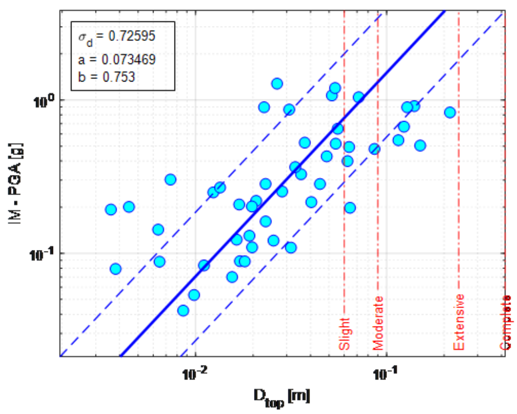

(d) 6-story 2018 in y-direction

Figure 4.30. Results of Cloud Analysis for 6-story buildings, IM(PGA)-EDP(Dtop). The blue circles show the Dtop values obtained from nonlinear dynamic analyses, and the vertical red dashed lines denote slight, moderate, extensive and complete damage state thresholds from left to the right, respectively.

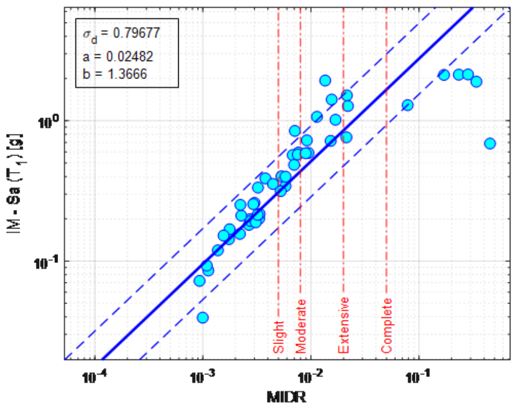

(a) 3-story 1975

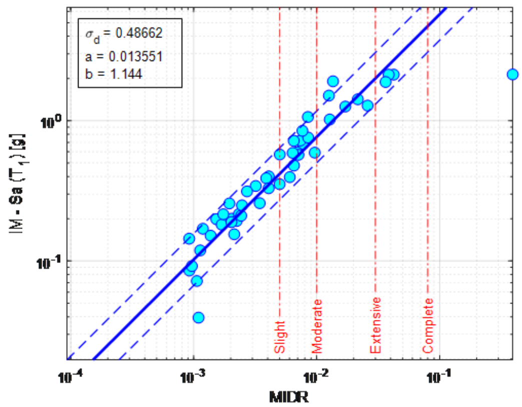

(b) 3-story 2018

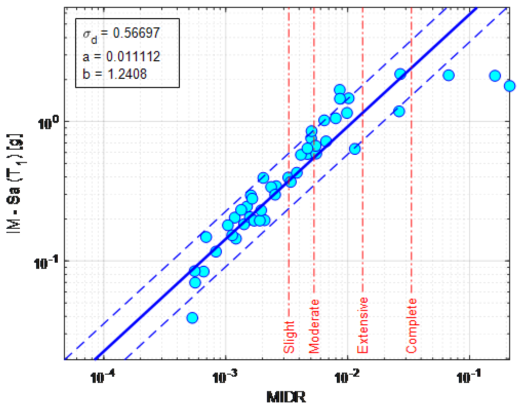

(c) 6-story 1975

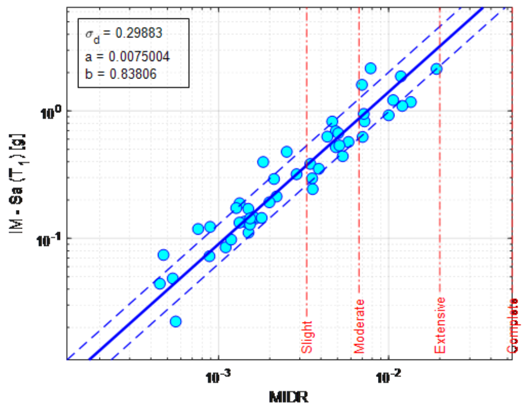

(d) 6-story 2018

Figure 4.31. Direction-free results of Cloud Analysis for all buildings, IM(Sa)-EDP(MIDR). The blue circles show the MIDR values obtained from nonlinear dynamic analyses, and the vertical red dashed lines denote slight, moderate, extensive and complete damage state thresholds from left to the right, respectively.

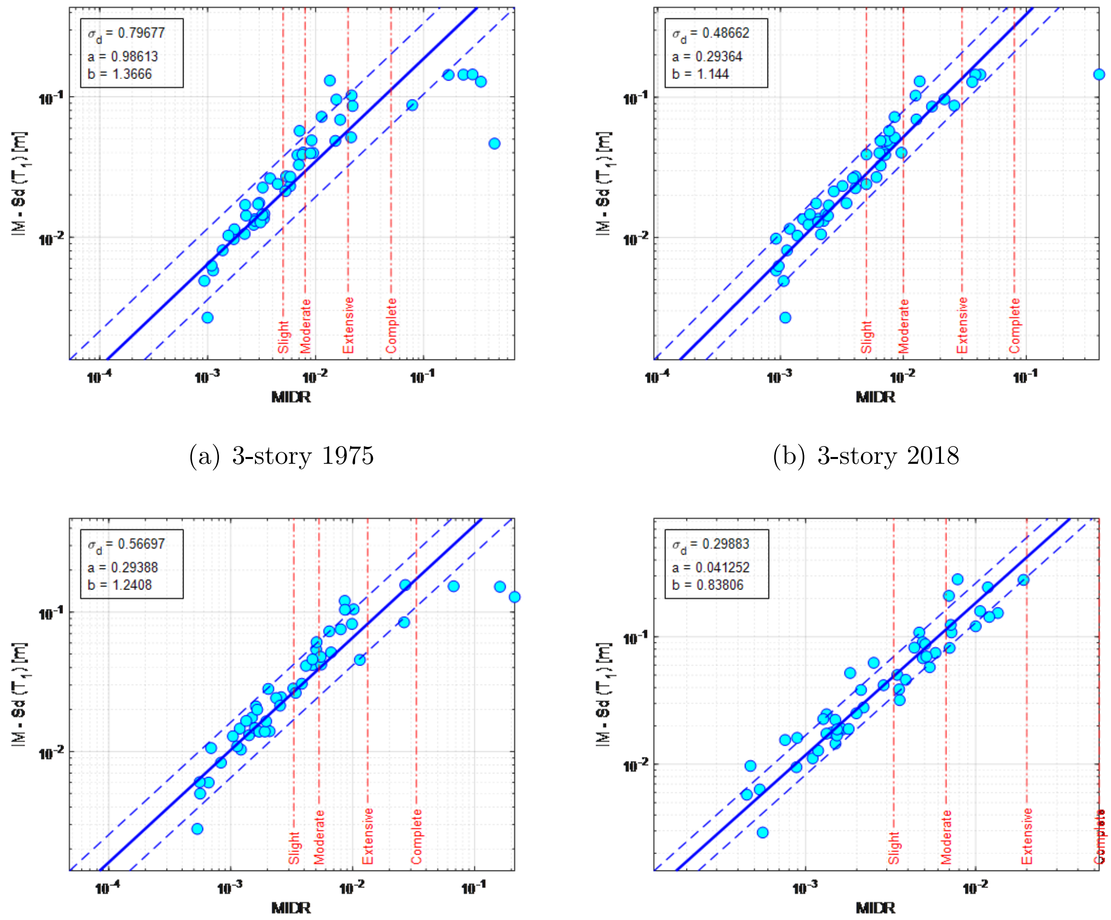

(a) 3-story 1975

(b) 3-story 2018

(c) 6-story 1975

(d) 6-story 2018

Figure 4.32. Direction-free results of Cloud Analysis for all buildings, IM(Sd)-EDP(MIDR). The blue circles show the MIDR values obtained from nonlinear dynamic analyses, and the vertical red dashed lines denote slight, moderate, extensive and complete damage state thresholds from left to the right, respectively.

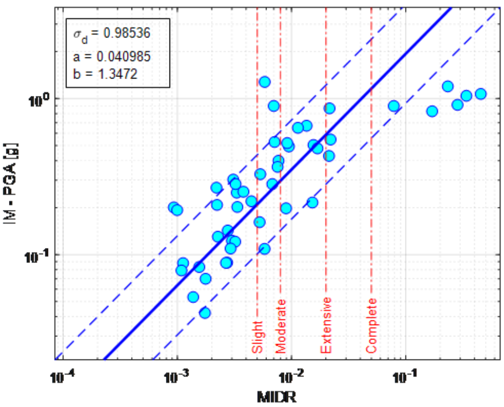

(a) 3-story 1975

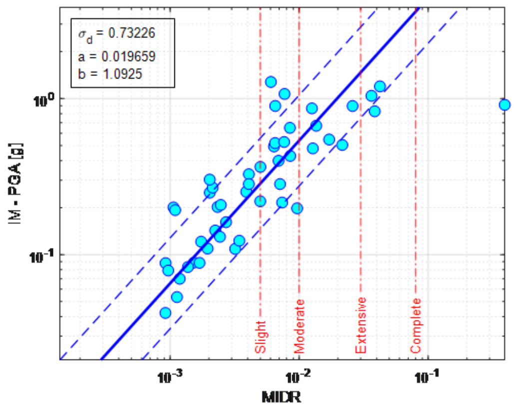

(b) 3-story 2018

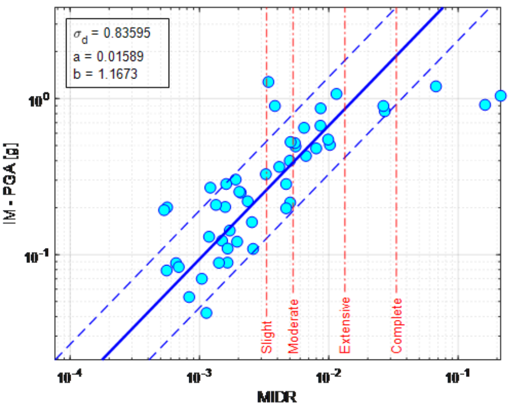

(c) 6-story 1975

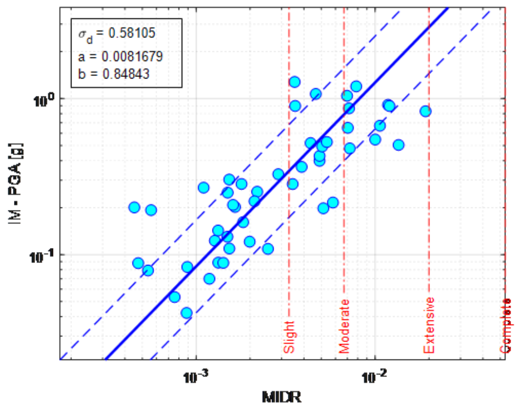

(d) 6-story 2018

Figure 4.33. Direction-free results of Cloud Analysis for all buildings, IM(PGA)-EDP(MIDR). The blue circles show the MIDR values obtained from nonlinear dynamic analyses, and the vertical red dashed lines denote slight, moderate, extensive and complete damage state thresholds from left to the right, respectively.

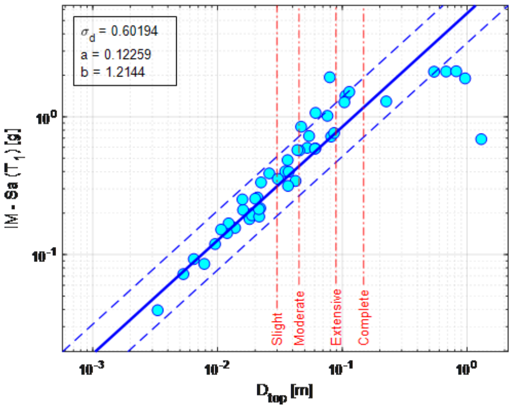

(a) 3-story 1975

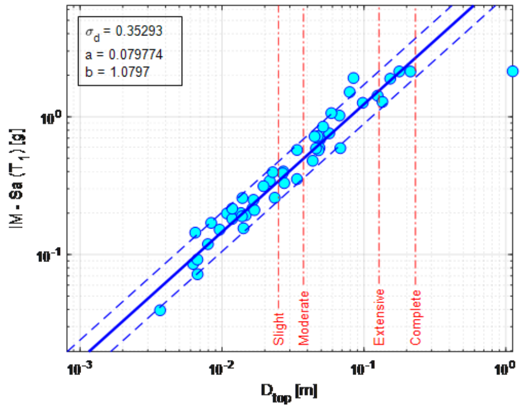

(b) 3-story 2018

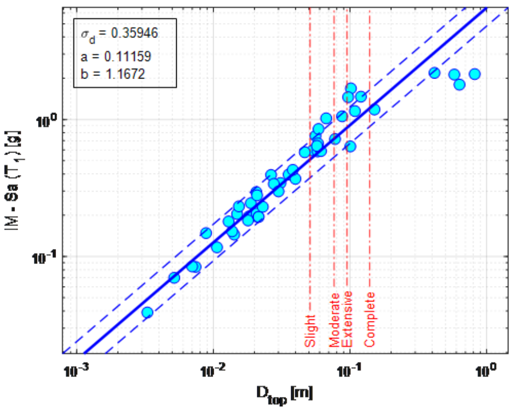

(c) 6-story 1975

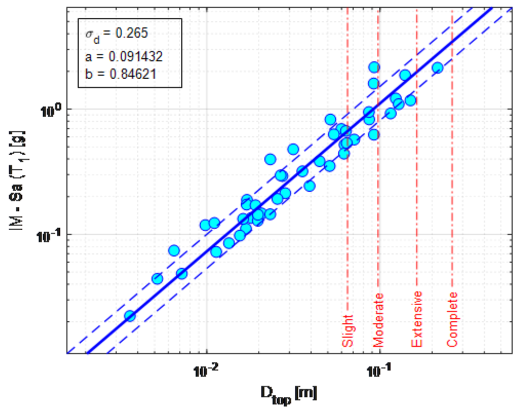

(d) 6-story 2018

Figure 4.34. Direction-free results of Cloud Analysis for all buildings, IM(Sa)-EDP(Dtop). The blue circles show the Dtop values obtained from nonlinear dynamic analyses, and the vertical red dashed lines denote slight, moderate, extensive and complete damage state thresholds from left to the right, respectively.

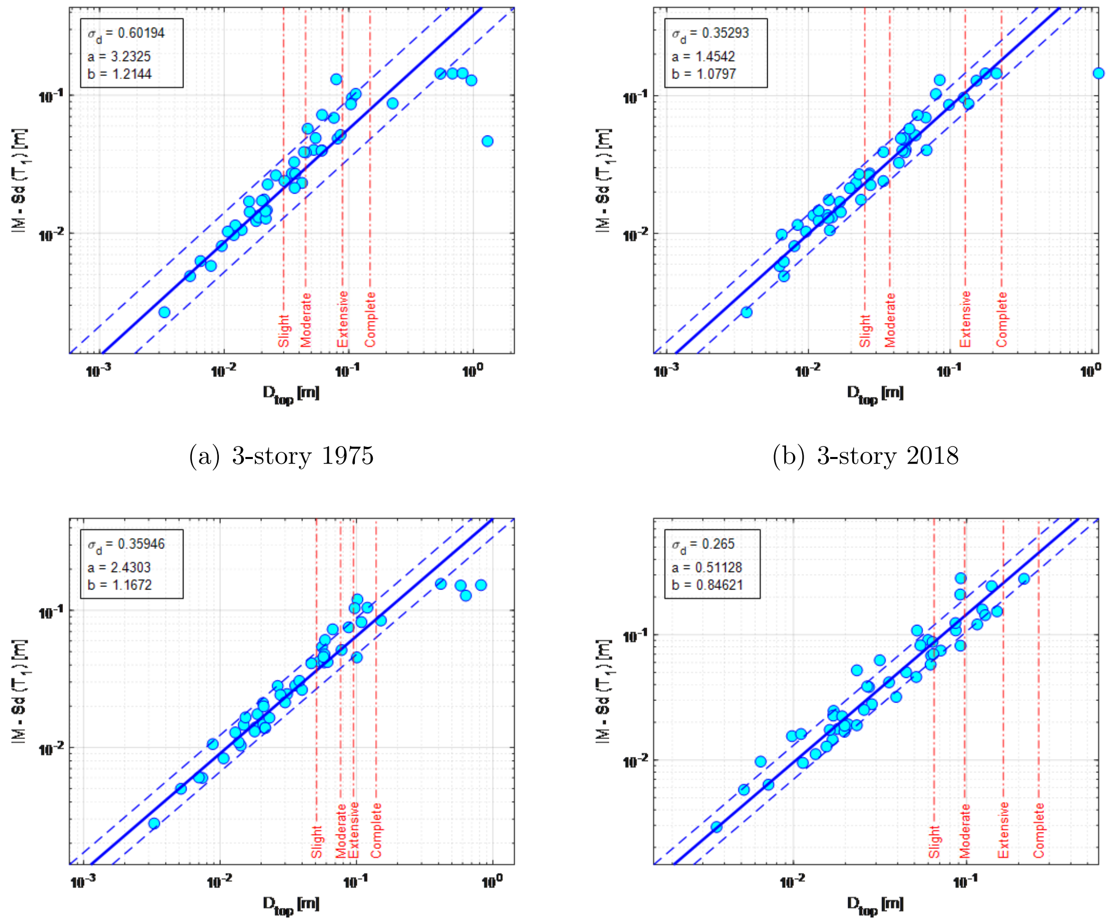

(a) 3-story 1975

(b) 3-story 2018

(c) 6-story 1975

(d) 6-story 2018

Figure 4.35. Direction-free results of Cloud Analysis for all buildings, IM(Sd)-EDP(Dtop). The blue circles show the Dtop values obtained from nonlinear dynamic analyses, and the vertical red dashed lines denote slight, moderate, extensive and complete damage state thresholds from left to the right, respectively.

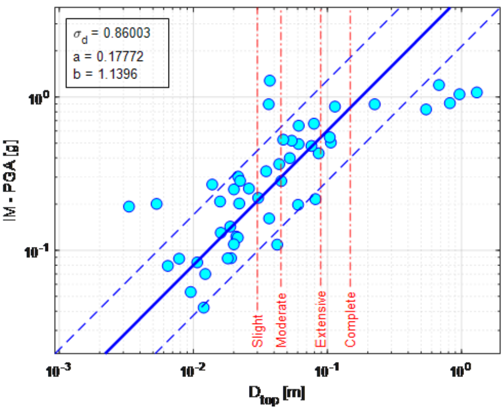

(a) 3-story 1975

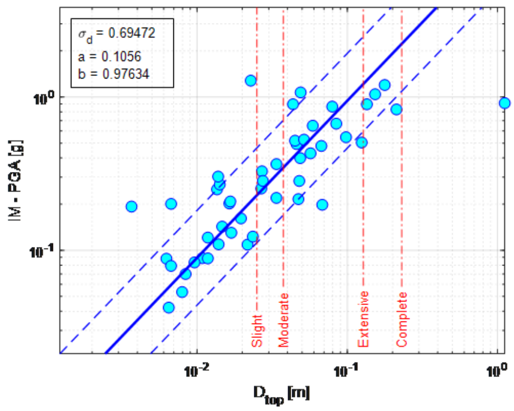

(b) 3-story 2018

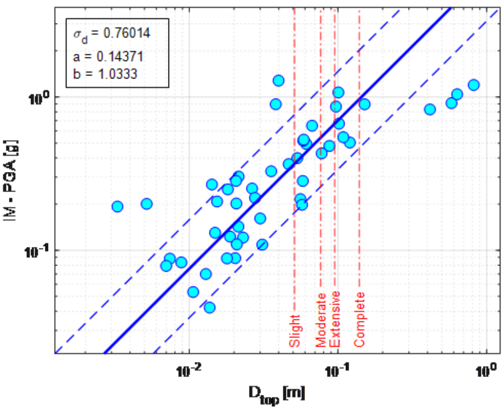

(c) 6-story 1975

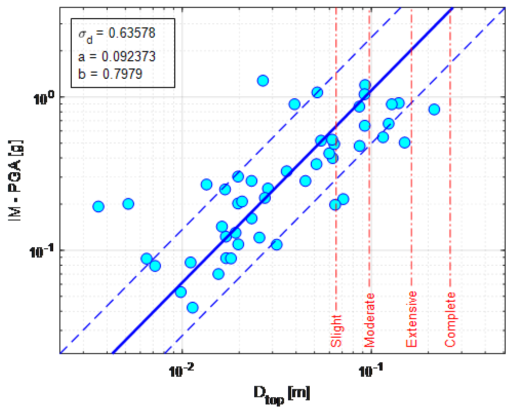

(d) 6-story 2018

Figure 4.36. Direction-free results of Cloud Analysis for all buildings, IM(PGA)-EDP(Dtop). The blue circles show the Dtop values obtained from nonlinear dynamic analyses, and the vertical red dashed lines denote slight, moderate, extensive and complete damage state thresholds from left to the right, respectively.

4.3. Development of Fragility Functions for the Buildings using the MSA Results

The maximum likelihood estimation (MLE) method is utilized to generate the fragility functions. The procedure of the MLE method is explained in the article written by Jack Baker (2015). The study (Baker, 2015) defines the statistical methods to get the fragility functions parameters by using the nonlinear dynamic analysis results.

Fragility functions are obtained by using a lognormal cumulative distribution function which is given in Equation (4.4). The goal is to find the best θ and β values which are the median and logarithmic standard deviation of the fragility function, respectively.

$$P(DS/IM \geq x) = \phi\left(\frac{In\,(x/\theta)}{\beta}\right). \tag{4.4}$$

$P(DS/IM \geq x)$ is probability of exceeding a damage state (DS) for a given intensity measure (IM=x). $\phi\,()$ is the standard normal cumulative distribution function and θ, β are the median of IM and the standard deviation of $In(IM)$, respectively.

By using the maximum likelihood estimation (MLE) method, θ and β are predicted. For a given IM level, the probability of observing z_j collapses in n_j ground motions for a certain IM is obtained by the binomial distribution in Equation (4.5).

$$P(z_j\, collapses\, in\, n_j\, ground\, motions) = \binom{n_j}{z_j} p_j^{z_j}\,(1 - p_j)^{n_j - z_j}. \tag{4.5}$$

In equation (4.5), p_j is the probability of ground motions with IM=xj to exceed a DS for a given building that is previously defined as $P(DS/IM \geq x)$ in Equation (4.4). The maximum likelihood method provides the highest probability of p_j.

When different IM levels are used for the analyses, the likelihood function that is the product of the binomial probabilities (from Equation (4.5)) at each IM level is defined by using Equation (4.6).

$$Likelihood = \prod_{j}^{m} \binom{n_j}{z_j} p_j^{z_j} (1 - p_j)^{n_j - z_j}. \tag{4.6}$$

If p_j is written in the Likelihood equation, Equation (4.6) is converted to;

$$Likelihood = \prod_{j}^{m} \binom{n_j}{z_j} \phi \left(\frac{In\,(x/\theta)}{\beta} \right)^{z_j} (1 - \phi \left(\frac{In\,(x/\theta)}{\beta} \right))^{n_j - z_j}. \tag{4.7}$$

Since it is easier to maximize a sum equation than maximizing a product equation, Equation (4.6) is converted into Equation (4.7) by taking the natural logarithm of both sides of Equation (4.7).

The θ and β values which maximize Equation (4.8) are selected as the parameters of the fragility functions.

$$\{\theta, \beta\} = arg_{\theta,\beta} max \sum_{j_1}^{n} \left\{ In \binom{n_j}{z_j} + In\phi \left(\frac{In\,(x/\theta)}{\beta} \right) + (n_j - z_j) In(1 - \phi \left(\frac{In\,(x/\theta)}{\beta} \right) \right\}. \tag{4.8}$$

By using the MSA results and the MLE method explained above, the fragility functions are developed for the 3 and 6-story buildings. The fragility curves and the fragility parameters' values are given in Figures 4.37 to 4.54 and Tables 4.1 to 4.6.

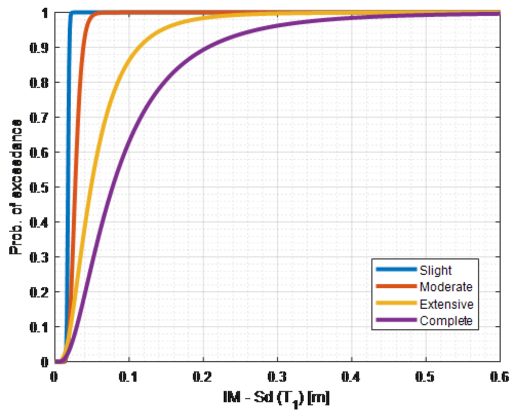

(a) 3-story 1975 in x-direction

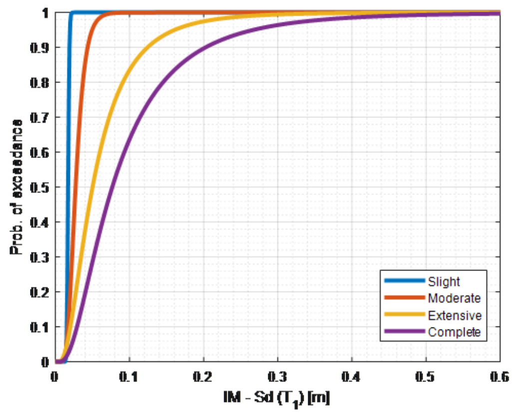

(b) 3-story 1975 in y-direction

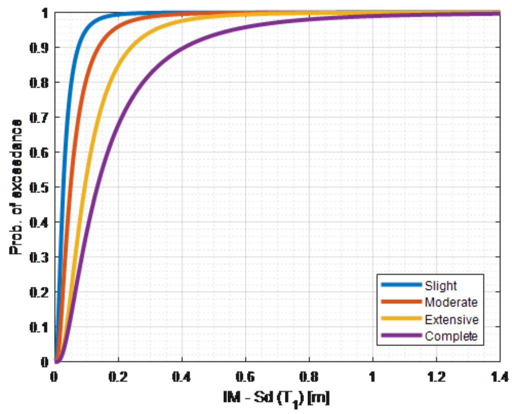

(c) 3-story 2018 in x-direction

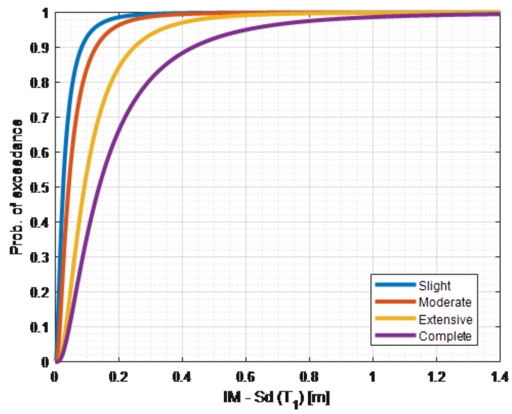

(d) 3-story 2018 in y-direction

Figure 4.37. Fragility curves for 3-story buildings obtained from MSA (IM: Sd and EDP: MIDR).

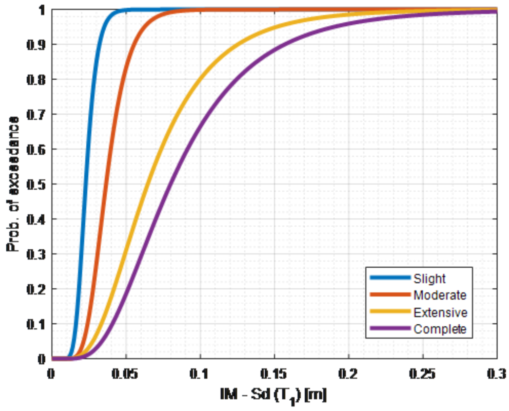

(a) 6-story 1975 in x-direction

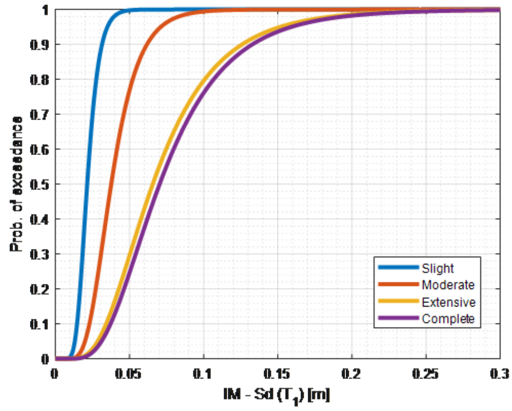

(b) 6-story 1975 in y-direction

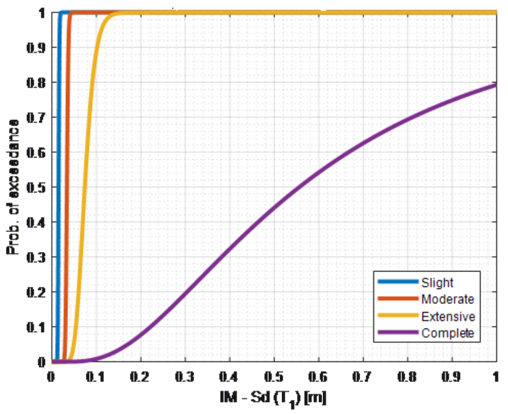

(c) 6-story 2018 in x-direction

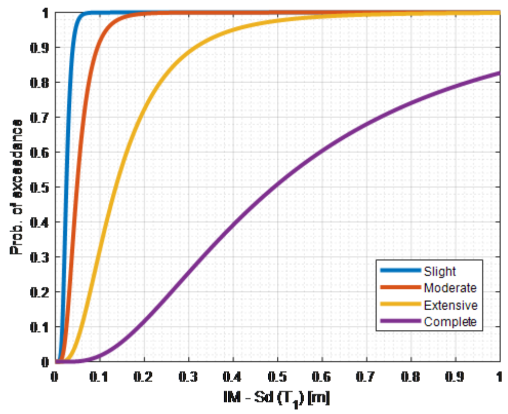

(d) 6-story 2018 in y-direction

Figure 4.38. Fragility curves for 6-story buildings obtained from MSA (IM: Sd and EDP: MIDR).

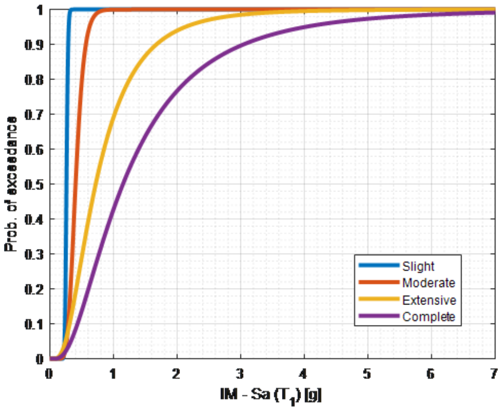

(a) 3-story 1975 in x-direction

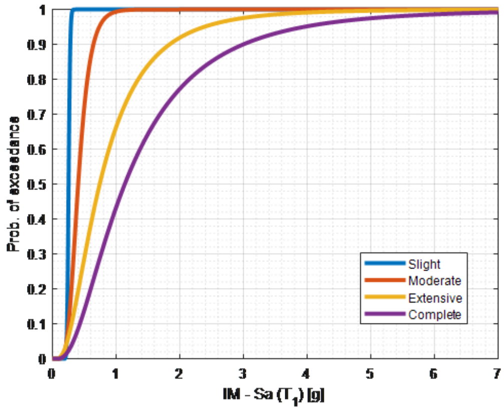

(b) 3-story 1975 in y-direction

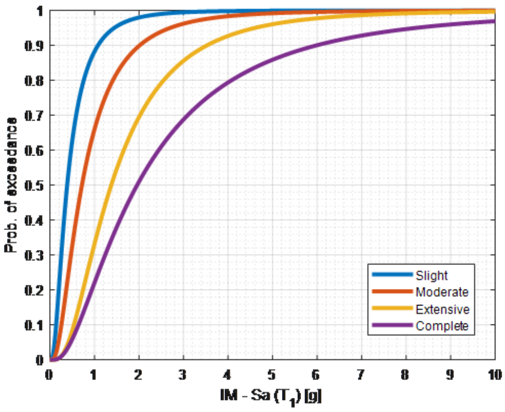

(c) 3-story 2018 in x-direction

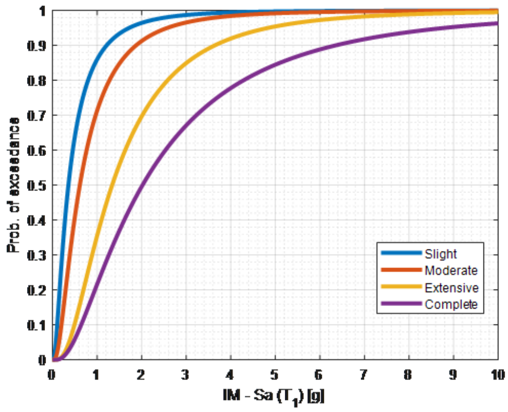

(d) 3-story 2018 in y-direction

Figure 4.39. Fragility curves for 3-story buildings obtained from MSA (IM: Sa and EDP: MIDR).

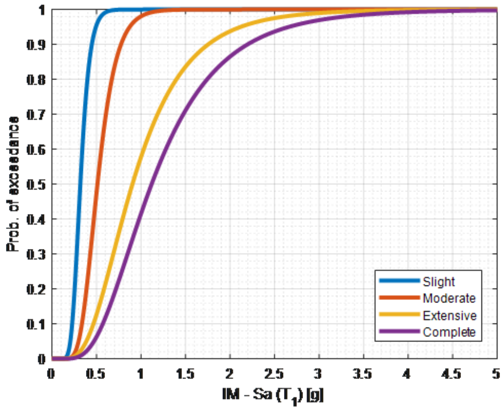

(a) 6-story 1975 in x-direction

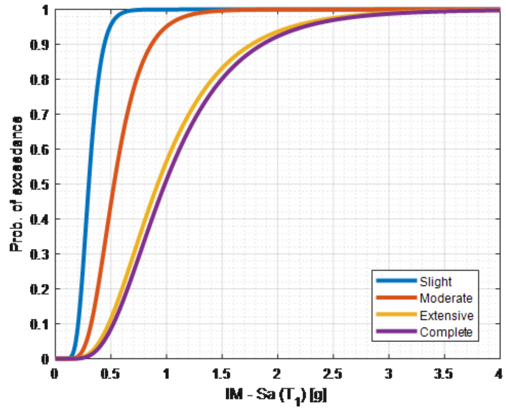

(b) 6-story 1975 in y-direction

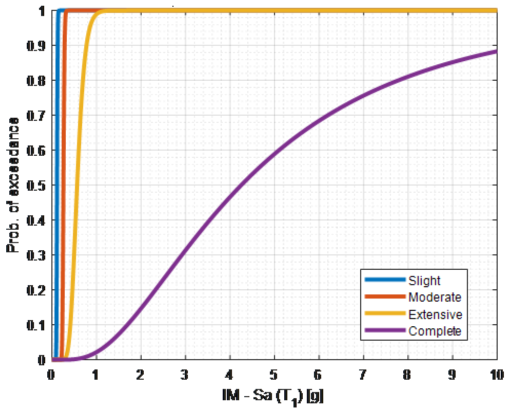

(c) 6-story 2018 in x-direction

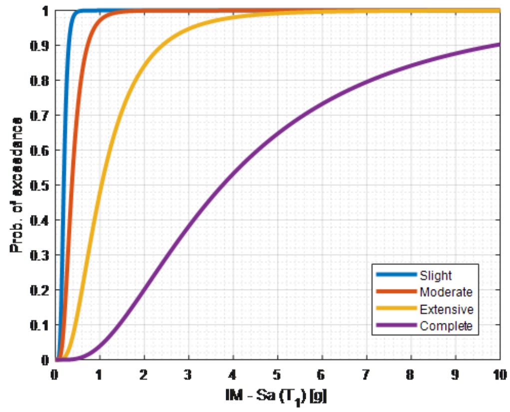

(d) 6-story 2018 in y-direction

Figure 4.40. Fragility curves for 6-story buildings obtained from MSA (IM: Sa and EDP: MIDR).

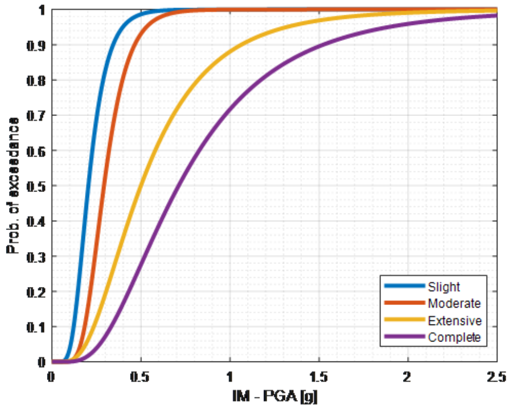

(a) 3-story 1975 in x-direction

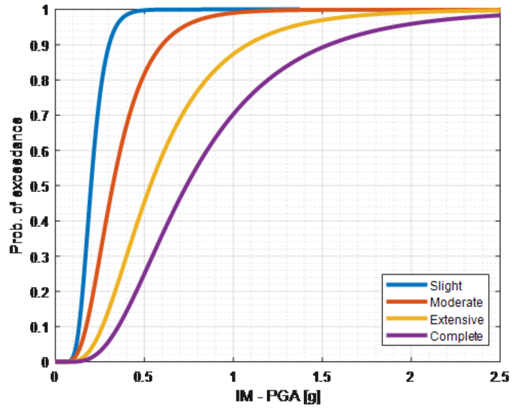

(b) 3-story 1975 in y-direction

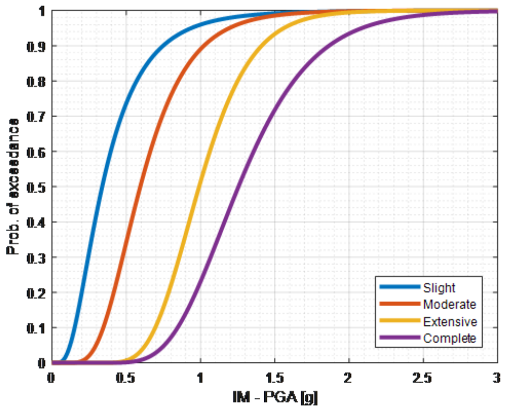

(c) 3-story 2018 in x-direction

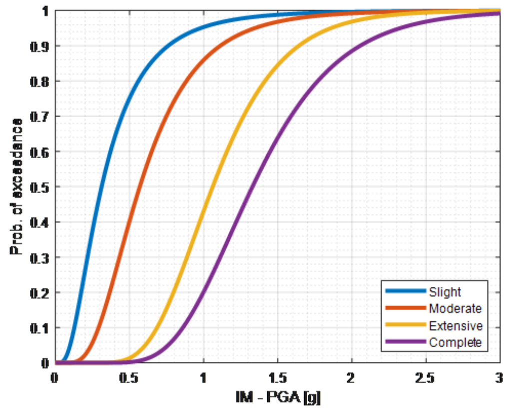

(d) 3-story 2018 in y-direction

Figure 4.41. Fragility curves for 3-story buildings obtained from MSA (IM: PGA and EDP: MIDR).

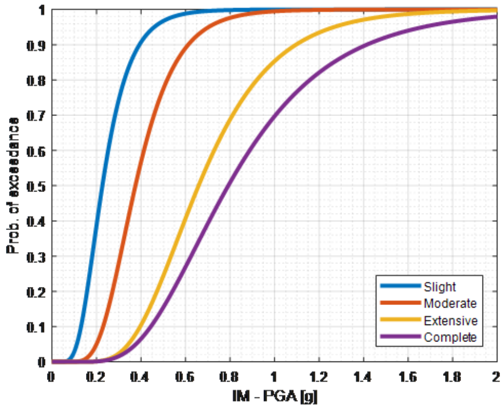

(a) 6-story 1975 in x-direction

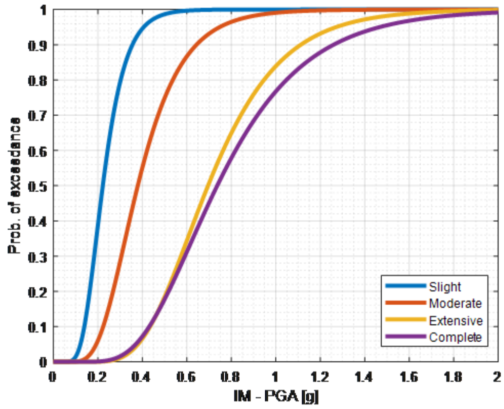

(b) 6-story 1975 in y-direction

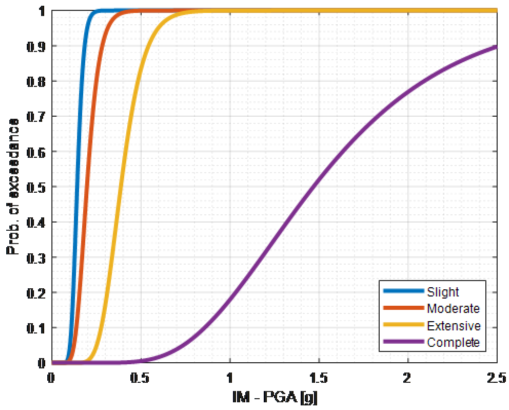

(c) 6-story 2018 in x-direction

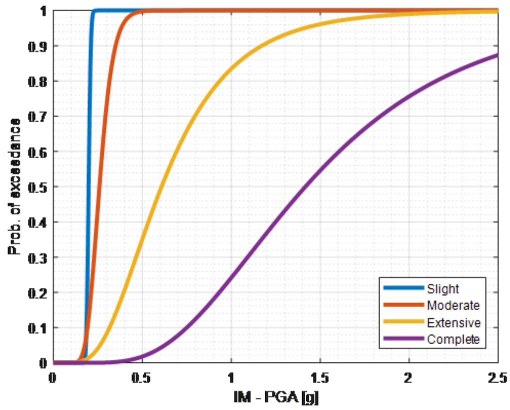

(d) 6-story 2018 in y-direction

Figure 4.42. Fragility curves for 6-story buildings obtained from MSA (IM: PGA and EDP: MIDR).

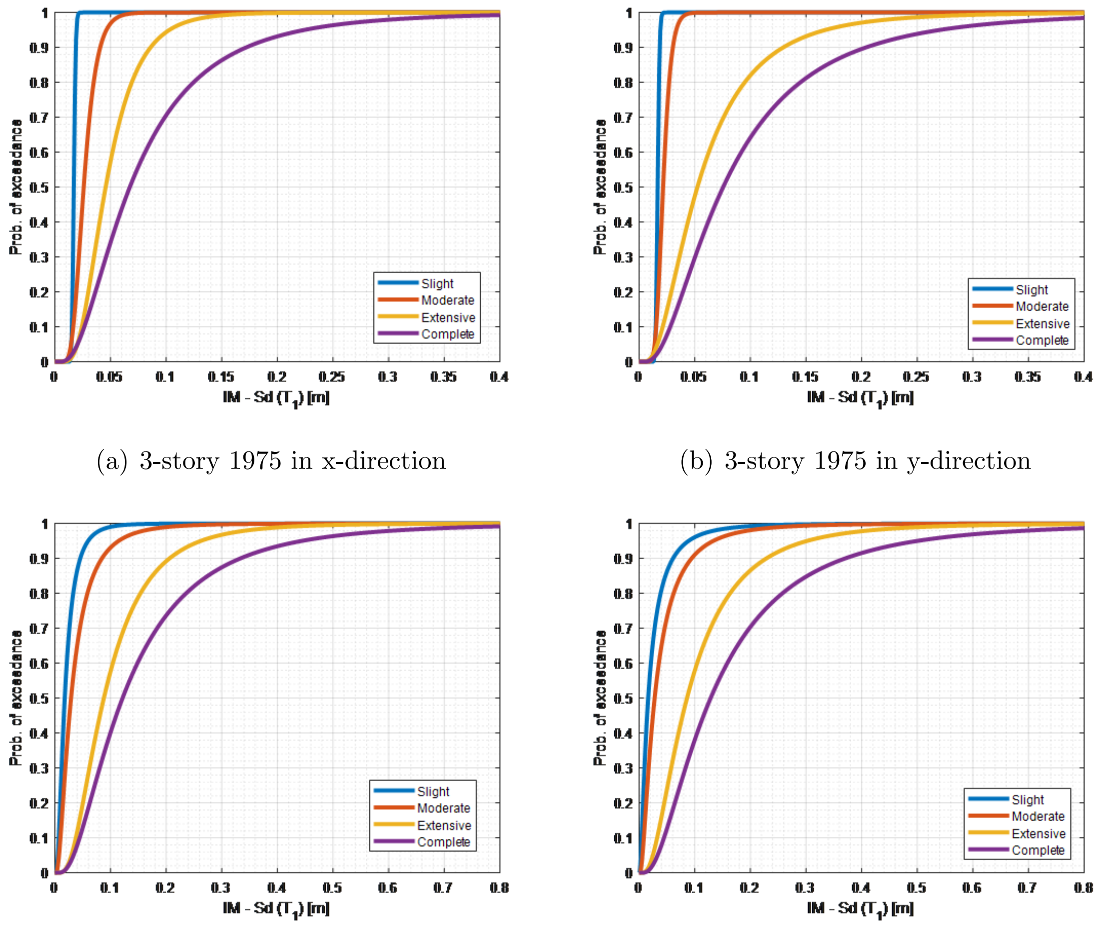

(a) 3-story 1975 in x-direction

(b) 3-story 1975 in y-direction

(c) 3-story 2018 in x-direction

(d) 3-story 2018 in y-direction

Figure 4.43. Fragility curves for 3-story buildings obtained from MSA (IM: Sd and EDP: Dtop).

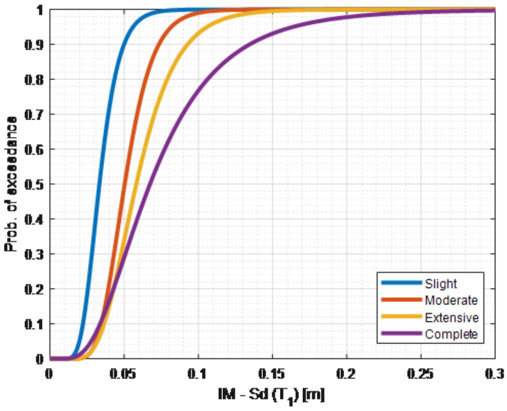

(a) 6-story 1975 in x-direction

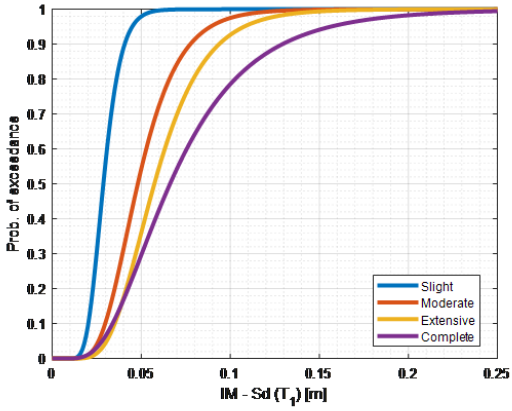

(b) 6-story 1975 in y-direction

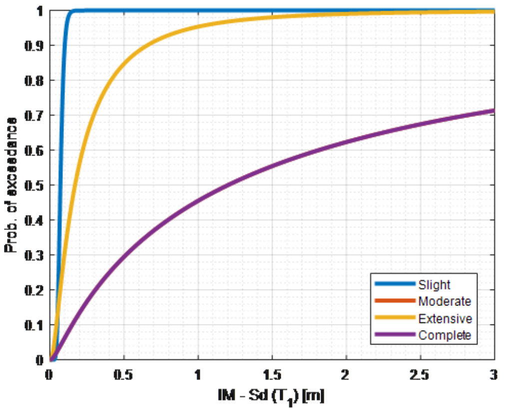

(c) 6-story 2018 in x-direction

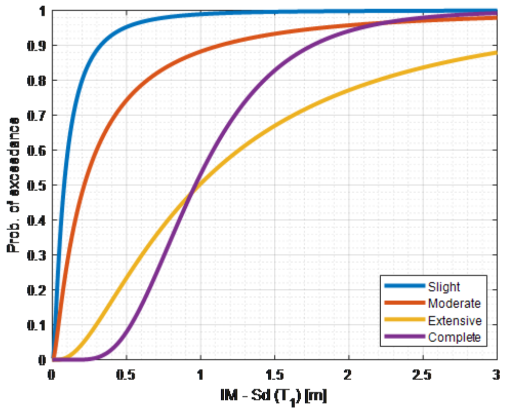

(d) 6-story 2018 in y-direction

Figure 4.44. Fragility curves for 6-story buildings obtained from MSA (IM: Sd and EDP: Dtop).

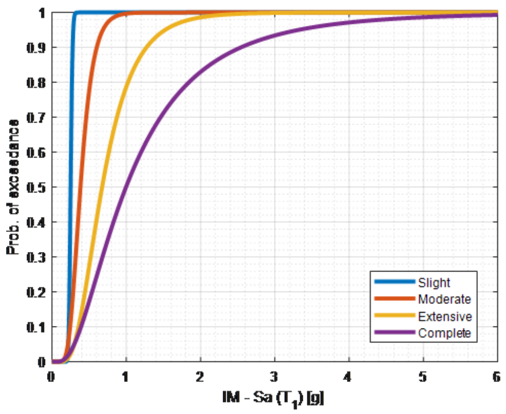

(a) 3-story 1975 in x-direction

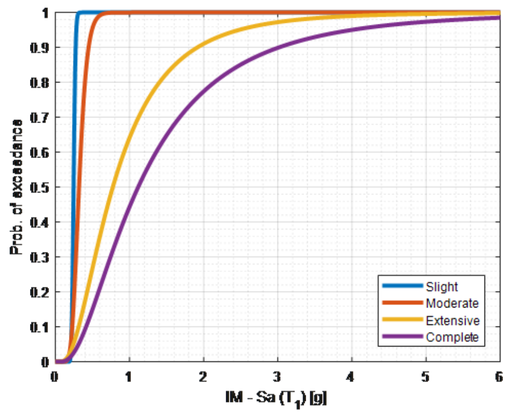

(b) 3-story 1975 in y-direction

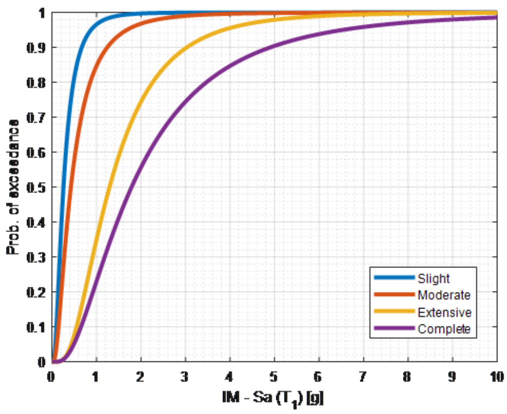

(c) 3-story 2018 in x-direction

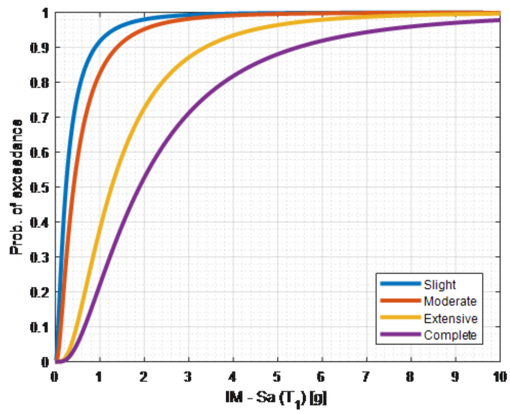

(d) 3-story 2018 in y-direction

Figure 4.45. Fragility curves for 3-story buildings obtained from MSA (IM: Sa and EDP: Dtop).

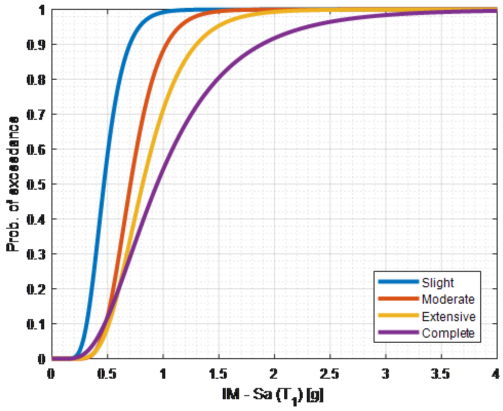

(a) 6-story 1975 in x-direction

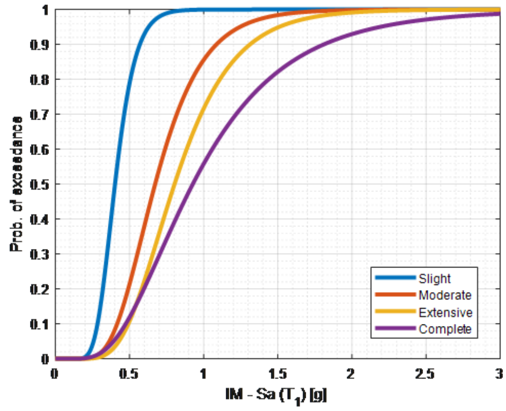

(b) 6-story 1975 in y-direction

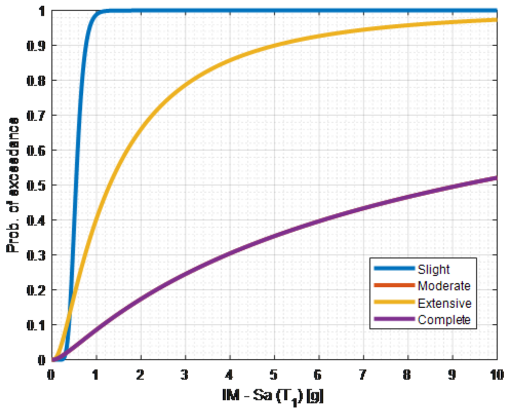

(c) 6-story 2018 in x-direction

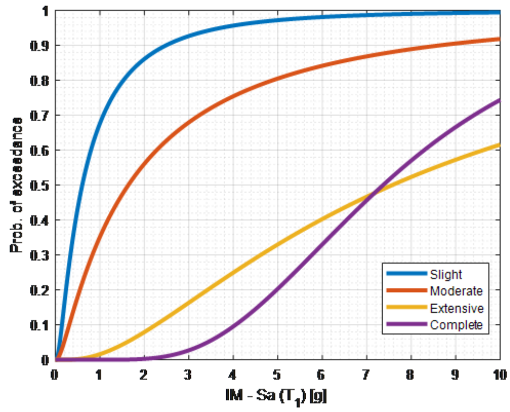

(d) 6-story 2018 in y-direction

Figure 4.46. Fragility curves for 6-story buildings obtained from MSA (IM: Sa and EDP: Dtop).

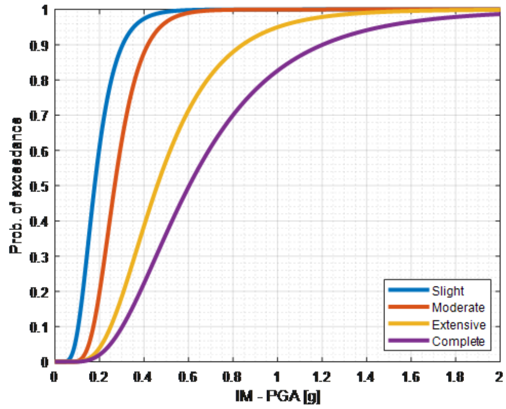

(a) 3-story 1975 in x-direction

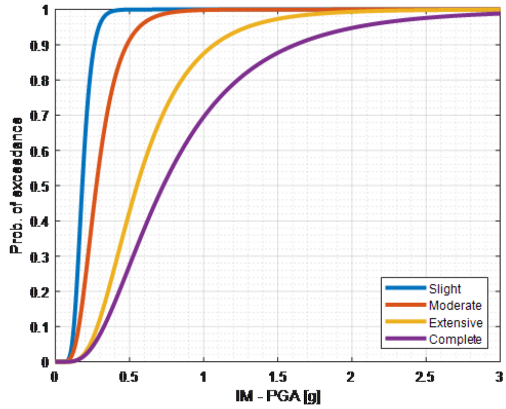

(b) 3-story 1975 in y-direction

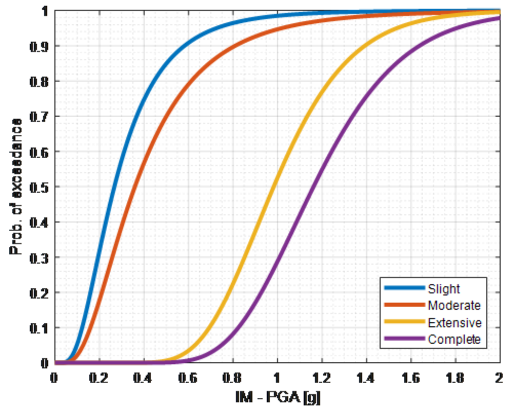

(c) 3-story 2018 in x-direction

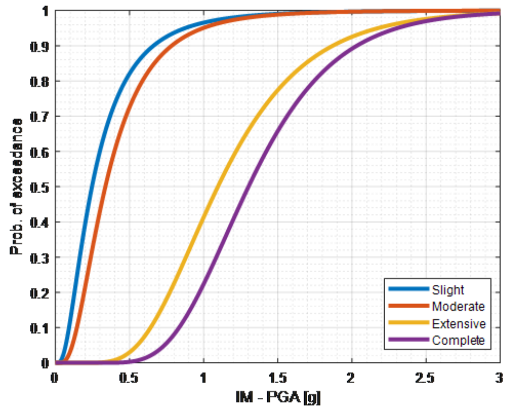

(d) 3-story 2018 in y-direction

Figure 4.47. Fragility curves for 3-story buildings obtained from MSA (IM: PGA and EDP: Dtop).

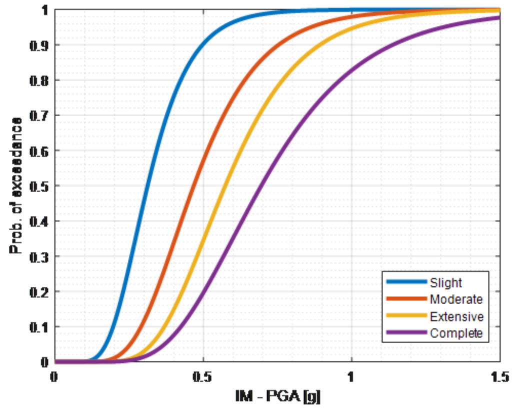

(a) 6-story 1975 in x-direction

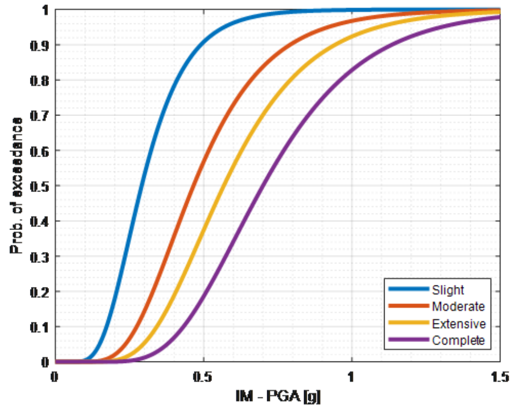

(b) 6-story 1975 in y-direction

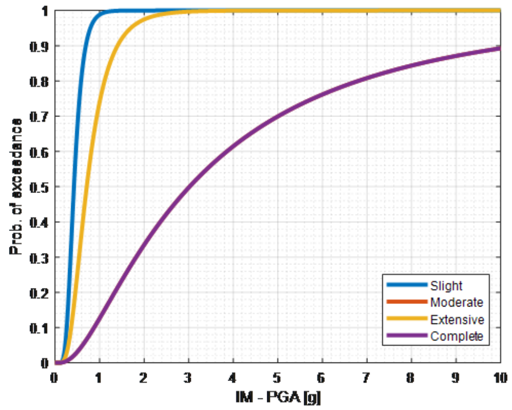

(c) 6-story 2018 in x-direction

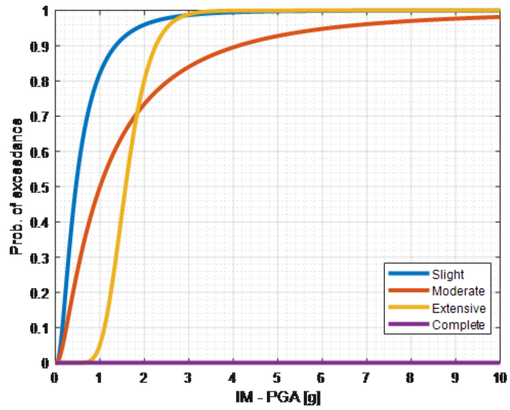

(d) 6-story 2018 in y-direction

Figure 4.48. Fragility curves for 6-story buildings obtained from MSA (IM: PGA and EDP: Dtop).

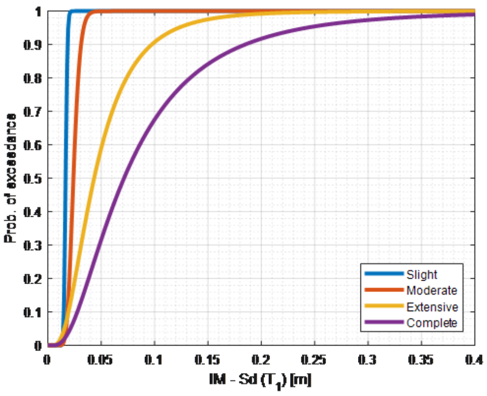

(a) 3-story 1975

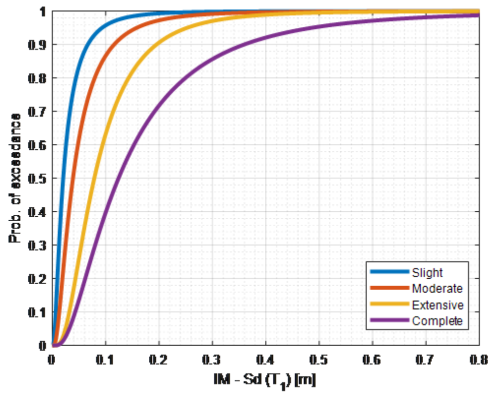

(b) 3-story 2018

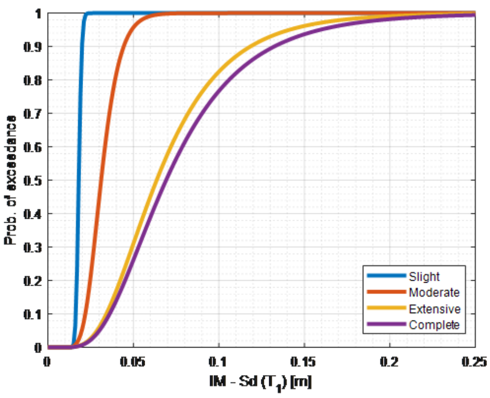

(c) 6-story 1975

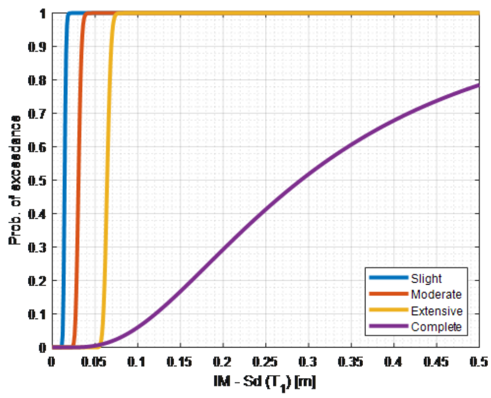

(d) 6-story 2018

Figure 4.49. Direction-free fragility curves for all buildings obtained from MSA (IM: Sd and EDP: MIDR).

Table 4.1. Parameters of direction-free fragility curves obtained from MSA (EDP = MIDR, IM = Sd(m). (Θ=Sd[m], β=In(Sd[m]))

Building Type	**Slight**		**Moderate**		**Extensive**		**Complete**	
	Θ	β	Θ	β	Θ	β	Θ	β
3-1975	0.0166	0.0841	0.0239	0.2049	0.0433	0.6319	0.0713	0.7430
3-2018	0.0202	0.9290	0.0385	0.8578	0.0785	0.7096	0.1238	0.8307
6-1975	0.0180	0.0784	0.0311	0.2759	0.0635	0.4858	0.0691	0.5071
6-2018	0.0143	0.0976	0.0306	0.0902	0.0641	0.0564	0.2907	0.6871

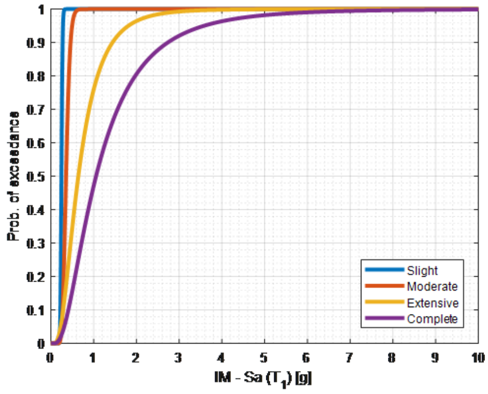

(a) 3-story 1975

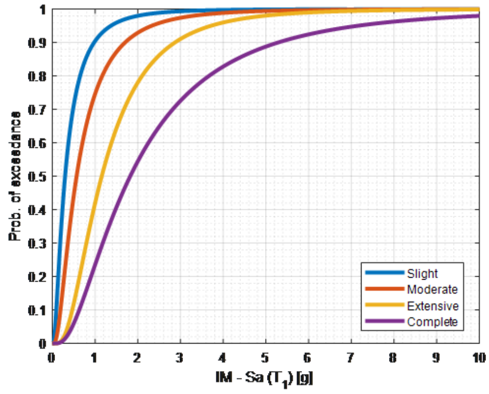

(b) 3-story 2018

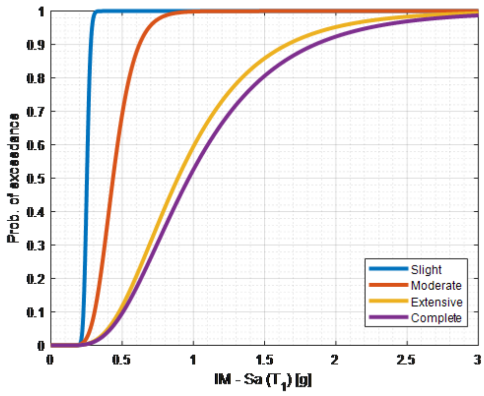

(c) 6-story 1975

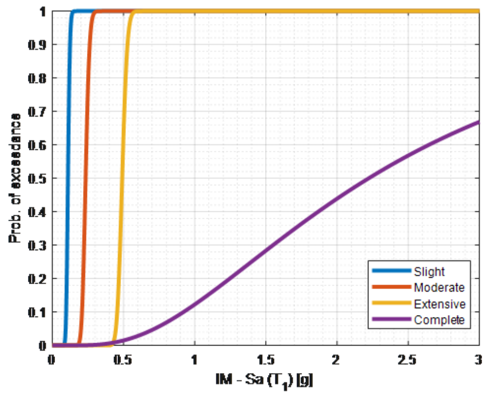

(d) 6-story 2018

Figure 4.50. Direction-free fragility curves for all buildings obtained from MSA (IM: Sa and EDP: MIDR).

Table 4.2. Parameters of direction-free fragility curves obtained from MSA (EDP = MIDR, IM = Sa(g). (Θ=Sa[g], β=In(Sa[g]))

Building Type	**Slight**		**Moderate**		**Extensive**		**Complete**	
	Θ	β	Θ	β	Θ	β	Θ	β
3-1975	0.2452	0.0851	0.3535	0.2049	0.6404	0.6319	1.0545	0.7430
3-2018	0.2969	0.9291	0.5666	0.8578	1.1551	0.7095	1.8219	0.8306
6-1975	0.2523	0.0803	0.4356	0.2760	0.8902	0.4851	0.9676	0.5071
6-2018	0.1093	0.0982	0.2336	0.0909	0.4901	0.0576	2.2223	0.6871

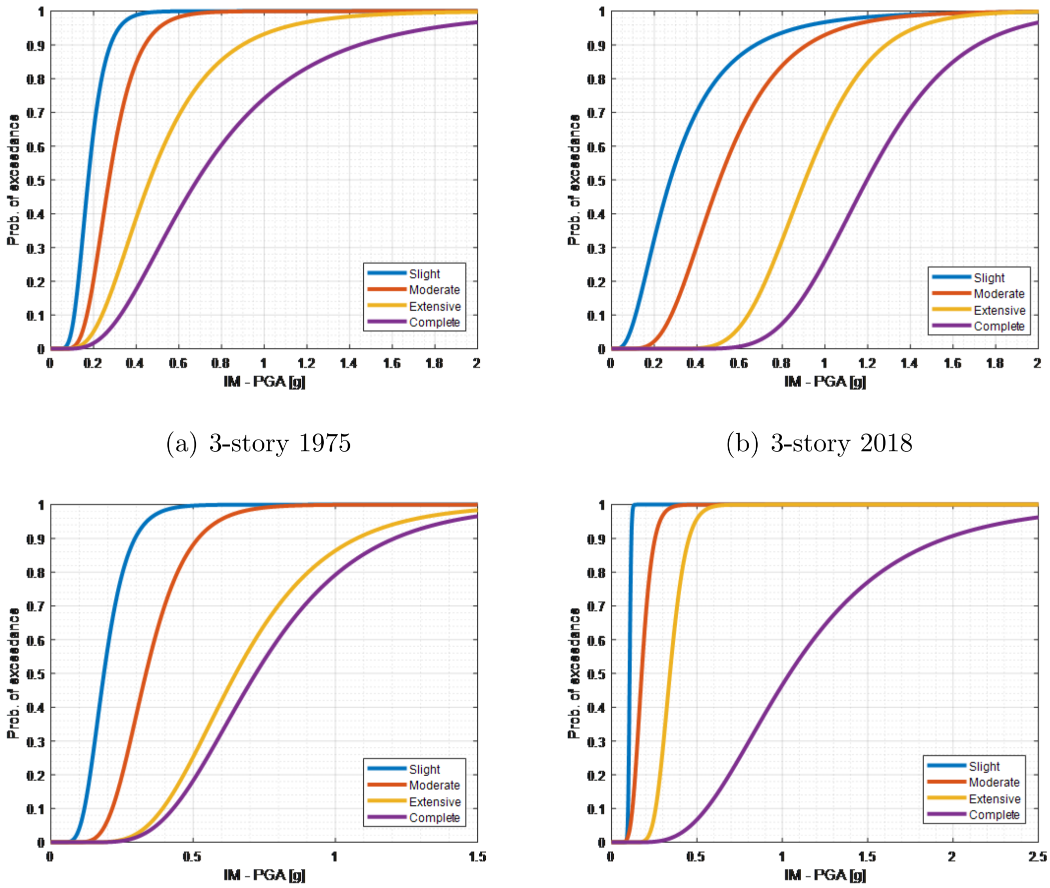

(a) 3-story 1975 (b) 3-story 2018

(c) 6-story 1975 (d) 6-story 2018

Figure 4.51. Direction-free fragility curves for all buildings obtained from MSA (IM: PGA and EDP: MIDR).

Table 4.3. Parameters of direction-free fragility curves obtained from MSA (EDP = MIDR, IM = PGA(g). (Θ=PGA[g], β=In(PGA[g]))

Building Type	**Slight**		**Moderate**		**Extensive**		**Complete**	
	Θ	β	Θ	β	Θ	β	Θ	β
3-1975	0.1748	0.3658	0.2725	0.3745	0.4637	0.5151	0.6862	0.5810
3-2018	0.2748	0.7006	0.5058	0.4628	0.9070	0.2731	1.1970	0.2804
6-1975	0.1865	0.3594	0.3341	0.3414	0.6497	0.3929	0.7202	0.4030
6-2018	0.2074	0.0727	0.3764	0.2872	0.7751	0.2201	1.0884	0.4913

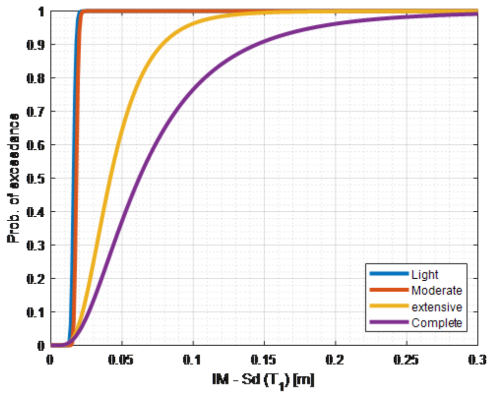

(a) 3-story 1975

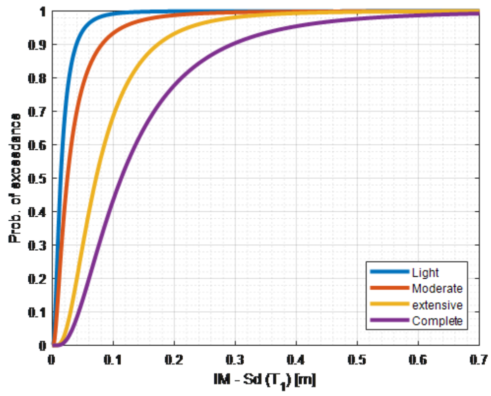

(b) 3-story 2018

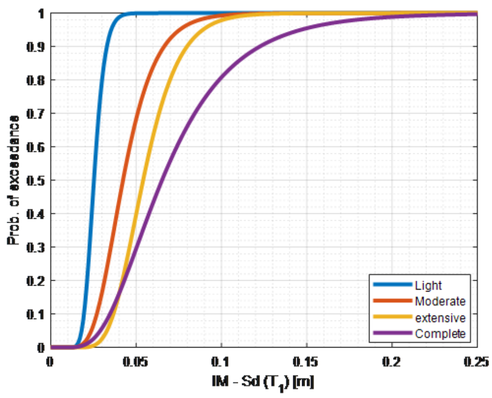

(c) 6-story 1975

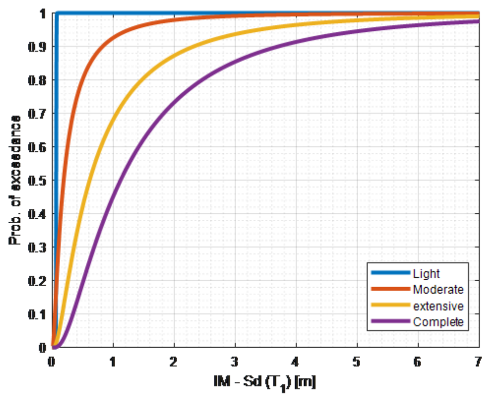

(d) 6-story 2018

Figure 4.52. Direction-free fragility curves for all buildings obtained from MSA (IM: Sd and EDP: Dtop).

Table 4.4. Parameters of direction-free fragility curves obtained from MSA (EDP = Dtop, IM = Sd(m). (Θ=Sd[m], β=In(Sd[m]))

Building Type	**Slight**		**Moderate**		**Extensive**		**Complete**	
	Θ	β	Θ	β	Θ	β	Θ	β
3-1975	0.0160	0.0878	0.0179	0.0739	0.0417	0.4906	0.0620	0.6598
3-2018	0.0136	0.8278	0.0245	0.9323	0.0715	0.6879	0.1127	0.7481
6-1975	0.0252	0.2049	0.0423	0.3520	0.0541	0.3033	0.0651	0.4925
6-2018	0.0618	0.0631	0.1846	1.1653	0.6108	1.0393	1.1170	0.9343

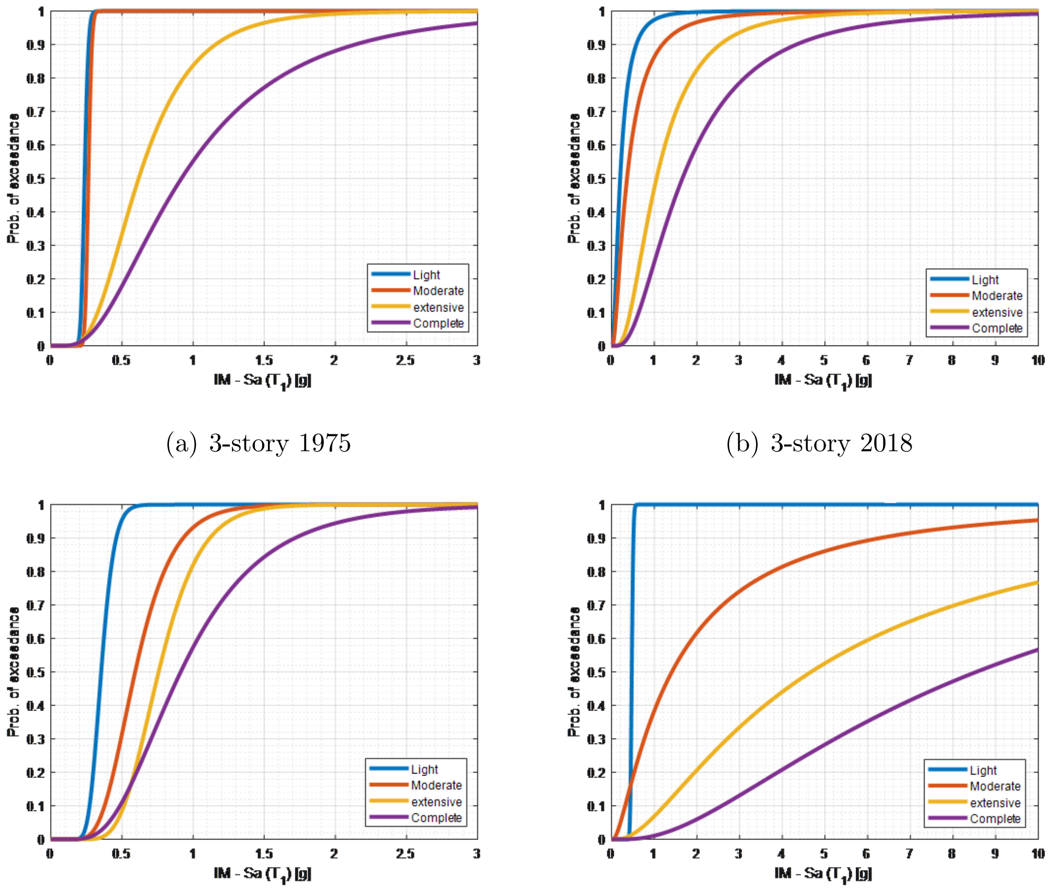

(a) 3-story 1975

(b) 3-story 2018

(c) 6-story 1975

(d) 6-story 2018

Figure 4.53. Direction-free fragility curves for all buildings obtained from MSA (IM: Sa and EDP: Dtop).

Table 4.5. Parameters of direction-free fragility curves obtained from MSA (EDP = Dtop, IM = Sa(g). (Θ=Sa[g], β=In(Sa[g]))

Building Type	**Slight**		**Moderate**		**Extensive**		**Complete**	
	Θ	β	Θ	β	Θ	β	Θ	β
3-1975	0.2368	0.0897	0.2637	0.0712	0.6168	0.4906	0.9174	0.6598
3-2018	0.2001	0.8278	0.3604	0.9322	1.0518	0.6879	1.6582	0.7481
6-1975	0.3535	0.2049	0.5922	0.3519	0.7574	0.3032	0.9122	4925
6-2018	0.4725	0.0622	1.4112	1.1653	4.6700	1.0394	8.5401	0.9343

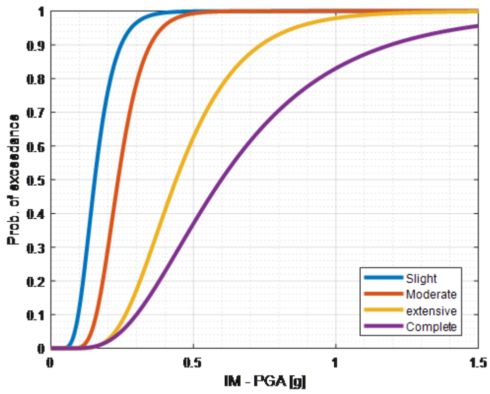

(a) 3-story 1975

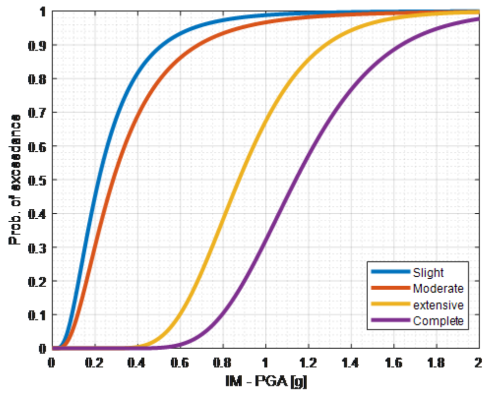

(b) 3-story 2018

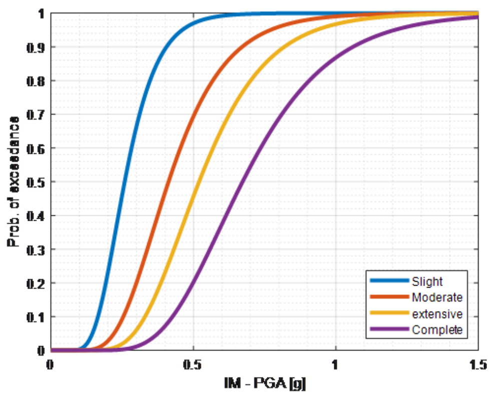

(c) 6-story 1975

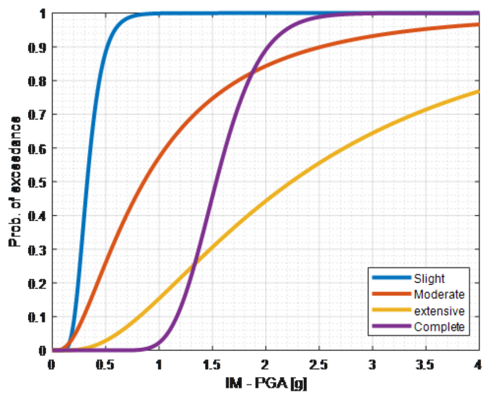

(d) 6-story 2018

Figure 4.54. Direction-free fragility curves for all buildings obtained from MSA (IM: PGA and EDP: Dtop).

Table 4.6. Parameters of direction-free fragility curves obtained from MSA (EDP = Dtop, IM = PGA(g). (Θ=PGA[g], β=In(PGA[g]))

Building Type	**Slight**		**Moderate**		**Extensive**		**Complete**	
	Θ	β	Θ	β	Θ	β	Θ	β
3-1975	0.1536	0.3680	0.2356	0.3062	0.4391	0.4041	0.5979	0.5383
3-2018	0.2170	0.6759	0.2845	0.6849	0.8740	0.2978	1.1395	0.2816
6-1975	0.2587	0.3507	0.4127	0.3793	0.5198	0.3547	0.6724	0.3552
6-2018	0.3260	0.3554	0.8574	0.8404	2.2388	0.7902	1.5347	0.2147

4.4. Development of Fragility Functions for the Buildings using the Cloud Analyses Results

By using the Cloud Analysis' results (Figures 4.19 to 4.36) , the fragility functions are developed for the 3-story and 6-story buildings. The fragility curves and the fragility parameters' values are given in Figures 4.55 to 4.72 and Tables 4.7 to 4.12.

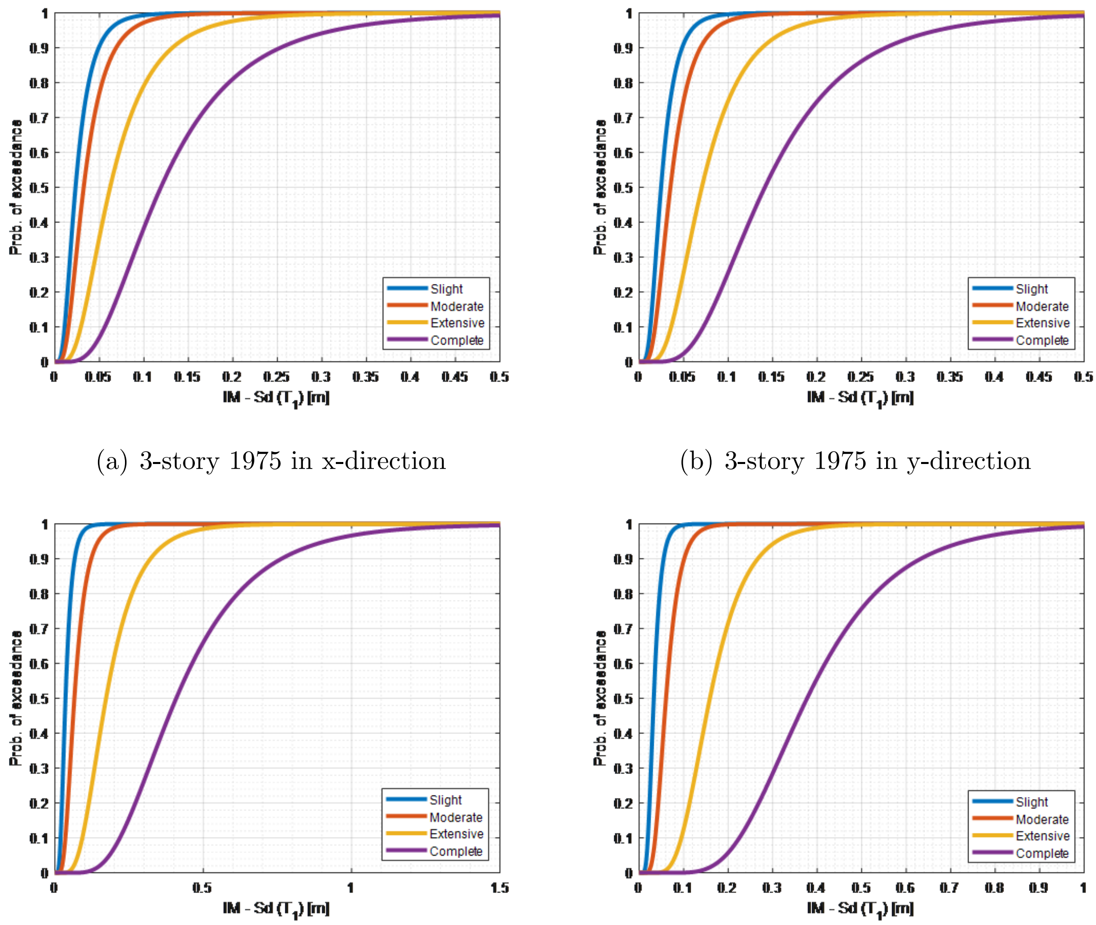

(a) 3-story 1975 in x-direction

(b) 3-story 1975 in y-direction

(c) 3-story 2018 in x-direction

(d) 3-story 2018 in y-direction

Figure 4.55. Fragility curves for 3-story buildings obtained from cloud analyses (IM: Sd and EDP: MIDR).

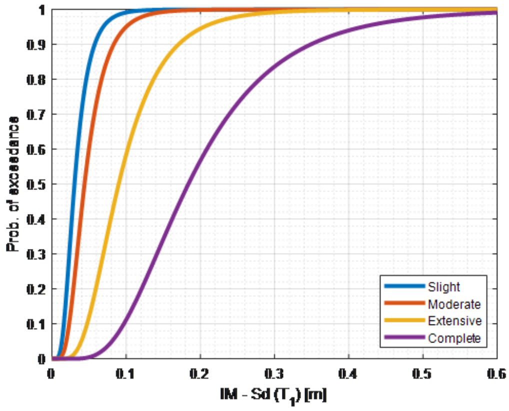

(a) 6-story 1975 in x-direction

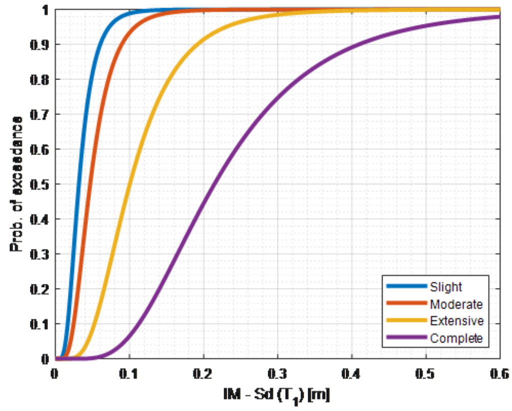

(b) 6-story 1975 in y-direction

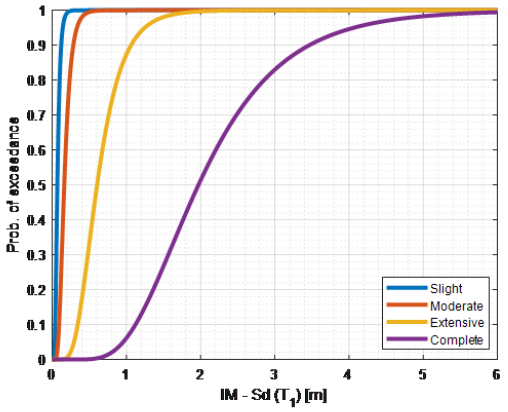

(c) 6-story 2018 in x-direction

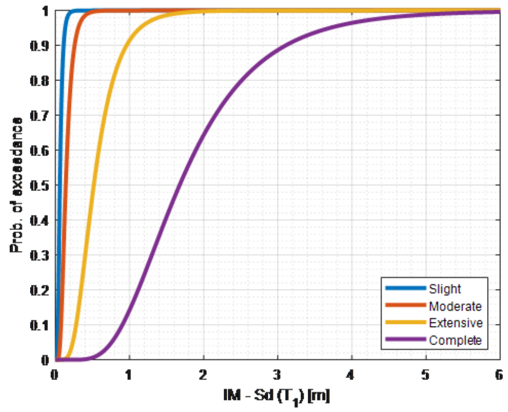

(d) 6-story 2018 in y-direction

Figure 4.56. Fragility curves for 6-story buildings obtained from cloud analyses (IM: Sd and EDP: MIDR).

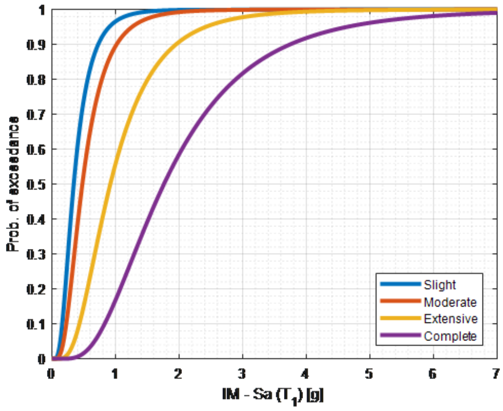

(a) 3-story 1975 in x-direction

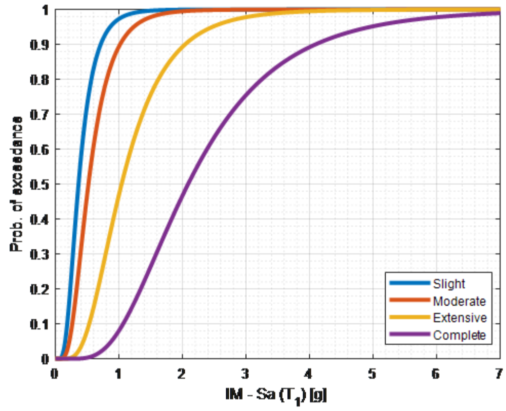

(b) 3-story 1975 in y-direction

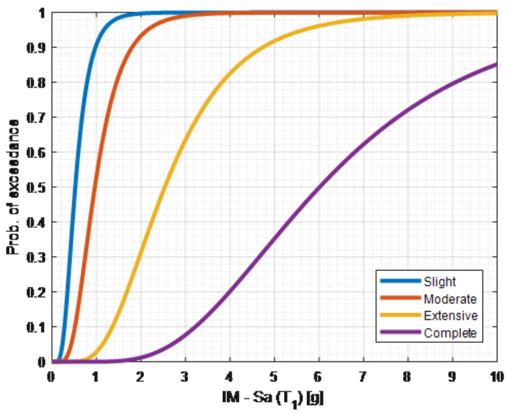

(c) 3-story 2018 in x-direction

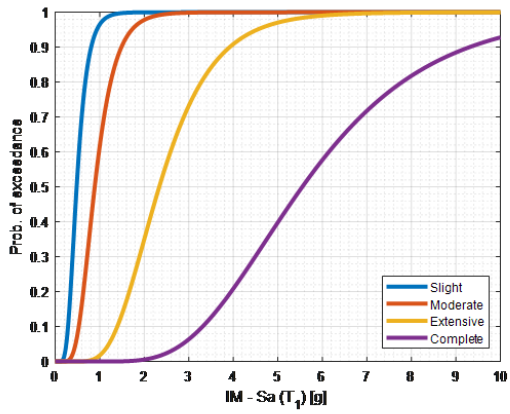

(d) 3-story 2018 in y-direction

Figure 4.57. Fragility curves for 3-story buildings obtained from cloud analyses (IM: Sa and EDP: MIDR).

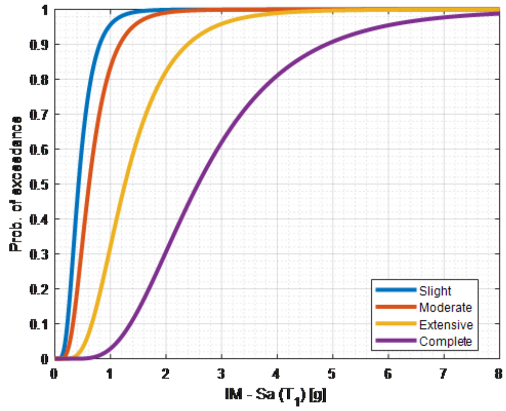

(a) 6-story 1975 in x-direction

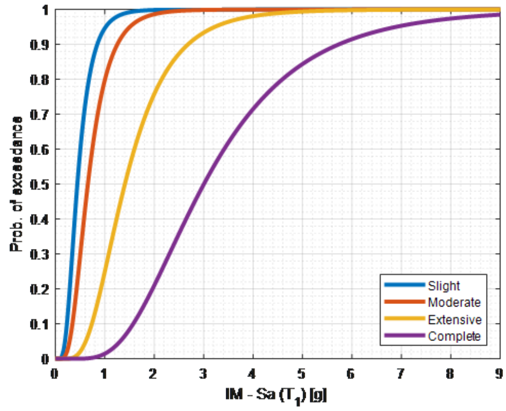

(b) 6-story 1975 in y-direction

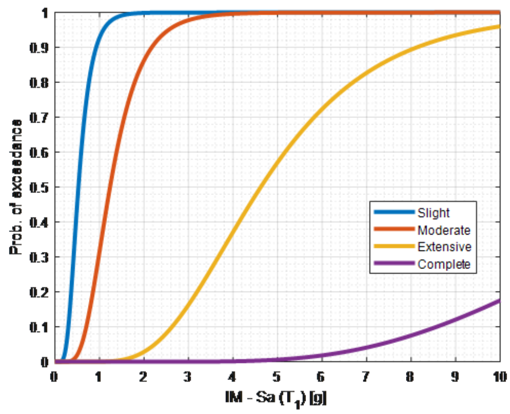

(c) 6-story 2018 in x-direction

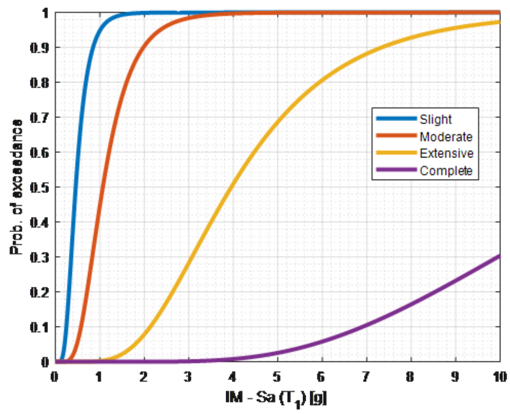

(d) 6-story 2018 in y-direction

Figure 4.58. Fragility curves for 6-story buildings obtained from cloud analyses (IM: Sa and EDP: MIDR).

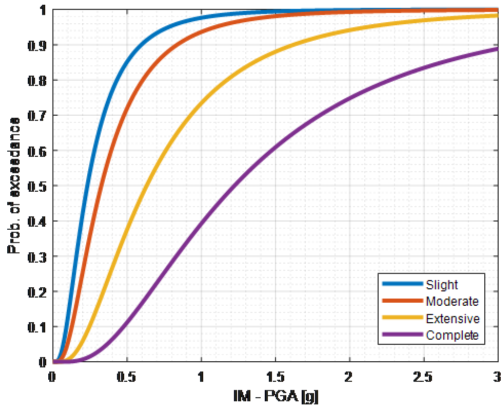

(a) 3-story 1975 in x-direction

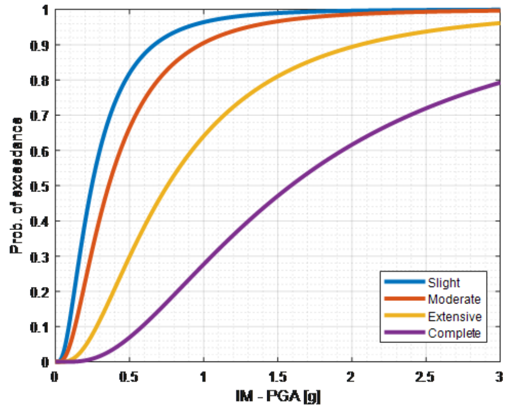

(b) 3-story 1975 in y-direction

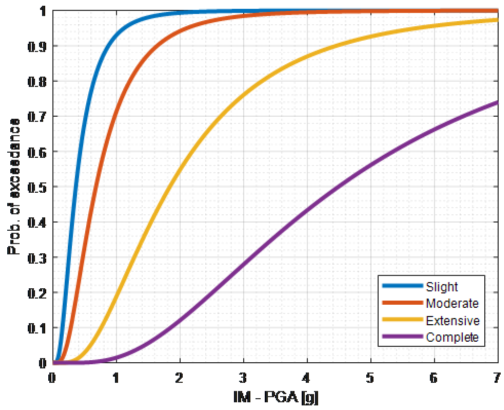

(c) 3-story 2018 in x-direction

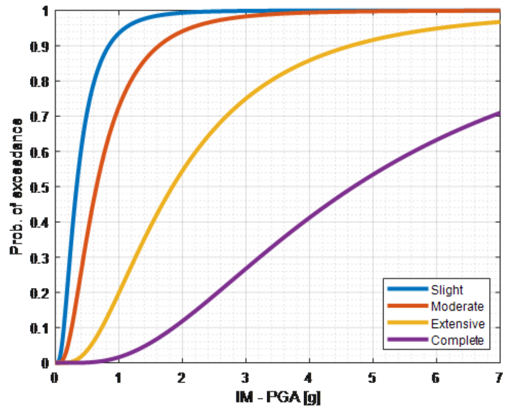

(d) 3-story 2018 in y-direction

Figure 4.59. Fragility curves for 3-story buildings obtained from cloud analyses (IM: PGA and EDP: MIDR).

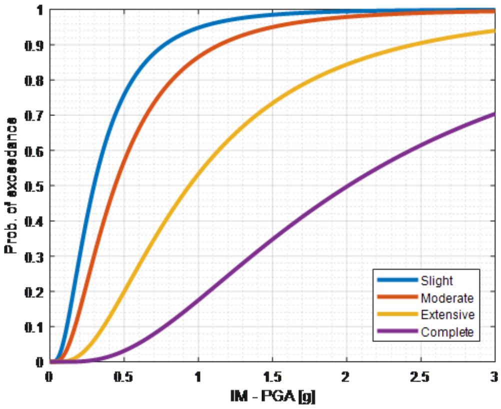

(a) 6-story 1975 in x-direction

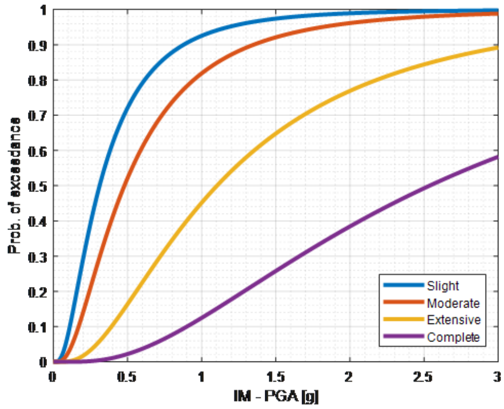

(b) 6-story 1975 in y-direction

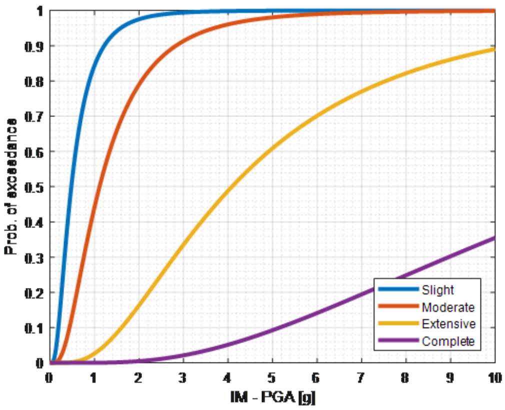

(c) 6-story 2018 in x-direction

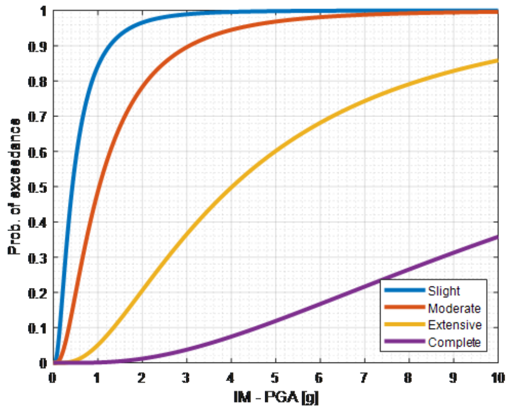

(d) 6-story 2018 in y-direction

Figure 4.60. Fragility curves for 6-story buildings obtained from cloud analyses (IM: PGA and EDP: MIDR).

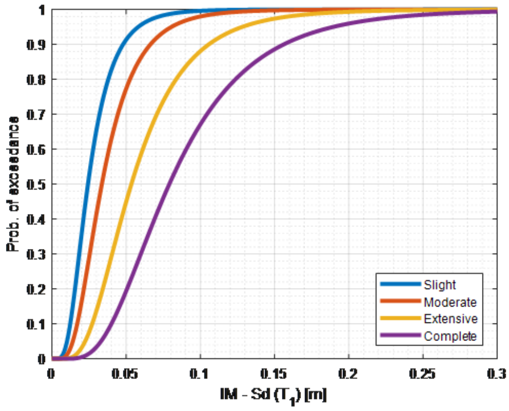

(a) 3-story 1975 in x-direction

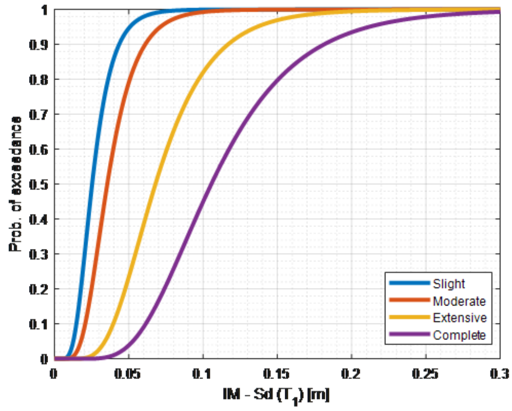

(b) 3-story 1975 in y-direction

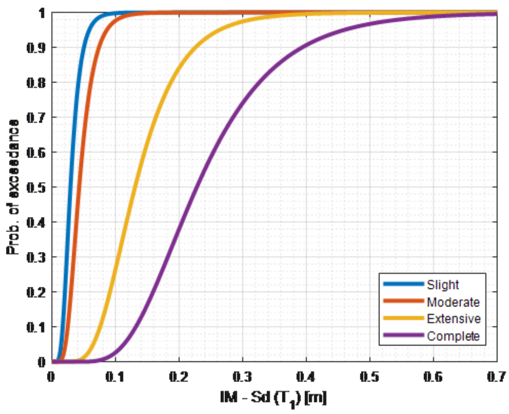

(c) 3-story 2018 in x-direction

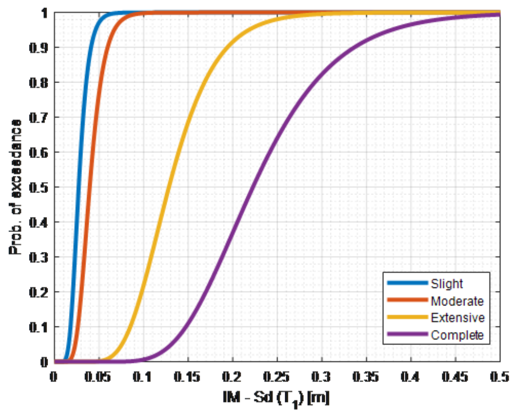

(d) 3-story 2018 in y-direction

Figure 4.61. Fragility curves for 3-story buildings obtained from cloud analyses (IM: Sd and EDP: Dtop).

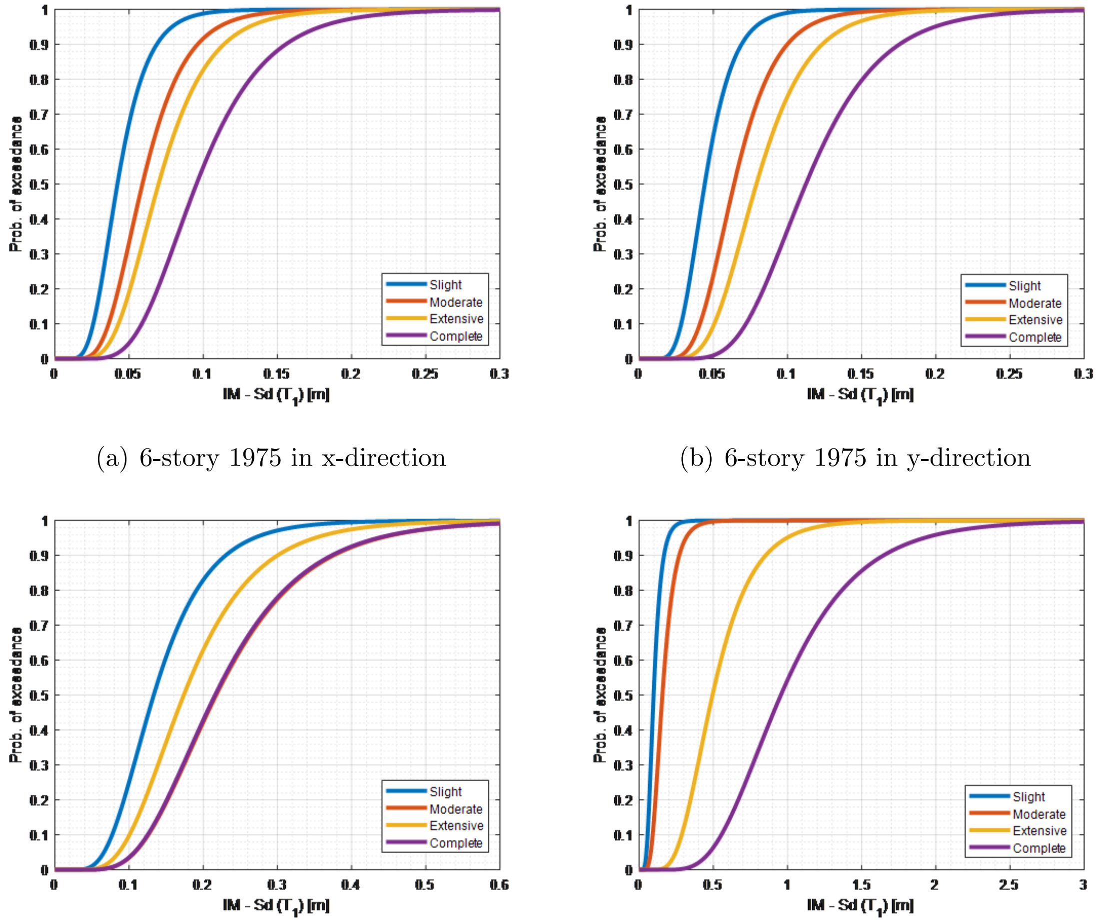

(a) 6-story 1975 in x-direction

(b) 6-story 1975 in y-direction

(c) 6-story 2018 in x-direction

(d) 6-story 2018 in y-direction

Figure 4.62. Fragility curves for 6-story buildings obtained from cloud analyses (IM: Sd and EDP: Dtop).

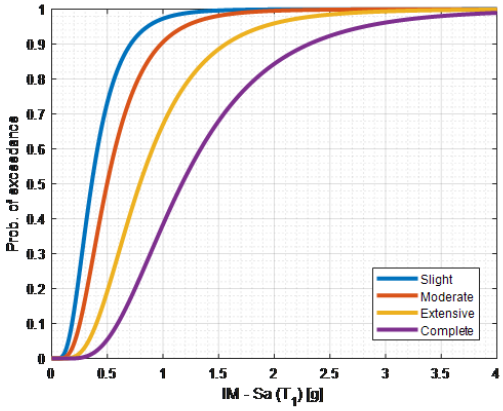

(a) 3-story 1975 in x-direction

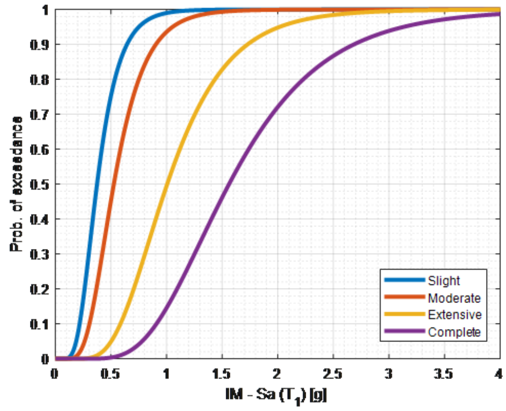

(b) 3-story 1975 in y-direction

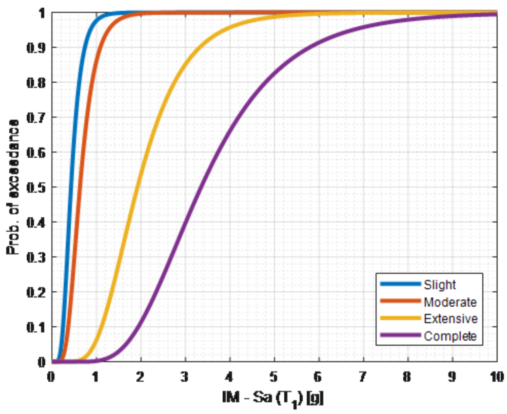

(c) 3-story 2018 in x-direction

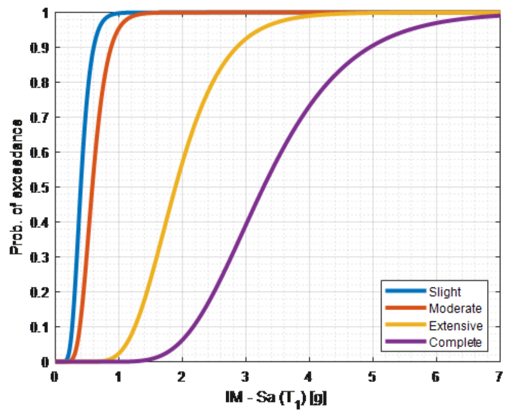

(d) 3-story 2018 in y-direction

Figure 4.63. Fragility curves for 3-story buildings obtained from cloud analyses (IM: Sa and EDP: Dtop).

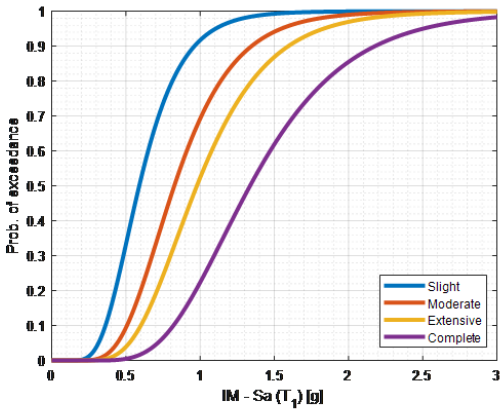

(a) 6-story 1975 in x-direction

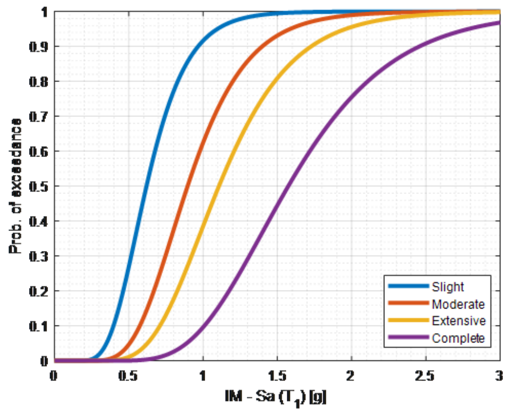

(b) 6-story 1975 in y-direction

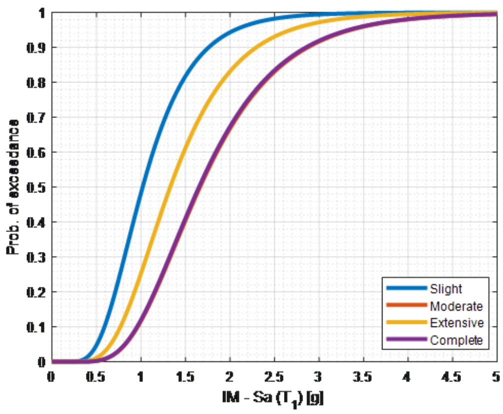

(c) 6-story 2018 in x-direction

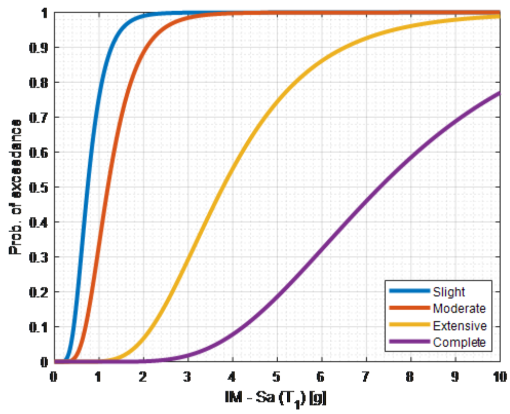

(d) 6-story 2018 in y-direction

Figure 4.64. Fragility curves for 6-story buildings obtained from cloud analyses (IM: Sa and EDP: Dtop).

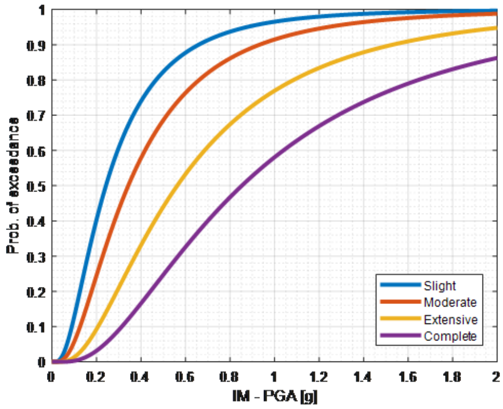

(a) 3-story 1975 in x-direction

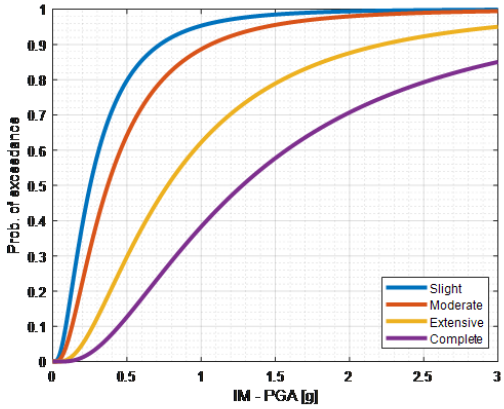

(b) 3-story 1975 in y-direction

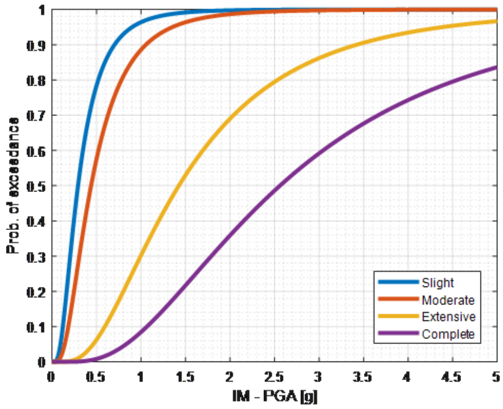

(c) 3-story 2018 in x-direction

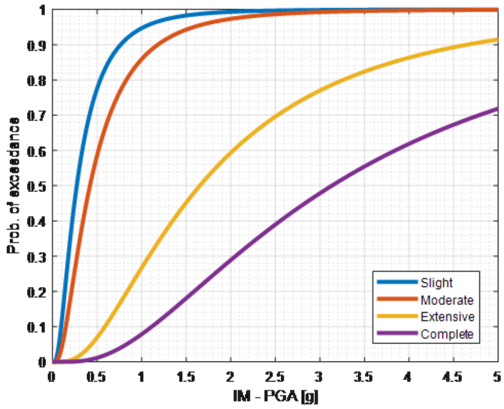

(d) 3-story 2018 in y-direction

Figure 4.65. Fragility curves for 3-story buildings obtained from cloud analyses (IM: PGA and EDP: Dtop).

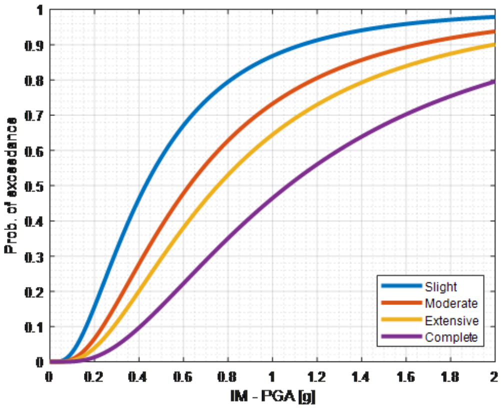

(a) 6-story 1975 in x-direction

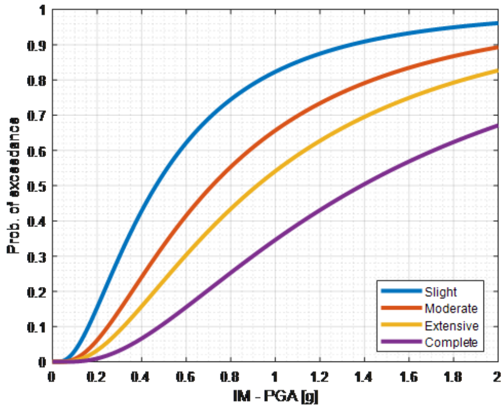

(b) 6-story 1975 in y-direction

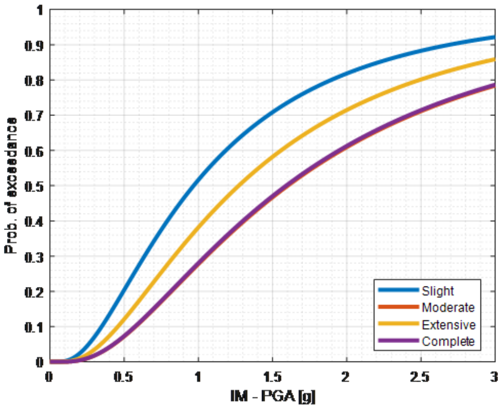

(c) 6-story 2018 in x-direction

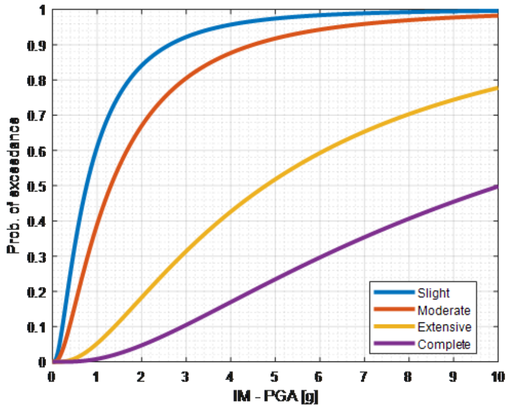

(d) 6-story 2018 in y-direction

Figure 4.66. Fragility curves for 6-story buildings obtained from cloud analyses (IM: PGA and EDP: Dtop).

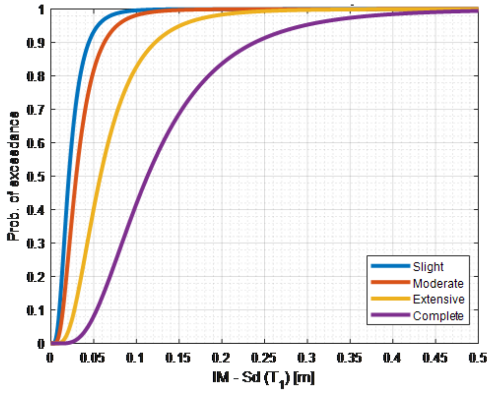

(a) 3-story 1975

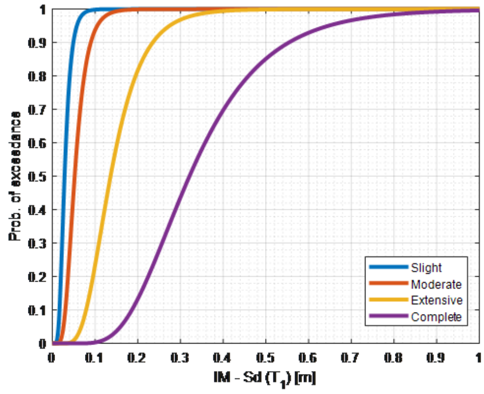

(b) 3-story 2018

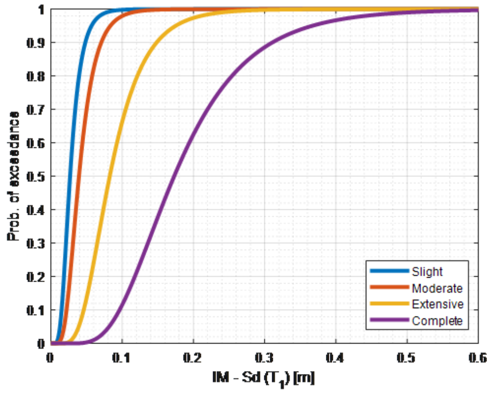

(c) 6-story 1975

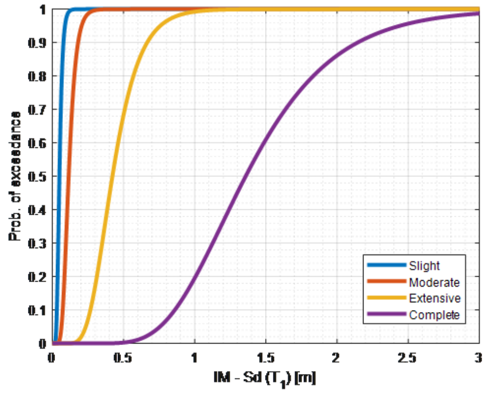

(d) 6-story 2018

Figure 4.67. Direction-free fragility curves for all buildings obtained from cloud analyses (IM: Sd and EDP: MIDR).

Table 4.7. Parameters of direction-free fragility curves obtained from cloud analyses (EDP = MIDR, IM = Sd(m). (Θ=Sd[m], β=In(Sd[m]))

Building Type	**Slight**		**Moderate**		**Extensive**		**Complete**	
	Θ	β	Θ	β	Θ	β	Θ	β
3-1975	0.0209	0.5830	0.0295	0.5830	0.0577	0.5830	0.1128	0.5830
3-2018	0.0284	0.4254	0.0521	0.4254	0.1361	0.4254	0.3209	0.4254
6-1975	0.0268	0.4569	0.0393	0.4569	0.0825	0.4569	0.1729	0.4569
6-2018	0.0491	0.3566	0.1143	0.3566	0.4215	0.3566	1.3577	0.3566

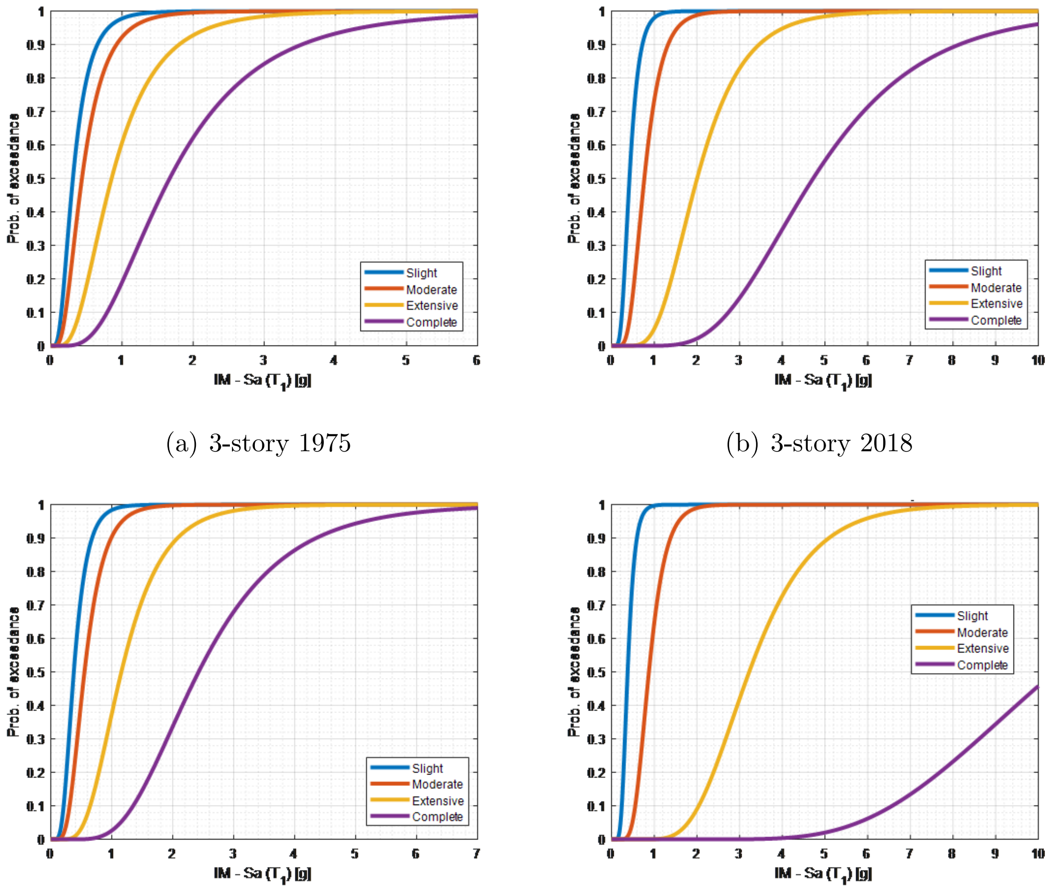

(a) 3-story 1975 (b) 3-story 2018

(c) 6-story 1975 (d) 6-story 2018

Figure 4.68. Direction-free fragility curves for all buildings obtained from cloud analyses (IM: Sa and EDP: MIDR).

Table 4.8. Parameters of direction-free fragility curves obtained from cloud analyses (EDP = MIDR, IM = Sa(g). (Θ=Sa[g], β=In(Sa[g]))

Building Type	**Slight**		**Moderate**		**Extensive**		**Complete**	
	Θ	β	Θ	β	Θ	β	Θ	β
3-1975	0.3096	0.5830	0.4367	0.5830	0.8538	0.5830	1.6695	0.5830
3-2018	0.4183	0.4254	0.7667	0.4254	2.0031	0.4254	4.7212	0.4254
6-1975	0.3759	0.4569	0.5507	0.4569	1.1559	0.4569	2.4219	0.4569
6-2018	0.3754	0.3566	0.8740	0.3566	3.2229	0.3566	10.3802	0.3566

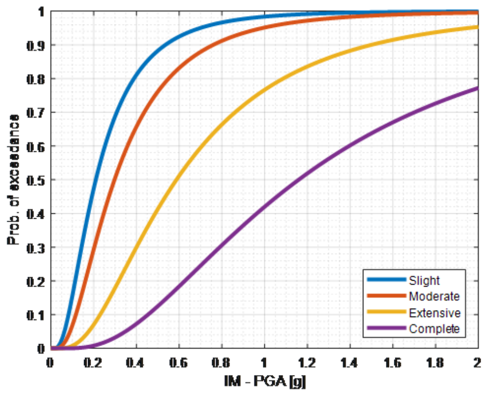

(a) 3-story 1975

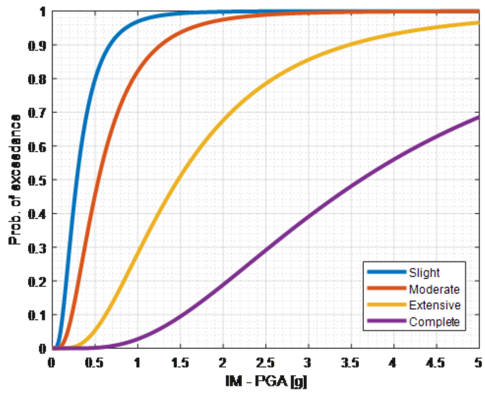

(b) 3-story 2018

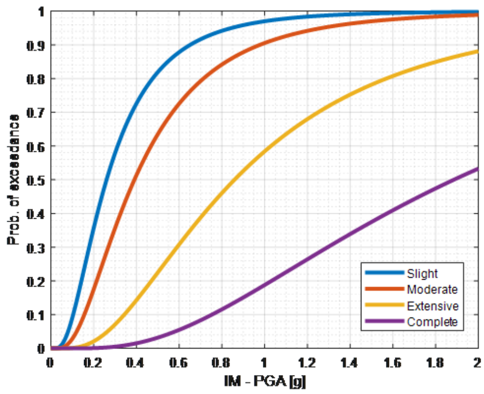

(c) 6-story 1975

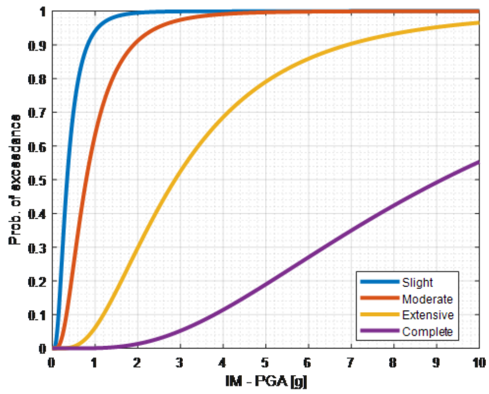

(d) 6-story 2018

Figure 4.69. Direction-free fragility curves for all buildings obtained from cloud analyses (IM: PGA and EDP: MIDR).

Table 4.9. Parameters of direction-free fragility curves obtained from cloud analyses (EDP = MIDR, IM = PGA(g). (Θ=PGA[g], β=In(PGA[g]))

Building Type	**Slight**		**Moderate**		**Extensive**		**Complete**	
	Θ	β	Θ	β	Θ	β	Θ	β
3-1975	0.2098	0.7314	0.2974	0.7314	0.5871	0.7314	1.1590	0.7314
3-2018	0.2856	0.6702	0.5386	0.6702	1.4724	0.6702	3.6133	0.6702
6-1975	0.2602	0.7161	0.3904	0.7161	0.8586	0.7161	1.8848	0.7161
6-2018	0.3436	0.6849	0.7918	0.6849	2.8734	0.6849	9.1232	0.6849

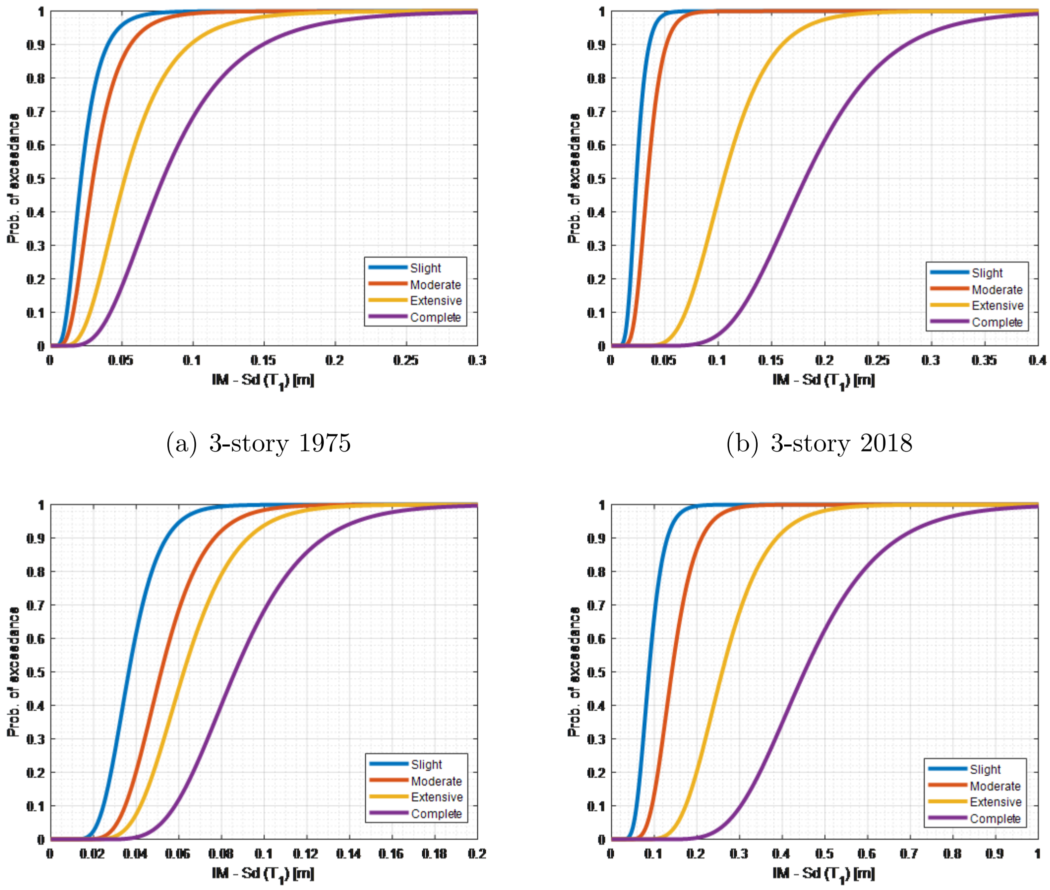

(a) 3-story 1975 (b) 3-story 2018

(c) 6-story 1975 (d) 6-story 2018

Figure 4.70. Direction-free fragility curves for all buildings obtained from cloud analyses (IM: Sd and EDP: Dtop).

Table 4.10. Parameters of direction-free fragility curves obtained from cloud analyses (EDP = Dtop, IM = Sd(m). (Θ=Sd[m], β=In(Sd[m]))

Building Type	**Slight**		**Moderate**		**Extensive**		**Complete**	
	Θ	β	Θ	β	Θ	β	Θ	β
3-1975	0.0212	0.4957	0.0296	0.4957	0.0519	0.4957	0.0789	0.4957
3-2018	0.0232	0.3269	0.0338	0.3269	0.1051	0.3269	0.1816	0.3269
6-1975	0.0365	0.3080	0.0517	0.3080	0.0622	0.3080	0.0863	0.3080
6-2018	0.0874	0.3132	0.1411	0.3132	0.2590	0.3132	0.4518	0.3132

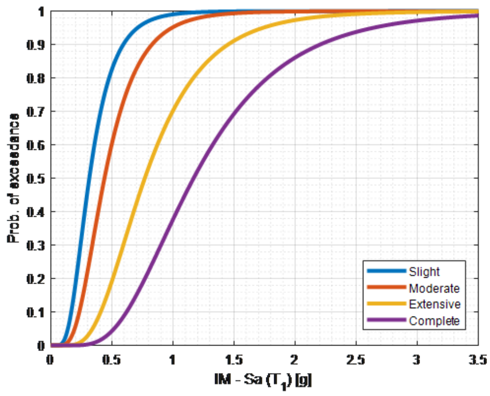

(a) 3-story 1975

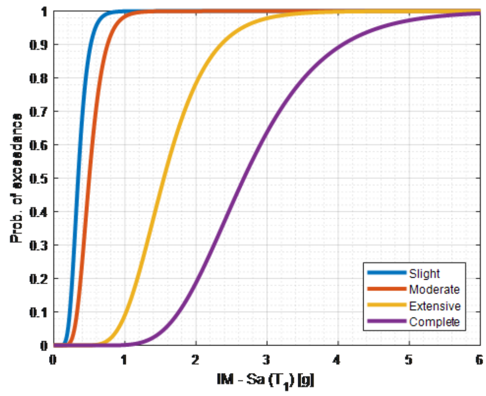

(b) 3-story 2018

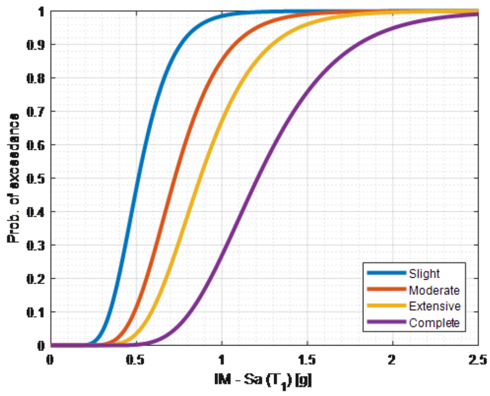

(c) 6-story 1975

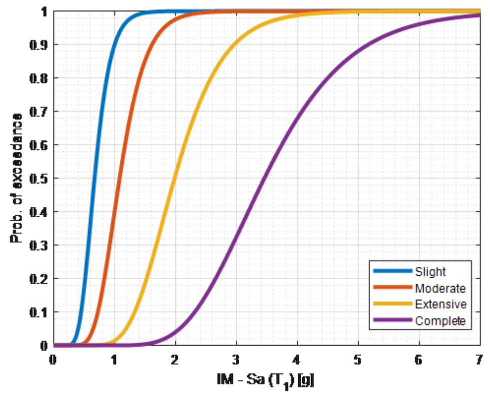

(d) 6-story 2018

Figure 4.71. Direction-free fragility curves for all buildings obtained from cloud analyses (IM: Sa and EDP: Dtop).

Table 4.11. Parameters of direction-free fragility curves obtained from cloud analyses (EDP = Dtop, IM = Sa(g). (Θ=Sa[g], β=ln(Sa[g]))

Building Type	**Slight**		**Moderate**		**Extensive**		**Complete**	
	Θ	β	Θ	β	Θ	β	Θ	β
3-1975	0.3138	0.4957	0.4381	0.4957	0.7682	0.4957	1.1677	0.4957
3-2018	0.3414	0.3269	0.4970	0.3269	1.5470	0.3269	2.6723	0.3269
6-1975	0.5113	0.3080	0.7236	0.3080	0.8720	0.3080	1.2085	0.3080
6-2018	0.6682	0.3132	1.0789	0.3132	1.9803	0.3132	3.4542	0.3132

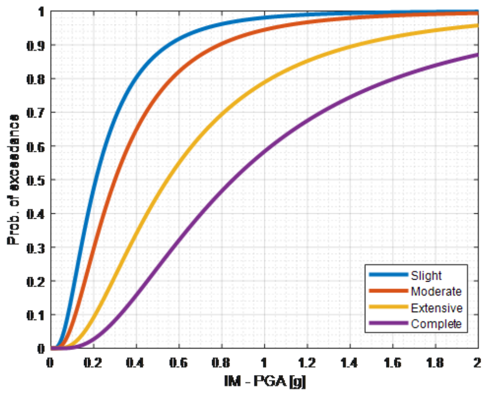

(a) 3-story 1975

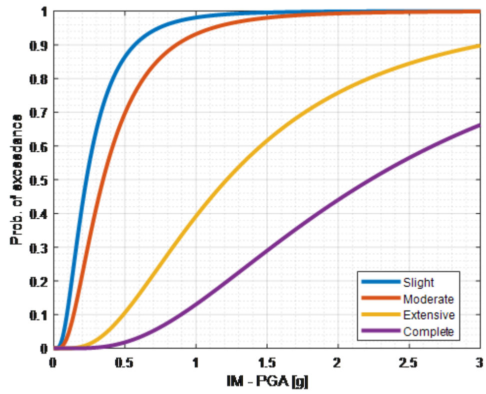

(b) 3-story 2018

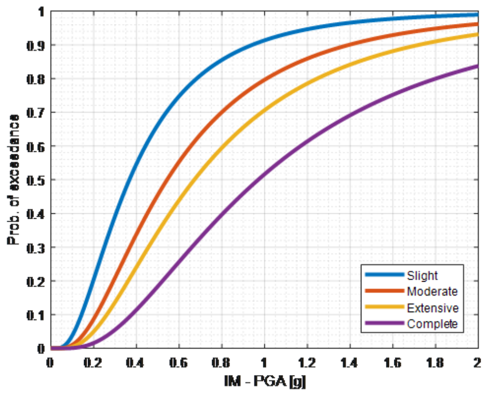

(c) 6-story 1975

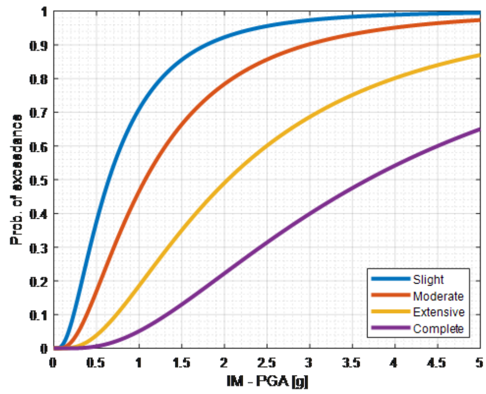

(d) 6-story 2018

Figure 4.72. Direction-free fragility curves for all buildings obtained from cloud analyses (IM: PGA and EDP: Dtop).

Table 4.12. Parameters of direction-free fragility curves obtained from cloud analyses (EDP = Dtop, IM = PGA(g). (Θ=PGA[g], β=In(PGA[g]))

Building Type	**Slight**		**Moderate**		**Extensive**		**Complete**	
	Θ	β	Θ	β	Θ	β	Θ	β
3-1975	0.2099	0.7547	0.2996	0.7547	0.5450	0.7547	0.8516	0.7547
3-2018	0.2286	0.7116	0.3463	0.7116	1.2156	0.7116	2.2249	0.7116
6-1975	0.3670	0.7356	0.5433	0.7356	0.6706	0.7356	0.9696	0.7356
6-2018	0.6437	0.7968	1.0700	0.7968	2.0377	0.7968	3.6760	0.7968

5. RESULTS AND DISCUSSIONS

In this study, in order to account for epistemic uncertainty in the derivation of fragility functions, fragility functions are derived by using two different methods namely, multiple stripe analysis and cloud analysis for low-rise and mid-rise (3 and 6-stories) MRF, RC buildings which are designed by considering the minimum conditions of Turkish Seismic Codes released in 1975 and 2018. The buildings' responses are obtained by performing multiple stripe analysis (MSA) and cloud analysis. The fragility curves are compared conveniently in Figures 5.1 to 5.6 and in Tables 5.1 to 5.12.

As can be seen from Figures 5.1 to 5.6, fragility curves are examined for four damage levels. Firstly, for the 3-story buildings, it can be observed that for slight, moderate and extensive damage levels both methods give similar results while for complete damage state they give slightly different results. On the other hand, when the curves are superimposed for the 6-story buildings, for complete damage state, methods give different results.

So, it can be observed that different methods can result in different fragility curves. One of the reason of this situation is because while regression analysis is performed for the cloud analysis, maximum likelihood estimation method is used for multiple stripe analysis.

In order to increase the representativeness of a fragility function, combinations of the fragility functions can be taken for each fragility curve. One can combine the fragility functions developed via different methods as in the logic tree. This is a common way to handle the epistemic uncertainty. In addition, logic trees are also used to allow multiple models to be considered with weights that reflected the degree of belief of the analysts in the alternative models. In this way, all proposed models that were credible could be considered without having to select a single best model.

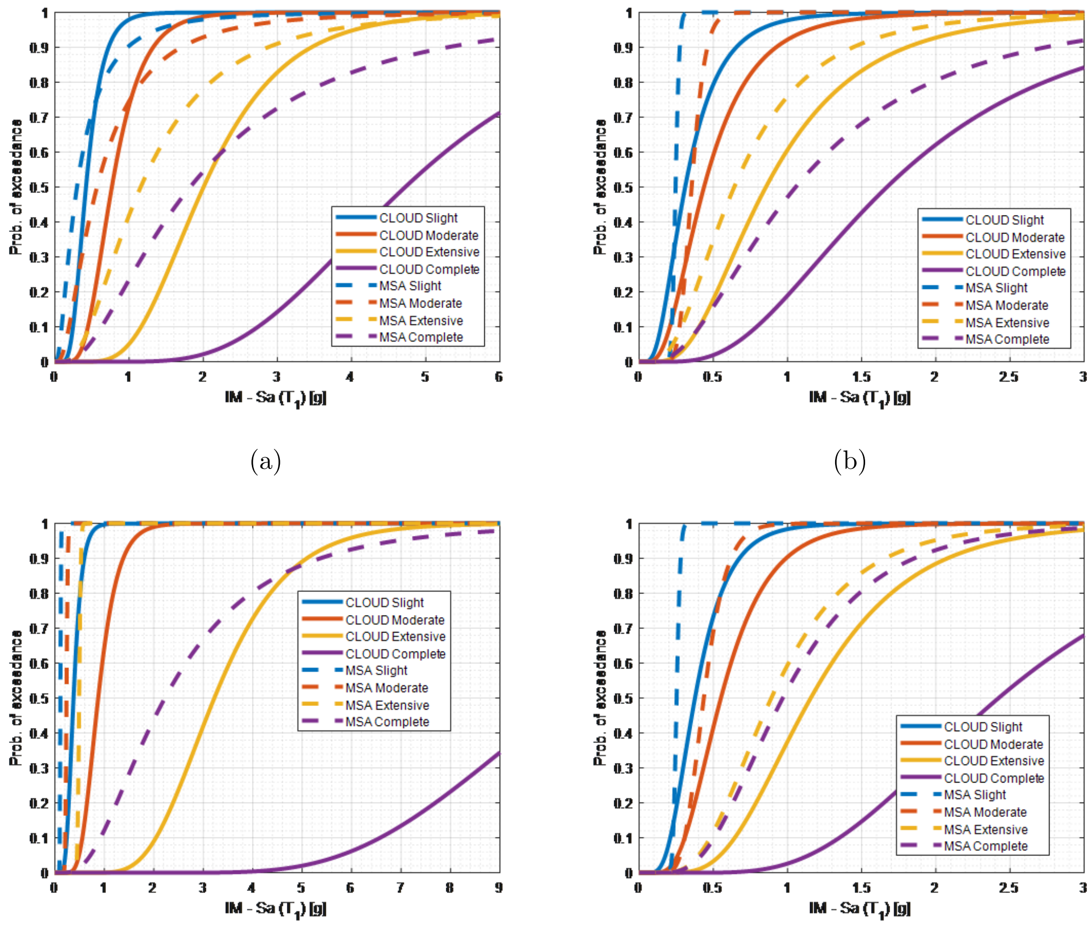

(a) (b)

(c) (d)

Figure 5.1. Comparison of direction-free fragility curves of MSA and Cloud Analysis of all buildings for different damage states (a) 3-story TSC 2018 (b) 3-story TSC 1975, (c) 6-story TSC 2018, (d) 6-story TSC 1975, IM(Sa)-EDP(MIDR).

Table 5.1. Parameters of direction-free fragility curves obtained from MSA (IM(Sa)-EDP(MIDR)).

Building Type	**Slight**		**Moderate**		**Extensive**		**Complete**	
	Θ	β	Θ	β	Θ	β	Θ	β
3-1975	0.2452	0.0851	0.3535	0.2049	0.6404	0.6319	1.0545	0.7430
3-2018	0.2969	0.9291	0.5666	0.8578	1.1551	0.7095	1.8219	0.8306
6-1975	0.2523	0.0803	0.4356	0.2760	0.8902	0.4851	0.9676	0.5071
6-2018	0.1093	0.0982	0.2336	0.0909	0.4901	0.0576	2.2223	0.6871

Table 5.2. Parameters of direction-free fragility curves obtained from Cloud Analysis (IM(Sa)-EDP(MIDR)).

Building Type	**Slight**		**Moderate**		**Extensive**		**Complete**	
	Θ	β	Θ	β	Θ	β	Θ	β
3-1975	0.3096	0.5830	0.4367	0.5830	0.8538	0.5830	1.6695	0.5830
3-2018	0.4183	0.4254	0.7667	0.4254	2.0031	0.4254	4.7212	0.4254
6-1975	0.3759	0.4569	0.5507	0.4569	1.1559	0.4569	2.4219	0.4569
6-2018	0.3754	0.3566	0.8740	0.3566	3.2229	0.3566	10.3802	0.3566

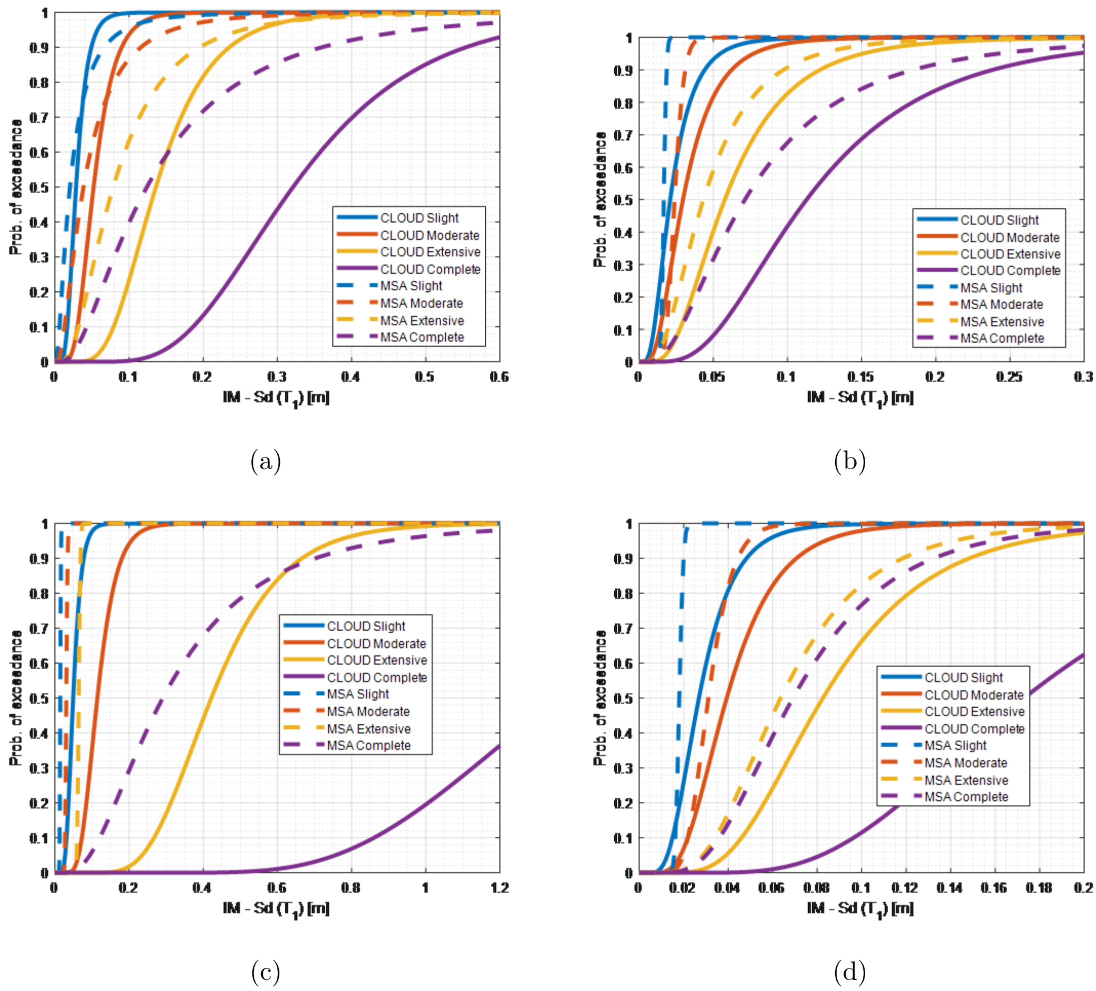

Figure 5.2. Comparison of direction-free fragility curves of MSA and Cloud Analysis of all buildings for different damage states (a) 3-story TSC 2018 (b) 3-story TSC 1975, (c) 6-story TSC 2018, (d) 6-story TSC 1975, IM(Sd)-EDP(MIDR).

Table 5.3. Parameters of direction-free fragility curves obtained from MSA (IM(Sd)-EDP(MIDR)).

Building Type	**Slight**		**Moderate**		**Extensive**		**Complete**	
	Θ	β	Θ	β	Θ	β	Θ	β
3-1975	0.0166	0.0841	0.0239	0.2049	0.0433	0.6319	0.0713	0.7430
3-2018	0.0202	0.9290	0.0385	0.8578	0.0785	0.7096	0.1238	0.8307
6-1975	0.0180	0.0784	0.0311	0.2759	0.0635	0.4858	0.0691	0.5071
6-2018	0.0143	0.0976	0.0306	0.0902	0.0641	0.0564	0.2907	0.6871

Table 5.4. Parameters of direction-free fragility curves obtained from Cloud Analysis (IM(Sd)-EDP(MIDR)).

Building Type	**Slight**		**Moderate**		**Extensive**		**Complete**	
	Θ	β	Θ	β	Θ	β	Θ	β
3-1975	0.0209	0.5830	0.0295	0.5830	0.0577	0.5830	0.1128	0.5830
3-2018	0.0284	0.4254	0.0521	0.4254	0.1361	0.4254	0.3209	0.4254
6-1975	0.0268	0.4569	0.0393	0.4569	0.0825	0.4569	0.1729	0.4569
6-2018	0.0491	0.3566	0.1143	0.3566	0.4215	0.3566	1.3577	0.3566

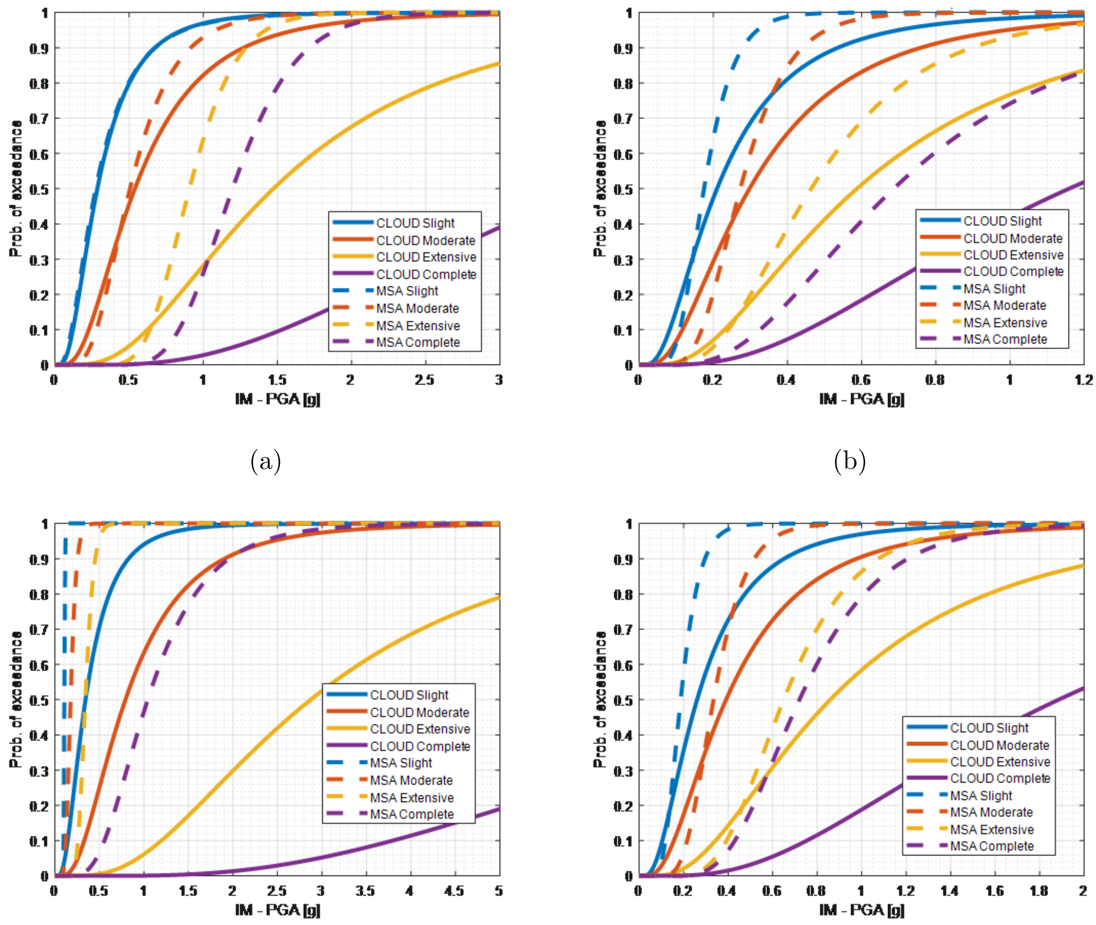

(a) (b)

(c) (d)

Figure 5.3. Comparison of direction-free fragility curves of MSA and Cloud Analysis of all buildings for different damage states (a) 3-story TSC 2018 (b) 3-story TSC 1975, (c) 6-story TSC 2018, (d) 6-story TSC 1975, IM(PGA)-EDP(MIDR).

Table 5.5. Parameters of direction-free fragility curves obtained from MSA (IM(PGA)-EDP(MIDR)).

Building Type	**Slight**		**Moderate**		**Extensive**		**Complete**	
	Θ	β	Θ	β	Θ	β	Θ	β
3-1975	0.1748	0.3658	0.2725	0.3745	0.4637	0.5151	0.6862	0.5810
3-2018	0.2748	0.7006	0.5058	0.4628	0.9070	0.2731	1.1970	0.2804
6-1975	0.1865	0.3594	0.3341	0.3414	0.6497	0.3929	0.7202	0.4030
6-2018	0.2074	0.0727	0.3764	0.2872	0.7751	0.2201	1.0884	0.4913

Table 5.6. Parameters of direction-free fragility curves obtained from Cloud Analysis (IM(PGA)-EDP(MIDR)).

Building Type	**Slight**		**Moderate**		**Extensive**		**Complete**	
	Θ	β	Θ	β	Θ	β	Θ	β
3-1975	0.2098	0.7314	0.2974	0.7314	0.5871	0.7314	1.1590	0.7314
3-2018	0.2856	0.6702	0.5386	0.6702	1.4724	0.6702	3.6133	0.6702
6-1975	0.2602	0.7161	0.3904	0.7161	0.8586	0.7161	1.8848	0.7161
6-2018	0.3436	0.6849	0.7918	0.6849	2.8734	0.6849	9.1232	0.6849

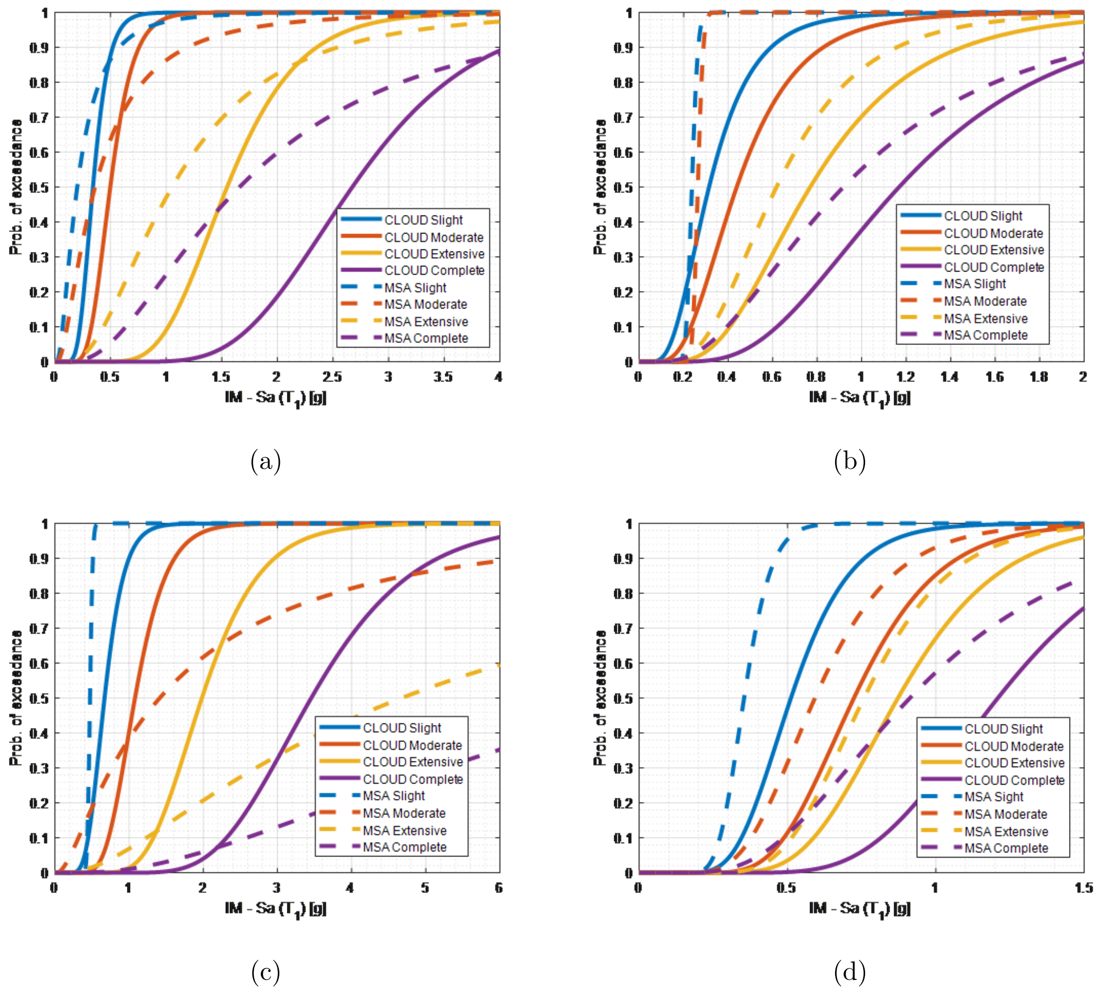

Figure 5.4. Comparison of direction-free fragility curves of MSA and Cloud Analysis of all buildings for different damage states (a) 3-story TSC 2018 (b) 3-story TSC 1975, (c) 6-story TSC 2018, (d) 6-story TSC 1975, IM(Sa)-EDP(Dtop).

Table 5.7. Parameters of direction-free fragility curves obtained from MSA (IM(Sa)-EDP(Dtop)).

Building Type	**Slight**		**Moderate**		**Extensive**		**Complete**	
	Θ	β	Θ	β	Θ	β	Θ	β
3-1975	0.2368	0.0897	0.2637	0.0712	0.6168	0.4906	0.9174	0.6598
3-2018	0.2001	0.8278	0.3604	0.9322	1.0518	0.6879	1.6582	0.7481
6-1975	0.3535	0.2049	0.5922	0.3519	0.7574	0.3032	0.9122	4925
6-2018	0.4725	0.0622	1.4112	1.1653	4.6700	1.0394	8.5401	0.9343

Table 5.8. Parameters of direction-free fragility curves obtained from Cloud Analysis (IM(Sa)-EDP(Dtop)).

Building Type	**Slight**		**Moderate**		**Extensive**		**Complete**	
	Θ	β	Θ	β	Θ	β	Θ	β
3-1975	0.3138	0.4957	0.4381	0.4957	0.7682	0.4957	1.1677	0.4957
3-2018	0.3414	0.3269	0.4970	0.3269	1.5470	0.3269	2.6723	0.3269
6-1975	0.5113	0.3080	0.7236	0.3080	0.8720	0.3080	1.2085	0.3080
6-2018	0.6682	0.3132	1.0789	0.3132	1.9803	0.3132	3.4542	0.3132

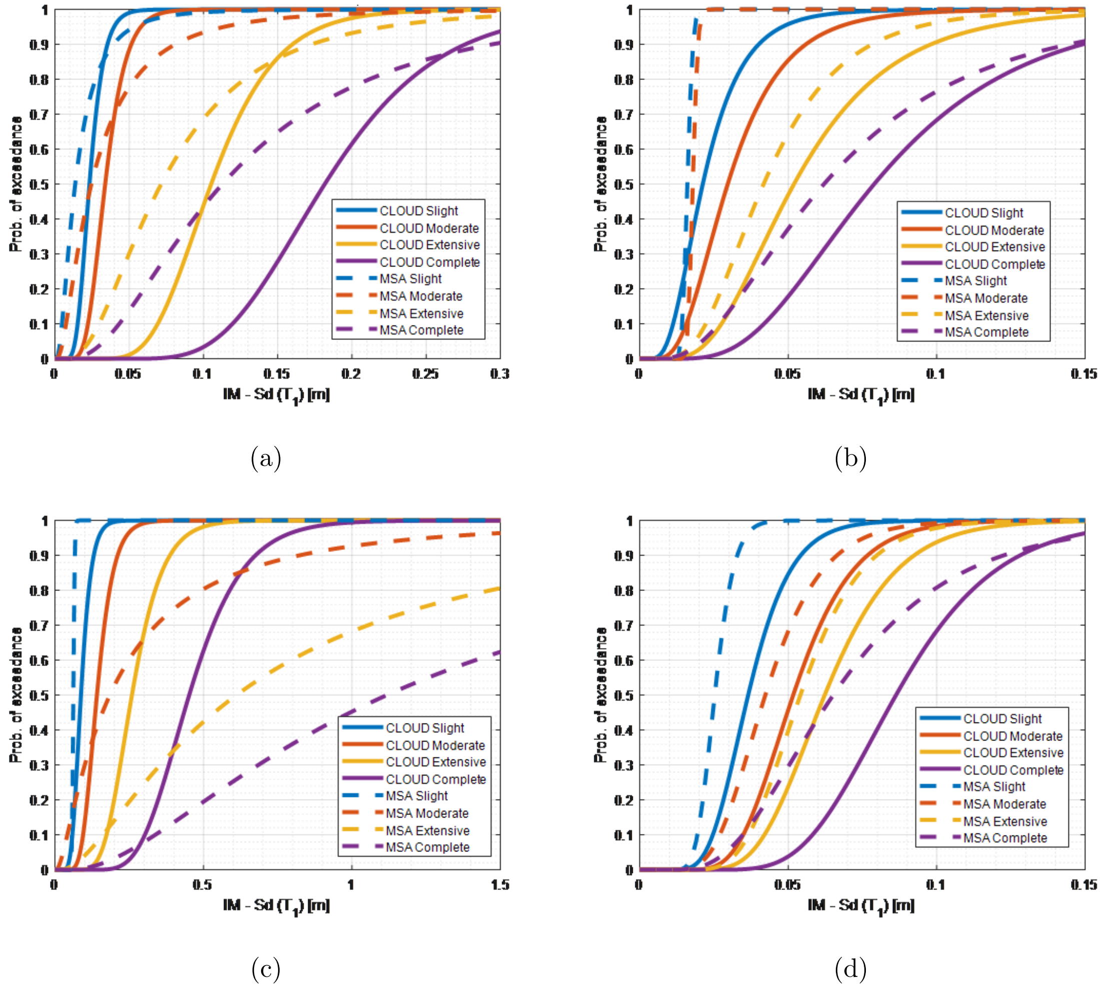

Figure 5.5. Comparison of direction-free fragility curves of MSA and Cloud Analysis of all buildings for different damage states (a) 3-story TSC 2018 (b) 3-story TSC 1975, (c) 6-story TSC 2018, (d) 6-story TSC 1975, IM(Sd)-EDP(Dtop).

Table 5.9. Parameters of direction-free fragility curves obtained from MSA (IM(Sd)-EDP(Dtop)).

Building Type	**Slight**		**Moderate**		**Extensive**		**Complete**	
	Θ	β	Θ	β	Θ	β	Θ	β
3-1975	0.0160	0.0878	0.0179	0.0739	0.0417	0.4906	0.0620	0.6598
3-2018	0.0136	0.8278	0.0245	0.9323	0.0715	0.6879	0.1127	0.7481
6-1975	0.0252	0.2049	0.0423	0.3520	0.0541	0.3033	0.0651	0.4925
6-2018	0.0618	0.0631	0.1846	1.1653	0.6108	1.0393	1.1170	0.9343

Table 5.10. Parameters of direction-free fragility curves obtained from Cloud Analysis (IM(Sd)-EDP(Dtop)).

Building Type	**Slight**		**Moderate**		**Extensive**		**Complete**	
	Θ	β	Θ	β	Θ	β	Θ	β
3-1975	0.0212	0.4957	0.0296	0.4957	0.0519	0.4957	0.0789	0.4957
3-2018	0.0232	0.3269	0.0338	0.3269	0.1051	0.3269	0.1816	0.3269
6-1975	0.0365	0.3080	0.0517	0.3080	0.0622	0.3080	0.0863	0.3080
6-2018	0.0874	0.3132	0.1411	0.3132	0.2590	0.3132	0.4518	0.3132

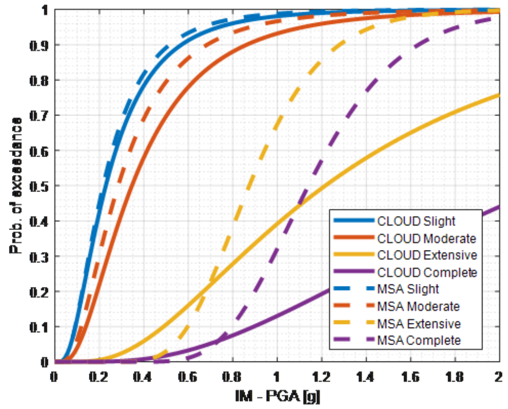

(a)

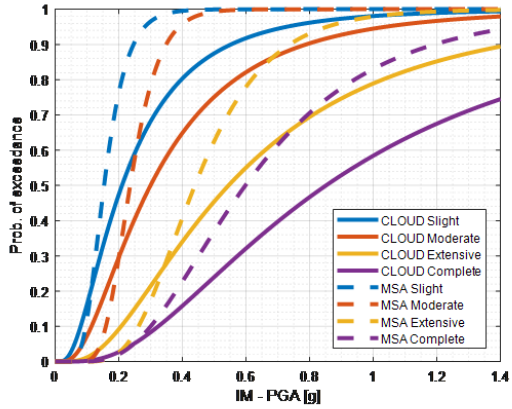

(b)

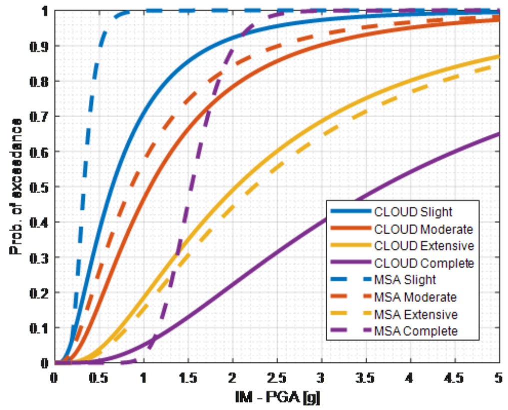

(c)

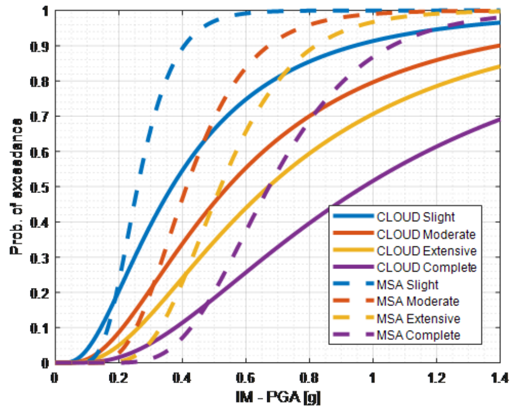

(d)

Figure 5.6. Comparison of direction-free fragility curves of MSA and Cloud Analysis of all buildings for different damage states (a) 3-story TSC 2018 (b) 3-story TSC 1975, (c) 6-story TSC 2018, (d) 6-story TSC 1975, IM(PGA)-EDP(Dtop).

Table 5.11. Parameters of direction-free fragility curves obtained from MSA (IM(PGA)-EDP(Dtop)).

Building Type	**Slight**		**Moderate**		**Extensive**		**Complete**	
	Θ	β	Θ	β	Θ	β	Θ	β
3-1975	0.1536	0.3680	0.2356	0.3062	0.4391	0.4041	0.5979	0.5383
3-2018	0.2170	0.6759	0.2845	0.6849	0.8740	0.2978	1.1395	0.2816
6-1975	0.2587	0.3507	0.4127	0.3793	0.5198	0.3547	0.6724	0.3552
6-2018	0.3260	0.3554	0.8574	0.8404	2.2388	0.7902	1.5347	0.2147

Table 5.12. Parameters of direction-free fragility curves obtained from Cloud Analysis (IM(PGA)-EDP(Dtop)).

Building Type	**Slight**		**Moderate**		**Extensive**		**Complete**	
	Θ	β	Θ	β	Θ	β	Θ	β
3-1975	0.2099	0.7547	0.2996	0.7547	0.5450	0.7547	0.8516	0.7547
3-2018	0.2286	0.7116	0.3463	0.7116	1.2156	0.7116	2.2249	0.7116
6-1975	0.3670	0.7356	0.5433	0.7356	0.6706	0.7356	0.9696	0.7356
6-2018	0.6437	0.7968	1.0700	0.7968	2.0377	0.7968	3.6760	0.7968

6. CONCLUSION

In this study, fragility functions are developed by using two different methods namely, cloud analysis and multiple stripe analysis in order to address the effects of modeling uncertainty (i.e. for epistemic uncertainty) on the fragility functions derived for low-rise and mid-rise (3 and 6-story), reinforced concrete (RC), moment-resisting frame (MRF) buildings, which are designed as per the Turkish Seismic Codes (TSC) released in 1975 and 2018.

To generate fragility functions, nonlinear dynamic analyses of study buildings are performed within the frameworks of cloud analysis and multiple stripe analysis (MSA), separately. Spectral displacement (Sd), spectral acceleration (Sa) and peak ground acceleration (PGA) are selected as the intensity measures (IM) whereas the maximum inter-story drift ratio (MIDR) and top displacement (Dtop) are used as engineering demand parameters (EDP). The fragility functions are developed for four damage states which are defined as slight damage, moderate damage, extensive damage, and complete damage.

For both 3 and 6-story buildings and for all IMs and EDPs, the fragility curves derived through cloud and multiple stripe analyses are well compared with each other for lower damage state levels, i.e. for slight and moderate damage states. When the damage level increases, i.e. for extensive and complete damage states, the estimated median values of the fragility curves are getting very different. In general, fragility curves resulting from multiple stripe analyses estimate higher damage exceedance probabilities than the curves obtained from cloud analyses. One exception to this is that the cases for 6-story TSC 2018 building in which the IMs are Sa and Sd, and the EDP is top displacement. In these cases, even the shapes of the curves are dissimilar. Another observation is that the differences between the fragility functions resulting from cloud and multiple stripe analyses are much more prominent for the buildings designed as per the TSC 2018. This might be related to the ductile behavior of the buildings and the number of inelastic displacement responses reaching or not reaching the damage state thresholds, which are assessed with different numbers of ground motion records in multiple stripe and cloud analyses.

Thus, different analytical frameworks/approaches, i.e. cloud and multiple stripe analyses, produces different fragility functions as it might be expected. In order to increase the representativeness of a fragility function, combinations of the fragility functions can be taken for each fragility curve. One can combine the fragility functions developed via different methods as in the logic tree. This is a common way to handle the epistemic uncertainty. In addition, logic trees are also used to allow multiple models to be considered with weights that reflected the degree of belief of the analysts in the alternative models. In this way, all proposed models that were credible could be considered without having to select a single best model.

REFERENCES

1. Erdik, M., "Earthquake Risk Assessment", *Bulletin of Earthquake Engineering*, Vol. 15, No. 12, pp. 5055–5092, 2017.

2. Porter, K., "A Beginner's Guide to Fragility, Vulnerability, and Risk", *Encyclopedia of Earthquake Engineering*, Vol. 2015, pp. 235–260, 2015.

3. Duran, H. İ., "PGV Based No-Code Mid-Rise Reinforced Concrete Frame-Type Building Fragilities in İstanbul", *M.Sc. Thesis, Department of Earthquake Engineering, Bogazici University, Istanbul, Turkey*, 2020.

4. Akkar, S. and Ö. Özen, "Effect of Peak Ground Velocity on Deformation Demands for SDOF Systems", *Earthquake Engineering* & $Structural Dynamics, Vol.\ 34, No.\ 13, pp. 1551--1571, 2005.$

5. FEMA-356, N., "NEHRP, Prestandard and Commentary for the Seismic Rehabilitation of Buildings", *Technical Report*, 2000.

6. Hancilar, U. and E. Çaktı, "Fragility Functions for Code Complying RC Frames via Best Correlated IM–EDP Pairs", *Bulletin of Earthquake Engineering*, Vol. 13, No. 11, pp. 3381–3400, 2015.

7. D'Ayala, D., A. Meslem, D. Vamvatsikos, K. Porter, T. Rossetto and V. Silva, "Guidelines for Analytical Vulnerability Assessment—Low/Mid-Rise (GEM Technical Report No. 2014–12 V1. 0.0).", *GEM Technical Report*, 2019.

8. Erdik, M., K. Sesetyan, M. Demircioglu, U. Hancilar, C. Zulfikar, E. Cakti, Y. Kamer, C. Yenidogan, C. Tuzun, Z. Cagnan *et al.*, "Rapid Earthquake Hazard and Loss Assessment for Euro-Mediterranean Region", *Acta Geophysica*, Vol. 58, No. 5, pp. 855–892, 2010.

9. Hancilar, U., E. Çaktı, M. Erdik, G. E. Franco and G. Deodatis, “Earthquake Vulnerability of School Buildings: Probabilistic Structural Fragility Analyses”, *Soil Dynamics and Earthquake Engineering*, Vol. 67, pp. 169–178, 2014.

10. Kirçil, M. S. and Z. Polat, “Fragility Analysis of Mid-Rise R/C Frame Buildings”, *Engineering Structures*, Vol. 28, No. 9, pp. 1335–1345, 2006.

11. Tüzün, C., “A Seismic Vulnerability Analysis Procedure for Urban Loss Assessment”, *M.Sc. Thesis, Department of Earthquake Engineering, Bogazici University, İstanbul, Turkey*, 2008.

12. Dolağan, İ., “Development of Peak Ground Acceleration (PGA) Based Pre-Code Reinforced Concrete Frame Building Fragilities for Istanbul”, *M.Sc. Thesis, Department of Earthquake Engineering, Bogazici University, İstanbul, Turkey*, 2019.

13. Computer and Structures, Inc., ETABS V18, *ETABS V18*, 2019.

14. ATC, “Preliminary Evaluation of Methods for Defining Performance, ATC-58-2”, *ATC Redwood City, CA*, 2003.

15. FEMA, “HAZUS MH MR4 Earthquake Technical Manual Multi-hazard Loss Estimation Methodology”, *Prepared by the National Institute of Building Sciences for FEMA*, 2003.

16. Vamvatsikos, D. and C. A. Cornell, “Incremental Dynamic Analysis”, *Earthquake Engineering & StructuralDynamics, Vol.* 31, *No.* 3, *pp.*491 − −514, 2002.

17. The Mathworks, Inc., Natick, Massachusetts, *MATLAB version (R2019a)*, 2019.

18. Jalayer, F., H. Ebrahimian, A. Miano, G. Manfredi and H. Sezen, “Analytical Fragility Assessment Using Unscaled Ground Motion Records”, *Earthquake Engineering & StructuralDynamics, Vol.* 46, *No.* 15, *pp.*2639 − −2663, 2017.

19. Pang, Y. and X. Wang, “Cloud-IDA-MSA Conversion of Fragility Curves for Effi-

cient and High-Fidelity Resilience Assessment", *Journal of Structural Engineering*, Vol. 147, No. 5, 2021.

20. Cornell, C. A., F. Jalayer, R. O. Hamburger and D. A. Foutch, "Probabilistic Basis for 2000 SAC Federal Emergency Management Agency Steel Moment Frame Guidelines", *Journal of Structural Engineering*, Vol. 128, No. 4, pp. 526–533, 2002.

APPENDIX A: REINFORCEMENT DETAILINGS OF LATERAL LOAD CARRYING SYSTEMS

The model and reinforcement of designed buildings for 3 and 6-story buildings designed as per TSC 2018 and TSC 1975 are given in this section. The following tables summarize the selected amount of steel bars for 3 and 6-story buildings designed as per TSC 2018 and TSC 1975.

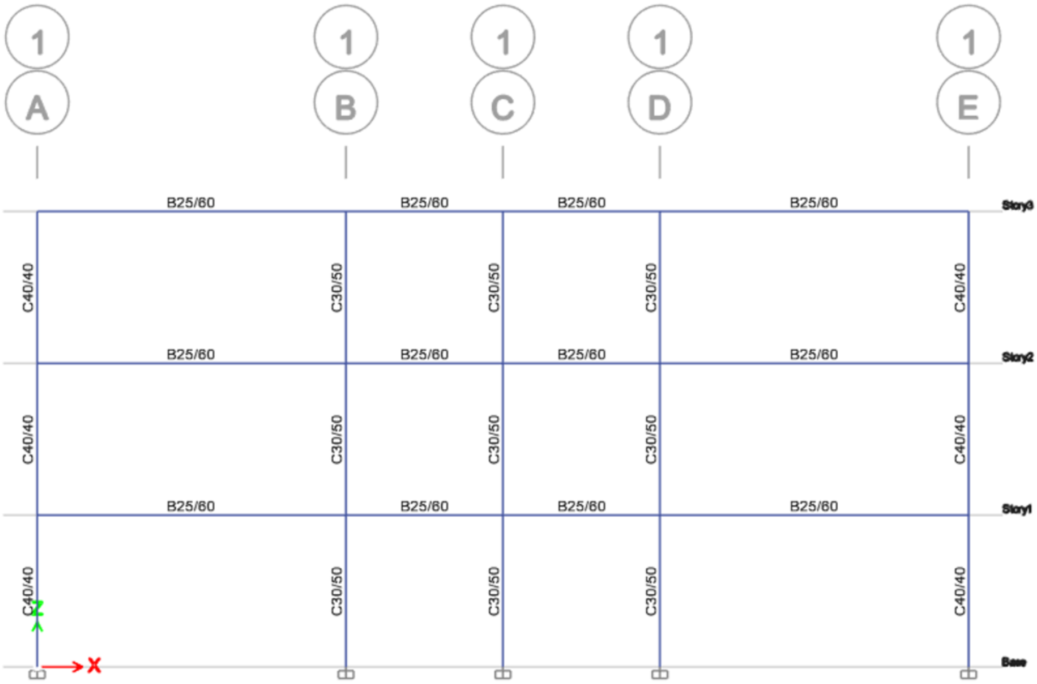

(a)

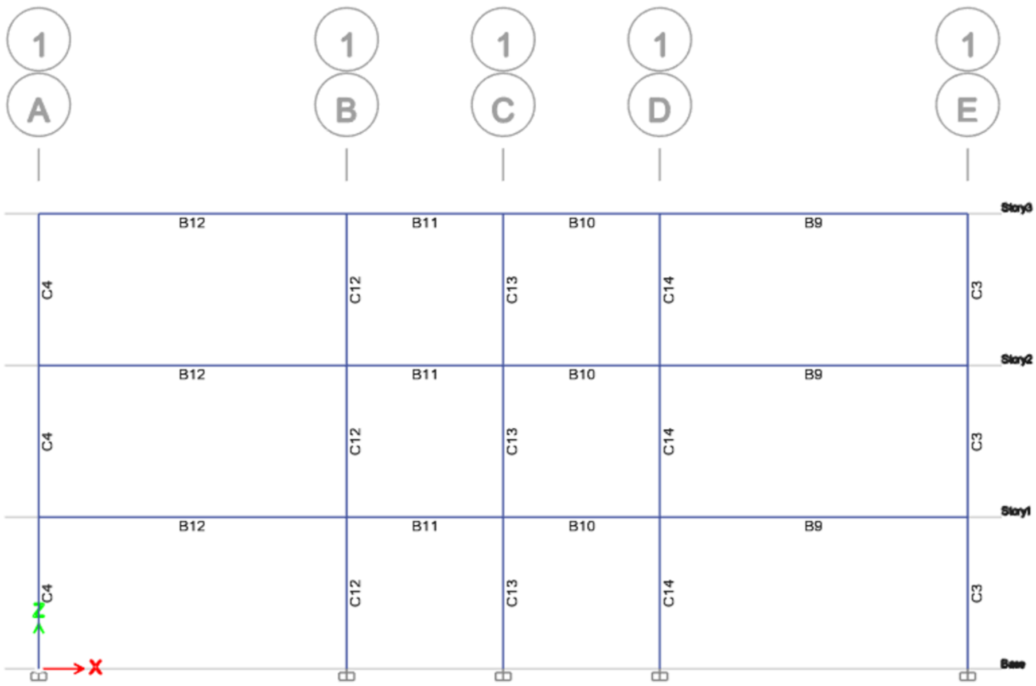

(b)

Figure A.1. 3-story building model TSC 2018.

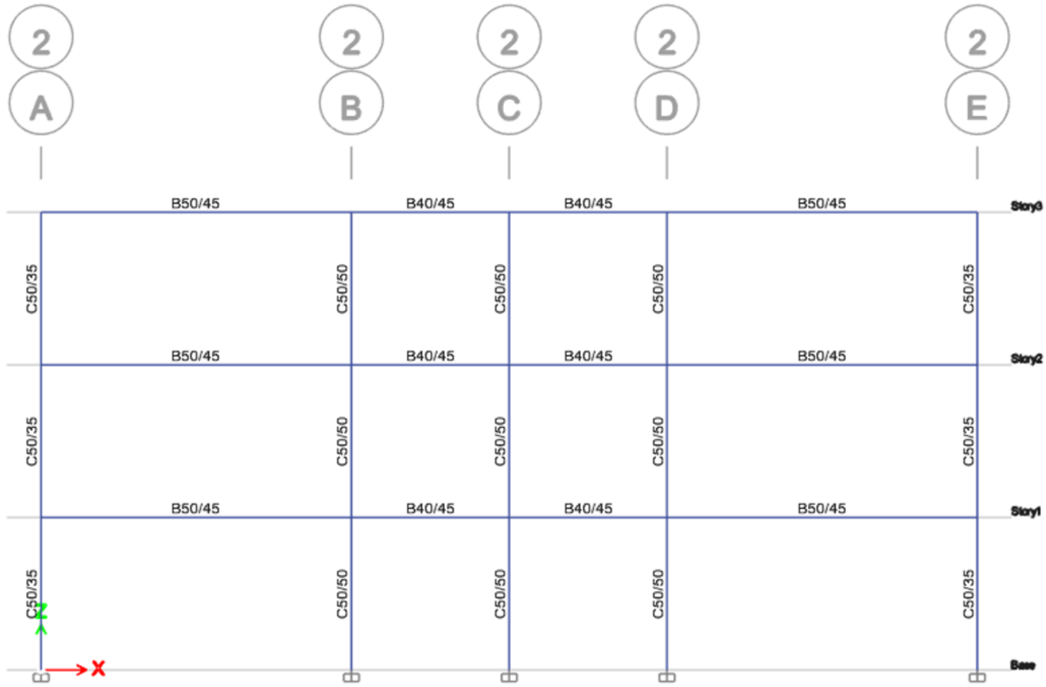

(a)

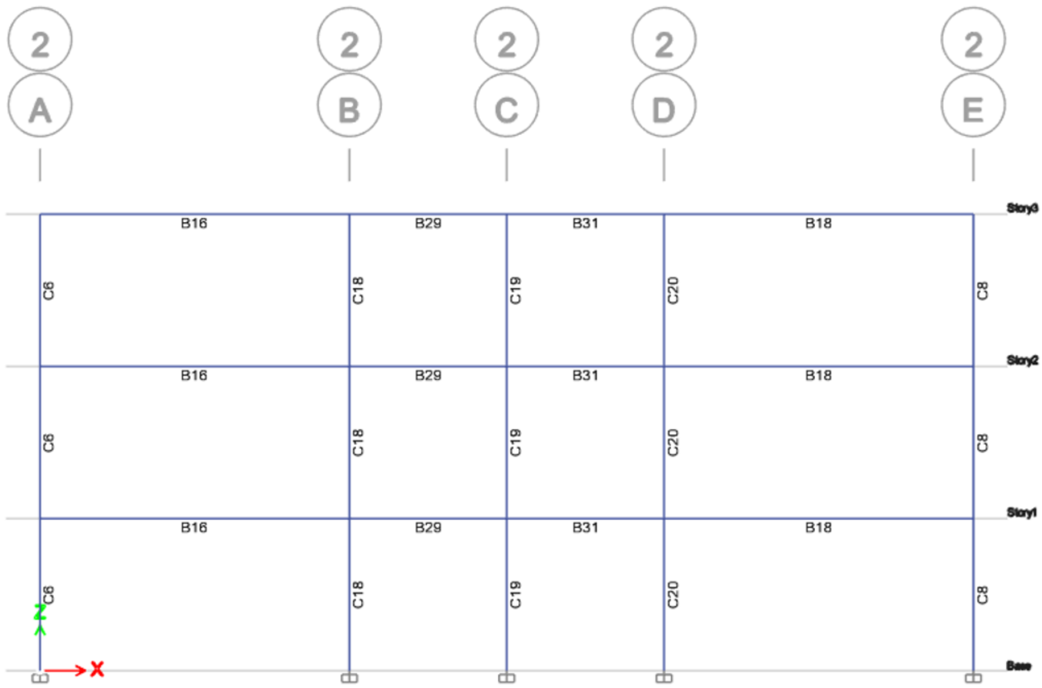

(b)

Figure A.2. 3-story building model TSC 2018. cont.

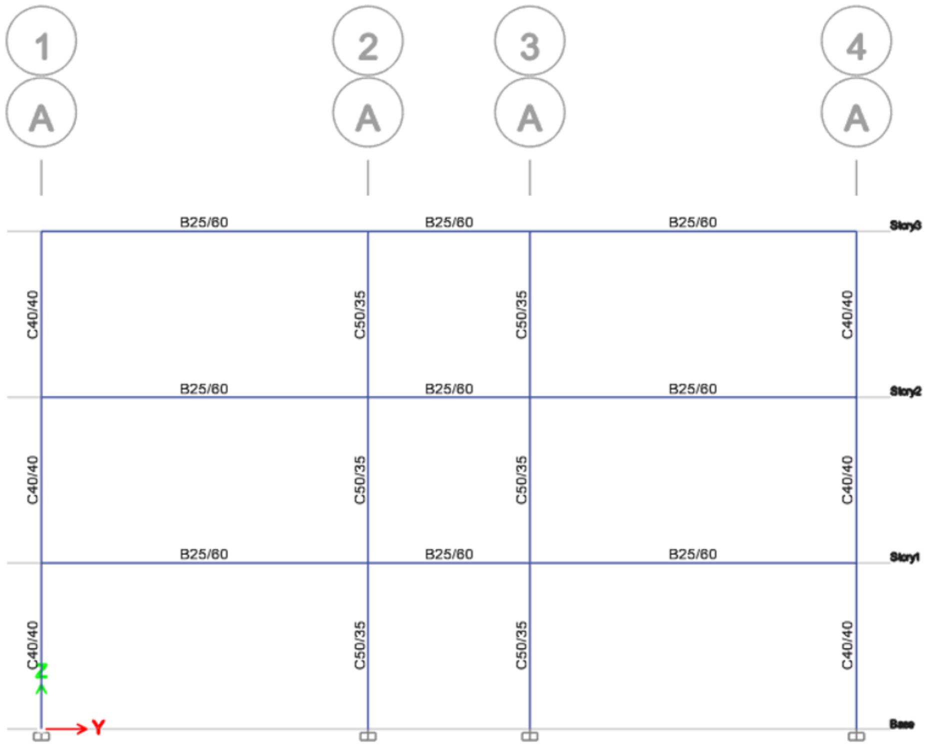

(a)

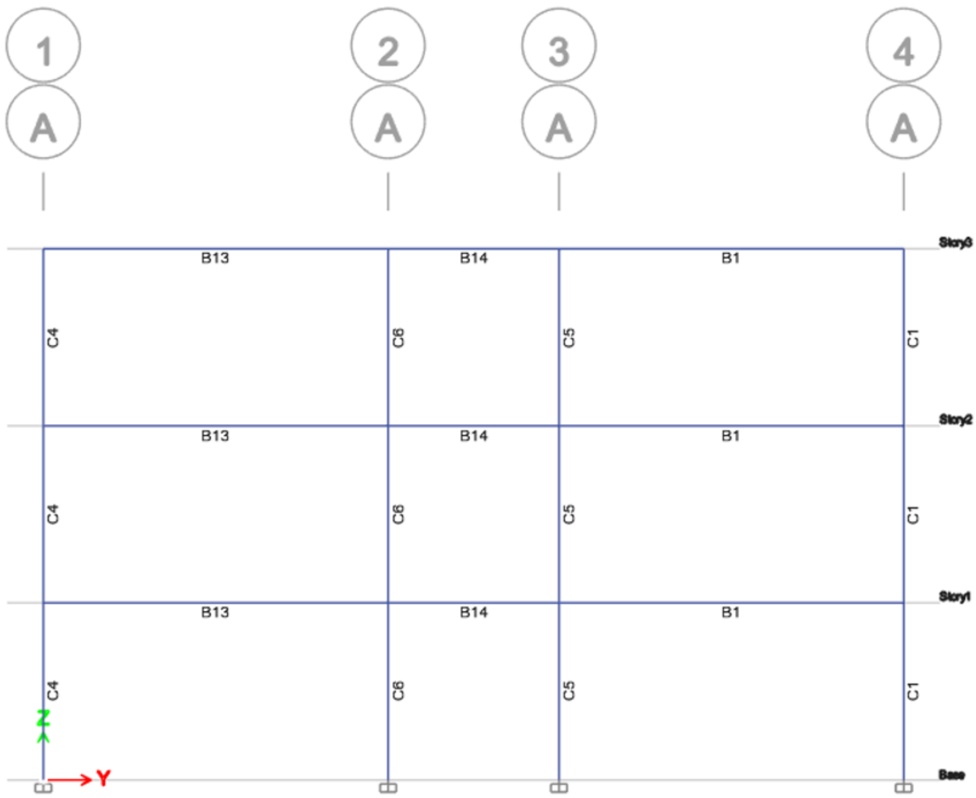

(b)

Figure A.3. 3-story building model TSC 2018. cont.

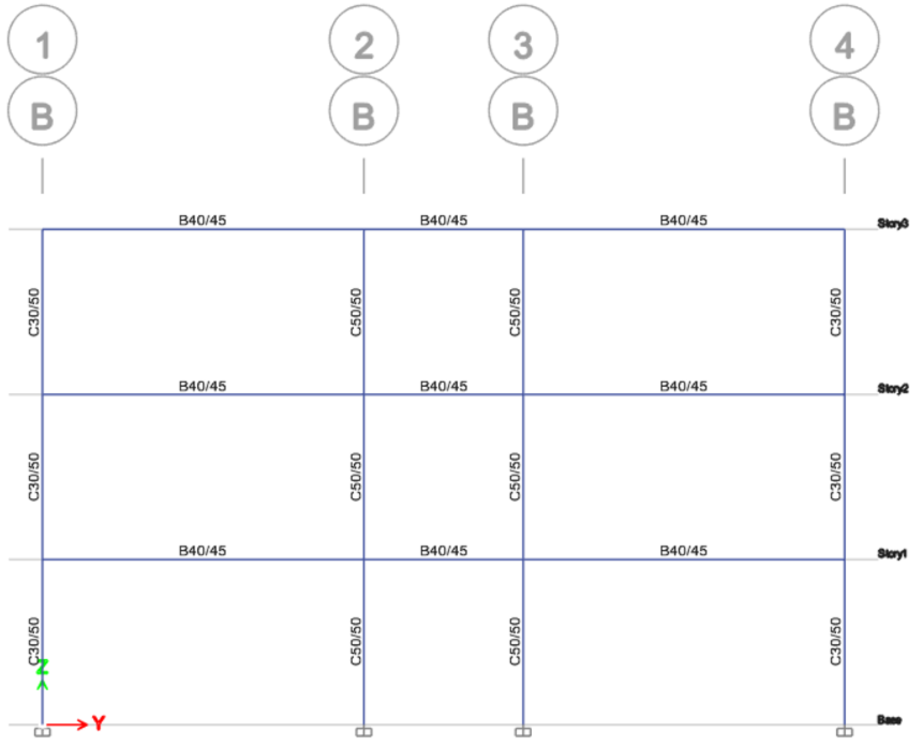

(a)

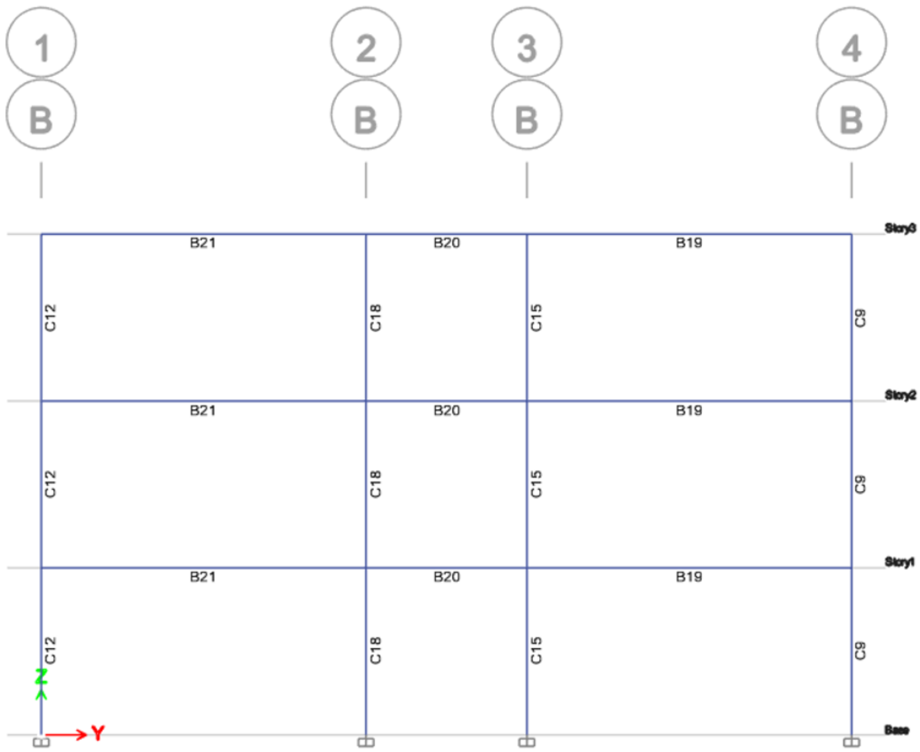

(b)

Figure A.4. 3-story building model TSC 2018. cont.

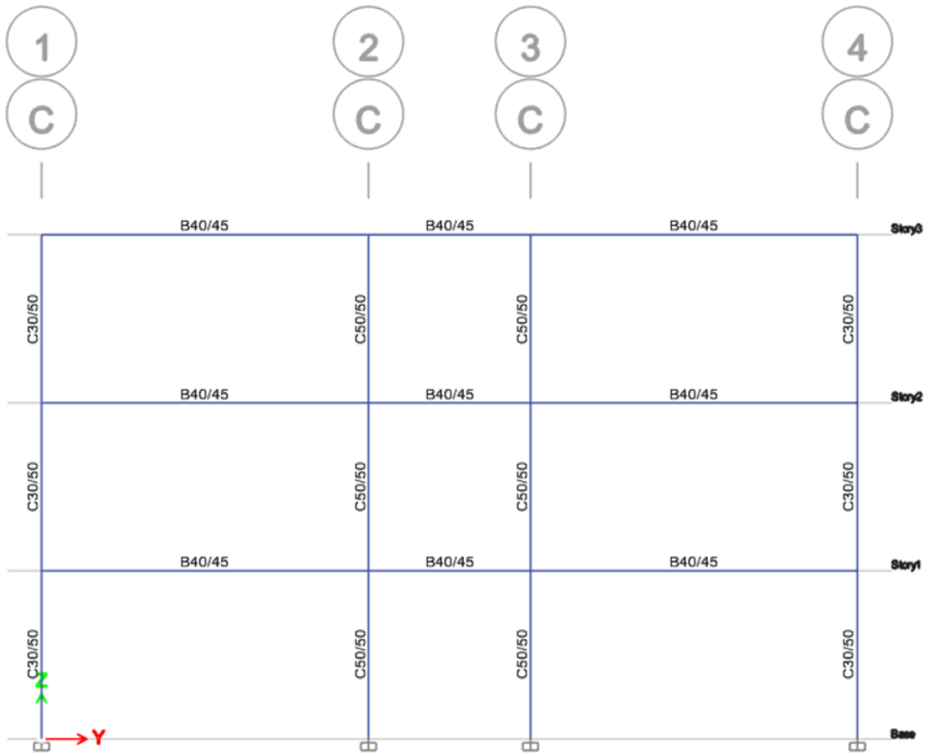

(a)

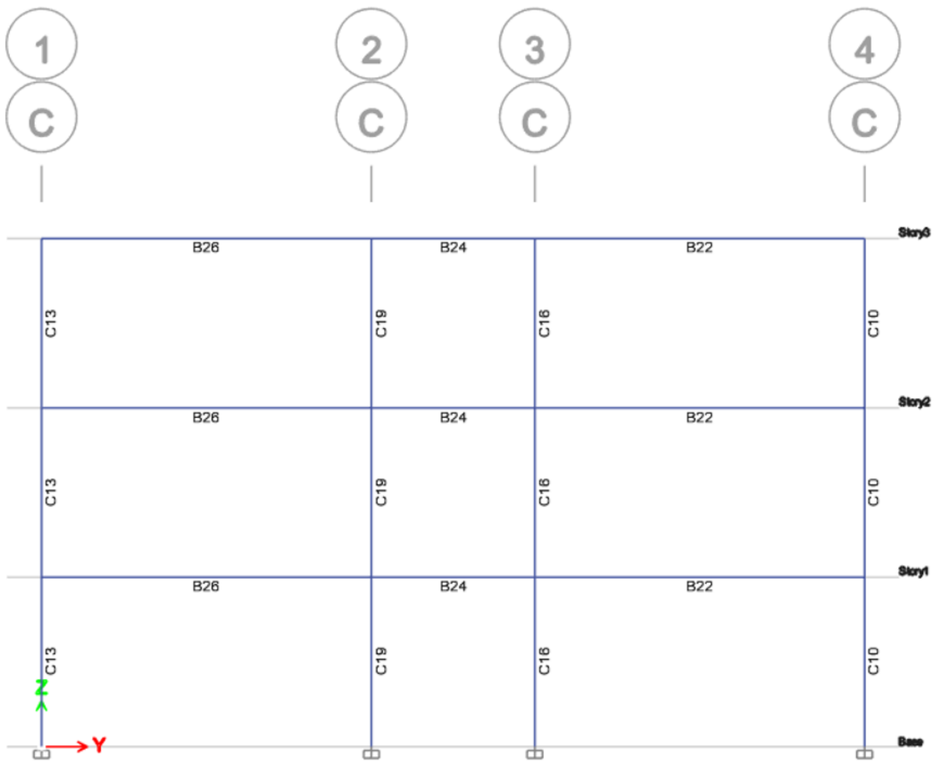

(b)

Figure A.5. 3-story building model TSC 2018. cont.

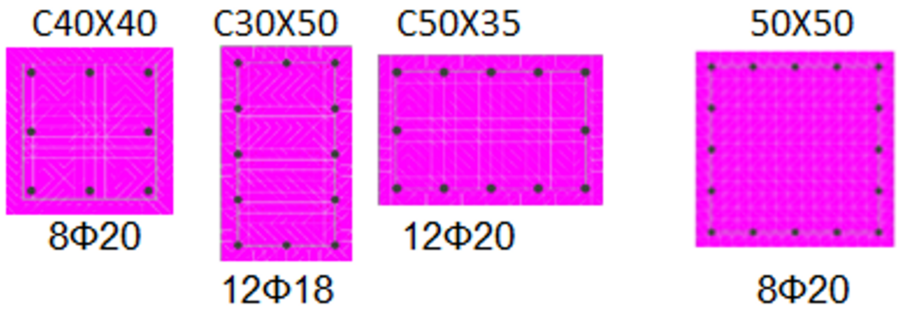

(a)

Figure A.6. 3-story building model designed per TSC 2018.

B9		B10	
Top	Bottom	Top	Bottom
2Φ14	2Φ16	2Φ14	2Φ16
3Φ14	0	3Φ14	0

B11		B12	
Top	Bottom	Top	Bottom
2Φ14	2Φ16	2Φ14	2Φ16
3Φ14	0	3Φ14	0

(a)

B16		B29	
Top	Bottom	Top	Bottom
2Φ18	2Φ16	2Φ16	2Φ16
3Φ16	1Φ16	3Φ14	1Φ14

B31		B18	
Top	Bottom	Top	Bottom
2Φ16	2Φ16	2Φ18	2Φ16
3Φ14	1Φ14	3Φ16	1Φ16

(b)

Figure A.7. Reinforcement for 3-story building model designed per TSC 2018.

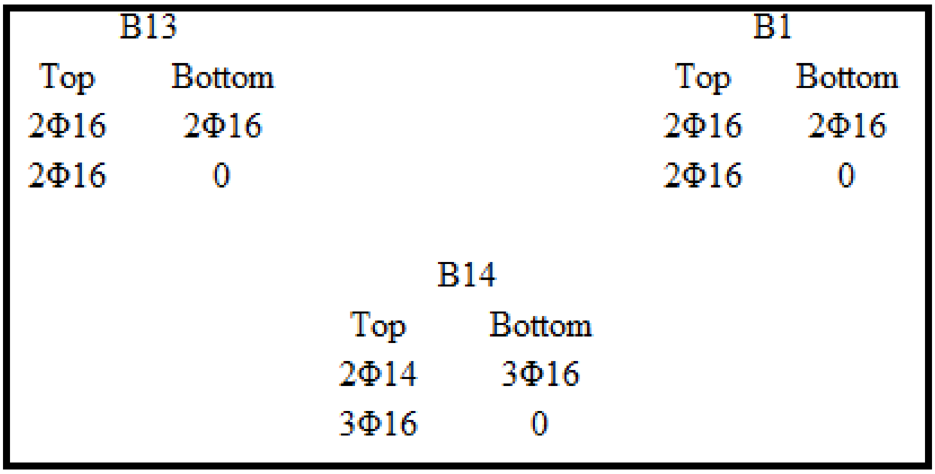

(a)

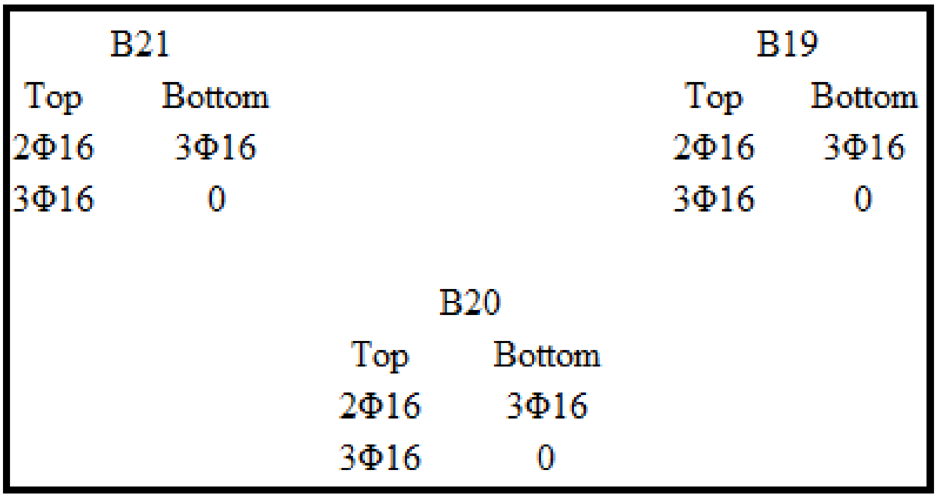

(b)

Figure A.8. Reinforcement for 3-story building model designed per TSC 2018. cont.

B21

Top	Bottom
2Φ16	3Φ16
3Φ16	0

B19

Top	Bottom
2Φ16	3Φ16
3Φ16	0

B20

Top	Bottom
2Φ16	3Φ16
3Φ16	0

(a)

Figure A.9. Reinforcement for 3-story building model designed per TSC 2018. cont.

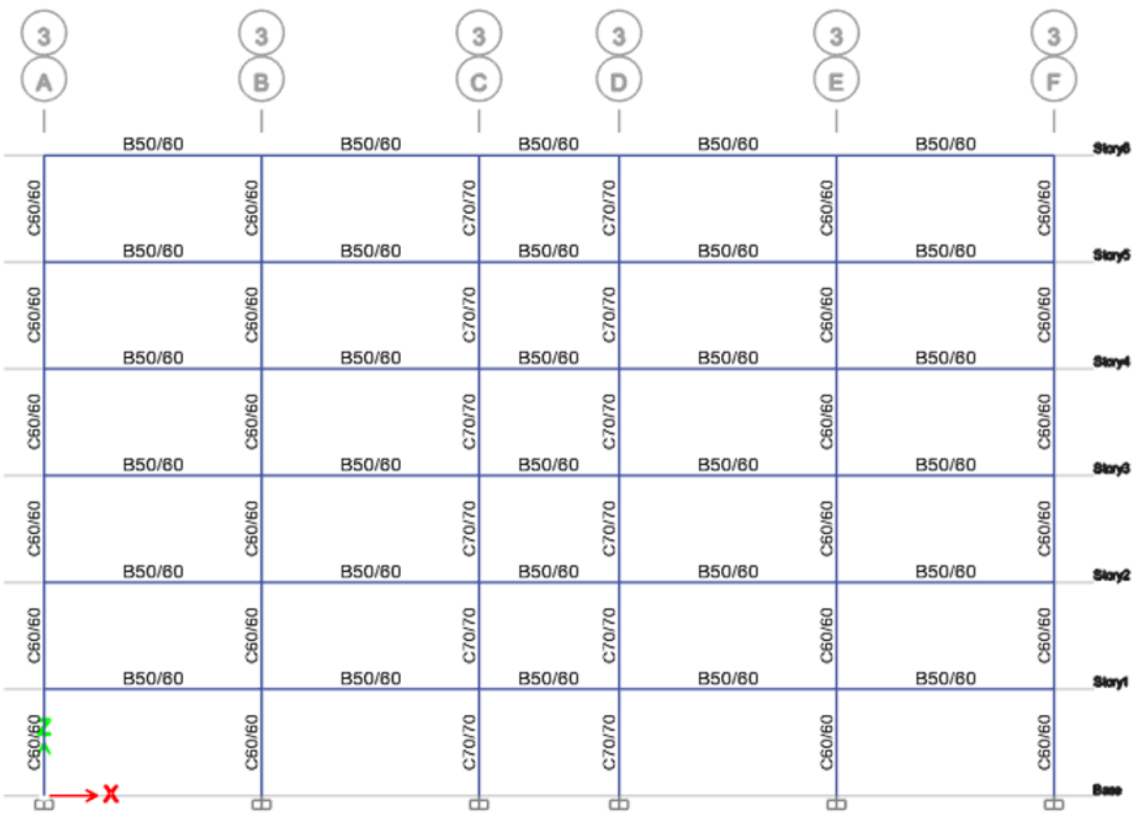

Figure A.10. 6-story building model TSC 2018.

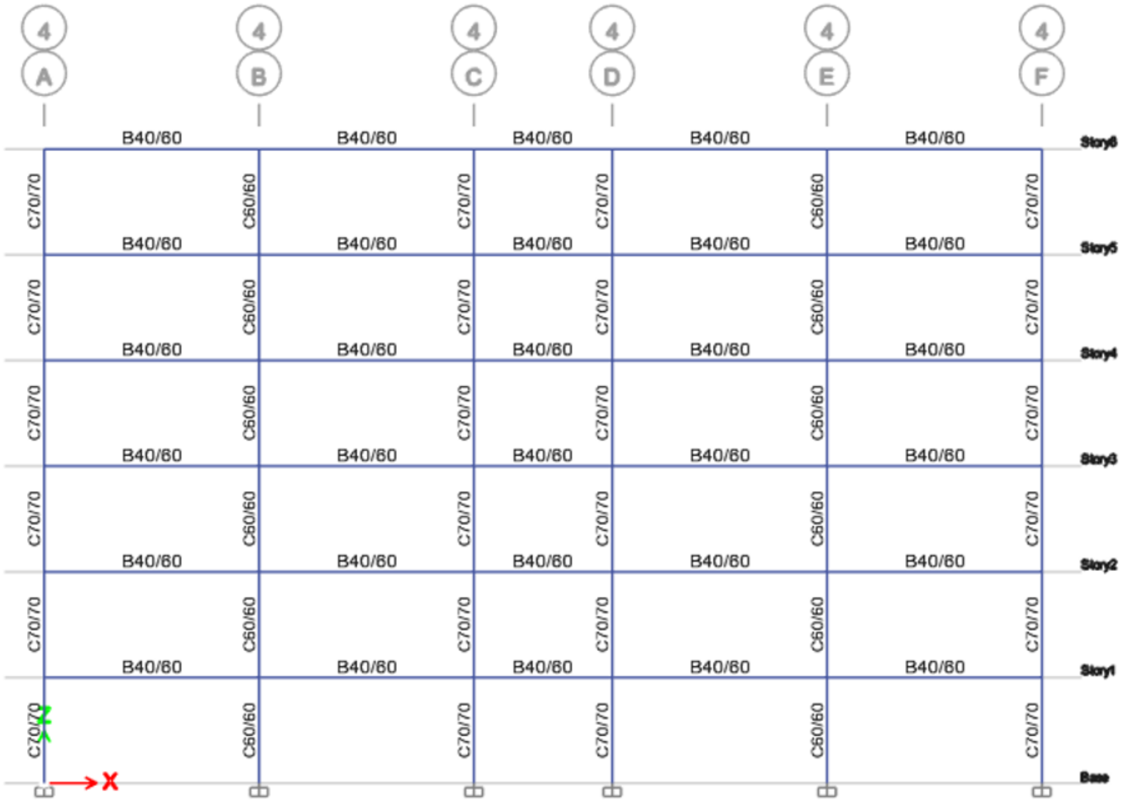

Figure A.11. 6-story building model TSC 2018. cont.

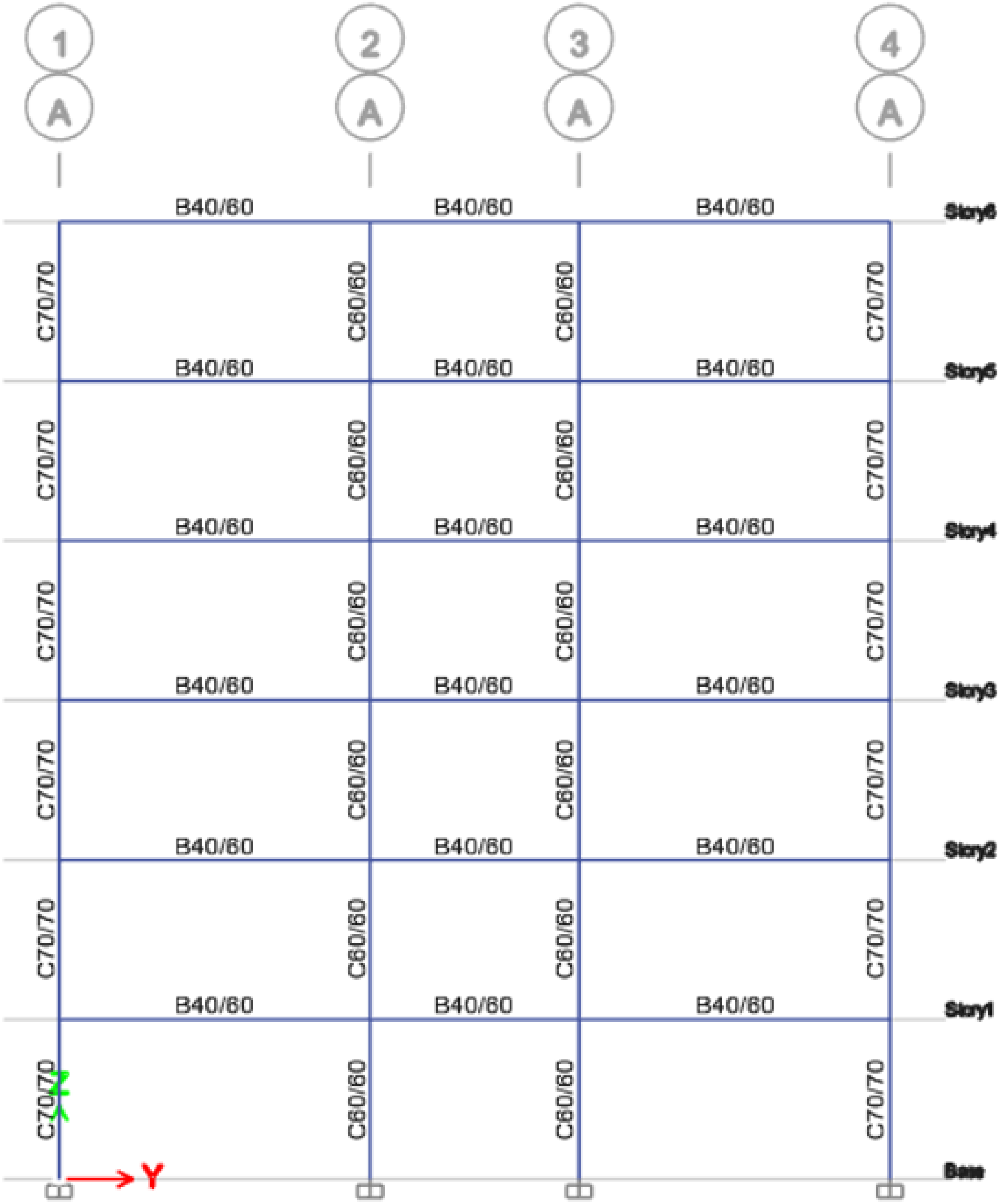

Figure A.12. 6-story building model TSC 2018. cont.

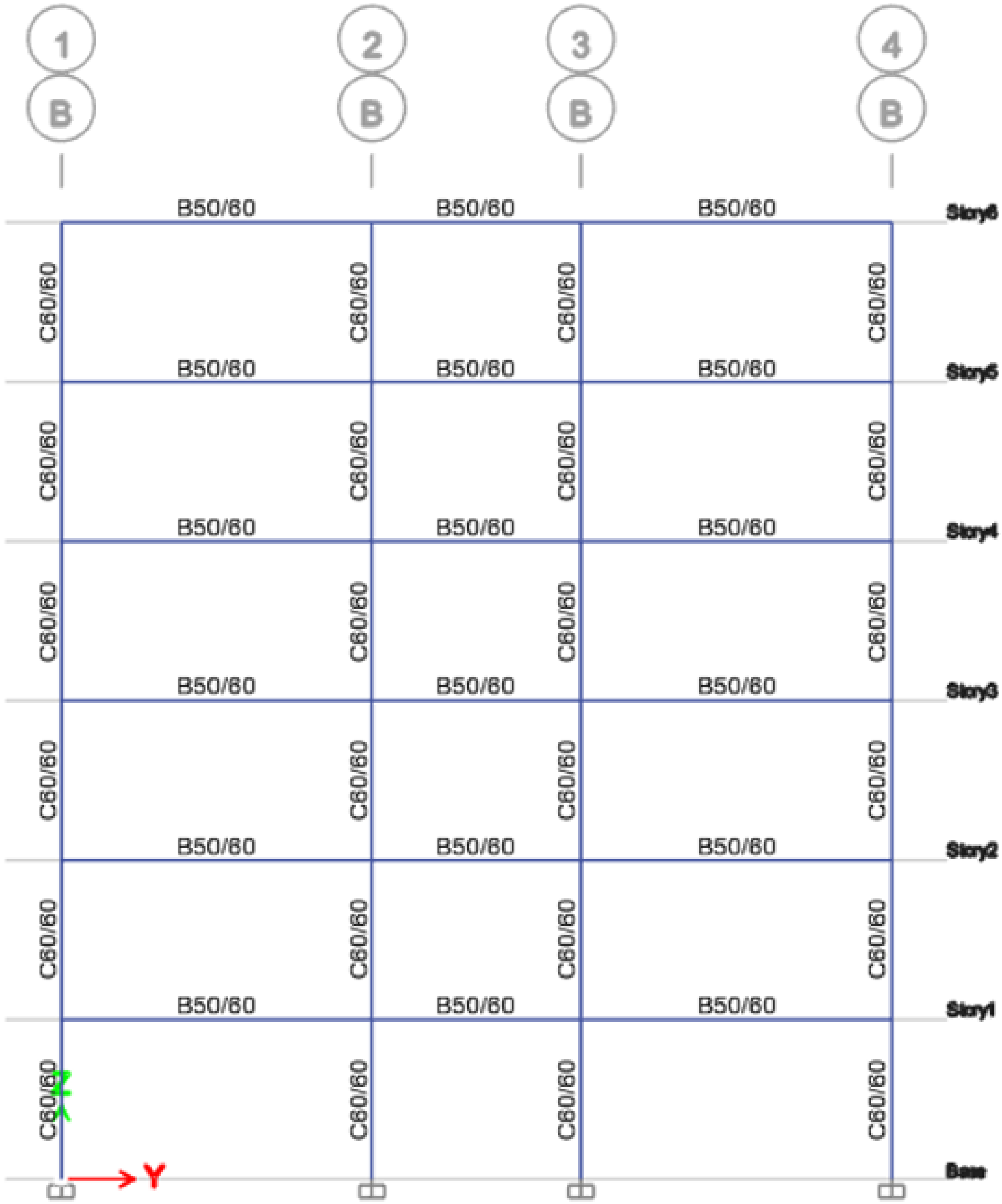

Figure A.13. 6-story building model TSC 2018. cont.

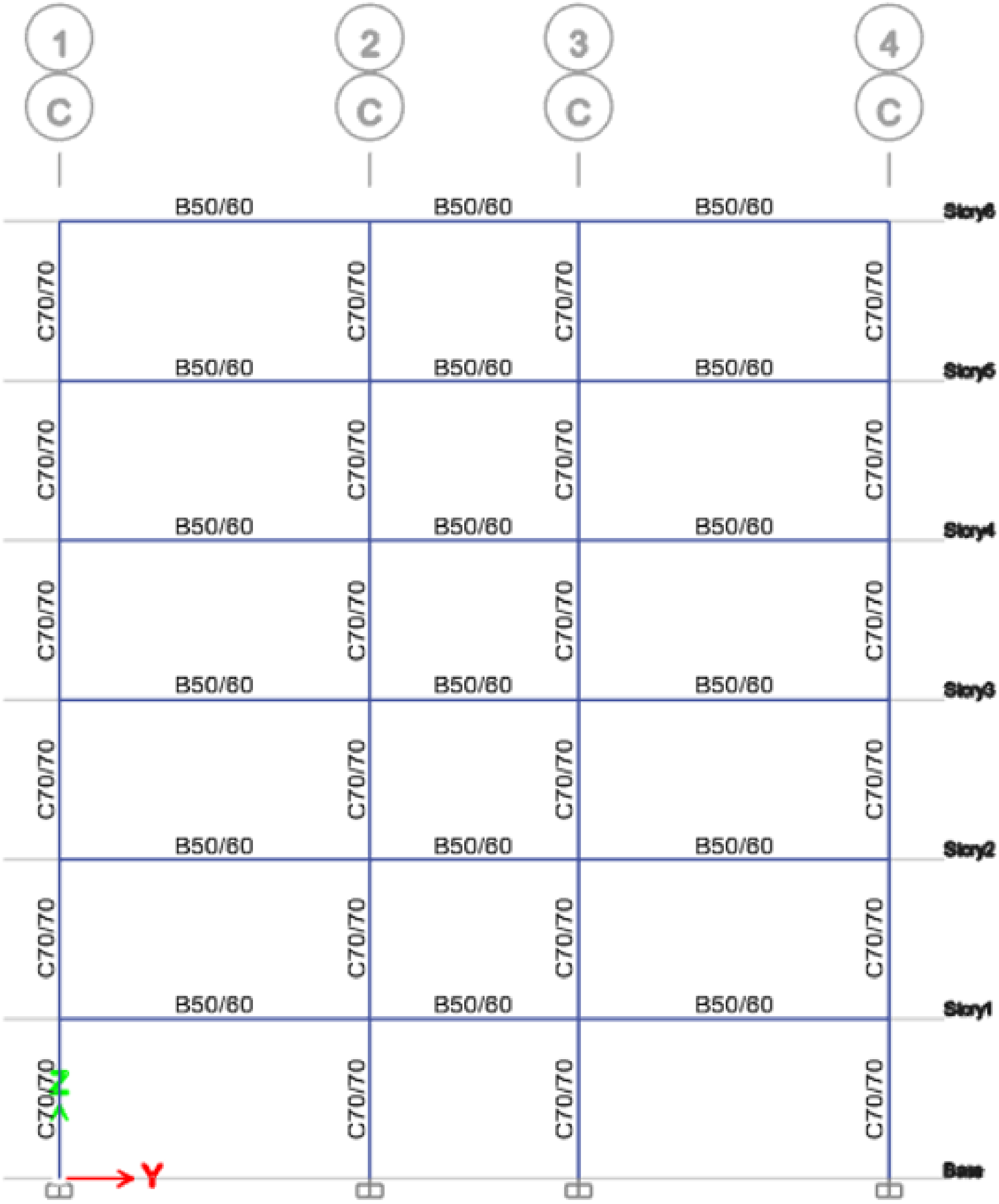

Figure A.14. 6-story building model TSC 2018. cont.

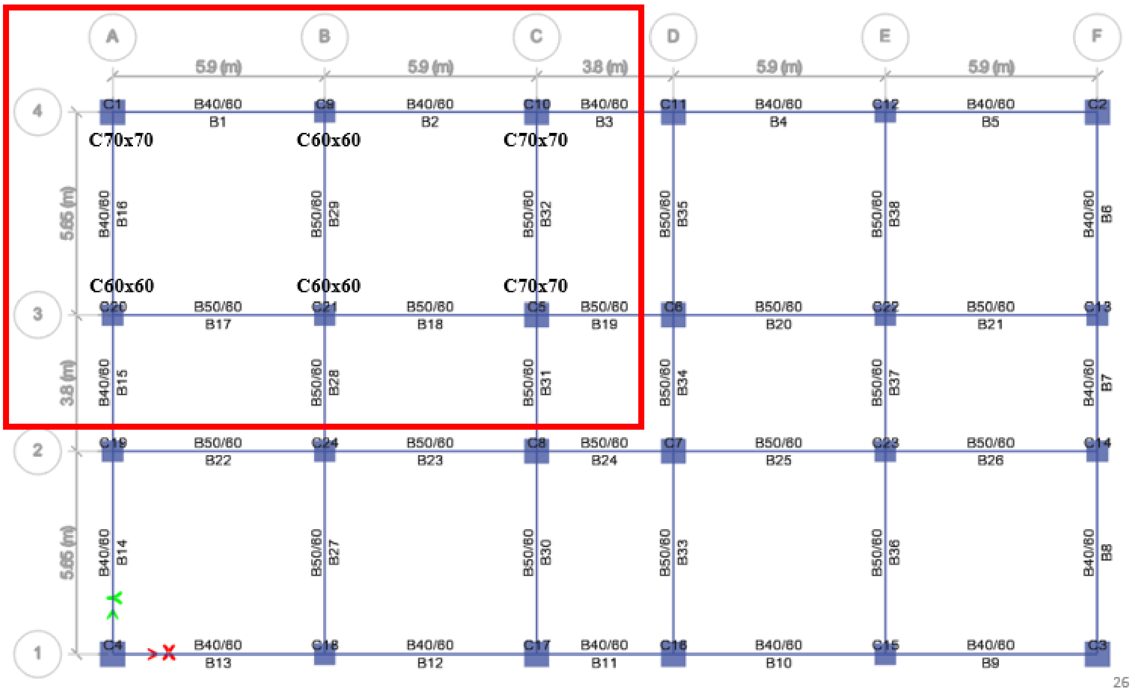

Figure A.15. 6-story building model TSC 2018. cont.

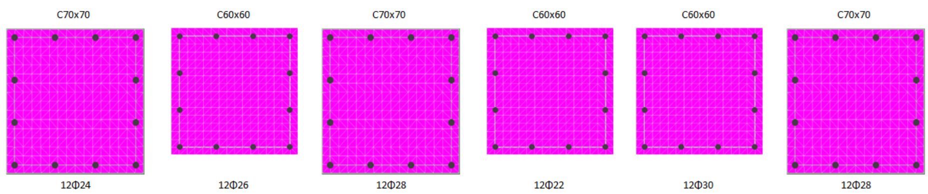

(a)

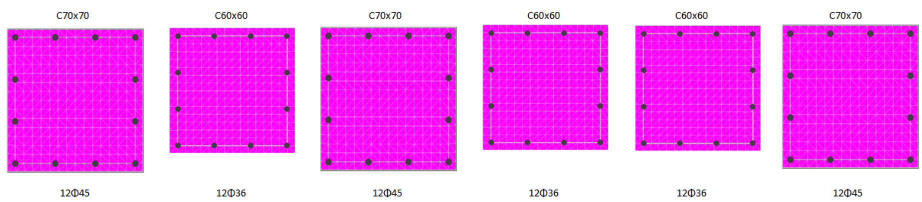

(b)

Figure A.16. Reinforcement for 6-story building model designed per TSC 2018 (a) Columns between 3-6 story (b) Columns between 1-2 story

Beam	Top	Bottom
B1	3Φ26	3Φ20
B2	3Φ26	3Φ20
B3	3Φ26	4Φ16
B17	4Φ24 1Φ16	4Φ18 -
B18	5Φ28	4Φ24
B19	4Φ24 1Φ16	4Φ18 -
B16	4Φ18	4Φ16
B15	4Φ18	4Φ16
B32	4Φ16	4Φ16
B29	4Φ16 1Φ14	4Φ16 -
B28	4Φ16 1Φ14	4Φ16 -
B31	4Φ16	4Φ16

(a)

Beam	Top	Bottom
B1	5Φ26	4Φ22
B2	5Φ26	4Φ22
B3	4Φ26 2Φ28	4Φ24 -
B17	5Φ28	4Φ24
B18	5Φ28	4Φ24
B19	4Φ28 3Φ26	4Φ26 -
B16	4Φ20	4Φ16
B15	4Φ22	4Φ16
B32	3Φ24	4Φ16
B29	3Φ26	4Φ16
B28	3Φ26	4Φ16
B31	3Φ24	4Φ16

(b)

Figure A.17. Reinforcement for 6-story building model designed per TSC 2018 (a) Beams between 5-6 story (b) Beams between 1-4 story

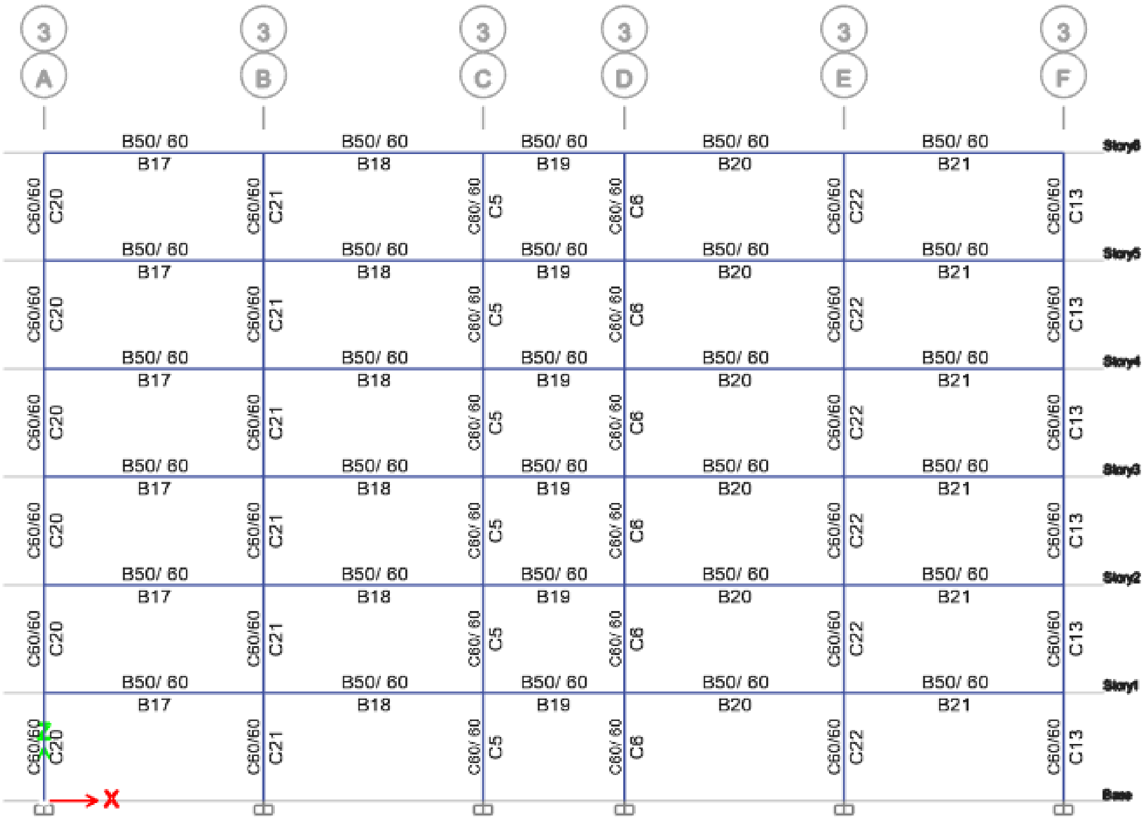

Figure A.18. 6-story building model TSC 1975.

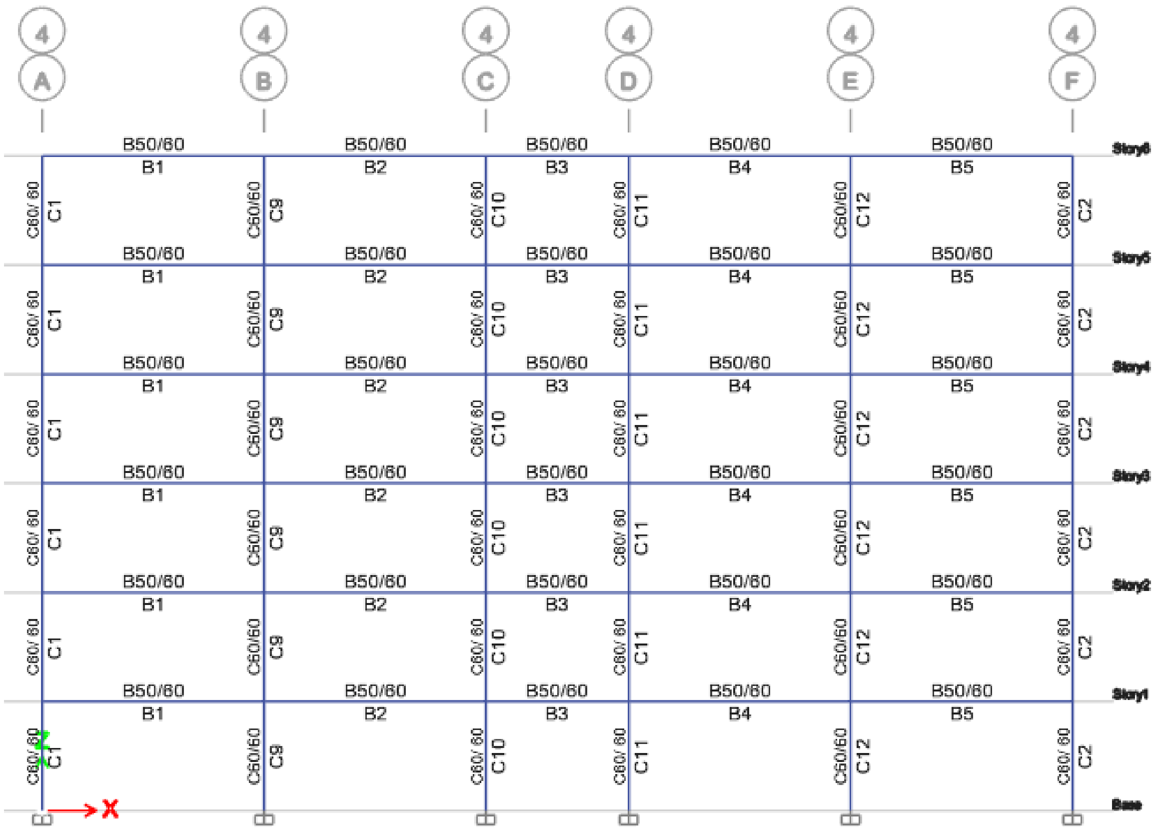

Figure A.19. 6-story building model TSC 1975. cont.

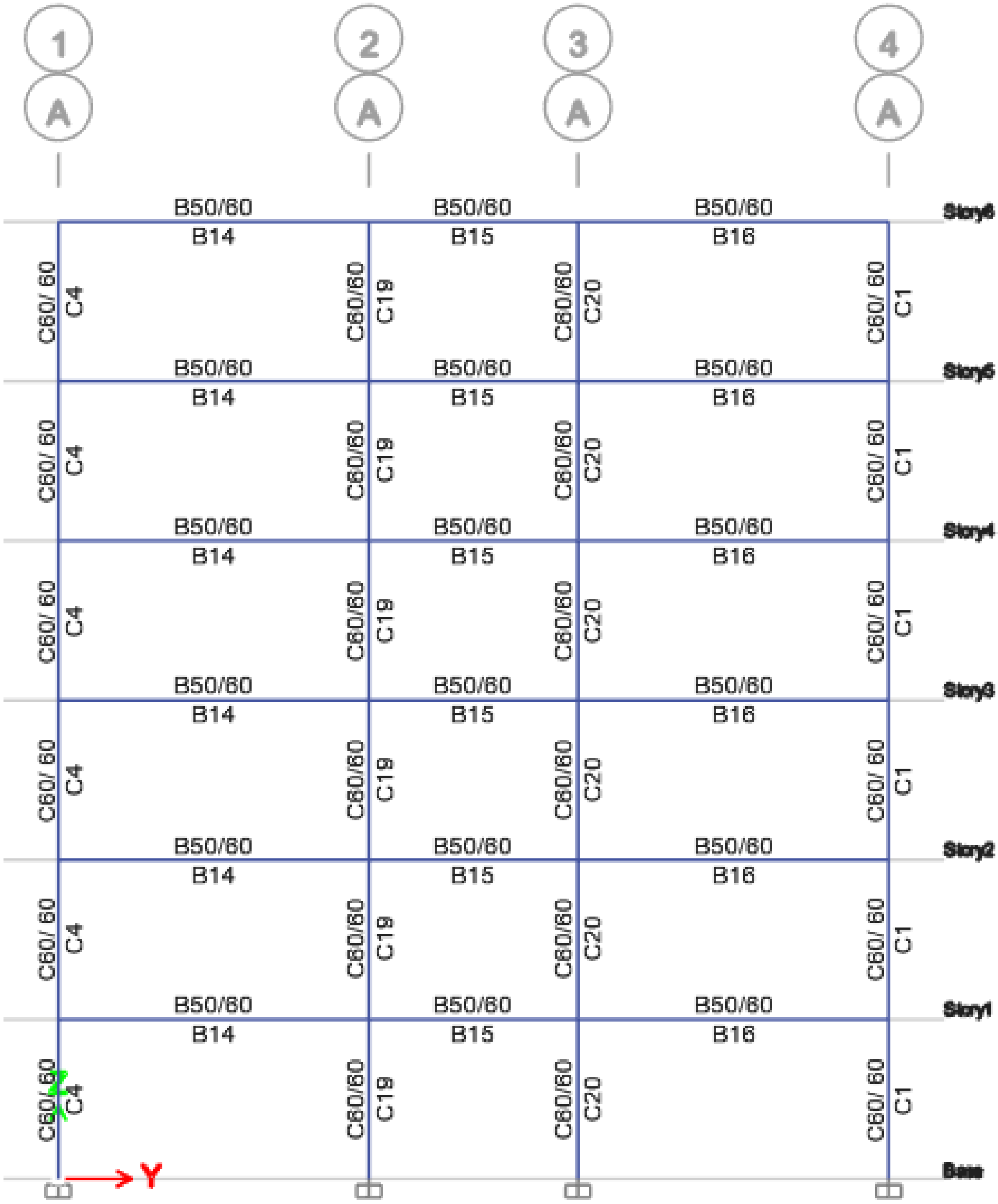

Figure A.20. 6-story building model TSC 1975. cont.

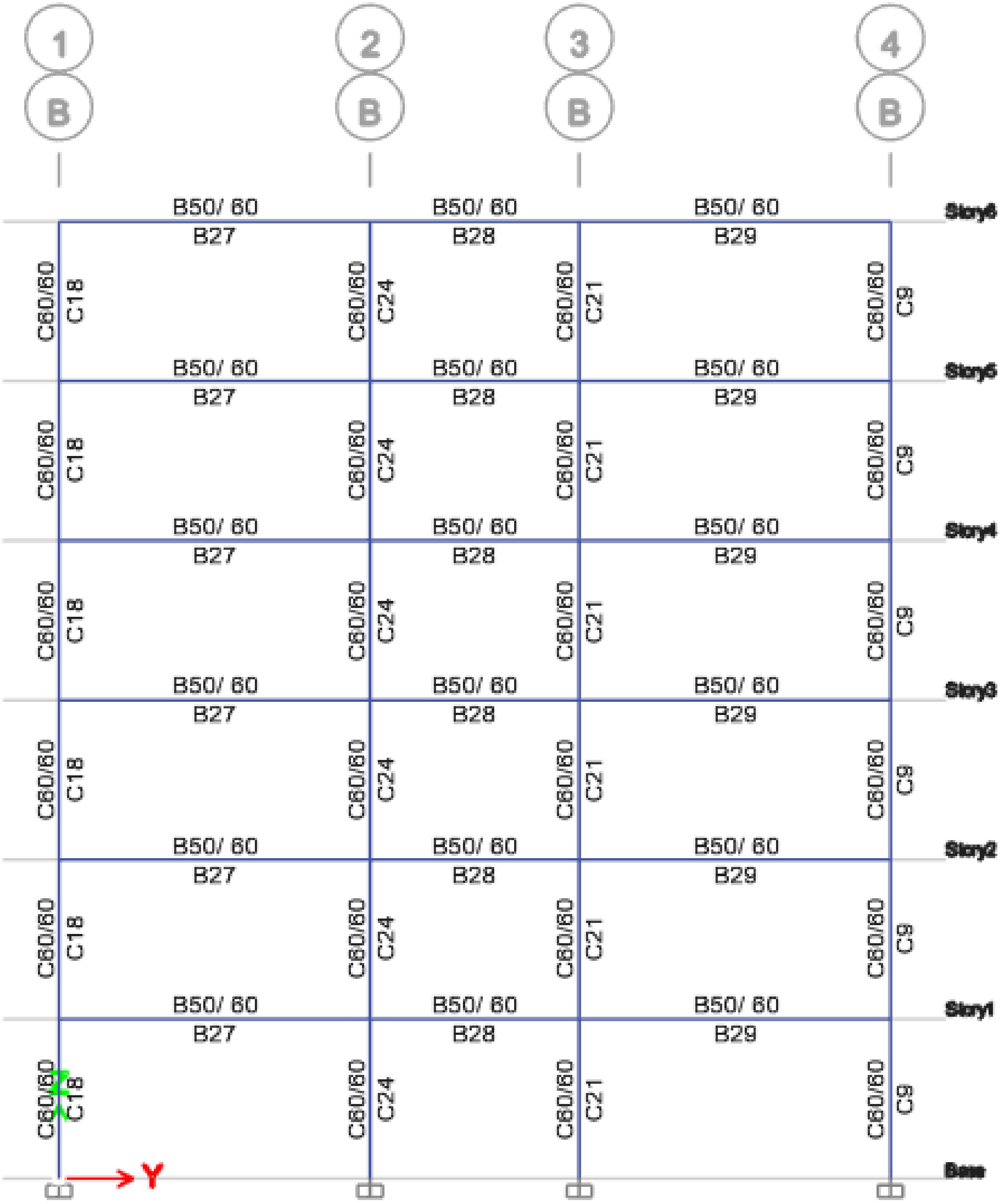

Figure A.21. 6-story building model TSC 1975. cont.

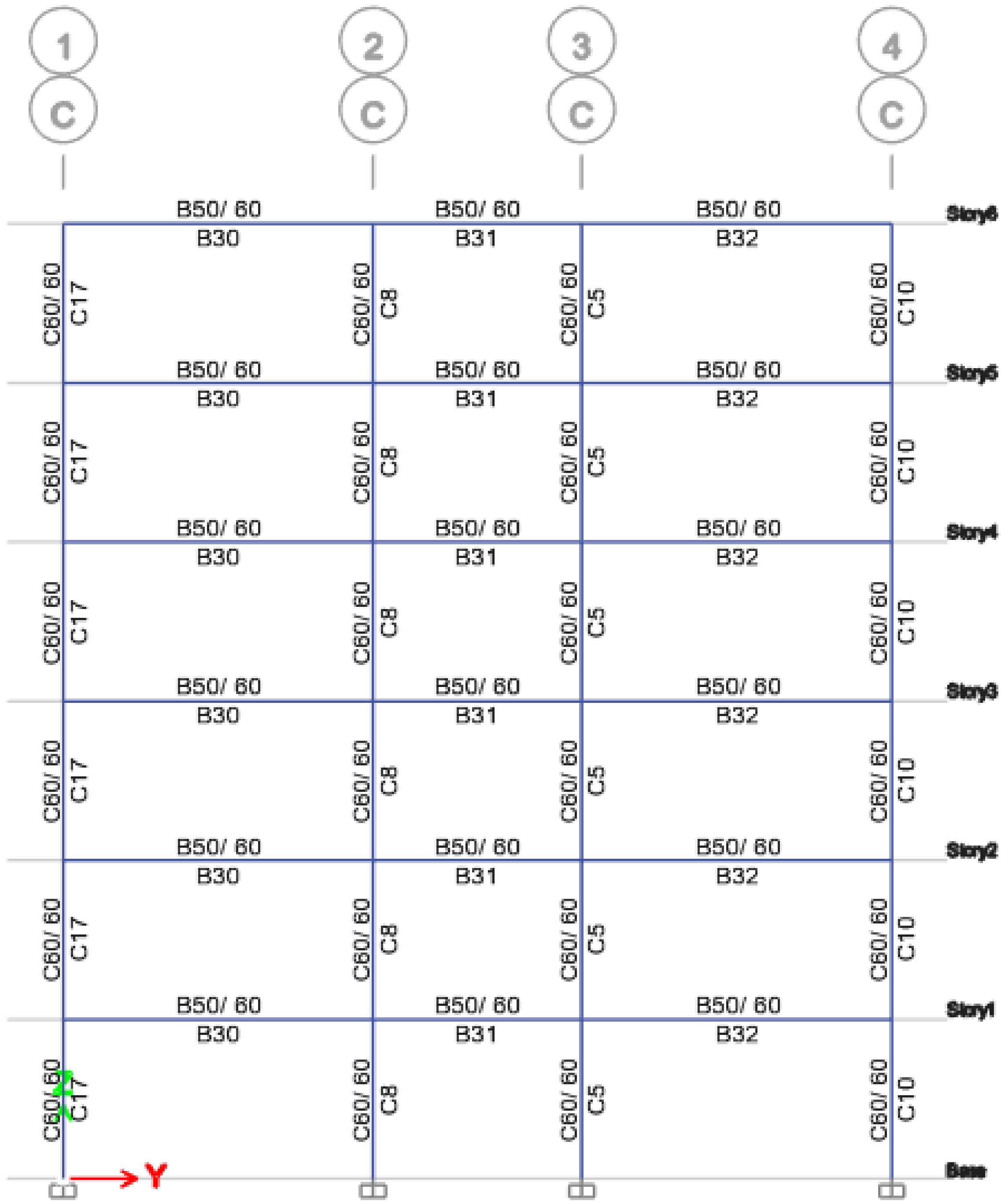

Figure A.22. 6-story building model TSC 1975. cont.

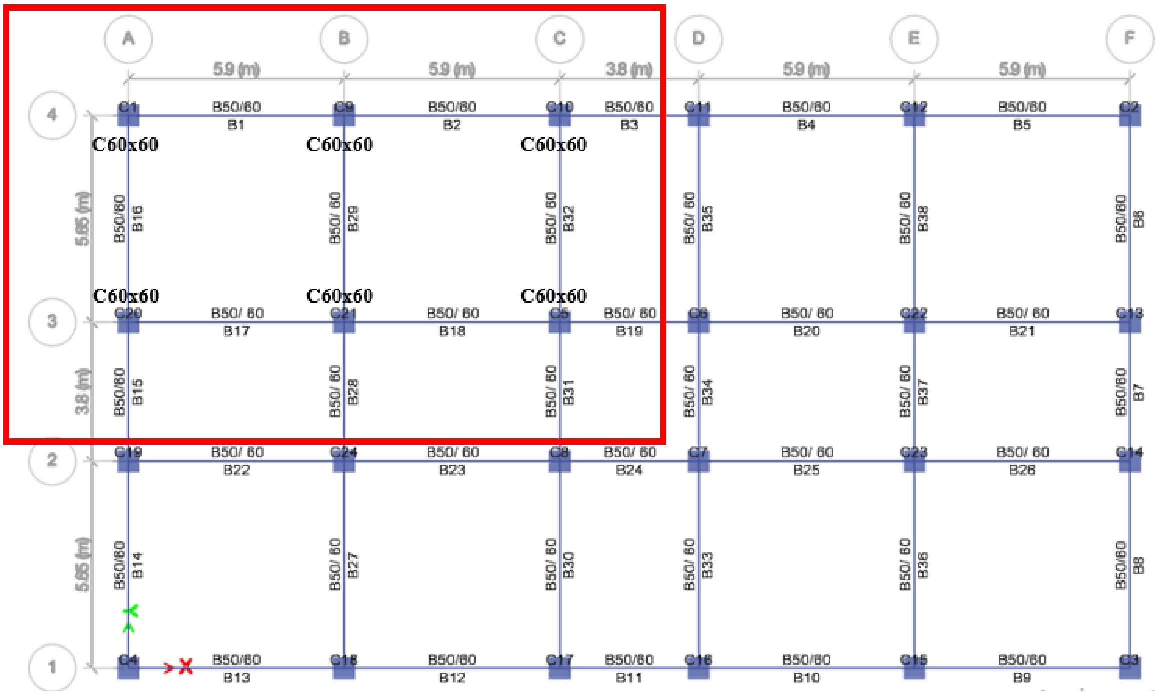

Figure A.23. 6-story building model TSC 1975. cont.

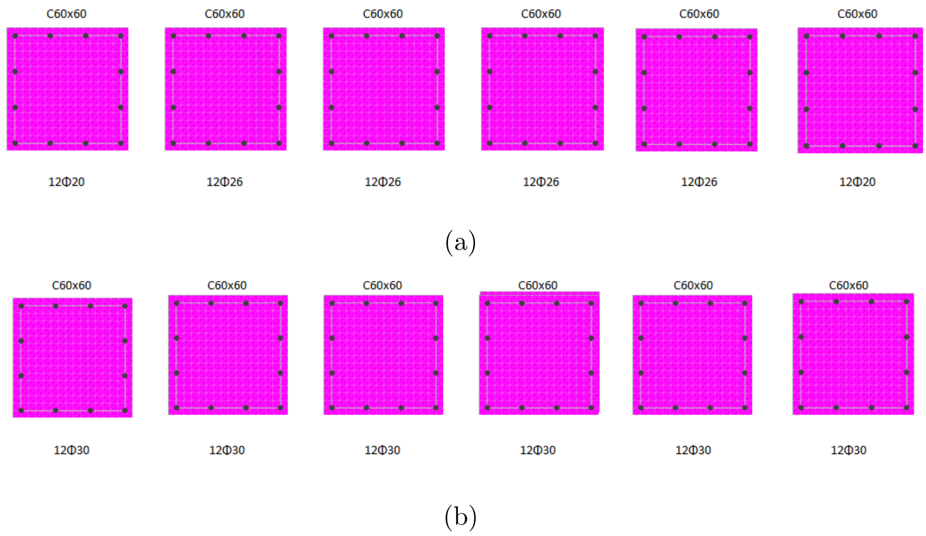

Figure A.24. Reinforcement for 6-story building model designed per TSC 1975 (a) Columns between 3-6 story (b) Columns between 1-2 story

Beam	Top	Bottom
B1	4Φ24	4Φ22
B2	4Φ24	4Φ22
B3	4Φ22	4Φ22
B17	4Φ24	4Φ22
B18	4Φ24	4Φ22
B19	4Φ22	4Φ22
B15	4Φ22	4Φ22
B16	4Φ22	4Φ22
B28	4Φ22	4Φ22
B29	4Φ22	4Φ22
B31	4Φ22	4Φ22
B32	4Φ22	4Φ22

(a)

Beam	Top	Bottom
B1	4Φ28 2Φ24	4Φ22 -
B2	4Φ28 2Φ22	4Φ22 -
B3	4Φ28 2Φ22	4Φ22 -
B17	4Φ28 2Φ22	4Φ22 -
B18	4Φ28 2Φ22	4Φ22 -
B19	4Φ28 2Φ22	4Φ22 -
B15	4Φ22	4Φ22
B16	4Φ22	4Φ22
B28	4Φ22	4Φ22
B29	4Φ22	4Φ22
B31	4Φ22	4Φ22
B32	4Φ22	4Φ22

(b)

Figure A.25. Reinforcement for 6-story building model designed per TSC 1975 (a) Beams between 5-6 story (b) Beams between 1-4 story

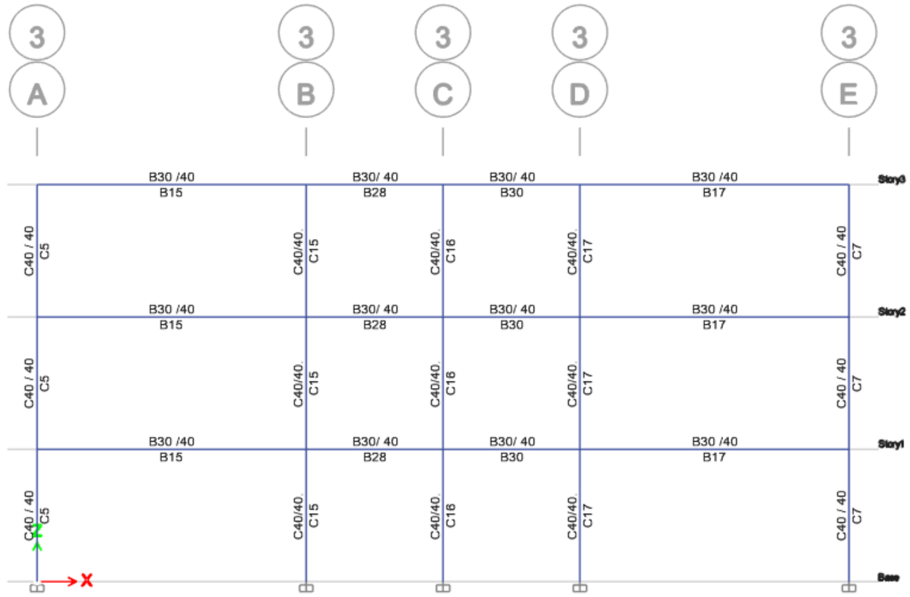

(a)

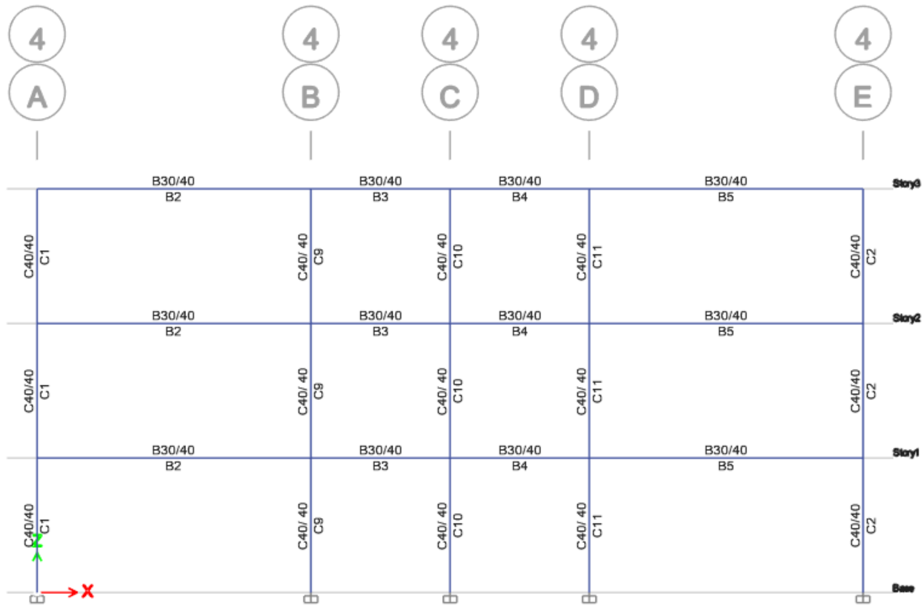

(b)

Figure A.26. 3-story building model TSC 1975.

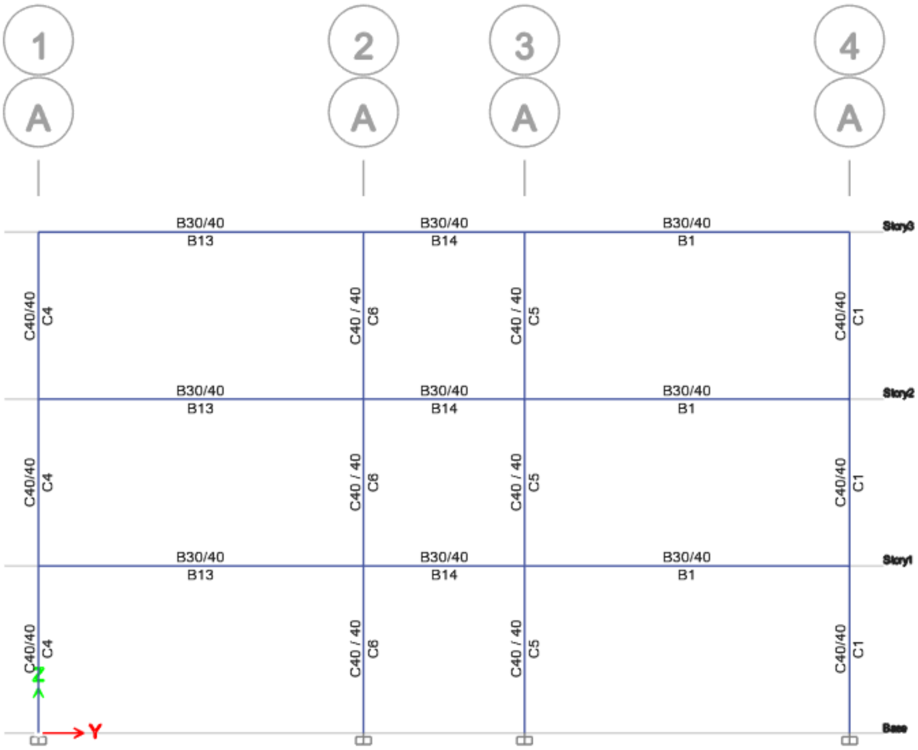

(a)

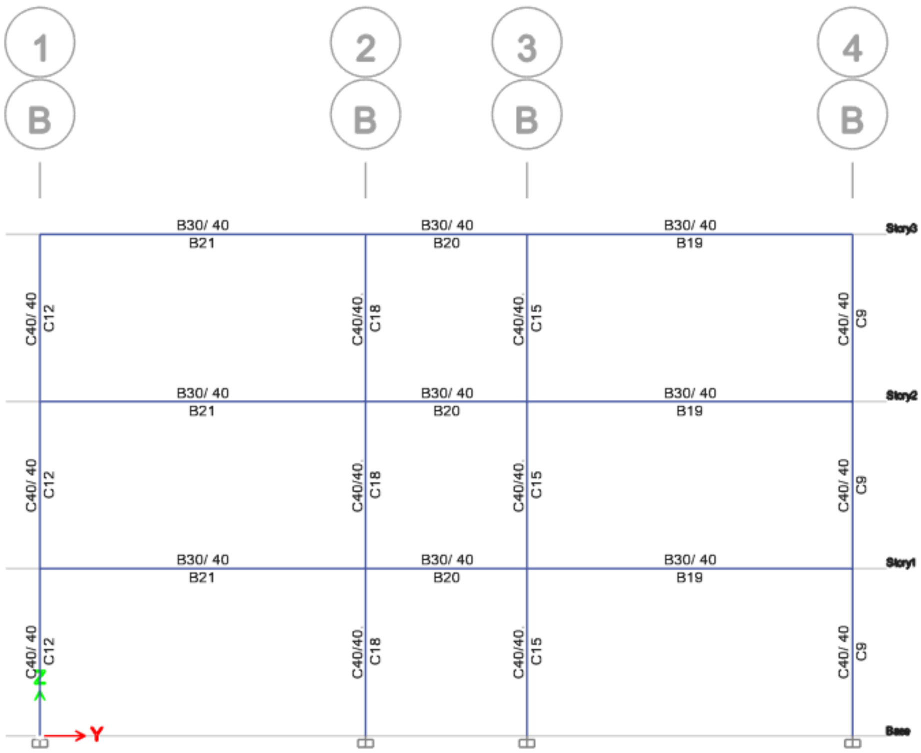

(b)

Figure A.27. 3-story building model TSC 1975. cont.

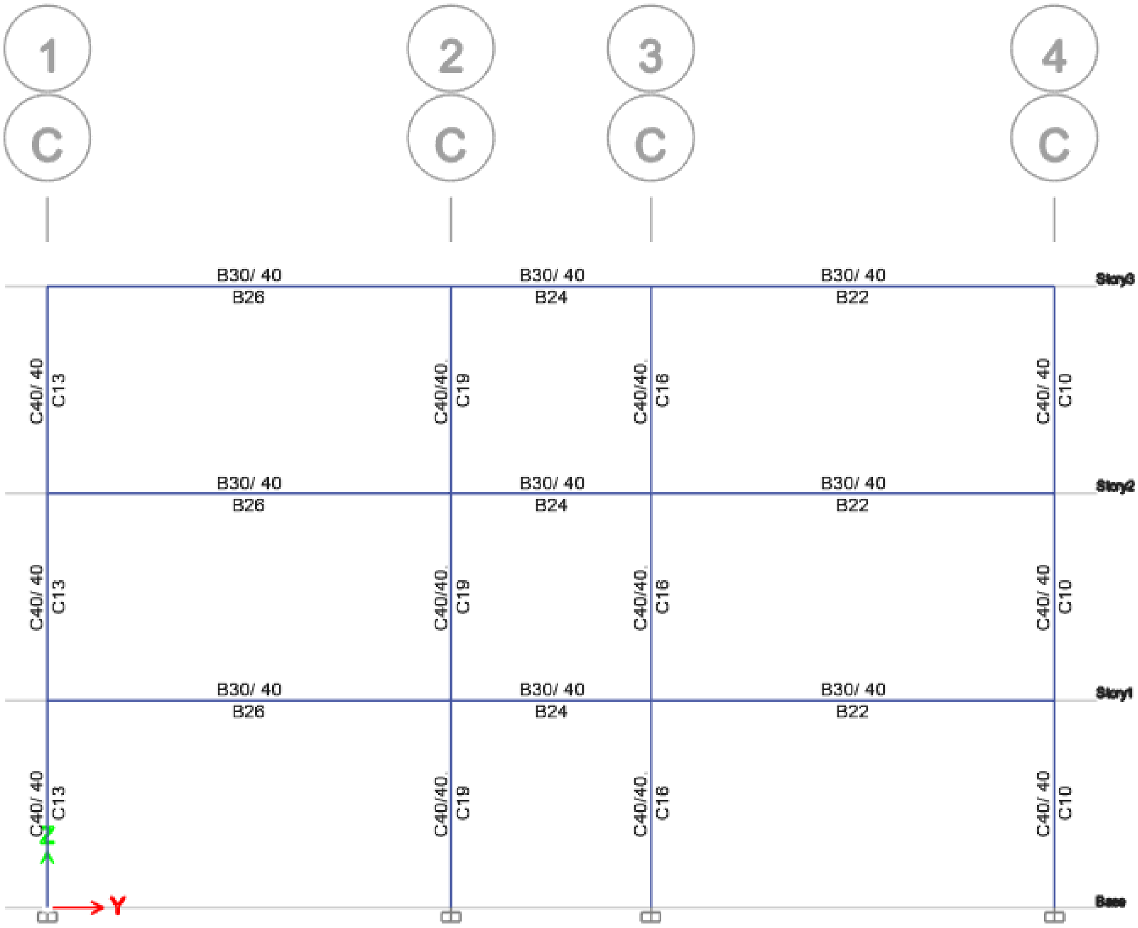

Figure A.28. 3-story building model TSC 1975. cont.

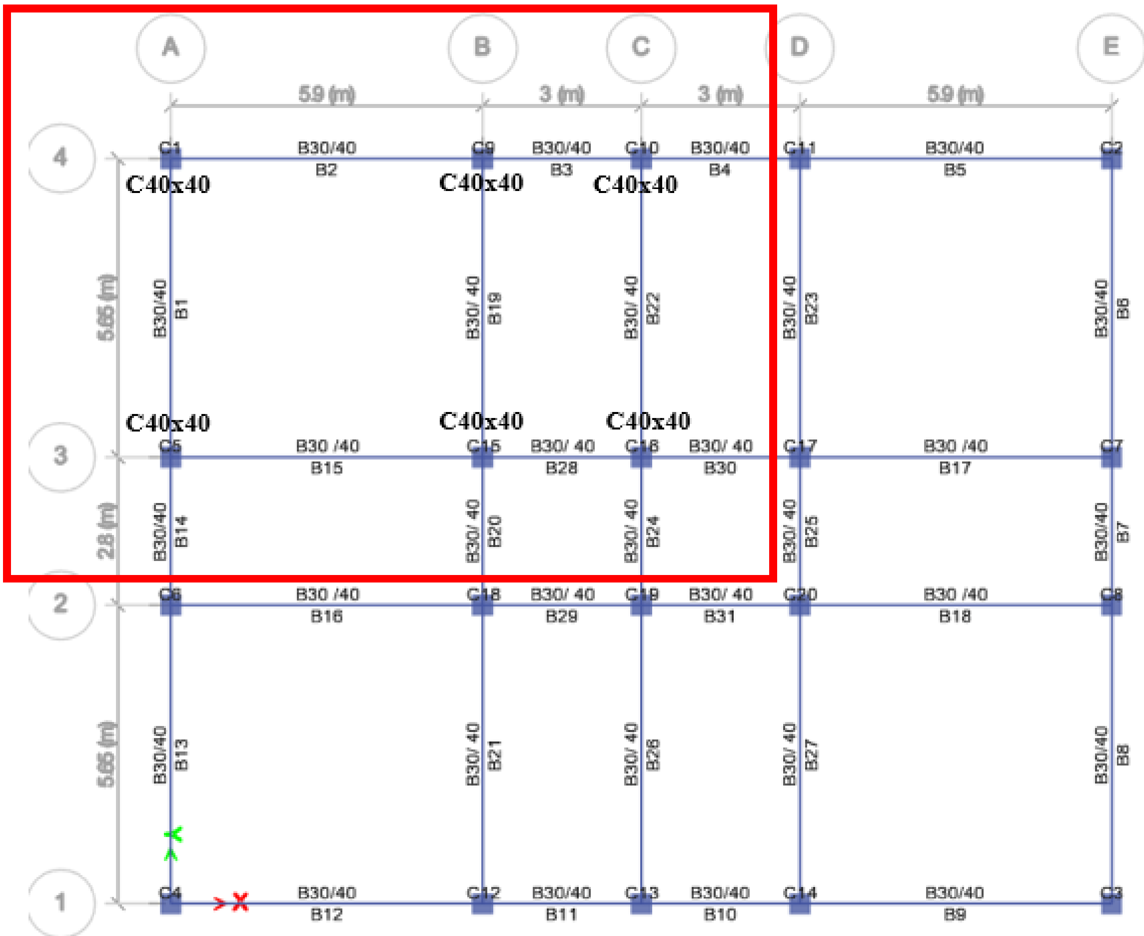

Figure A.29. 3-story building model TSC 1975.

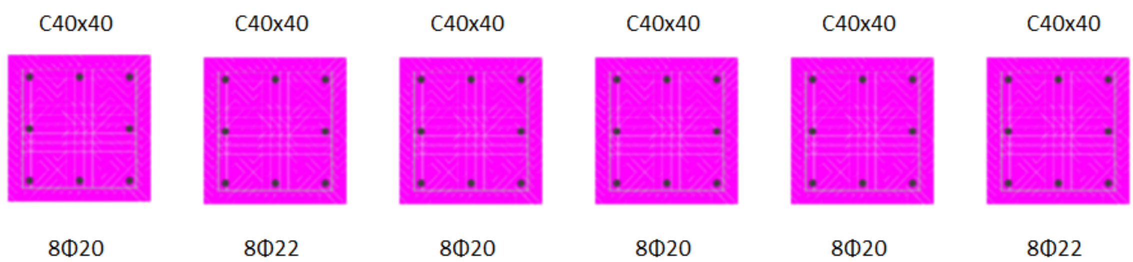

Figure A.30. Reinforcement of columns for 3-story building model designed per TSC 1975.

B2			**B3**		
Top	Bottom		Top	Bottom	
4Φ22	3Φ20		4Φ20	2Φ20	
B15			**B28**		
Top	Bottom		Top	Bottom	
4Φ22	3Φ20		4Φ20	2Φ20	
B1			**B14**		
Top	Bottom		Top	Bottom	
4Φ22	3Φ20		4Φ20	2Φ20	
B19			**B20**		
Top	Bottom		Top	Bottom	
4Φ22	3Φ20		4Φ20	2Φ20	
B22			**B24**		
Top	Bottom		Top	Bottom	
4Φ22	3Φ20		4Φ20	2Φ20	

Figure A.31. Reinforcement of beams for 3-story building model designed per TSC 1975.